



THE UNIVERSITY
of ADELAIDE

Normal fault growth analysis using 3D seismic datasets
located along Australia's southern margin

Alexander George Robson

Geology and Geophysics

School of Physical Sciences

University of Adelaide

This thesis is submitted in fulfilment of the requirements for the
degree of Doctor of Philosophy

September 2017

Abstract

Understanding and constraining the growth of normal faults continues to remain a grand challenge for geoscientists. Normal faults have long been interpreted to grow symplistically with an elliptical fault surface growing radially and accrued displacement increasing from the fault tip-line to the centre of the fault surface. However, continued rigorous analysis of normal fault arrays in rock outcrop and 3D seismic datasets has revealed that normal fault growth is substantially more complex. This is due to the growth and interaction of multiple fault segments, spatial heterogeneity in rock properties and a more detailed three-dimensional analytical approach to understanding displacement variations, rather than in two-dimensional analysis in the plane of view. The interpretation of normal fault growth has long been analysed on the centimetre and metre scale in rock outcrop. However, with increasingly available, high quality seismic datasets, constraints on normal fault growth can now be interpreted on the kilometre scale. Our present understanding of small-scale normal fault growth using rock outcrop is crucial information if we are to constrain the growth of normal faults on the kilometre scale in 3D seismic datasets, with limitations such as data quality, resolution, depth penetration and spatial coverage.

Seismic interpretation of normal fault geometry and development, explicitly or implicitly, will be influenced by, and in some cases rely on, preconceived and idealized conceptual models. Continued analysis of high quality seismic datasets, in order to further understand the development of normal fault systems, will create greater predictive ability in seismic interpretation and static modelling of the subsurface when a poorer quality seismic dataset does not provide a complete and obvious answer. Factors controlling normal fault growth, such as crustal extension, gravitational instability, thermal subsidence and sediment loading need to be better understood and constrained to allow for greater prediction of normal fault evolution in any given tectono-stratigraphic setting.

This thesis consists of four papers, each of which analyses the growth of Upper Cretaceous normal fault arrays along Australia's rifted-to-passive southern margin providing implications for other rifted and passive margins around the world, including the North Sea, Suez Rift, East African Rift, Niger Delta, Gulf of Mexico and Baram Delta. Australia's southern margin and its constituent basins (Bight, Otway, Sorell, Gippsland and Bass basins) was formed from the Australian-Antarctica continental break-up since the Middle to Late Jurassic. The four papers comprising this thesis provide analysis, interpretation and discussion on the development of normal fault arrays located in the Ceduna Sub-Basin of the Bight Basin and the Gambier Embayment, the present-day shelf-edge break and the Shipwreck Trough of the Otway Basin. This thesis aims to qualitatively constrain the influence of controls such as crustal extension, gravitational instability, deltaic sediment loading, perturbation of stress orientations and basin compartmentalisation on the spatial and temporal development of normal fault arrays in differing tectono-stratigraphic settings. Therefore, the findings of this thesis may be used as a predictive tool for normal fault geometry, linkage, displacement distribution and the spatial and temporal development of normal fault arrays in known tectono-stratigraphic settings around the world.

Table of Contents

Publication List	i
Declaration	ii
Acknowledgements	iii
1. Contextual Statement	8
1.1 Structural evolution of a gravitationally detached normal fault array: analysis of a 3D seismic dataset from the Ceduna Sub-Basin, Great Australian Bight	10
1.2 3D seismic analysis of gravity-driven and basement influenced normal fault growth in the deepwater Otway Basin, Australia	11
1.3 Structural evolution of a normal fault array using 3D seismic data from the Gambier Embayment, offshore Otway Basin, South Australia	12
1.4 Structural evolution of horst and half-graben structures proximal to a continental transform using a 3D seismic dataset from the Shipwreck Trough, offshore Otway Basin, Australia	13
2. Literature Review	14
2.1 Tectono-stratigraphic framework of Australia's southern margin, with emphasis on the Bight Basin and Otway Basin	14
2.2 Determining normal fault growth and kinematics: an overview	27
3. References	40
4. Thesis Body	47
4.1 Paper 1: Structural evolution of a gravitationally detached normal fault array: analysis of a 3D seismic dataset from the Ceduna Sub-Basin, Great Australian Bight	47
4.2 Paper 2: 3D seismic analysis of gravity-driven and basement influenced normal fault growth in the deepwater Otway Basin, Australia	69
4.3 Paper 3: Structural evolution of a normal fault array using 3D seismic data from the Gambier Embayment, offshore Otway Basin, South Australia	85
4.4 Paper 4: Structural evolution of horst and half-graben structures proximal to a continental transform using a 3D seismic dataset from the Shipwreck Trough, offshore Otway Basin, Australia	101

5.	Discussion: Controls on normal fault growth along Australia’s rifted-to-passive	
	southern margin	123
5.1	Normal fault growth in the Ceduna Sub-basin	123
5.2	Normal fault growth at the present-day shelf edge break and deepwater Otway Basin	125
5.3	Normal fault growth in the Gambier Embayment of the Otway Basin	125
5.4	Normal fault growth in the Shipwreck Trough of the Otway Basin	126
5.5	Contributions to the regional geology of Australia’s rifted-to-passive southern margin	127
5.6	Implications for normal fault growth and exploration	132
5.6.1	Implications for normal fault growth models	132
5.6.2	Implications for petroleum exploration	132
6.	Thesis Conclusions	135

Publication List

Robson, A. G., King, R. C., & Holford, S. P. (2017). Structural evolution of a gravitationally detached normal fault array: analysis of 3D seismic data from the Ceduna Sub-Basin, Great Australian Bight. *Basin Research*, 29, 605-624. DOI: 10.1111/bre.12191

Robson, A. G., King, R. C., & Holford, S. P. (2016). 3D seismic analysis of gravity-driven and basement influenced normal fault growth in the deepwater Otway Basin, Australia. *Journal of Structural Geology*, 89, 74-87. DOI:10.1080/08120099.2017.1324822

Robson, A. G., Holford, S. P., & King R. C. (2017). Structural evolution of a normal fault array in the Gambier Embayment, offshore Otway Basin, South Australia: insights from 3D seismic data. *Australian Journal of Earth Sciences*, 64(5), 611-624. DOI: 10.1080/08120099.2017.1324822.

Robson, A. G., Holford, S. P., King R. C., Kulikowski, D., (2018). Structural evolution of horst and half-graben structures proximal to a transtensional fault system using a 3D seismic dataset from the Shipwreck Trough, offshore Otway Basin, Australia. *Marine and Petroleum Geology*, 89(3), 615-634. DOI:10.1016/j.marpetgeo.2017.10.028

Conference Abstracts

Robson, A., King, R., & Holford, S. (2015). 3D seismic analysis of normal fault growth and interaction within a gravitational detachment delta system in the Ceduna Sub-Basin, Great Australian Bight. *ASEG Extended Abstracts, 2015(1)*, 1-4.

Robson, A., King, R., & Holford, S. Normal fault growth and segment linkage in a gravitationally detached delta system: evidence from 3D seismic reflection data from the Ceduna Sub-basin, Great Australian Bight. *The APPEA Journal*, 55(2), 467-467.

Robson, A. G., King, R. C., Holford, S. P., (2015). Normal Fault Growth Analysis of Australia's Southern Margin: Evidence From 3-D Seismic Reflection Data in the Ceduna Sub-Basin, Great Australian Bight and Deep-Water Otway Basin. In *International Conference and Exhibition, Melbourne, Australia 13-16 September 2015* (pp. 360-360). Society of Exploration Geophysicists and American Association of Petroleum Geologists.

Robson, A. G., Holford, S. P., King, R. C., (2015). Growth and reactivation of normal faults during the influx and interaction of two temporally and spatially distinct delta systems: an example of kilometre-scale mechanical stratigraphy using 3D seismic data from the Bight Basin, offshore southern Australia. *Geology of Geomechanics Conference, Geological Society of London, London, United Kingdom 28-29 October 2015*.

Robson, A., King, R., & Holford, S. (2016). Analysis of Gravity-Driven Normal Faults Using a 3D Seismic Reflection Dataset from the Present-Day Shelf-Edge Break of the Otway Basin, Australia. *ASEG Extended Abstracts, 2016(1)*, 1-6.

Robson, A. G., Holford, S. P., King, R. C., (2017). Controls on normal fault growth along Australia's southern margin. *American Association of Petroleum Geologists International Conference and Exhibition, London, United Kingdom, 14-18 October 2017*.

Declaration

I, Alexander Robson, certify that this work contains no material which has been accepted for the award of any other degree or diploma in any university or other tertiary institution and, to the best of my knowledge and belief, contains no material previously published or written by another person, except where due reference has been made in the text. In addition, I certify that no part of this work will, in the future, be used in a submission for any other degree or diploma in any university or other tertiary institution without the prior approval of the University of Adelaide and where applicable, any partner institution responsible for the joint-award of this degree.

I give consent to this copy of my thesis when deposited in the University Library, being made available for loan and photocopying, subject to the provisions of the Copyright Act 1968. The author acknowledges that copyright of published works contained within this thesis resides with the copyright holder(s) of those works.

I also give permission for the digital version of my thesis to be made available on the web, via the University's digital research repository, the Library catalogue and also through web search engines, unless permission has been granted by the University to restrict access for a period of time.

Alexander Robson —

7/09/2017

Date

Acknowledgements

The work produced within this thesis could not have been completed without the support, financial contribution and encouragement provided by, but not limited to, the following people:

My Supervisory Team; Dr. Rosalind King and Dr. Simon Holford.

I would like to thank you both for your encouragement, feedback and patience through this very challenging and memorable period of my life. Completing this degree is, and will always be, one of the highlights of my life, so thank you both for helping me make this possible. You are amazing geoscientists and it has been an honour and privilege to learn from you both.

Australian Society of Exploration Geophysicists (ASEG).

I would like to sincerely thank and acknowledge ASEG for the extra scholarship funding towards my research. Without this contribution, my research and conference travel would have been much more challenging.

The S³ Research Group.

I would like to thank all of the members of the S³ research group for listening to me present my work and for showing me the work you were all undertaking at the time, which certainly helped me develop as a geoscientist.

The Australian School of Petroleum (ASP).

Thank you to everyone at ASP for educating me over the last few years and for allowing me to work in the building when my scholarship was through the sciences faculty. I have really enjoyed the working and social culture at the ASP and will always have great memories of these years.

My Family & Friends.

Thank you to fellow PhD Candidates David Kulikowski and Michael Gray for all the good times in the office, our undergraduate years and honours year together and our AAPG Imperial Barrel Award successes prior to undertaking our PhD's. Thank you to my friends outside of work for keeping me sane when I needed a break. Thank you to my sisters Catherine, Emily and Jess, my brothers-in-law Sean, Dave and Dave for supporting me and believing in me over the 8 bumpy years at uni. Thank you to my amazing partner Iris for pushing and supporting me to finish my thesis while working fulltime and understanding that it's something I just have to finish. Most of all, thank you to my parents Chris and Leonie for allowing me to find my own path, pushing me to work hard and unconditionally supporting me the whole way through all of the ups and downs; this PhD is dedicated to you both.

1. Contextual Statement

Our understanding of the temporal, spatial and kinematic development of normal faults has improved significantly in the last few decades (e.g. Walsh and Watterson, 1988; Childs et al. 1995; Walsh et al. 2003; Giba et al. 2012; Jackson and Rotevatn, 2013). Normal fault growth on the kilometre-scale and in three dimensions has been significantly improved with the availability of high quality 3D seismic reflection datasets (Mansfield and Cartwright, 1996; Walsh et al. 1999; Tvedt et al., 2013; Lewis et al. 2013; Rotevatn and Jackson, 2014). Australia's rifted-to-passive southern margin provides a wealth of information of normal fault growth with numerous offshore 3D seismic datasets, which image normal fault arrays.

Australia's southern margin is understudied and underexplored compared to other hydrocarbon prolific passive margins around the world, such as the Niger Delta (Doust and Omatsola, 1990; Morley and Guerin, 1996; Cohen and McClay, 1996; Bilotti and Shaw, 2005; Corredor et al., 2005; Briggs et al; 2006; Cobbold et al, 2009) and Gulf of Mexico (Buffler et al. 1979; Winker and Edwards, 1983, Wu et al. 1990, Rowan, 1997). Australia's southern margin and its constituent basins (Bight and Otway basins) were formed from the break-up of Australia and Antarctica since the Middle to Late Jurassic (Norvick and Smith, 2001; Norvick, 2005). The Middle Jurassic to Upper Cretaceous aged, E-W to NW-SE oriented Bight Basin is located within the Great Australian Bight and is host to the Ceduna Sub-Basin, which has been characterized by two stacked delta systems of Cenomanian and late Santonian-Maastrichtian age (Totterdell et al. 2000; MacDonald et al. 2010). The NW-SE oriented, Upper Jurassic-Cenozoic aged Otway Basin extends from SE South Australia to NW offshore Tasmania and is characterised as a rifted-to-passive margin basin, with rifting transitioning to thermal subsidence in the late Maastrichtian (Moore et al., 2000; Krassay et al., 2004; Stacey et al., 2013; Holford et al., 2014).

Using four 3D seismic datasets located along Australia's southern margin in the Ceduna Sub-Basin and Otway Basin we aim to temporally and spatially constrain the development of normal fault systems and to describe the controls on their development. We provide examples of normal faults which developed as a result of both mechanical extension and transtension and gravitational instability. Therefore, our findings have implication towards the development of normal faults in both continental rift basins, such as the North Sea (e.g. Childs et al. 1995; Jackson and Larsen, 2009; Kane et al., 2010; Lewis et al., 2013; Tvedt et al., 2013) and Suez Rift (e.g. Gawthorpe et al. 2003; Jackson and Rotevatn, 2013), and passive margin basins, such as the Gulf of Mexico (Buffler et al. 1979; Winker and Edwards, 1983, Wu et al. 1990, Rowan, 1997) and Niger Delta (Doust and Omatsola, 1990; Morley and Guerin, 1996; Cohen and McClay, 1996; Bilotti and Shaw, 2005; Corredor et al., 2005; Briggs et al; 2006; Cobbold et al, 2009).

Given that the structural evolution of the surrounding geological province should be (to some degree) expressed in the temporal and spatial constraints interpreted for the development of a normal fault (Boult et al. 2008), our research significantly contributes to temporal and kinematic evolution of the Ceduna Sub-Basin and Otway Basin. Furthermore, our study has direct implications for hydrocarbon prospectivity, given that faults may be sealing, allowing for hydrocarbon entrapment, or permeable, allowing the vertical and/or cross-fault migration of hydrocarbons (Smith, 1980; Allan, 1989; Harding and Tuminas, 1989; Hooper, 1991; Knott, 1993; Anderson et al. 1994).

1.1 Structural evolution of a gravitationally detached normal fault array: analysis of a 3D seismic dataset from the Ceduna Sub-Basin, Great Australian Bight (paper 1)

The growth, interaction and controls on normal fault systems developed within stacked delta systems at extensional delta-top settings have not been extensively examined. We aim to analyse the kinematic, spatial and temporal growth of a Cretaceous aged, thin-skinned, listric fault system in order to further the understanding of how gravity-driven fault segments and fault systems develop and interact at an extensional delta-top setting. Furthermore, we aim to explore the influence of a pre-existing structural framework on the development of gravity-driven normal faults through the examination of two overlapping, spatially and temporally distinct delta systems. To do this, we use three-dimensional (3D) seismic reflection data from the central Ceduna Sub-basin, offshore southern Australia. The seismic reflection data images a Cenomanian-Santonian fault system, and a post-Santonian fault system, which are dip-linked through an intervening Turonian-early Campanian section. Both of these fault systems contain four hard-linked strike assemblages oriented NW-SE (127-307), each composed of 13 major fault segments. The Cenomanian-Santonian fault system detaches at the base of a shale interval of late Albian age, and is characterised by kilometre-scale growth faults in the Cenomanian-Santonian interval. The post-Santonian fault system nucleated in vertical isolation from the Cenomanian-Santonian fault system. This is evident through displacement minima observed at Turonian-early Campanian levels, which is indicative of vertical segmentation and eventual hard dip-linkage. Our analysis constrains fault growth into four major evolutionary stages: [1] early Cenomanian nucleation and growth of fault segments, resulting from gravitational instability, and with faults detaching on the lower Albian interval; [2] Santonian cessation of growth for the majority of faults; [3] erosional truncation of fault upper tips coincident with the continental breakup of Australia and Antarctica (~ 83 Ma); [4] Campanian-Maastrichtian reactivation of the underlying Cenomanian-Santonian fault system, inducing the nucleation, growth and consequential dip-linkage of the post-Santonian fault system with the underlying fault system. Our results highlight

the along-strike linkage of fault segments and the interaction through dip-linkage and fault reactivation, between two overlapping, spatially and temporally independent delta systems of Cenomanian and late Santonian-Maastrichtian age in the frontier Ceduna Sub-Basin. This study has implications regarding the growth of normal fault assemblages, through vertical and lateral segment linkage, for other stacked delta systems (such as the Gulf of Mexico) where upper delta systems develop over a pre-existing structural framework.

1.2 3D seismic analysis of gravity-driven and basement influenced normal fault growth in the deepwater Otway Basin, Australia (paper 2)

In this study we have used a three-dimensional (3D) seismic dataset to analyse the development of a normal fault array located at the present-day shelf-edge break of the Otway Basin, southern Australia. The seismic dataset images an Upper Cretaceous aged, NW-SE (128-308) striking, normal fault array, consisting of ten fault segments. The ten faults are arranged in the form of two hard-linked fault assemblages, separated by only 2 km in the dip direction. The down-dip fault assemblage is gravity-driven, located over a basement plateau and displays Campanian-Maastrichtian growth, with a maximum of 1.45 km of accumulated throw. The up-dip normal fault assemblage penetrates below the seismic survey and is interpreted to be partially dip-linked to major basement-involved normal faults that can be observed on regional 2D seismic lines. This fault assemblage displays growth initiating in the Turonian-Santonian and has accumulated up to 1.74 km of throw.

This study has constrained post-Cenomanian fault growth into four evolutionary stages: [1] basement reactivation during Turonian-Santonian crustal extension between Australia and Antarctica. This resulted in either the nucleation of a vertically isolated normal fault array in shallow cover sediments directly above the reactivated basement-involved faults or the upward propagation of basement-involved normal faults; [2] continued Campanian-Maastrichtian crustal extension and

sediment loading induced gravitational instability on the basement plateau, nucleating a second, vertically isolated normal fault array in the cover sediments; [3] hard-linkage of fault segments in both fault arrays eventuated to form two along-strike, NW-SE striking fault assemblages, and; [4] termination of fault growth in the latest Maastrichtian. We provide evidence for growth via lateral and vertical segment linkage by documenting high variability of throw along-strike and down-dip for both fault assemblages. This study has highlighted the complexities involved in the growth of both gravity-driven normal fault arrays (such as those present in the Niger Delta and Gulf of Mexico) and basement-linked normal fault arrays (such as those present in the North Sea and Suez Rift) with the interaction of an underlying and reactivating basement framework. This study has also showcased a superb example of spatial variability in growth of two normal fault assemblages over relatively short distances (~2 km separation down-dip).

1.3 Structural evolution of a normal fault array using 3D seismic data from the Gambier

Embayment, offshore Otway Basin, South Australia (paper 3)

This study contributes to the growing pool of research on normal fault growth by determining the structural evolution of a normal fault array using detailed kinematic analysis of normal fault tip propagation and linkage. Furthermore, this study provides further insight into the structural evolution of the offshore Otway Basin, Australia. Using three-dimensional (3D) seismic reflection data we have investigated the development of a Late Cretaceous–Cenozoic age normal fault array located in the Gambier Embayment of the offshore Otway Basin. Using the seismic reflection data we have observed an array of six NW–SE-oriented normal faults, which have grown via the linkage of numerous, smaller segments. Underlying, and with partial dip-linkage to, this fault array are E–W-striking, basement-involved faults that formed during the initial Tithonian–Barremian rifting event in the Otway Basin. From the observations of fault displacement analysis, post-Cenomanian growth

history of the upper array can be summarised into four key stages: (1) resumed crustal extension during the early Late Cretaceous resulted in the nucleation of the majority of faults; (2) fault quiescence during the intra-Late Cretaceous period, with only one newly formed fault nucleating; (3) nucleation of another newly formed fault and further growth of all other faults in the latest Cretaceous; and (4) continued growth of all faults, forming the Cenozoic Gambier Sub-basin in the Otway Basin.

This study shows that Late Cretaceous faults, which dip-link to underlying basement-involved faults, display earlier nucleation and greater overall throw and length, compared to those which are spatially isolated from basement-involved faults. This is likely caused by increased rift-related stress concentrations in cover strata above the upper tips of basement-involved faults. By analysing the segmented growth style of a Late Cretaceous normal fault array that interacts with an underlying reactivated basement framework, this study progresses our understanding of the geological evolution of the presently under-explored Gambier Embayment, offshore Otway Basin, South Australia.

1.4 Structural evolution of horst and half-graben structures proximal to a continental transform using a 3D seismic dataset from the Shipwreck Trough, offshore Otway Basin, Australia (paper 4)

This study uses a three-dimensional (3D) seismic reflection dataset from the Shipwreck Trough, offshore Otway Basin, southern Australia, with the aim to document the growth of the Shipwreck Fault Zone (SFZ) and related extensional structures. The SFZ marks a major transition point from the southern margin rift system to the west and the oceanic-continental transform margin to the SE. The SFZ has previously been interpreted as a N-S striking transtensional fault zone, which is the northern en echelon extension of the transform margin to the south. The downward thrown (western) side of the SFZ is known as the Shipwreck Trough and contains numerous horst and half-graben structures, two of which host the producing Geographe and Thylacine gas fields. This study highlights examples

of structures along the SFZ that are indicative of left-lateral transtensional deformation and has identified zones of increased basement fault block relief, attributing to gravitational faulting in cover sediments. This study has also implemented throw-distance and throw-depth analysis on four horst and half-graben structures, which has indicated that the associated normal faults have had continuous Upper Cretaceous growth via the linkage of smaller normal fault segments. Lastly, the two-way-time (TWT) and isochronal mapping conducted in this study shows the larger-scale structural evolution of the Shipwreck Trough. This analysis has also highlighted several other structural closures similar to (and with close vicinity of) the Thylacine and Geographe gas fields, providing implications for petroleum exploration.

2. Literature Review

The first section of this literature review provides an overview of the regional geology of the southern margin of Australia, including more detailed reviews of the Bight and Otway basins, where this study is located. The second part of this literature review focusses on normal fault growth in three stages: [1] previous research on normal fault growth in rock outcrop and seismic datasets; [2] a summary of the presently accepted normal fault growth models; and [3] techniques to determine the growth and kinematics of syndepositional normal fault growth.

2.1 Regional tectonics of Australia's southern margin and the tectono-stratigraphic framework of the Ceduna Sub-Basin and Otway Basin

2.1.1 Regional Setting of Australia's southern margin

The southern margin of Australia extends for over 4,000 km from just south of the Naturalist Plateau in the west to the transform plate boundary in the east, abutting the south Tasman Rise (Totterdell et al. 2012; Stacey et al. 2013). The southern Margin of Australia is one of the most underexplored

passive margins of the world, with hydrocarbon production in only the Gippsland and Otway basins (Totterdell et al., 2000). Extensional break-up of Australia and Antarctica from the Middle to Upper Jurassic formed the Bight, Otway, Gippsland, Bass and Sorell basins (Norvick and Smith, 2001), along with smaller depocentres on the South Tasman Rise, which collectively constitute the southern rift system (Stagg et al., 1990; Willcox and Stagg, 1990; Stacey et al. 2013). The southern margin has developed via episodic extension and thermal subsidence prior to, and proceeding, the initiation of seafloor spreading between Australia and Antarctica in the late Santonian (Totterdell et al., 2000; Totterdell and Bradshaw, 2004; Stacey et al., 2013). Middle to Late Jurassic extension was oblique, with east-west basement structures extended under northwest-southeast tension creating *en échelon* half graben structures (Norvick and Smith, 2001). Asymmetric break-up of Australia and Antarctica resulted in low angle detachment faulting, creating a simple shear mechanism, cutting through crust and lithospheric mantle (Espurt et al., 2009). This was followed by post-rift subsidence during the Early Cretaceous, with heavily accelerated subsidence from the Albian-Santonian, coinciding with global sea level rise (Totterdell et al., 2000; Totterdell and Bradshaw, 2004).

Commencement of NW-SE ultra-slow to slow Seafloor spreading in the latest Santonian continued until the Middle Eocene and was preceded by N-S fast seafloor spreading (Totterdell et al., 2011). This resulted in a normal to normal-oblique rifted margin extending from the western limit of the Bight Basin to the central Otway Basin, which transitions across the southern Otway Basin and Sorell Basin to a transform plate boundary in the far SE of the margin, adjacent to Western Tasmania and the South Tasman Rise (Totterdell et al., 2011; 2012; Stacey et al., 2013). Regional uplift during the Maastrichian saw the erosion of Upper Cretaceous deposition in the northern areas of the southern margin (Totterdell et al., 2000). However, a return to regional subsidence and sea floor spreading, during the Palaeocene resulted in the deposition of cool-water carbonates, with very little clastic sediment influx, until the present day (Tikku and Cande, 1999).

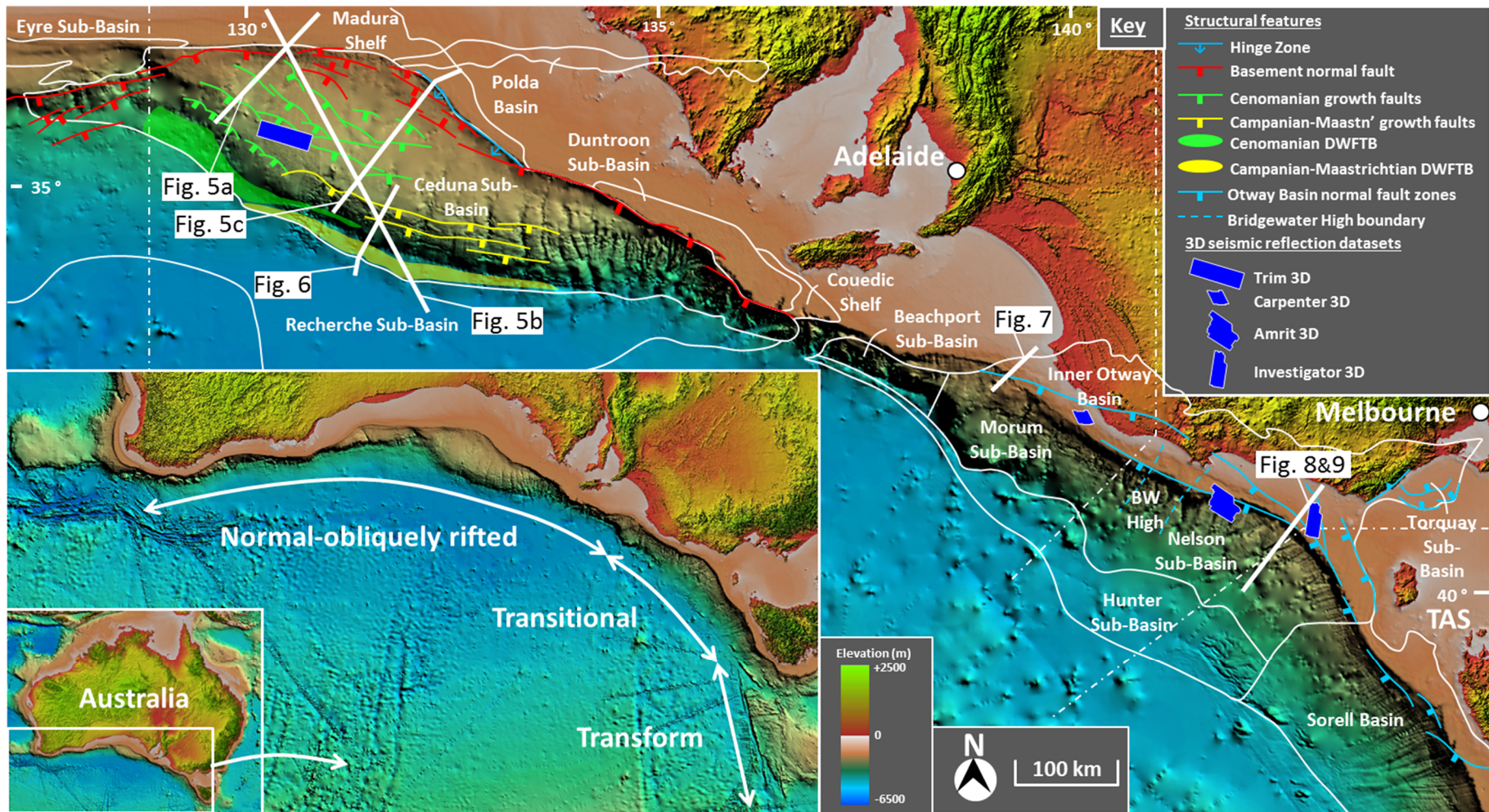
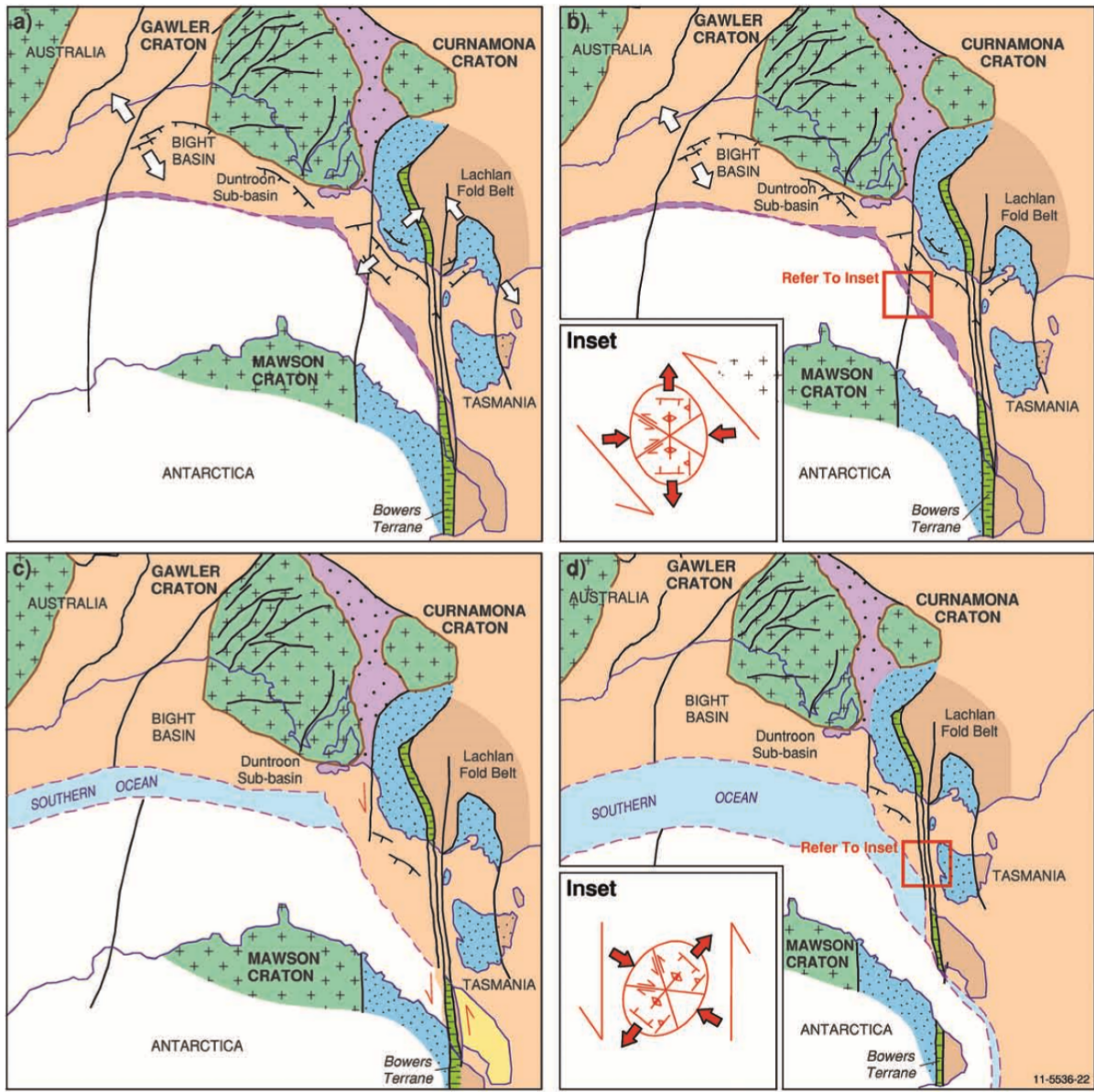


Fig. 1: Location map of the southern margin of Australia, highlighting (bottom left corner) the transition from normal-oblique rifting in the west to the transform margin in the east. Note the location of the four 3D seismic reflection datasets we analyse in this study, which comprise the four papers presented in the thesis body.

2.1.2 Basement Architecture

Pre-existing basement architecture appears to have had a strong influence on the partitioning of the southern margin. The normal-oblique section of the margin spanning the Bight Basin and the eastern and central Otway Basin is considered an extensive zone of lithospheric thinning and thick extensional basin development, with a well-established distal ocean-continent transition zone (Totterdell et al., 2011; 2012). Lithospheric thinning is not as prevalent east of the central Otway Basin, with rift and transform elements comprising the ocean-continent boundary, resulting from NW-SE to NE-SW extension developing transtensional basins (Totterdell et al., 2011; 2012). The Tasman Fracture Zone forms the ocean-continent boundary in the southern Sorell Basin and South Tasman Rise (Totterdell et al., 2011; 2012; Stacey et al., 2013). The southern margin rifted architecture and the focus of initial extensional strain were both heavily controlled by the underlying basement terrain. Archean and Neoproterozoic basement structure and rheology controlled the rift compartmentalisation in the central and western portions of the margin (Gibson et al., 2012). The transition from an E-W oriented rift to a N-S oriented transform plate boundary in the eastern portions of the margin was predominantly controlled by dominant, and pre-existing, N-S structural grain of the Neoproterozoic-Early Paleozoic fold belts (Gibson et al., 2011).



Schematic diagram

Fig. 2: Plate tectonic reconstructions for the Australian-Antarctic conjugate margin (after Gibson et al., 2013).

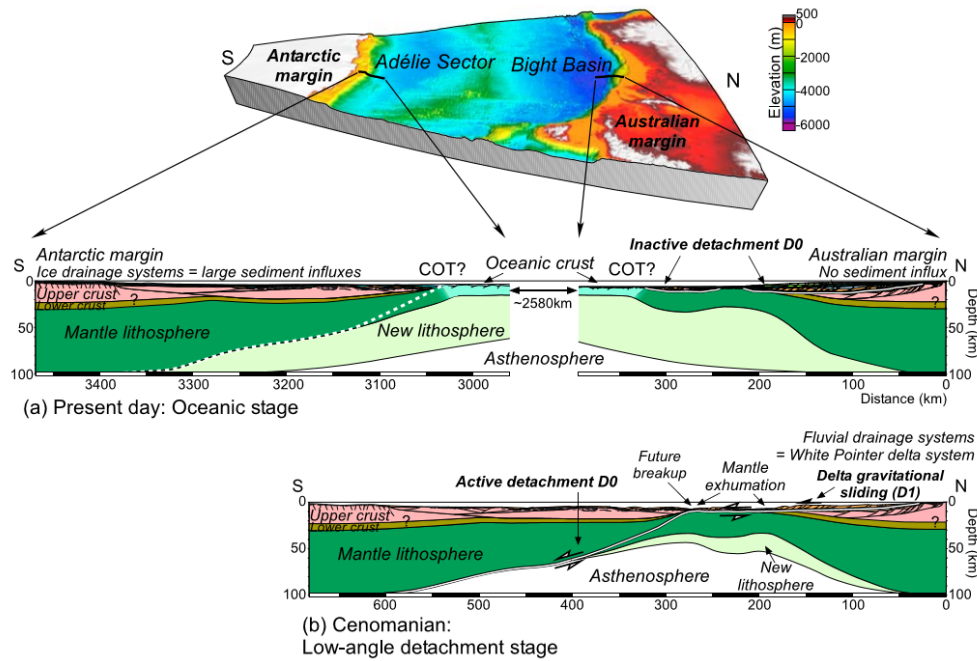


Fig. 3: Possible conceptual scenario for the Australian-Antarctic continental passive margins evolution based on paleo-Alps margin geometries. (a): Oceanic present-day state with strongly asymmetrical shape of the Australian and Antarctic conjugate margins. COT: Continent-Ocean Transition zone. (b): Before the Late Santonian breakup event, a simple shear mechanism results in the development of a low-angle detachment fault (D0 modelled). The top-to-the-south sense of displacement accommodates exhumation of the continental mantle ahead of the southern Australian margin. The continental crust is highly stretched with formation of a crustal klippe (after Espurt et al., 2009).

2.1.3 Tectono-stratigraphic framework of the Ceduna Sub-Basin

The Ceduna Sub-Basin is the largest sub-basin of the Bight Basin, which contains four other depocentres: the Eyre, Recherche, Duntroon and Bremer sub-basins. The NW-trending Ceduna Sub-basin spans approximately 90,000 km² of the E-W to NW-SE oriented Bight Basin (Fig. 2d), and which contains up to 15 km of Middle Jurassic to Upper Cretaceous sediments (Totterdell and Krassay, 2003; MacDonald et al., 2010). The formation of the Ceduna Sub-Basin resulted from the rifting of Australia and Antarctica during the break-up of eastern Gondwana (Fraser and Tilbury, 1979; Bein and Taylor, 1981; Stagg et al. 1990; Willcox and Stagg, 1990; Totterdell et al. 2000; Holford et al., 2011), made apparent by the south-southwest steeply dipping, inboard Jurassic to Lower Cretaceous Pademelon and Potoroo fault systems (see basement normal faults on location map, Figure 1; Totterdell and Bradshaw, 2004).

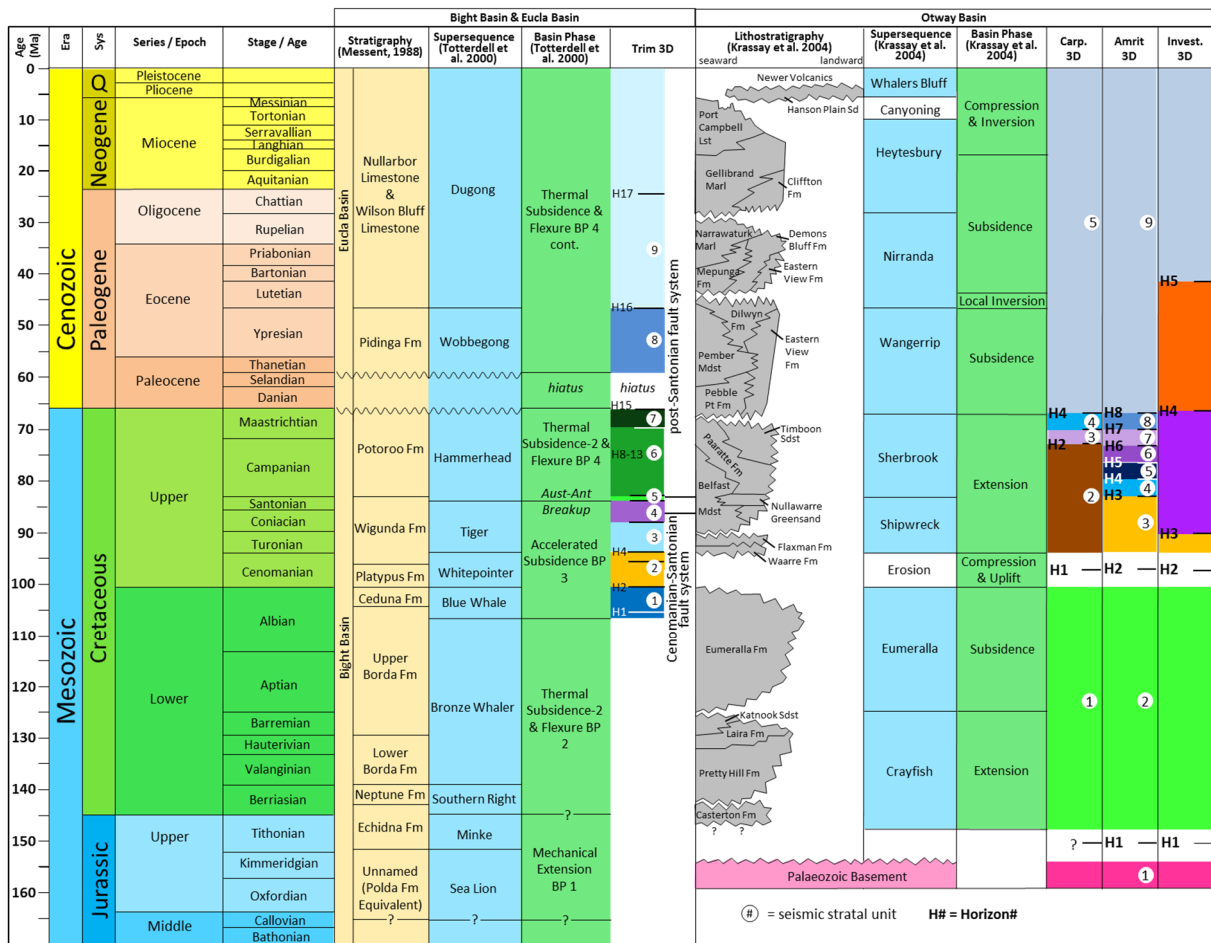


Fig. 4: Tectono-stratigraphic framework of the Bight and Otway basins, with the litho-stratigraphy included of the Otway Basin. Horizons and stratal units for all four studies comprising the main body of the thesis have been included here for later reference (modified from Geary and Reid, 1998; Messent, 1998; Totterdell et al., 2000; 2004; Krassay et al., 2004)

Four basin phases characterise the Ceduna Sub-Basin (after Totterdell et al. 2000): [1] Middle-Late Jurassic mechanical oblique extension (Norvick and Smith, 2001); [2] Lower Cretaceous slow basin subsidence; [3] late Lower Cretaceous accelerated thermal subsidence; and [4] Upper Cretaceous-Cenozoic post Australia-Antarctica break-up thermal subsidence (Veevers 1986; Sayers et al. 2001). The sediment succession in the Ceduna Sub-Basin transitions from Middle Jurassic-Lower Cretaceous fluvio-lacustrine deposits through to marine siltstones and mudstones and deltaic influx in the Upper Cretaceous and a Paleogene cool-water carbonate succession (Totterdell et al. 2000; Totterdell and Krassay, 2003; Totterdell and Bradshaw, 2004). The structure of the Ceduna Sub-Basin is typical of delta systems around the world, such as the Niger Delta (Doust and Omatsola, 1990; Morley and

Guerin, 1996; Cohen and McClay, 1996; Bilotti and Shaw, 2005; Corredor et al., 2005; Briggs et al.; 2006; Cobbold et al, 2009), Baram Delta (James, 1984; Koopman, 1996; Schreurs, 1997; King et al. 2010) and Gulf of Mexico (Buffler et al. 1978; Winker and Edwards, 1983, Wu et al. 1990, Rowan, 1997). However, the Ceduna Sub-Basin hosts two structurally and geometrically independent delta systems with associated delta deep-water fold-thrust belts (DDWFTBs); the Whitepointer and Hammerhead deltas, that are synonymous with the Whitepointer and Hammerhead supersequences respectively (Totterdell and Krassay, 2003; King and Backé, 2010; MacDonald et al., 2010).

The delta-top extensional province is characterised by an array of listric faults known as the Mulgara Fault Family (Totterdell and Bradshaw, 2004). These faults were formed from the rapid deltaic influx of the Whitepointer Supersequence during the Cenomanian, resulting in a gentle SW (basinward) dipping detachment forming within the underlying shales of the Blue Whale Supersequence (Totterdell et al. 2000; MacDonald et al., 2010). This detachment accommodated delta-top extension causing the nucleation and rapid growth of the listric fault array, spanning an area in the central-western Ceduna Sub-Basin of ~250 km along strike and ~100 km down dip (Totterdell and Bradshaw, 2004). Fault growth terminated during the late Cenomanian, with some fault reactivation occurring during the Turonian-Santonian deposition of the Tiger Supersequence, accompanied by thinning of the lower crust, inferring a significant period of extension (Totterdell et al. 2000; Sayers et al. 2001). Initiation of sea floor spreading began in the latest Santonian, coinciding with strong erosional features in the northern and eastern Ceduna Sub-Basin and this was followed by a second phase of thermal subsidence (Veevers, 1986; Sayers et al. 2001; Totterdell et al. 2000; Totterdell and Bradshaw, 2004; MacDonald et al, 2012a). Campanian-Maastrichtian rapid deposition of the deltaic Hammerhead Supersequence resulted in a detachment within the Tiger Supersequence in the eastern Ceduna Sub-Basin (Totterdell et al. 2000) with down dip compression driven by up-dip gravitational extension (*sensu* King et al. 2009; King and Backé, 2010; MacDonald et al. 2010). Fault growth continued into the Cenozoic, following a post-Maastrichtian 5-7 M.y. hiatus, with some faults offsetting seismic reflectors as shallow as 100 m below seafloor (MacDonald et al. 2012a).

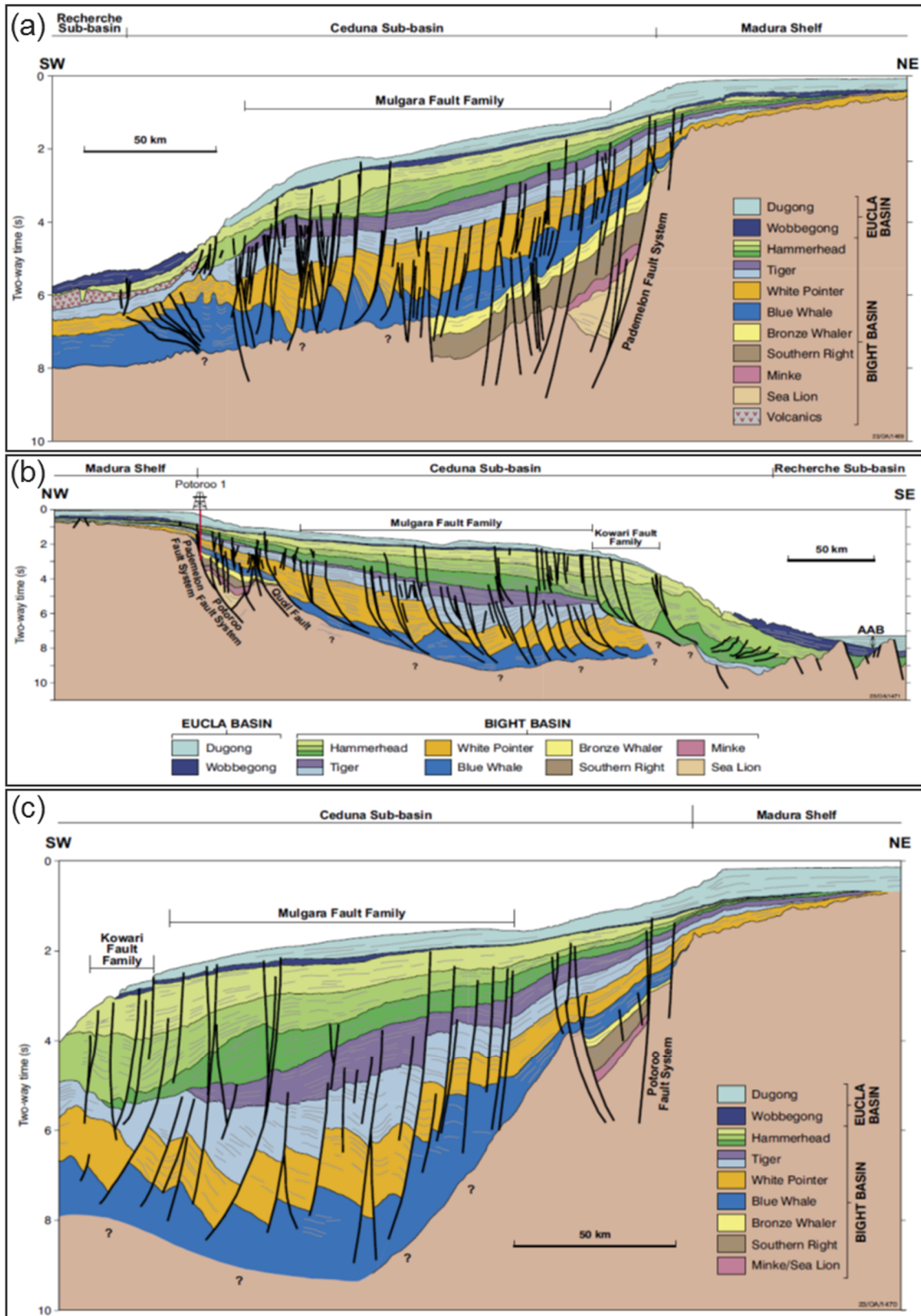


Figure 5: Regional seismic profiles (a, b, c) showing the geometry of White Pointer (blue-orange) and Hammerhead (green) DDWFTB systems. The location of these lines can be found in Figure 1. The location and geometry of the White Pointer and Hammerhead delta systems can also be found in Figure 1. The Blue Whale supersequence (Blue) hosts the basal detachment for the White Pointer delta system and the Hammerhead delta system is detached at the base of the Tiger supersequence (purple) (after Totterdell and Bradshaw, 2004).

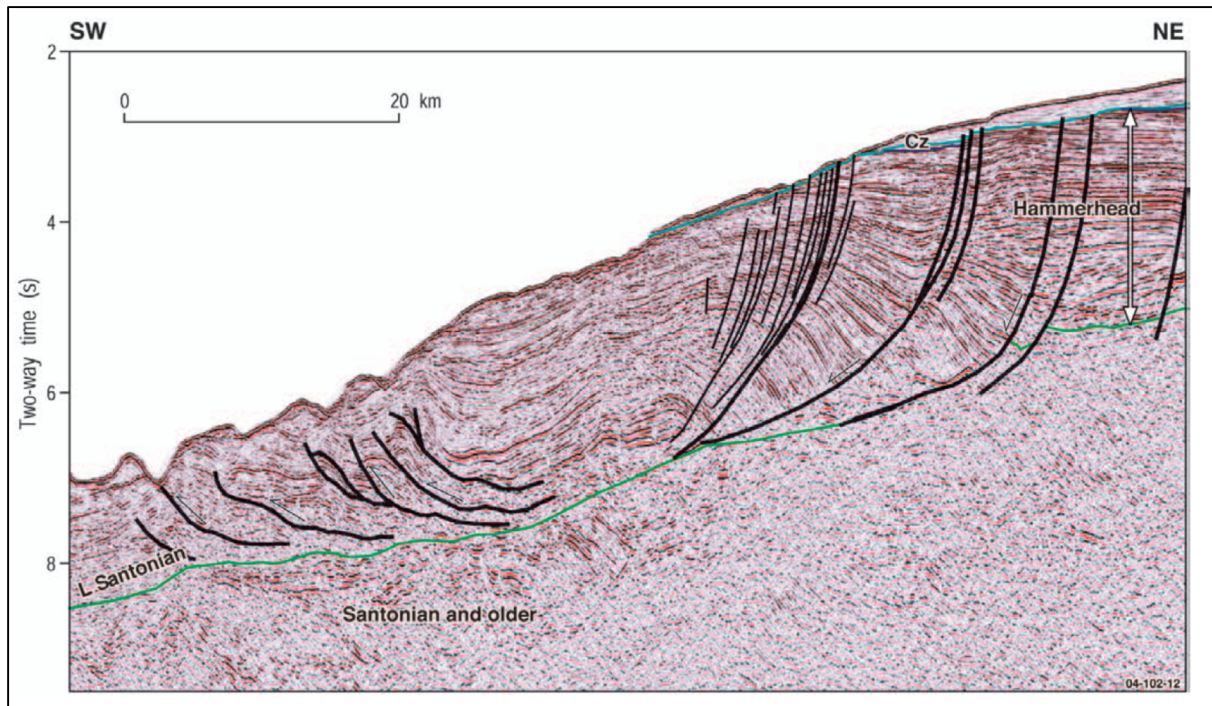


Figure 6: Seismic profile 199-07 of well-established extensional, transitional and compressional provinces of the Hammerhead DDWFTB. A seaward dip can be observed on the basal detachment within the Tiger supersequence (green) (after Totterdell and Bradshaw, 2004).

2.1.4 Tectono-stratigraphic framework of the Otway Basin

The Upper Jurassic-Cenozoic, NW oriented Otway Basin also formed during the break-up of eastern Gondwana and is located to the east of the Ceduna Sub-Basin, spanning an area of 150,000 km² from SE South Australia to NW Tasmania, where it is continuous with the Sorell Basin (Willcox and Stagg, 1990; Moore et al. 2000; Krassay et al. 2004; Norvick, 2005; Holford et al., 2011; Totterdell et al. 2011). The majority of the Otway Basin (120,000 km²) lies offshore under the present day continental shelf and deep-water province in water depths up to 3000 m (Stacey et al. 2013). The Otway Basin is comprised of five major depocenters: the primarily onshore Inner Otway Basin, the eastern Torquay Sub-Basin and the deepwater Morum, Nelson and Hunter Sub-Basins (Moore et al. 2000; Krassay et al. 2004; Stacey et al. 2013). These depocenters all contain an Upper Jurassic to Upper Cretaceous siliciclastic sedimentary succession and a Cenozoic mixed siliciclastic and carbonate succession. Reaching up to 8 km in thickness are the Upper Jurassic-Lower Cretaceous

Crayfish and Eumeralla Supersequences (Fig. 7), deposited into major depocenters formed through Tithonian-Barremian basement rifting creating E-W to NW-SE striking half-graben structures, with variable normal fault orientation influenced by pre-existing Palaeozoic structure (Moreton et al. 1994; Perincek and Cockshell, 1995; Finlayson et al. 1996; Krassay et al. 2004; Gibson et al., 2011). The Tithonian-Barremian Crayfish Supersequence is characterised by organic-rich mudstones, sandstones and basalts (Ryan et al. 1995; Krassay et al. 2004). This is unconformably overlain by the post-rift, deposition Aptian-Albian Eumeralla Supersequence, during thermal subsidence, which is comprised of westerly and northerly thinning fluviolacustrine shales and thin coal measures with observed volcanoclastic influence (Hill et al. 1995; Krassay et al. 2004; Duddy, 2003). Little or no Cenomanian strata has been preserved above the Eumeralla Supersequence, which has created a regional unconformity (Partridge, 2001; Krassay et al. 2004; Palmowski et al. 2004; Tassone et al. 2014).

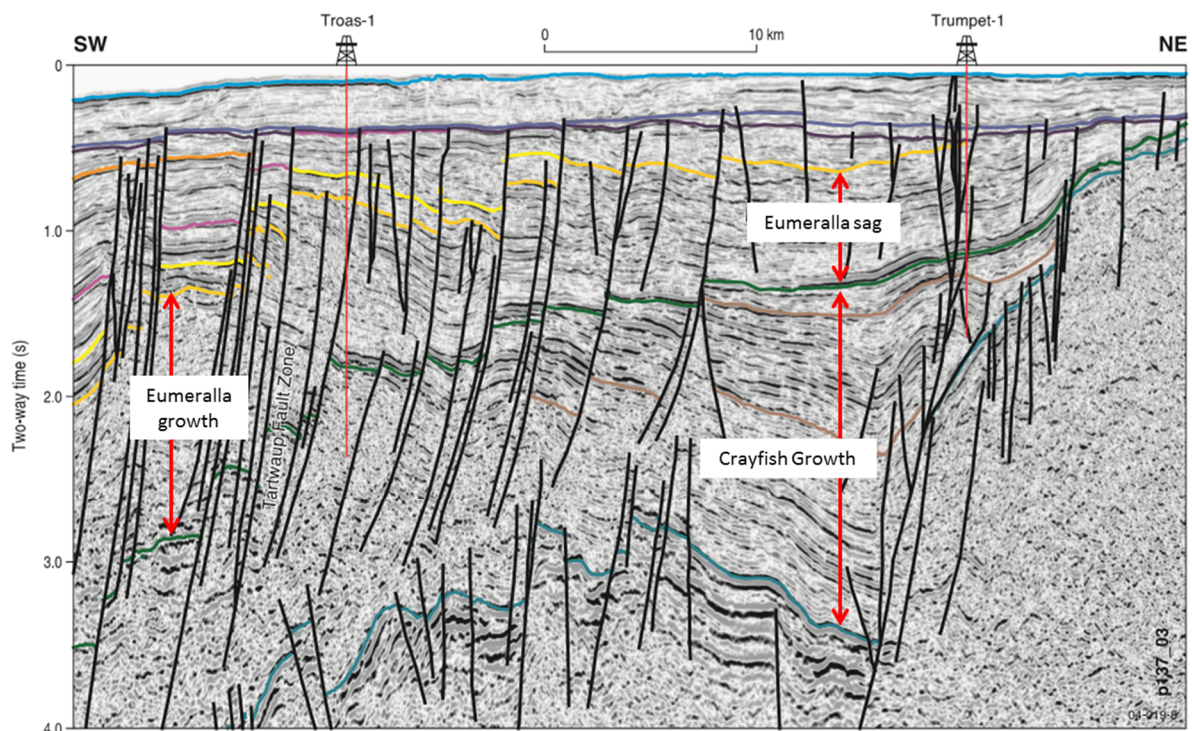


Fig. 7: Seismic line s137p-03 showing the growth wedges of the Crayfish Supersequence and the general sag nature of the Eumeralla Supersequence, with exceptions of growth across some faults. The location of this seismic line is shown in Figure 1 (modified from Krassay et al., 2004).

This is succeeded by the Upper Cretaceous Shipwreck and Sherbrook Supersequences (Fig. 8), reaching up to 5 km in thickness, basinward of the present-day shelf edge break, deposited during a second period of crustal extension in the Otway Basin (Krassay et al. 2004; Stacey et al. 2013). The Turonian-Santonian Shipwreck Supersequence is highly variable across the basin, but is generally characterised by Turonian syn-rift non-marine sediments, grading up to fluvio-deltaic sands (Krassay et al. 2004). This is succeeded by Coniacian-late Santonian marine mudstones in the eastern Otway Basin and Coniacian-late Santonian interbedded siltstones and sandstones grading up to deltaic sandstones in the western Otway Basin (Krassay et al. 2004). The Campanian-Maastrichtian Sherbrook Supersequence is characterised by a major period of deltaic deposition across the basin, with a decrease in mechanical extension compared to the Turonian-Santonian (Partridge, 2001; Krassay et al. 2004; Stacey et al. 2013). The Cenozoic sedimentary succession is characterised by mixed siliciclastic and carbonate rocks divided into the Wangerrip, Nirranda, Heytesbury and Whalers Bluff supersequences (Fig. 9), which together have the greatest thickness at the present-day shelf edge break (Stacey et al. 2013). Cenozoic thermal subsidence was sporadically interrupted by periods of inversion and uplift (Holford et al. 2014; Bailey et al. 2014).

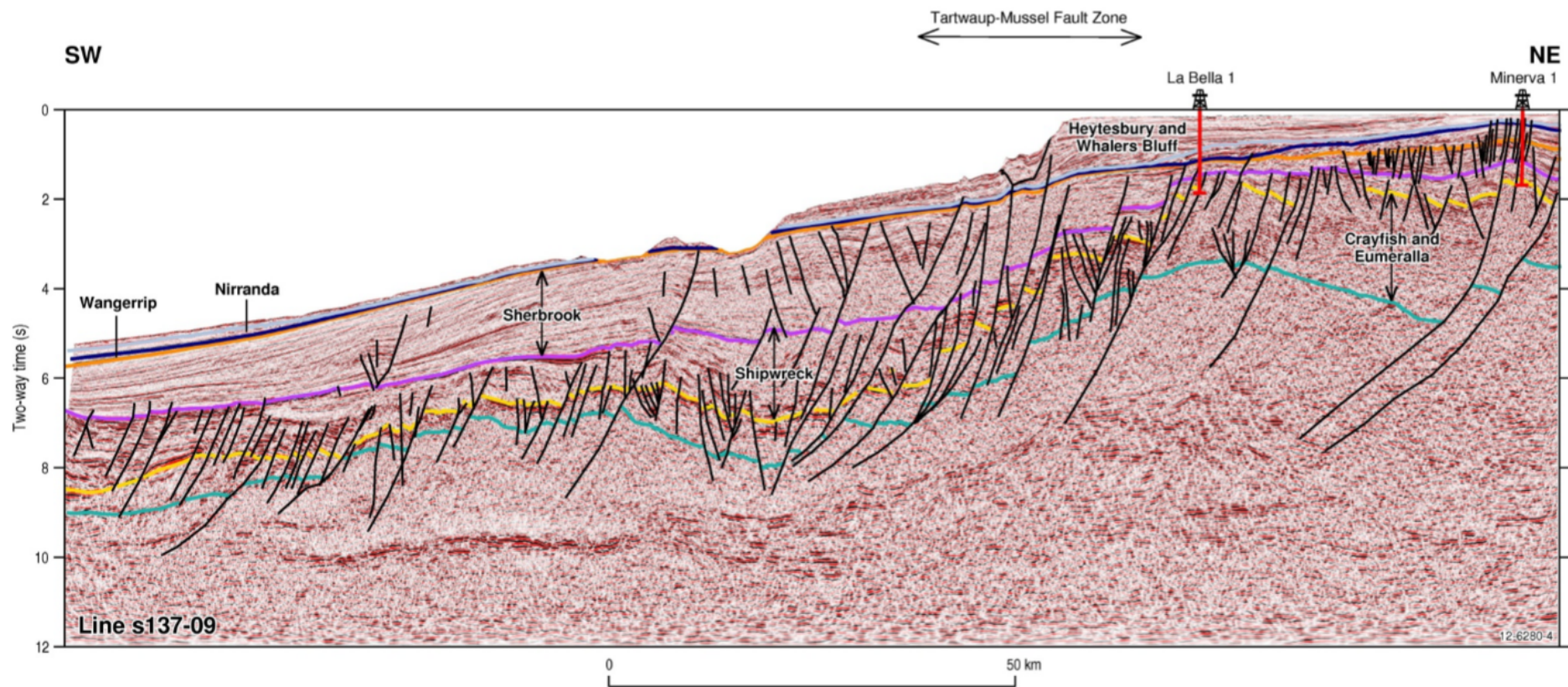


Fig. 8: Seismic line s137p-09 showing the thickening of the Shipwreck and Sherbrook Supersequences, basinward of the present-day shelf break. Also note the growth wedge of Crayfish and Eumeralla Supersequences under the present-day shelf. The location of this line is shown in Figure 1 (after from Stacey et al., 2013).

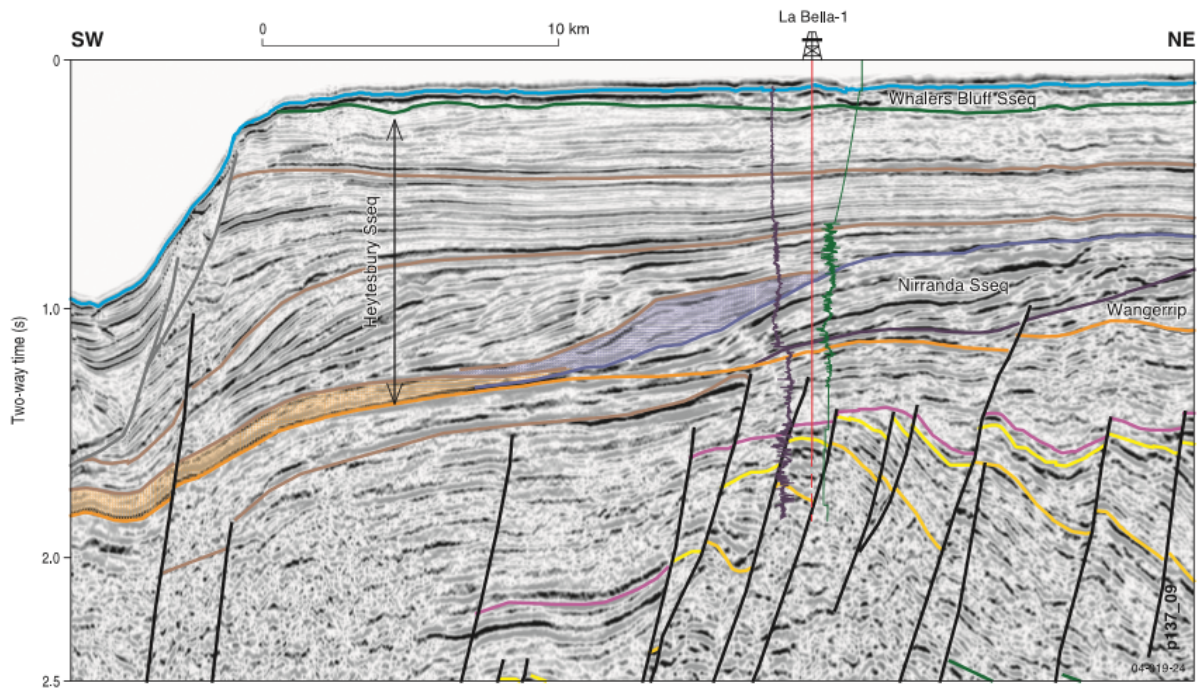


Fig. 9: Zoom in of Figure 8 (seismic line s137-p09) to the present-day shelf break to show the Cenozoic Wangerrip, Nirranda, Heytesbury and Whalers Bluff Supersequences. Note the lack of structural control on deposition of these Supersequences, compared to the underlying (and faulted) Shipwreck and Sherbrook Sequences. The location of this line is shown in Figure 1 (after Krassay et al., 2004).

2.2 Determining normal fault growth and kinematics: an overview

2.2.1 Overview of normal fault growth in rock outcrop and seismic datasets

Understanding the growth and motion of normal faults endures to deliver an imposing challenge for geoscientists. Interpreting normal fault growth from three-dimensional or two-dimensional seismic data provides an even greater challenge, given the issues that remain with data quality, reliability, depth penetration and spatial coverage. The more incomplete a seismic dataset is, the more a seismic interpretation of normal fault geometry and growth, explicitly or implicitly, will rely on empirical methods and idealized and preconceived conceptual models. One such conceptual model, as suggested by Walsh and Watterson (1991), is the means by which faults are linked and how they have evolved to their present day geometry. Further research to build our understanding on the growth of normal fault systems will create greater certainty in seismic interpretation and static

modelling of the subsurface when a seismic dataset does not provide a complete and obvious answer. A better understanding of the controlling factors on normal fault growth, such as crustal extension and gravitational instability, will also allow for a better prediction of fault evolution in known tectono-stratigraphic settings.

Fault arrays developing in sedimentary basins are commonly observed to be segmented in rock outcrop and seismic reflection data (Fig.10), containing multiple fault segments on a large range of scales (Walsh and Watterson, 1989, 1990, 1991; Peacock and Sanderson, 1991, 1994; Stewart and Hancock, 1991; Trudgill and Cartwright, 1994; Cartwright et al., 1995; Childs et al., 1995; Dawers and Anders, 1995; Huggins et al., 1995; Mansfield and Cartwright, 2001; Walsh et al. 2002, 2003; Childs et al. 2003, 2009; Giba et al. 2012; Jackson and Rotevatn; 2013; Lewis et al. 2013; Tvedt et al. 2013). Faults may be interpreted to have grown via segment linkage when they appear to have map view segmented geometry, have highly variable along-strike displacement profiles and are isolated at depth (*sensu* Cartwright et al. 1995, Fig. 4). Segment linkage may also occur vertically down a fault plane (Fig. 11), with faults vertically linking through downward or upward propagation of fault tip-lines; a process known as dip-linkage (Childs et al., 1996; Mansfield and Cartwright, 1996; Rykkelid and Fossen, 2002; Baudon and Cartwright, 2008; Jackson and Rotevatn, 2013).

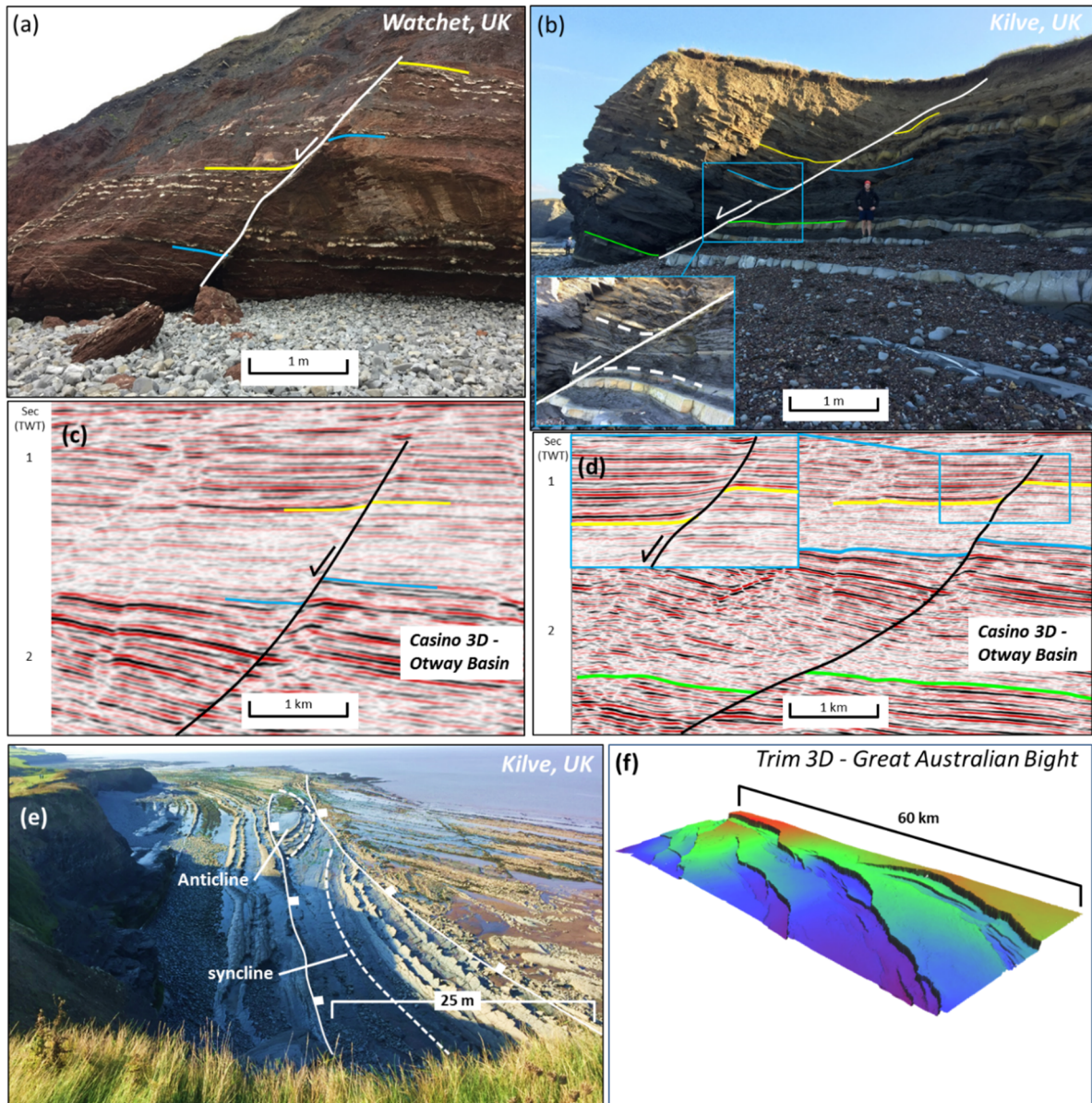


Fig. 10. Examples of normal faults interpreted in rock outcrop from a field trip in 2015 to Watchet (a) and Kilve (b; e), United Kingdom, compared with examples interpreted from 3D seismic data in the Otway Basin (c; d) and Great Australian Bight (f), Australia.

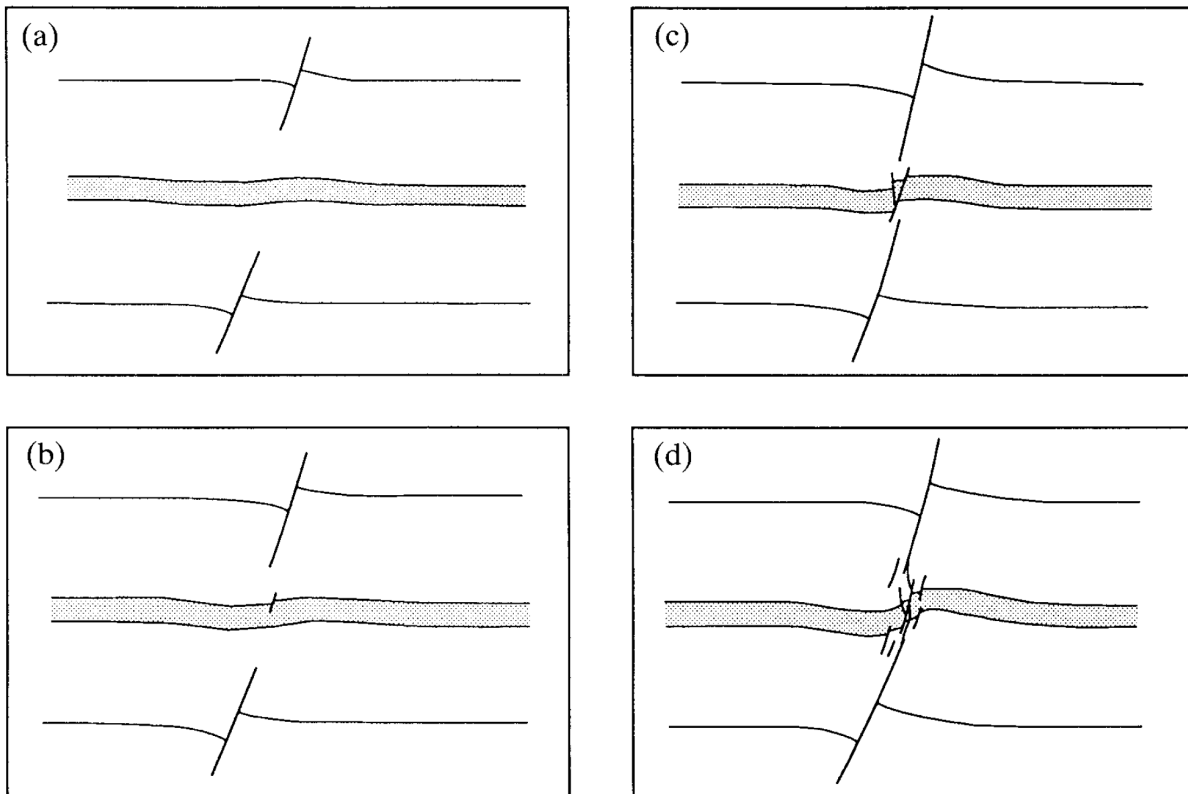


Fig. 11. Four stage evolution of two initially isolated faults, which progressively link vertically; a process known as dip-linkage (after Mansfield and Cartwright, 1996).

These characteristics of segment linkage describe the growth of normal faults which have grown in brittle rock (e.g. Peacock and Sanderson, 1991; Dawers and Anders, 1995; Huggins et al. 1995). Somewhat more complex is constraining the growth of normal faults in the presence of and influenced by mechanically weak detachments (e.g. salt or mudstone). Fault propagation can be hindered by the presence of ductile strata, given that displacement and strain may be accommodated through fault-related folding and this complicates the analysis and understanding of displacement distribution, fault segmentation and kinematic evolution of fault arrays (Fig. 12; Withjack et al. 1990; Rowan et al., 1998; 1999; Withjack and Callaway, 2000; Jackson and Larsen, 2009; Kane et al. 2010; Marsh et al. 2010; Jackson and Rotevatn, 2013; Lewis et al. 2013; Tvedt et al. 2013).

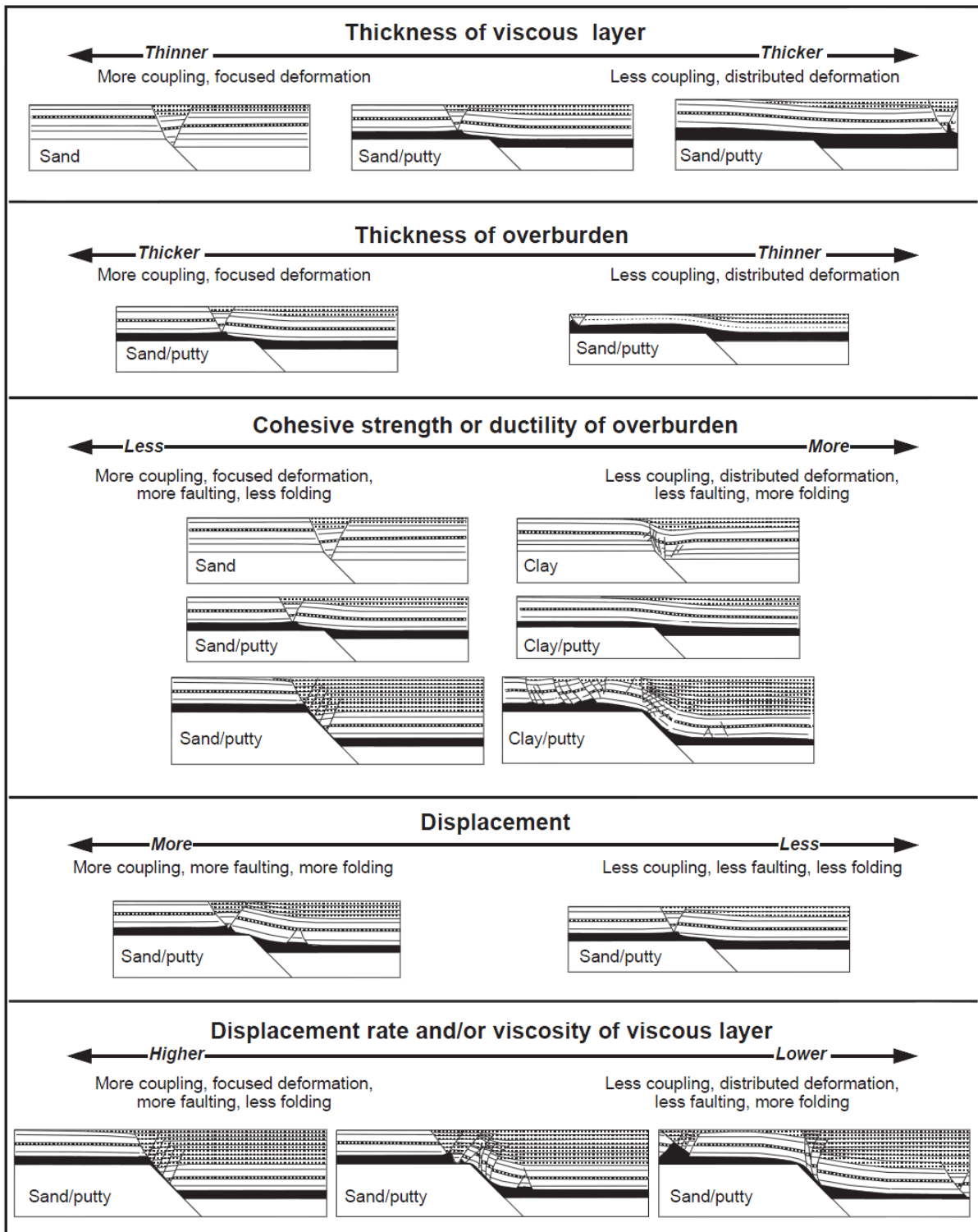


Fig. 12. Sandbox Modelling results showing how the different properties of a ductile layer, thickness of the overburden and displacement rate can affect normal fault growth in cover sediments above a ductile layer (after Withjack and Callaway, 2000).

Interpretation of fault geometry and growth is generally based on an underlying preconceived conceptual model that a fault is elliptical with displacement increasing from the tip-line into the centre of the fault (Watterson, 1986; Walsh and Watterson, 1987). However, continuous research and the availability of high quality 3D seismic datasets has shown that fault growth is much more complex, due to spatial variation in rock properties and the interaction of multiple fault segments (Childs et al., 1993, 2003; Nicol et al., 1996; Jackson and Rotevatn, 2013; Lewis et al. 2013; Rotevatn and Jackson., 2014). These new findings stem from detailed analysis of displacement profiling on the fault surface, which Giba et al. (2012) suggest has been somewhat absent in previous studies of fault arrays. With the increase in availability in 3D seismic datasets, normal fault growth has been increasingly studied in rift basins, such as the North Sea (Jackson and Larsen, 2009; Kane et al., 2010; Lewis et al., 2013; Tvedt et al., 2013), Suez Rift (Gawthorpe et al. 2003; Jackson and Rotevatn, 2013) and East African Rift (Morley et al. 1990; Chorowicz, 2005; Aanyu and Koehn, 2011). This has also been the case with passive margins such as the Niger Delta (Koledoye et al., 2000; Khani and Back, 2012), Gulf of Mexico (Rowan et al. 1998) and Baram Delta (Imber et al. 2003).

2.2.2 Summary of normal fault growth models

Studies using both rock outcrop and seismic datasets, along with physical models of the subsurface, suggest that normal faults grow via one of two ways: [1] radially, with a displacement increasing congruent with fault length, commonly known as the 'isolated fault model' (Fig. 13a, 14a; Watterson 1986; Walsh & Watterson 1988; Dawers et al. 1993; Cartwright et al. 1995; Dawers & Anders 1995); and [2] near-final length establishment prior to significant displacement accumulation, commonly known as the 'coherent fault model' (Fig. 13d; 14b; Morley 2002; Walsh et al. 2002, 2003; Childs et al. 2003; Schlagenhauf et al. 2008; Giba et al. 2012; Jackson & Rotevatn 2013; Nicol et al. 2016; Tvedt et al. 2016; Jackson et al. 2017). The 'isolated fault model' has been the favoured interpretation of structural geologist for the last ~30 years, given that it accounts for the presence of

breached relays and along-strike displacement variations. However, a recent emergence of studies using 3D seismic datasets attest to the validity of the 'coherent fault model' (Fig. 13c; 13d; 14b; 14c) with detailed displacement profiling, encapsulating the entire fault surface, which Giba et al., (2012) suggest has been somewhat absent in previous studies of fault arrays.

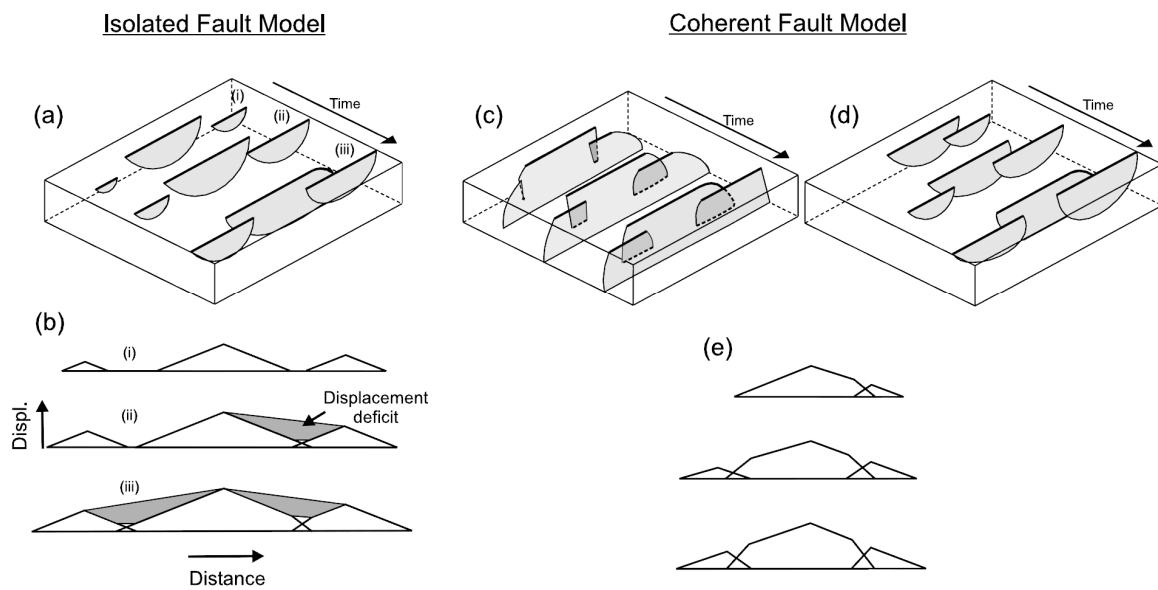
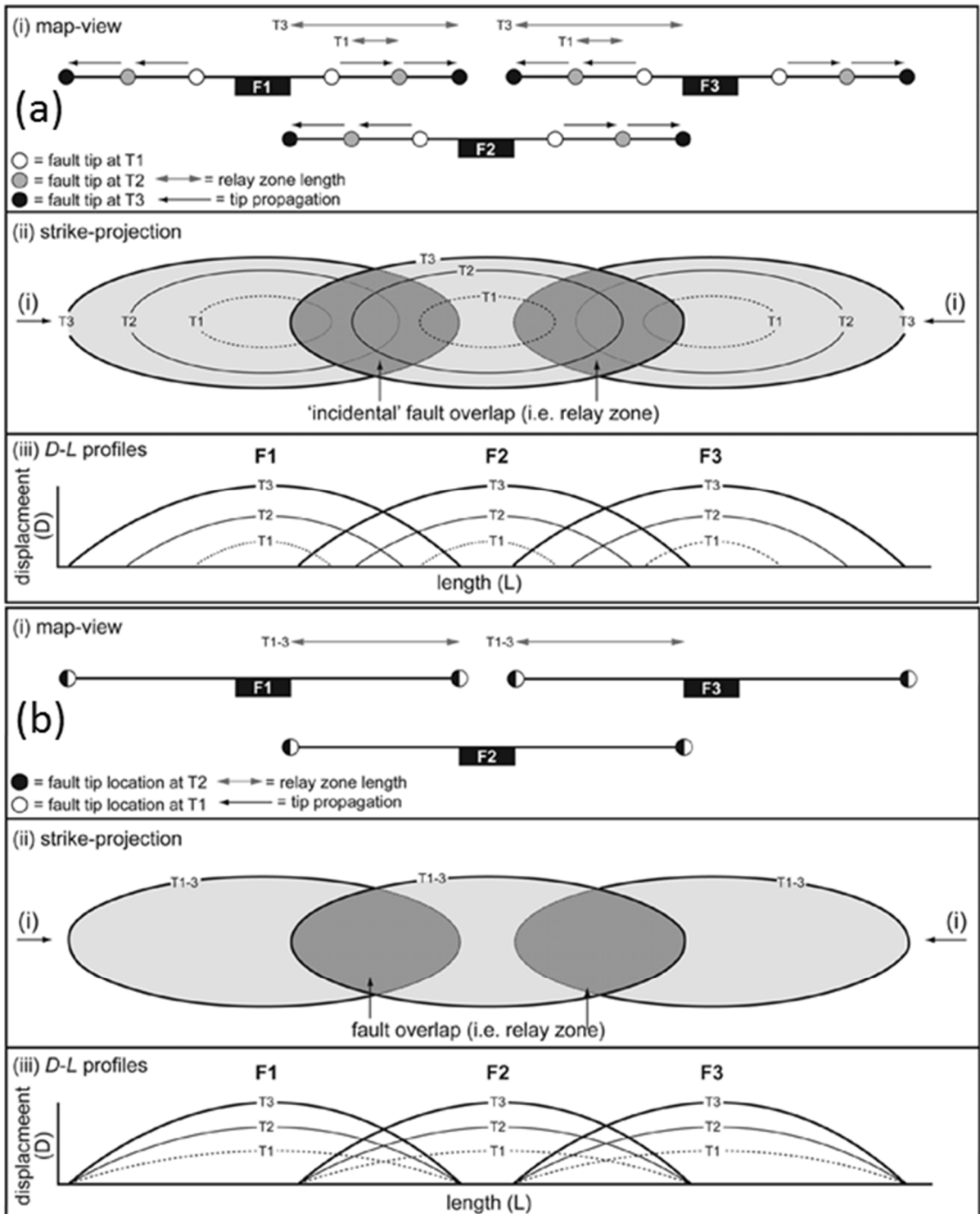


Fig. 13. Schematic diagram and corresponding displacement-distance graph for the (a) 'isolated fault model' (b) bifurcation 'coherent fault model' and (c) segmented 'coherent fault model' (after Walsh et al., 2003)



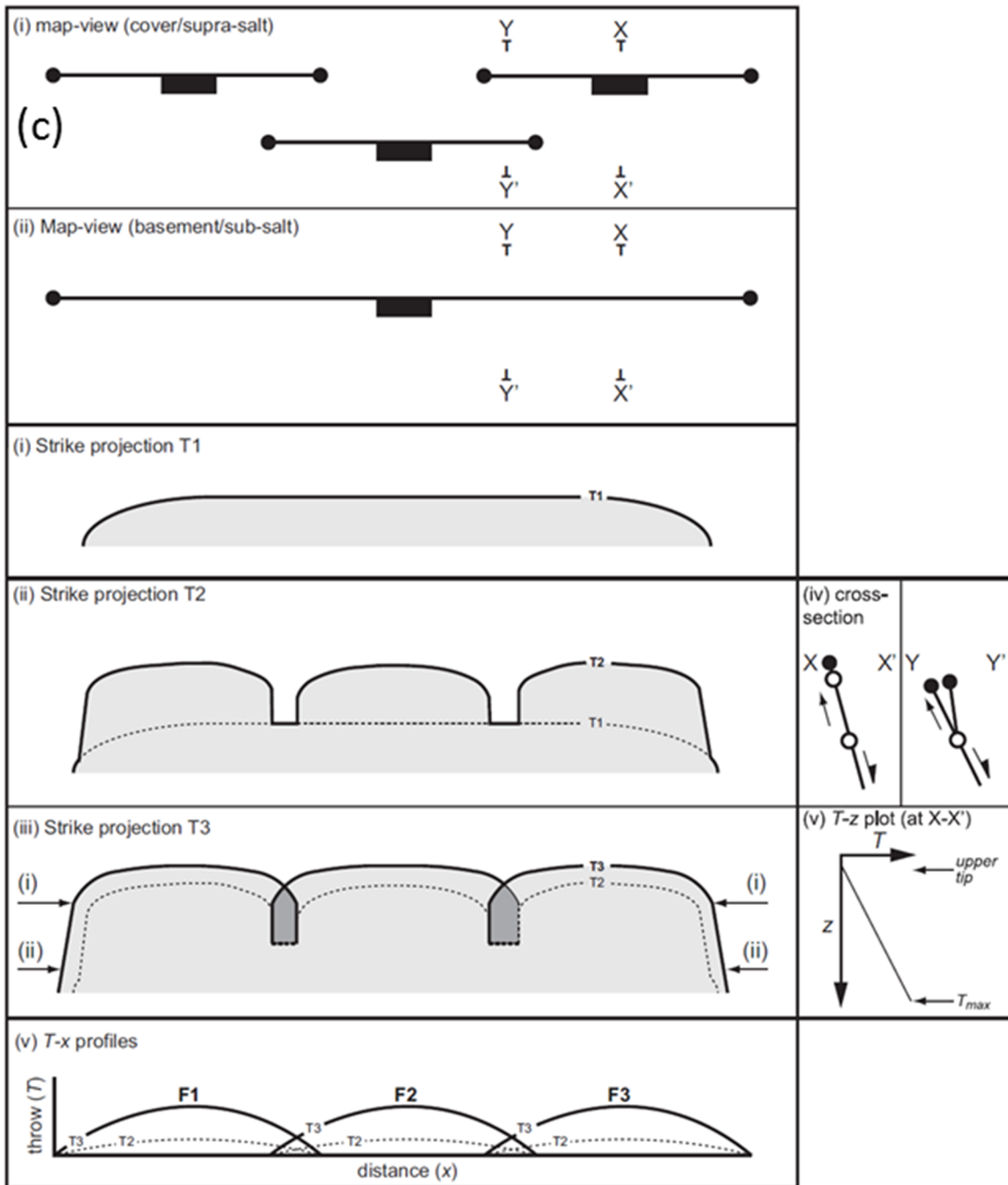


Fig. 14. Map-view, strike projection and corresponding throw-distance graph for the (a) 'isolated fault model' (b) segmented 'coherent fault model' and (c) bifurcation 'coherent fault model' (after Jackson and Rotevatn, 2013).

These two fault models are extremely hard to discriminate between using present-day geometric measures (Jackson et al., 2017). Jackson et al., (2017) shows how an 'under-displaced' fault (i.e. less than predicted displacement, based on length) can be interpreted to have grown in three very different ways, all of which are plausible based on geometric observations alone. This fault may have: [1] grown via the 'coherent fault model' with near-final length establishment prior to significant displacement accumulation (Fig. 13d; 14b; e.g. Morley 2002; Walsh et al. 2002, 2003; Giba et al. 2012; Jackson & Rotevatn 2013); [2] developed via the recent linkage of several smaller segments, all of which have a small displacement, as expected of a smaller fault (e.g. Cartwright et al., 1995); or [3] due to mechanical heterogeneity of layered strata, the vertical fault tip propagation into ductile layers was severely hindered due to decoupling, in comparison to lateral fault tip propagation through brittle rock (Benedicto et al. 2003; Soliva & Benedicto 2005). While it may seem a minor difference in growth style between these two fault models, the implications towards the geological evolution of an extensional setting (gravity or mechanically driven) are profound. A basin formed by faults growing in accordance with the 'isolated fault model' would initialise as (and grow for a substantial amount of time as) a series of isolated depocentres/ compartments, where the sediments would collect in the hanging wall of normal fault. This type of fault arrangement with a late stage of relay ramp development would have much less control over sediment dispersal (Jackson et al., 2017). In contrast, a fault which grew via the 'coherent fault model' would have much greater control over sediment deposition in the earlier stages of rift development, with the near-instantaneous development of relay ramps (Jackson et al., 2017).

A second order (third) fault growth model (Fig. 13c; 14c) exists, which accounts for faults that have grown via the 'coherent fault model' but have also bifurcated as they have grown upwards (e.g. Walsh and Watterson, 1991; Childs et al. 1995, 2003; Giba et al. 2012; Jackson and Rotevatn, 2013). Faults that have grown in this manner may commonly be mistaken as faults which have grown via the 'isolated fault model' (Watterson 1986; Walsh & Watterson 1988; Dawers et al. 1993; Cartwright et al. 1995; Dawers & Anders 1995) in cover strata, if the fault is not analysed at depth, where these

branchlines meet to form one single throughgoing structure (Fig. 13c; 14c). Individual branchlines in cover sediments may display the same displacement profile of an isolated fault segment. However, if the displacements of all branchlines are summed together, the coherent displacement pattern (growth) of the entire structure will be revealed (e.g. Walsh and Watterson, 1991; Childs et al. 1995, 2003; Giba et al. 2012; Jackson and Rotevatn, 2013).

2.2.3 Techniques to determine the growth and kinematics of syndepositional normal faults

Four techniques may be applied to analyse the temporal and spatial evolution of a normal fault array: [1] displacement-distance ($D-x$) graphs and displacement backstripping; [2] displacement-depth ($T-z$) analysis; [3] Expansion Index analysis; and [4] Isochronal mapping. Displacement-distance (or throw-distance) analysis displays the throw of horizons displaced by the fault surface to show the along-strike throw variation of entire fault assemblages, which may highlight individual fault segments (see displacement-depth graphs, Fig. 13; 14). Displacement (or throw) backstripping involves analysis of fault systems employing the 'vertical subtraction method' (Chapman & Meneilly, 1991; Childs et al., 1993; Dutton & Trudgill, 2009; Jackson & Rotevatn, 2013). This method allows the displacement variation at the time of deposition of a given horizon to be determined by subtracting the displacement of the given horizon from displacement values of deeper horizons (Chapman & Meneilly, 1991; Childs et al., 1993; Dutton & Trudgill, 2009; Jackson & Rotevatn, 2013).

Displacement-depth (or throw-depth) measurements may be used to analyse downward tip-line propagation and dip-linkage, by highlighting anomalous throw deficits down the fault surface (Fig. 15; Mansfield and Cartwright, 1996; Rykkelid and Fossen, 2002; Baudon and Cartwright, 2008; Jackson and Rotevatn, 2013; Jackson et al., 2017). A linear increase in displacement with depth implies a continuous fault growth history. Meanwhile, a point of inflection, creating a steepening of the $D-x$ graph, implies a period of fault dormancy between growth stages (see reactivated fault

example, Fig. 15). Finally, a localised minimum between two maxima implies the dip-linkage of two normal faults, with the minimum corresponding to the linkage point between the faults (see dip-linked fault, Fig. 15).

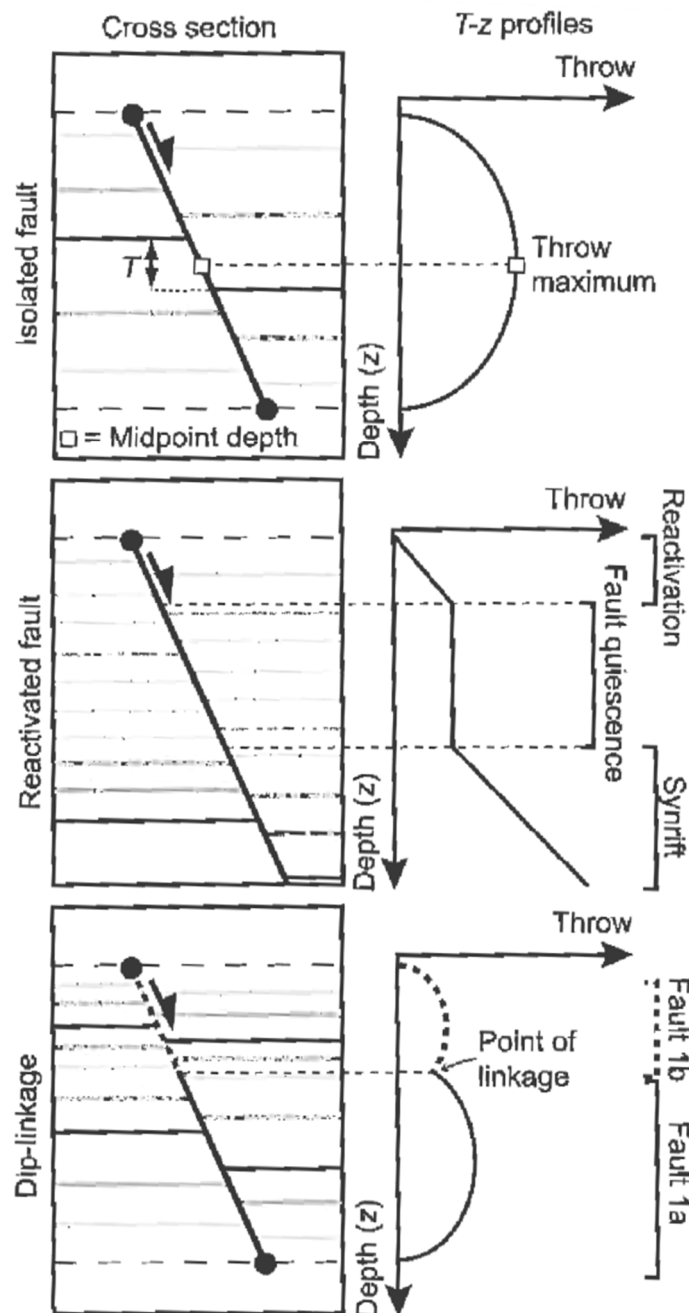


Fig. 15. Three cross-sections of normal fault stratal geometries; an isolated, reactivated and dip-linked fault (left column), their corresponding throw-depth (or displacement-depth) plots (right column) with plot interpretation included where necessary (after Ryan et al., 2017).

Expansion index plots (Fig. 16) measure and constrain the timing and magnitude of growth strata by dividing the hanging-wall thickness of a given stratal unit by the corresponding footwall thickness and plotting these measurements for each stratal unit that the fault intersects (Thorsen 1963; see also Cartwright et al. 1998; Bouroullec et al. 2004; Jackson & Rotevatn 2013; Tvedt et al. 2013). Indexes greater than one suggest thickening from the footwall into the hanging-wall and thus would be interpreted as a period of syndepositional fault growth. Indexes of or within the error range of one are considered a period of fault dormancy (Thorsen 1963; Cartwright et al. 1998; Bouroullec et al. 2004; Jackson & Rotevatn, 2013; Jackson et al., 2017). Isochronal mapping identifies variations of stratal thickness in relation to the accommodation space provided through syn-depositional faulting. Isochronal mapping is perhaps the most visual way of showing the evolution of fault systems via a map exposing the depocentres created by fault activity at the time of deposition.

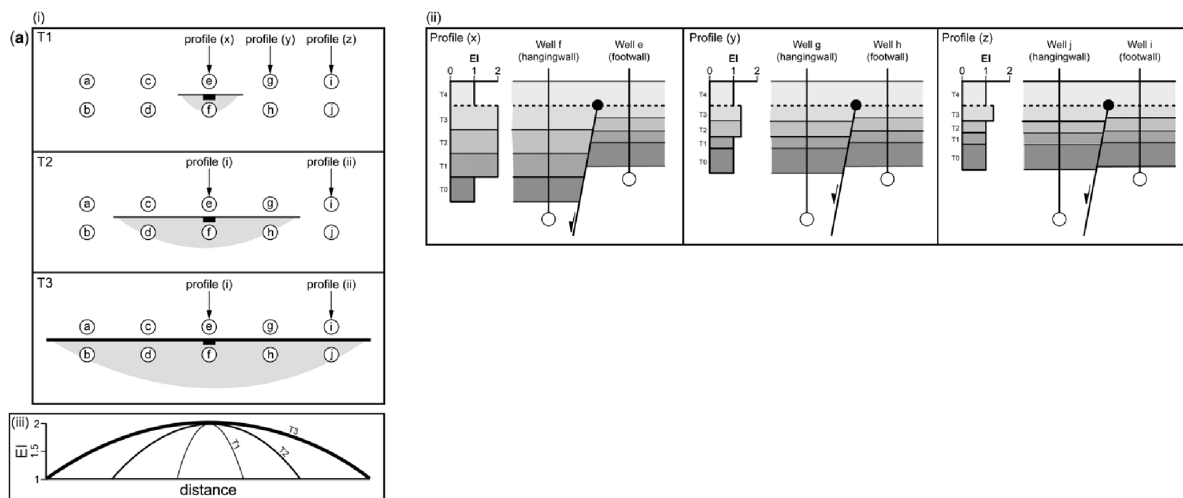


Fig. 16. An example of an isolated fault which grows in length from point e/f (profile x), to point g/h (profile y), to point i/j (profile z), with accumulating throw in accordance with the 'isolated fault model'. Expansion index (EI) graphs are shown on the right hand side, with their corresponding cross section hanging-wall and footwall geometries (after Jackson et al., 2017).

3. References

- Aanyu, K., & Koehn, D. (2011). Influence of pre-existing fabrics on fault kinematics and rift geometry of interacting segments: analogue models based on the Albertine Rift (Uganda), Western Branch-East African Rift System. *Journal of African Earth Sciences*, 59(2-3), 168-184.
- Bailey, A., King, R., Holford, S., Sage, J., Backe, G., & Hand, M. 2014. Remote sensing of subsurface fractures in the Otway Basin, South Australia. *Journal of Geophysical Research: Solid Earth*, 119(8), 6591-6612.
- Baudon, C., & Cartwright, J., 2008. The kinematics of reactivation of normal faults using high resolution throw mapping. *Journal of Structural Geology*, 30(8), 1072-1084.
- Bein, J., & Taylor, M. L. (1981). The Eyre Sub-basin: recent exploration results. *The APPEA Journal*, 21(1), 91-98.
- Benedicto, A., Schultz, R.A. & Soliva, R. 2003. Layer thickness and the shape of faults. *Geophysical Research Letters*, 30, 2076, <https://doi.org/10.1029/2003GL018237>
- Bilotti, F., & Shaw, J. H. (2005). Deep-water Niger Delta fold and thrust belt modelled as a critical taper wedge: The influence of elevated basal fluid pressure on structural styles. *AAPG bulletin*, 89(11), 1475-1491.
- Bouroullec, R., Cartwright, J.A., Johnson, H.D., Lansigu, C., Que ´mener, J.M. & Savanier, D. 2004. Syndepositional faulting in the Gre `s d'Annot Formation, SE France: high-resolution kinematic analysis and stratigraphic response to growth faulting. In: Joseph, P. & Lomas, S.A. (eds) *Deep-Water Sedimentation in the Alpine Basin of SE France: New Perspectives on the Gre `s d'Annot and Related Systems*. Geological Society, London, Special Publications, 221, 241–265, <https://doi.org/10.1144/GSL.SP.2004.221.01.13>
- Briggs, S. E., Davies, R. J., Cartwright, J. A., & Morgan, R., 2006. Multiple detachment levels and their control on fold styles in the compressional domain of the deepwater west Niger Delta. *Basin Research*, 18(4), 435-450.
- Buffler, R. T., Shaub, F. J., Watkins, J. S., & Worzel, J. L. (1979). Anatomy of the Mexican ridges, southwestern Gulf of Mexico. *Geological and geophysical investigations of continental margins: AAPG Memoir*, 29, 319-327.
- Cartwright, J. A., Bouroullec, R., James, D., Johnson, H. D., 1998. Polycyclic motion history of Gulf Coast Growth Faults from high resolution kinematic analysis. *Geology* 26, 819-822.
- Cartwright, J. A., Trudgill, B. D., & Mansfield, C. S., 1995. Fault growth by segment linkage: an explanation for scatter in maximum displacement and trace length data from the Canyonlands Grabens of SE Utah. *Journal of Structural Geology*, 17(9), 1319-1326.
- Chapman, T. J., & Meneilly, A. W. (1991). The displacement patterns associated with a reverse reactivated, normal growth fault. In A. M. Roberts, G. Yielding & B. Freeman (Eds.). *The geometry of normal faults* (pp. 183–191). London UK: Geological Society, London, Special Publications, 56 (1).
- Childs, C., Easton, S. J., Vendeville, B. C., Jackson, M. P. A., Lin, S. T., Walsh, J. J., & Watterson, J. (1993). Kinematic analysis of faults in a physical model of growth faulting above a viscous salt analogue. *Tectonophysics*, 228(3), 313-329.
- Childs, C., Manzocchi, T., Walsh, J.J., Bonson, C.G., Nicol, A. & Scho ¨pfer, M.P.J. 2009. A geometric model of fault zone and fault rock thickness variations. *Journal of Structural Geology*, 31, 117–127.
- Childs, C., Nicol, A., Walsh, J. J., & Watterson, J., 1996. Growth of vertically segmented normal

- faults. *Journal of Structural Geology*, 18(12), 1389-1397.
- Childs, C., Nicol, A., Walsh, J. J., & Watterson, J., 2003. The growth and propagation of synsedimentary faults. *Journal of Structural Geology*, 25(4), 633-648.
- Childs, C., Watterson, J., & Walsh, J. J., 1995. Fault overlap zones within developing normal fault systems. *Journal of the Geological Society*, 152(3), 535-549.
- Chorowicz, J. (2005). The east African rift system. *Journal of African Earth Sciences*, 43(1), 379-410.
- Cobbold, P. R., Clarke, B. J., & Løseth, H., 2009. Structural consequences of fluid overpressure and seepage forces in the outer thrust belt of the Niger Delta. *Petroleum Geoscience*, 15(1), 3-15.
- Cohen, H. A., & McClay, K., 1996. Sedimentation and shale tectonics of the northwestern Niger Delta front. *Marine and Petroleum Geology*, 13(3), 313-328.
- Corredor, F., Shaw, J. H., & Bilotti, F., 2005. Structural styles in the deep-water fold and thrust belts of the Niger Delta. *AAPG bulletin*, 89(6), 753-780.
- Dawers, N. H., & Anders, M. H., 1995. Displacement length scaling and fault linkage. *Journal of Structural Geology*, 17(5), 607-614.
- Dawers, N.H., Anders, M.H. & Scholz, C.H. 1993. Growth of normal faults: displacement-length scaling. *Geology*, 21, 1107-1110.
- Doust, H., Omatsola, E., 1990. Niger Delta. In: Edwards, J.D., Santogrossi, P.A. (Eds.), *Divergent/Passive Margin Basins*. American Association of Petroleum Geologists Memoir 48, 201-238.
- Duddy, 2003 Duddy, I. R., Erout, B., Green, P. F., Crowhurst, P. V., & Boulton, P. J. (2003). Timing constraints on the structural history of the western Otway Basin and implications for hydrocarbon prospectivity around the Morum High, South Australia. *The APPEA Journal*, 43(1), 59-83.
- Dutton, D. M., & Trudgill, B. D. (2009). Four dimensional analysis of the Sembo relay system, offshore Angola: Implications for fault growth in salt-detached settings. *AAPG bulletin*, 93(6), 763-794.
- Espurt, N., Callot, J. P., Totterdell, J., Struckmeyer, H., & Vially, R. (2009). Interactions between continental breakup dynamics and large-scale delta system evolution: Insights from the Cretaceous Ceduna delta system, Bight Basin, Southern Australian margin. *Tectonics*, 28(6).
- Finlayson, D. M., Johnstone, D. W., Owen, A. J., & Wake-Dyster, K. D., 1996. Deep seismic images and the tectonic framework of early rifting in the Otway Basin, Australian southern margin. *Tectonophysics*, 264(1), 137-152.
- Gawthorpe, R.L., Jackson, C.A-L., Young, M.J., Sharp, I.R., Moustafa, A.R. & Leppard, C.W. 2003. Normal fault growth, displacement localisation and the evolution of normal fault populations: the Hammam Faraun fault block, Suez rift, Egypt. *Journal of Structural Geology*, 25, 883-895.
- Geary, G.C. and Reid, I.S.A., 1998. Hydrocarbon prospectivity of the offshore eastern Otway Basin, Victoria for the 1998 Acreage Release. Victorian Initiative for Minerals and Petroleum Report 55, Department of Natural Resources and Environment.
- Giba, M., Walsh, J. J., & Nicol, A., 2012. Segmentation and growth of an obliquely reactivated normal fault. *Journal of Structural Geology*, 39, 253-267.
- Gibson, G. M., Totterdell, J. M., White, L. T., Mitchell, C. H., Stacey, A. R., Morse, M. P., & Whitaker, A. 2013. Pre-existing basement structure and its influence on continental rifting and fracture zone development along Australia's southern rifted margin. *Journal of the Geological Society*, 170(2), 365-377.
- Fraser, A. R., & Tilbury, L. A. (1979). Structure and stratigraphy of the Ceduna Terrace region. *Great*

Australian Bight Basin: APEA Journal, 19, 53-65.

- Hill, K. A., Finlayson, D. M., Hill, K. C. & Cooper, G. T., 1995. Mesozoic tectonics of the Otway Basin: the legacy of Gondwana and the active Pacific margin- a review and ongoing research. *The APPEA Journal, 35(1), 467-493.*
- Holford, S.P., Hillis, R.R., Duddy, I.R., Green, P.F., Stoker, M.S., Tuitt, A.G., Backé, G., Tassone, D.R. & Macdonald, J.D., 2011. Cenozoic post-breakup compressional deformation and exhumation of the southern Australian margin. *APPEA Journal-Australian Petroleum Production and Exploration Association, 51(1), 613-638.*
- Holford, S. P., Tuitt, A. K., Hillis, R. R., Green, P. F., Stoker, M. S., Duddy, I. R., & Tassone, D. R., 2014. Cenozoic deformation in the Otway Basin, southern Australian margin: implications for the origin and nature of post-breakup compression at rifted margins. *Basin Research, 26(1), 10-37.*
- Huggins, P., Watterson, J., Walsh, J. J., & Childs, C., 1995. Relay zone geometry and displacement transfer between normal faults recorded in coal-mine plans. *Journal of Structural Geology, 17(12), 1741-1755.*
- Imber, J., Childs, C., Nell, P. A. R., Walsh, J. J., Hodgetts, D., Flint, S. S., 2003. Hanging wall fault kinematics and footwall collapse in listric growth fault systems. *Journal of Structural Geology 25, 197-208.*
- Jackson, C. A. L., Bell, R. E., Rotevatn, A., & Tvedt, A. B., 2017. Techniques to determine the kinematics of synsedimentary normal faults and implications for fault growth models. *Geological Society, London, Special Publications, 439, SP439-22.*
- Jackson, C. L., & Larsen, E., 2009. Temporal and spatial development of a gravity-driven normal fault array: Middle–Upper Jurassic, South Viking Graben, northern North Sea. *Journal of Structural Geology, 31(4), 388-402.*
- Jackson, C. A. L., & Rotevatn, A., 2013. 3D seismic analysis of the structure and evolution of a salt-influenced normal fault zone: A test of competing fault growth models. *Journal of Structural Geology, 54, 215-234.*
- James, D. M. D. (Ed.). (1984). *The geology and hydrocarbon resources of Negara Brueni Dalussalam. Muzium Brunei and Brunei Shell Petroleum Company Berhad Special Publication, 8, 2–21.*
- Kane, K. E., Jackson, C. A. L., & Larsen, E., 2010. Normal fault growth and fault-related folding in a salt influenced rift basin: South Viking Graben, offshore Norway. *Journal of Structural Geology, 32(4), 490-506.*
- Khani, H. F., & Back, S. (2012). Temporal and lateral variation in the development of growth faults and growth strata in western Niger Delta, Nigeria. *AAPG bulletin, 96(4), 595-614.*
- King, R. C., & Backé, G. (2010). A balanced 2D structural model of the Hammerhead Delta Deepwater Fold-Thrust Belt, Bight Basin, Australia. *Australian Journal of Earth Sciences, 57(7), 1005-1012.*
- King, R. C., Backé, G., Morley, C. K., Hillis, R. R., & Tingay, M. R., 2010. Balancing deformation in NW Borneo: Quantifying plate-scale vs. gravitational tectonics in a Delta and Deepwater Fold-Thrust Belt System. *Marine and Petroleum Geology, 27(1), 238-246.*
- King, R. C., Hillis, R. R., Tingay, M. R. P., Morley, C. K. (2009). Present-day stress and neotectonic provinces of the Baram Delta and deep-water fold thrust belt. *Journal of the Geological Society, 166, 197-200.*
- Koledoye, B. A., Aydin, A., & May, E., 2003. A new process-based methodology for analysis of shale smear along normal faults in the Niger Delta. *AAPG bulletin, 87(3), 445-463.*

- Koopman, A., Schreurs, J., & Ellenor, D. W., 1996. The oil and gas resources of Brunei Darussalam—The coastal and offshore oil and gas fields. *Geology and Hydrocarbon Resources of Negara Brunei Darussalam*, edited by ST Sandal, 155-192.
- Krassay, A.A., Cathro, D.L. AND Ryan, D.J., 2004. A regional tectonostratigraphic framework for the Otway Basin. In: Boulton, P.J., Johns, D.R. and Lang, S.C. (eds), *Eastern Australasian Basins Symposium II*. Petroleum Exploration Society of Australia, Special Publication, 97–116.
- Lewis, M. M., Jackson, C. A. L., & Gawthorpe, R. L., 2013. Salt-influenced normal fault growth and forced folding: The Stavanger Fault System, North Sea. *Journal of Structural Geology*, 54, 156-173.
- Macdonald, J. D., Backé, G., King, R., Holford, S., & Hillis, R. R. (2012). Geomechanical modelling of fault reactivation in the Ceduna Sub-basin, Bight Basin, Australia. In D. Healy, R. W. H. Butler, Z. K. Shipton, & R. H. Sibson (Eds.) *Faulting, fracturing and igneous intrusions in the Earth's crust* (pp. 71–89). London UK: Geological Society, London, Special Publications, 367.
- Macdonald, J. D., King, R., Hillis, R. R., & Backé, G. (2010). Structural style of the White Pointer and Hammerhead delta—deepwater fold-thrust belts, Bight Basin, Australia. *The Australian Petroleum Production and Exploration Association Journal*, 50, 487–510.
- Mansfield, C. S., & Cartwright, J. A., 1996. High resolution fault displacement mapping from three-dimensional seismic data: evidence for dip linkage during fault growth. *Journal of Structural Geology*, 18(2), 249-263.
- Mansfield, C., & Cartwright, J. (2001). Fault growth by linkage: observations and implications from analogue models. *Journal of Structural Geology*, 23(5), 745-763.
- Marsh, N., Imber, J., Holdsworth, R. E., Brockbank, P., & Ringrose, P. (2010). The structural evolution of the Halten Terrace, offshore Mid-Norway: extensional fault growth and strain localisation in a multi-layer brittle–ductile system. *Basin Research*, 22(2), 195-214.
- Messent, B.E.J. (1998) Great Australian Bight: well audit. Australian Geological Survey Organisation Record 1998/37.
- Moore, A.M.G., Stagg, H.M.J. & Norvick, M.S., 2000. Deep-water Otway Basin: a new assessment of the tectonics and hydrocarbon prospectivity. *The APPEA Journal*, 32(1), 66–85.
- Morley, C.K. 2002. Evolution of large normal faults: evidence from seismic reflection data. *American Association of Petroleum Geologists Bulletin*, 86, 961–978.
- Morley, C. K., & Guerin, G., 1996. Comparison of gravity driven deformation styles and behaviour associated with mobile shales and salt. *Tectonics*, 15(6), 1154-1170.
- Morton, J. G. G., Hill, A. J., Parker, G., & Tabassi, A. 1994. Towards a unified stratigraphy for the Otway Basin. In Finlayson, DM (compiler), *NGMA/Petroleum Exploration Society of Australia Otway Basin Symposium*, Melbourne, 20, 7-12.
- Morley, C.K., Nelson, R.A., Patton, T.L. & Munn, S.G. 1990. Transfer zones in the East African Rift System and their relevance to hydrocarbon exploration in rifts. *AAPG Bulletin*, 74, 1234–1253.
- Nicol, A., Watterson, J., Walsh, J.J. & Childs, C. 1996. The shapes, major axis orientations and displacement patterns of fault surfaces. *Journal of Structural Geology*, 18, 235–248.
- Nicol, A., Childs, C., Walsh, J.J., Manzocchi, T. & Schoepfer, M.P.J. 2016. Interactions and growth of faults in an outcrop-scale system. In: Childs, C., Holdsworth, R.E., Jackson, C.A.-L., Manzocchi, T., Walsh, J.J. & Yielding, G. (eds) *The Geometry and Growth of Normal Faults*. Geological Society, London, Special Publications, 439. First published online March 10, 2016, <https://doi.org/10.1144/SP439.9>

- Norvick, M.S., 2005. Plate Tectonic Reconstructions of Australia's Southern Margins. Geoscience Australia, Record 2005/07.
- Norvick, M. S., & Smith, M. A. (2001). Southeast Australia-Mapping the plate tectonic reconstruction of southern and southeastern Australia and implications for petroleum systems. *APPEA Journal-Australian Petroleum Production and Exploration Association*, 41(1), 15-36.
- Palmowski, D., Hill, K. C., & Hoffman, N., 2004. Structure and hydrocarbons in the Shipwreck Trough, Otway Basin: half-graben gas fields abutting a continental transform. *The APPEA Journal*, 44, 417-440.
- Peacock, D. C. P., & Sanderson, D. J., 1991. Displacements, segment linkage and relay ramps in normal fault zones. *Journal of Structural Geology*, 13(6), 721-733.
- Peacock, D. C. P., & Sanderson, D. J. (1994). Geometry and development of relay ramps in normal fault systems. *AAPG Bulletin*, 78 (2), 147-165.
- Perincek, D. and Cockshell, C.D., 1995. The Otway Basin: Early Cretaceous rifting to Neogene inversion. *The APPEA Journal*, 35, 451-466.
- Rotevatn, A., & Jackson, C. A. L. (2014). 3D structure and evolution of folds during normal fault dip linkage. *Journal of the Geological Society*, 171 (6), 821-829.
- Rowan, M. G., Hart, B. S., Nelson, S., Flemings, P. B., & Trudgill, B. D., 1998. Three-dimensional geometry and evolution of a salt-related growth-fault array: Eugene Island 330 field, offshore Louisiana, Gulf of Mexico. *Marine and petroleum geology*, 15(4), 309-328.
- Rowan, M.G., Jackson, M.P.A., Trudgill, B.D. (1999). Salt-related fault families and fault welds in the northern Gulf of Mexico. *AAPG Bulletin* 83, 1454-1484.
- Ryan, S.M., Knight, L.A. & Parker, G.J., 1995. The stratigraphy and structure of the Tyrendarra Embayment, Otway Basin, Victoria. Geological Survey of Victoria, VIMP report 15.
- Rykkelid, E., & Fossen, H., 2002. Layer rotation around vertical fault overlap zones: observations from seismic data, field examples, and physical experiments. *Marine and Petroleum Geology*, 19(2), 181-192.
- Sayers, J., Symonds, P. A., Direen, N. G., & Bernardel, G., 2001. Nature of the continent-ocean transition on the non-volcanic rifted margin of the central Great Australian Bight. *Geological Society, London, Special Publications*, 187(1), 51-76.
- Schlagenhauf, A., Manighetti, I., Malavieille, J. & Dominguez, S. 2008. Incremental growth of normal faults: Insights from a laser-equipped analog experiment. *Earth and Planetary Science Letters*, 273, 299-311.
- Schreurs, G., 1997. The petroleum geology of Negara Brunei Darussalem; an update. In: Howes, J.V.C. and Noble, R. A. (Eds) *Proceedings of the IPA Petroleum Systems of SE Asia and Australasia Conference*, Jakarta, Indonesia, May, 1997, Indonesian Petroleum Association, Jakarta, 751-766.
- Soliva, R. & Benedicto, A. 2005. Geometry, scaling relations and spacing of vertically restricted normal faults. *Journal of Structural Geology*, 27, 317-325.
- Stacey, A.R., Mitchell, C.H., Struckmeyer, H.I.M. AND Totterdell, J.M., 2013. Geology and hydrocarbon prospectivity of the deepwater Otway and Sorell basins, offshore southeastern Australia. Record 2013/02. Geoscience Australia: Canberra.
- Stagg, H. M. J., C. D. Cockshell, J. B. Willcox, A. J. Hill, D. V. C. Needham, B. Thomas, G. W. O'Brien And L. P. Hough (1990). Basins of the Great Australian Bight region—Geology and petroleum potential, Folio 5, Continental Margins Program, Bureau of Mineral Resources, Geology and Geophysics, Canberra, Australia.

- Stewart, I. S., & Hancock, P. L. (1991). Scales of structural heterogeneity within neotectonic normal fault zones in the Aegean region. *Journal of Structural Geology*, 13 (2), 191–204.
- Tassone, D. R., Holford, S. P., Duddy, I. R., Green, P. F., & Hillis, R. R., 2014. Quantifying Cretaceous Cenozoic exhumation in the Otway Basin, southeastern Australia, using sonic transit time data: Implications for conventional and unconventional hydrocarbon prospectivity. *AAPG Bulletin*, 98(1), 67-117.
- Thorsen, C. E., 1963. Age of growth faulting in southeast Louisiana. *Gulf Coast Association of Geological Societies Transactions* 13, 103-110.
- Tikku, A. A., & Cande, S. C. (1999). The oldest magnetic anomalies in the Australian-Antarctic Basin: Are they isochrons?. *Journal of Geophysical Research: Solid Earth*, 104(B1), 661-677.
- Totterdell, J. M., Blevin, J. E., Struckmeyer, H. I. M., Bradshaw, B. E., Colwell, J. B., & Kennard, J. M., (2000). Petroleum frontiers, systems and plays—A new sequence framework for the Great Australian Bight: Starting with a clean slate. *APPEA Journal*, 40 (1), 95–120.
- Totterdell, J. M., & Bradshaw, B. E. (2004). The structural framework and tectonic evolution of the Bight Basin. In *Eastern Australasian Basins Symposium II*, Petroleum Exploration Society of Australia, Special Publication, 41-61.
- Totterdell, J.M, Gibson, G.M., Stacey, A.R., Mitchell, C.H., Morse, M.P., Nayak, G.K. and Kuszniir, N.J., 2011. Structural architecture of Australia’s 4000 km-long southern rifted continental margin. EGU General Assembly 2011. Geophysical Research Abstracts, 13, EGU2011-1427-1.
- Totterdell, J. M., Gibson, G. M., Stacey, A. R., Mitchell, C. H., Morse, M. P., Nayak, G. K., & Kuszniir, N. J. (2012). The structure of Australia’s southern rifted margin: basement architecture, rifting processes and basin development. In *Proceedings of the 34th International Geological Congress 2012, Brisbane, Australia*.
- Totterdell, J. M., & Krassay, A. A. (2003). The role of shale deformation and growth faulting in the Late Cretaceous evolution of the Bight Basin, offshore southern Australia. *Geological Society, London, Special Publications*, 216(1), 429-442.
- Trudgill, B., & Cartwright, J., 1994. Relay-ramp forms and normal-fault linkages, Canyonlands National Park, Utah. *Geological Society of America Bulletin*, 106(9), 1143-1157.
- Tvedt, A.B.M., Rotevatn, A. & Jackson, C.A-L. 2016. Supra-salt normal fault growth during the rise and fall of a diapir: perspectives from 3D seismic reflection data, Norwegian North Sea. *Journal of Structural Geology*, 91, 1–26, <https://doi.org/10.1016/j.jsg.2016.08.001>
- Tvedt, A., Rotevatn, A., Jackson, C. A. L., Fossen, H., & Gawthorpe, R. L., 2013. Growth of normal faults in multilayer sequences: A 3D seismic case study from the Egersund Basin, Norwegian North Sea. *Journal of Structural Geology*, 55, 1-20.
- Veevers, J. J. (1986). Breakup of Australia and Antarctica estimated as mid-Cretaceous (95±5 Ma) from magnetic and seismic data at the continental margin. *Earth and Planetary Science Letters*, 77(1), 91-99.
- Walsh, J. J., Bailey, W. R., Childs, C., Nicol, A., & Bonson, C. G., 2003. Formation of segmented normal faults: a 3-D perspective. *Journal of Structural Geology*, 25(8), 1251-1262.
- Walsh, J. J., Nicol, A., & Childs, C., 2002. An alternative model for the growth of faults. *Journal of Structural Geology*, 24(11), 1669-1675.
- Walsh, J. J., & Watterson, J., 1988. Analysis of the relationship between displacements and dimensions of faults. *Journal of Structural Geology*, 10(3), 239-247.
- Walsh, J. J., & Watterson, J., 1991. Geometric and kinematic coherence and scale effects in normal fault systems. *Geological Society, London, Special Publications*, 56(1), 193-203.

- Watterson, J. 1986. Fault dimensions, displacement and growth. *Pure and Applied Geophysics*, 124, 365–373.
- Willcox, J. B., & Stagg, H. M. J., 1990. Australia's southern margin: a product of oblique extension. *Tectonophysics*, 173(1), 269-281.
- Winker, C.D. & Edwards, M.B., 1983. Unstable progradational clastic shelf margins. In: Stanley, D.J. & Moore, G.T. (eds) *The shelfbreak: critical interface on continental margins*. Society of Economic Paleontologists and Mineralogists, Special Publication 33, 139-157.
- Withjack, M. O., & Callaway, S. (2000). Active normal faulting beneath a salt layer: an experimental study of deformation patterns in the cover sequence. *AAPG bulletin*, 84(5), 627-651.
- Withjack, M. O., Olson, J., & Peterson, E. (1990). Experimental models of extensional forced folds. *Aapg Bulletin*, 74(7), 1038-1054.
- Wu, S., Bally, A. W., & Cramez, C., 1990. Allochthonous salt, structure and stratigraphy of the north-Eastern Gulf of Mexico. Part II: Structure. *Marine and Petroleum Geology*, 7(4), 334-370.

4. Thesis Body

4.1 Paper 1

Robson, A. G., King, R. C., & Holford, S. P. (2017). Structural evolution of a gravitationally detached normal fault array: analysis of 3D seismic data from the Ceduna Sub-Basin, Great Australian Bight. *Basin Research*, 29, 605-624. DOI: 10.1111/bre.12191

Statement of Authorship

Title of Paper	Structural evolution of a gravitationally detached normal fault array: analysis of 3D seismic data from the Ceduna Sub-Basin, Great Australian Bight.
Publication Status	<input checked="" type="checkbox"/> Published <input type="checkbox"/> Accepted for Publication <input type="checkbox"/> Submitted for Publication <input type="checkbox"/> Unpublished and Unsubmitted work written in manuscript style
Publication Details	Robson, A. G., King, R. C., & Holford, S. P. (2017). Structural evolution of a gravitationally detached normal fault array: analysis of 3D seismic data from the Ceduna Sub-Basin, Great Australian Bight. Basin Research, 29, 605-624. DOI:10.1111/bre.12191

Principal Author

Name of Principal Author (Candidate)	Alexander Robson			
Contribution to the Paper	<ul style="list-style-type: none"> Seismic interpretation fault analysis preparation of manuscript editing manuscript Corresponding author 			
Overall percentage (%)	70%			
Certification:	This paper reports on original research I conducted during the period of my Higher Degree by Research candidature and is not subject to any obligations or contractual agreements with a third party that would constrain its inclusion in this thesis. I am the primary author of this paper.			
Signature	<table border="1" style="width: 100%;"> <tr> <td style="width: 80%;"></td> <td style="width: 20%;">Date</td> <td>6/09/2017</td> </tr> </table>		Date	6/09/2017
	Date	6/09/2017		

Co-Author Contributions

By signing the Statement of Authorship, each author certifies that:

- i. the candidate's stated contribution to the publication is accurate (as detailed above);
- ii. permission is granted for the candidate to include the publication in the thesis; and
- iii. the sum of all co-author contributions is equal to 100% less the candidate's stated contribution.

Name of Co-Author				
Contribution to the Paper	<ul style="list-style-type: none"> Supervised development of work Helped in data interpretation and manuscript evaluation Multiple edits of manuscript during review 			
Signature	<table border="1" style="width: 100%;"> <tr> <td style="width: 80%;"></td> <td style="width: 20%;">Date</td> <td>6/09/2017</td> </tr> </table>		Date	6/09/2017
	Date	6/09/2017		

Name of Co-Author				
Contribution to the Paper	<ul style="list-style-type: none"> Supervised development of work Helped in data interpretation and manuscript evaluation Multiple edits of manuscript during review 			
Signature	<table border="1" style="width: 100%;"> <tr> <td style="width: 80%;"></td> <td style="width: 20%;">Date</td> <td>6/09/2017</td> </tr> </table>		Date	6/09/2017
	Date	6/09/2017		

Please cut and paste additional co-author panels here as required.

Structural evolution of a gravitationally detached normal fault array: analysis of 3D seismic data from the Ceduna Sub-Basin, Great Australian Bight

A. G. Robson^{*,†}, R. C. King^{*} and S. P. Holford[†]

^{*}*Department of Earth Sciences, Centre for Tectonics Resources and Exploration (TRaX), University of Adelaide, Adelaide 5005, South Australia, Australia*

[†]*Australian School of Petroleum, University of Adelaide, Adelaide 5005, South Australia, Australia*

ABSTRACT

The growth, interaction and controls on normal fault systems developed within stacked delta systems at extensional delta-top settings have not been extensively examined. We aim to analyse the kinematic, spatial and temporal growth of a Cretaceous aged, thin-skinned, listric fault system in order to further the understanding of how gravity-driven fault segments and fault systems develop and interact at an extensional delta-top setting. Furthermore, we aim to explore the influence of a pre-existing structural framework on the development of gravity-driven normal faults through the examination of two overlapping, spatially and temporally distinct delta systems. To do this, we use three-dimensional (3D) seismic reflection data from the central Ceduna Sub-basin, offshore southern Australia. The seismic reflection data images a Cenomanian–Santonian fault system, and a post-Santonian fault system, which are dip-linked through an intervening Turonian–early Campanian section. Both of these fault systems contain four hard-linked strike assemblages oriented NW–SE (127–307), each composed of 13 major fault segments. The Cenomanian–Santonian fault system detaches at the base of a shale interval of late Albian age, and is characterised by kilometre-scale growth faults in the Cenomanian–Santonian interval. The post-Santonian fault system nucleated in vertical isolation from the Cenomanian–Santonian fault system. This is evident through displacement minima observed at Turonian–early Campanian levels, which is indicative of vertical segmentation and eventual hard dip-linkage. Our analysis constrains fault growth into four major evolutionary stages: (1) early Cenomanian nucleation and growth of fault segments, resulting from gravitational instability, and with faults detaching on the lower Albian interval; (2) Santonian cessation of growth for the majority of faults; (3) erosional truncation of fault upper tips coincident with the continental breakup of Australia and Antarctica (*ca.* 83 Ma); (4) Campanian–Maastrichtian reactivation of the underlying Cenomanian–Santonian fault system, inducing the nucleation, growth and consequential dip-linkage of the post-Santonian fault system with the underlying fault system. Our results highlight the along-strike linkage of fault segments and the interaction through dip-linkage and fault reactivation, between two overlapping, spatially and temporally independent delta systems of Cenomanian and late Santonian–Maastrichtian age in the frontier Ceduna Sub-Basin. This study has implications regarding the growth of normal fault assemblages, through vertical and lateral segment linkage, for other stacked delta systems (such as the Gulf of Mexico) where upper delta systems develop over a pre-existing structural framework.

INTRODUCTION

Understanding the evolution of gravity-driven normal faults whose growth is influenced by the presence of mechanically weak detachments (e.g. evaporites or mudstones) is challenging, with most models for normal fault growth based on observations of faults that have grown in

the absence of a mechanically weak detachment (e.g. Peacock & Sanderson, 1991; Dawers & Anders, 1995; Huggins *et al.*, 1995). The ductility of mechanically weak layers of sedimentary rock can inhibit the propagation of faults and allow for the accommodation of displacement and strain, creating complexities in fault displacement (Withjack *et al.*, 1990; Withjack & Callaway, 2000; Kane *et al.*, 2010; Marsh *et al.*, 2010; Tvedt *et al.*, 2013). Recent research has significantly contributed to our understanding of gravity-driven normal fault growth (Rowan *et al.*, 1998, 1999; Jackson & Larsen, 2009; Kane

Correspondence: A. G. Robson, Australian School of Petroleum, The University of Adelaide, South Australia 5005, Australia. E-mail: alexander.robson@adelaide.edu.au

et al., 2010; Jackson & Rotevatn, 2013; Lewis *et al.*, 2013; Tvedt *et al.*, 2013). However, the growth, interaction and influence of normal fault systems developed within temporally and vertically isolated, stacked delta systems has not been extensively examined. Delta systems commonly occur on passive margins around the world (such as the Gulf of Mexico, the Niger Delta, the Baram Delta and the Great Australian Bight) and provide examples of normal fault growth developing over mechanically weak detachments at the extensional delta-top (*sensu* King *et al.*, 2009; Fig. 1).

Using a 3D seismic reflection dataset from the Ceduna Sub-Basin, located offshore, within the Great Australian Bight (Fig. 1), we aim to establish the structural evolution of four assemblages of hard-linked normal fault segments located at an extensional delta top setting, which detach in an underlying shale of late Albian age. The Middle Jurassic to Upper Cretaceous age Ceduna Sub-Basin (Fig. 1c) is characterized by a delta system consisting of two stacked deltas of Cenomanian and late Santonian–Maastriichtian age, that display evidence for gravity-driven extension at the delta top, balanced down-dip by a delta deepwater fold-thrust belt and accommodated by a late Albian shale detachment (Totterdell *et al.*, 2000; Macdonald *et al.*, 2010). The 3D seismic reflection data (Fig. 1a, b) allow us to spatially and temporally constrain fault growth through examination and measurement of synkinematic growth strata, both along-strike and down-dip, for individual fault segments and linked fault assemblages.

We have identified and individually analysed two vertically connected fault systems of Cenomanian–Santonian and post-Santonian age. The observation of along-strike segment linkage in map view, the isolation of faults at depth and of highly variable along-strike displacement profiles leads us to conclude that these fault assemblages formed due to the along-strike linkage of *ca.* 5–15 km long fault segments. Measurement of the variation in displacement with depth down fault planes reveals minor displacement minima at the Turonian–early Campanian level. Given the inherited map view geometry of the post-Santonian fault system and only minor displacement deficits between the fault systems, it is clear that the Cenomanian–Santonian fault system was active during, and had a large control over, the development of the post-Santonian fault system. Therefore, our results show that pre-existing gravity-driven faults may have a large influence over the geometric development of overlying faults in stacked delta systems. This has implications for fault growth models in other delta systems around the world, including the Gulf of Mexico (Buller *et al.*, 1979; Winker & Edwards, 1983; Wu *et al.*, 1990; Rowan, 1997), Niger Delta (Doust & Omatsola, 1989; Morley & Guerin, 1996; Cohen & McClay, 1996; Bilotti & Shaw, 2005; Corredor *et al.*, 2005; Briggs *et al.*, 2006; Cobbold *et al.*, 2009) and Baram Delta (James, 1984; Koopman *et al.*, 1996; Schreurs, 1997; King *et al.*, 2010).

GEOLOGICAL SETTING

The Ceduna Sub-basin (Fig. 1b, c) is a NW-trending depocentre that covers a surface area of *ca.* 90 000 km² within the E-W to NW-SE oriented Bight Basin (Fig. 1d). It contains up to 15 km of Middle Jurassic to Upper Cretaceous age sediments (Totterdell & Krassay, 2003; Macdonald *et al.*, 2010). The Bight Basin contains four other major depocentres, the Eyre, Recherche, Duntroon and Bremer sub-basins, though the sedimentary thickness in the Ceduna sub-basin far exceeds that in the other depocentres. The Ceduna Sub-basin formed following the rifting of Australia and Antarctica during the break-up of eastern Gondwana from the Late Jurassic onwards (Fraser & Tilbury, 1979; Bein & Taylor, 1981; Stagg *et al.*, 1990; Willcox & Stagg, 1990; Totterdell *et al.*, 2000; Holford *et al.*, 2011). The inboard, south-southwest-striking, steeply dipping Jurassic to Lower Cretaceous Pademelon and Potoroo rift systems, provide evidence for this mechanical extension (Totterdell & Bradshaw, 2004; see fig. 15). The Ceduna Sub-basin is bordered by Proterozoic and older terranes to the north, the Proterozoic–Archean Gawler Craton to the east, the Duntroon Sub-Basin to the SE and the Eyre Sub-Basin to the west. To the south, the sedimentary rocks of the Ceduna sub-basin thin out onto the abyssal plain in the Recherche Sub-Basin (Fig. 1c) (Fraser & Tilbury, 1979; Bein & Taylor, 1981; Willcox & Stagg, 1990; Hill, 1995; Norvick & Smith, 2001; Krassay & Totterdell, 2003).

Oblique extension (basin phase 1) occurred throughout the Middle and Upper Jurassic, resulting in *en-échelon*, west-northwest striking half-graben structures through all sub-basins, filled with fluvial and lacustrine sediments of the Sea Lion, Minke and Southern Right supersequences (Fig. 1a) (Totterdell *et al.*, 2000). A transition to slow basin subsidence (basin phase 2) occurred during the Valanginian, resulting in the deposition of the fluvial and lacustrine Bronze Whaler Supersequence until the middle Albian (Fig. 1a; Totterdell *et al.*, 2000). Basin phase 3 involves the acceleration of subsidence due to lower crustal extension from the middle Albian–late Santonian. Initiation of this phase led to the first marine flooding of the basin, during which nearshore marine siltstones and mudstones of the middle-late Albian Blue Whale Supersequence were deposited (Fig. 1a) (Totterdell *et al.*, 2000; Totterdell & Krassay, 2003). Accelerated thermal subsidence continued during the Cenomanian and brought on the rapid deposition of the deltaic Whitepointer Supersequence (Fig. 1a). A Southwest dipping detachment formed by the shales of the underlying Blue Whale Supersequence (Totterdell & Krassay, 2003; Macdonald *et al.*, 2010) accommodated movement of a series of listric faults known as the Mulgara Fault Family, which are developed *ca.* 250 km along strike and *ca.* 100 km down dip in the central-western Ceduna Sub-Basin (Totterdell & Bradshaw, 2004; see fig. 15; Fig. 1b). This style of listric faulting is similar to that seen in the Niger Delta (Doust & Omatsola, 1989; Morley & Guerin, 1996; Cohen

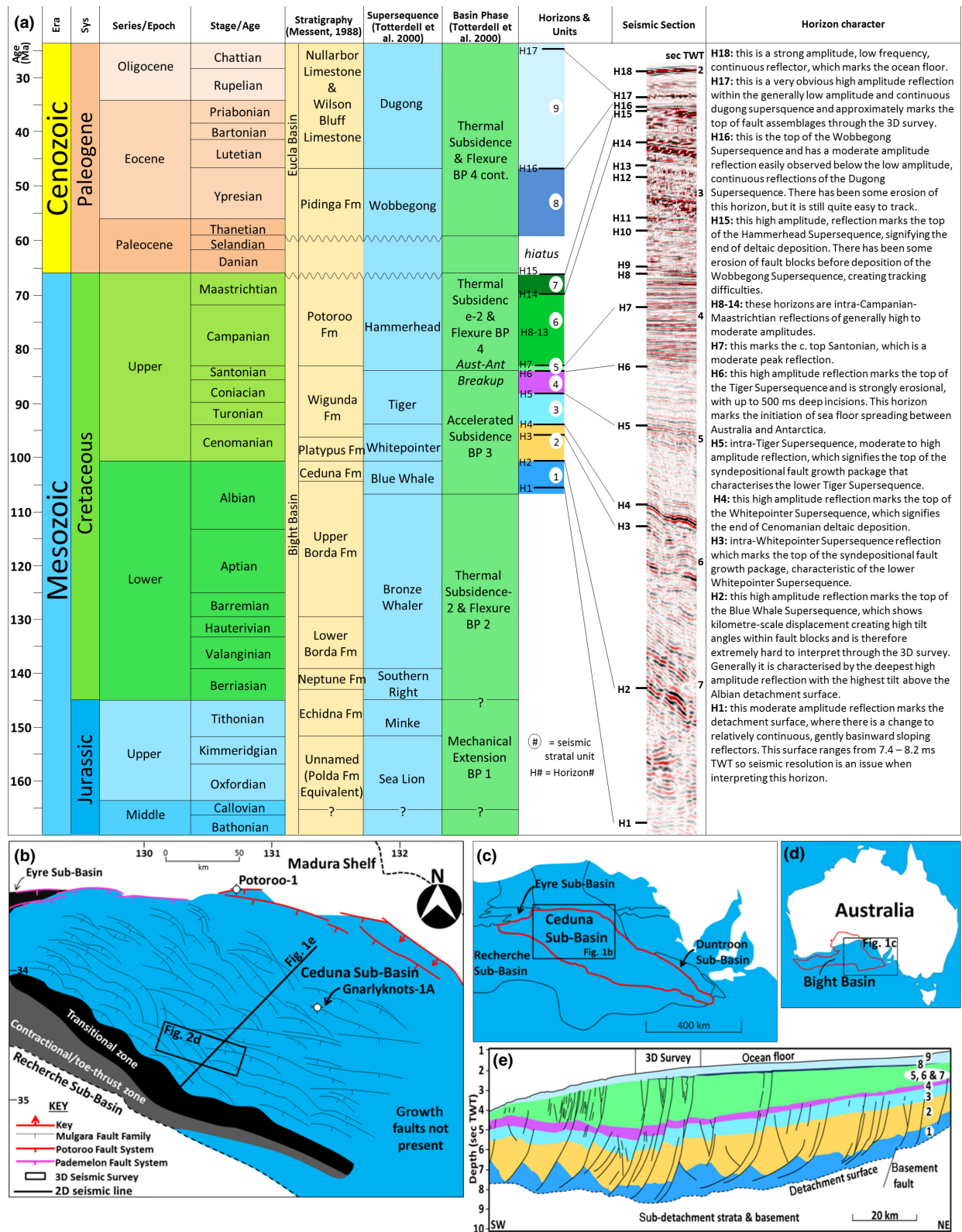


Fig. 1. (a) Bight Basin correlation chart, demonstrating the interpreted horizons and seismic stratal units from this study with stratigraphy (Messent, 1998), sequence stratigraphic scheme and basin phases (Totterdell *et al.*, 2000). (b) Map of the central Ceduna Sub-basin, illustrating the extensional, transitional and compressional zones. The extensional zone is comprised of the Potoroo and Pademelon basement fault systems and the thin-skinned Mulgara Fault Family, detached at the late Albian interval. (c) Locations of the Ceduna, Eyre, Duntroon and Recherche Sub-Basins. (d) Location of the Bight Basin. The location of the 3D seismic survey (Fig. 2d) used for this study and the 2D seismic line used for the geoseismic cross-section (e) is shown on the location map (b). The geoseismic line (e) was derived from interpretation by Geoscience Australia provided in the 2012 acreage release data set. Note the location of the 3D reflection survey on the geoseismic line and the listric faults forming a detachment at the base of stratal unit 1 (late Albian).

& McClay, 1996; Bilotti & Shaw, 2005; Corredor *et al.*, 2005; Briggs *et al.*, 2006; Cobbold *et al.*, 2009), Baram Delta (James, 1984; Koopman *et al.*, 1996; Schreurs, 1997; King *et al.*, 2010) and the Gulf of Mexico (Buffler *et al.*, 1979; Winker & Edwards, 1983; Wu *et al.*, 1990; Rowan, 1997). The style of fault geometry indicates that downslope deformation was driven by gravitational sliding (Morley & Guerin, 1996; Schultz-Ela, 2001; Totterdell & Krassay, 2003; Peel, 2014).

Further down-dip, a deep-water fold-thrust belt contains toe thrusts and intense folding above the Blue Whale shale detachment (Fig. 1b; Totterdell & Krassay, 2003; Tapley *et al.*, 2005; Macdonald *et al.*, 2010, 2012b). The growth of listric faults either terminated or became blind by the late Cenomanian, with little evidence for syndepositional faulting within the upper White Pointer Supersequence (Totterdell *et al.*, 2000). However, accelerated thermal subsidence rates (basin phase 3) continued into the *ca.* Santonian and this is exhibited by further growth of Cenomanian gravity-driven faults during the Turoonian, creating growth packages within the lower Turo-

nian-Santonian Tiger Supersequence (Fig. 1a), consisting of marginal marine and marine mudstones (Totterdell *et al.*, 2000). Fault growth during the Turoonian-Santonian was accompanied by thinning of the lower crust, signifying a significant phase of extension (Sayers *et al.*, 2001). The upper Tiger Supersequence does not exhibit evidence for synkinematic faulting (Totterdell *et al.*, 2000).

The onset of seafloor spreading between Australia and Antarctica likely began in the latest Santonian (*ca.* 83 Ma), and this coincides with the development of strong erosional features in the northern and eastern Ceduna Sub-Basin, including large incised valleys and angular unconformities within the Tiger Supersequence (Totterdell *et al.*, 2000; Sayers *et al.*, 2001; Totterdell & Bradshaw, 2004; MacDonald *et al.*, 2012a). These features are interpreted to result from regional uplift at the commencement of sea floor spreading (Totterdell & Bradshaw, 2004). Inversion of Cenomanian gravity-driven faults has been interpreted in the northern portions of the Ceduna Sub-Basin, *ca.* 60 km north of the study area

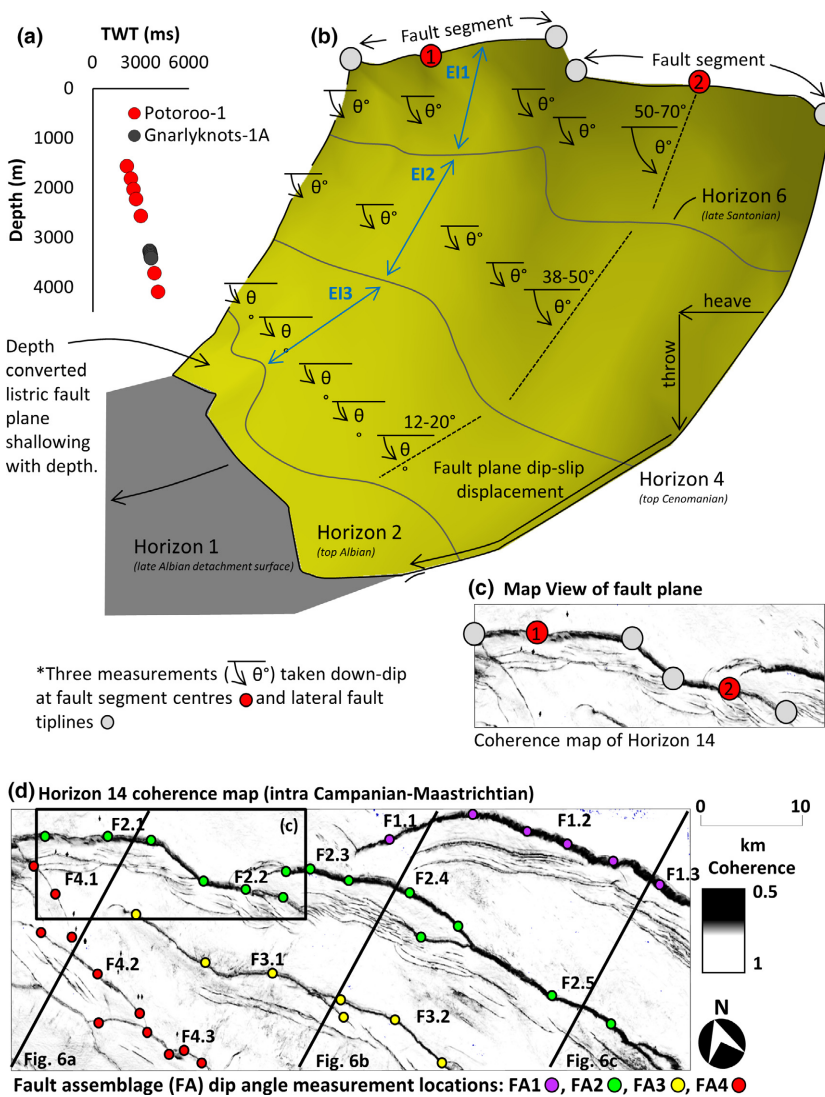


Fig. 2. Two-way-time (TWT) vs depth plot (a) of the velocity surveys for wells Potoroo-1 and Gnarlyknots-1A used for depth conversion. Three-dimensional perspective view (b) of an example listric fault plane from the 3D reflection survey to show fault plane model calculations. This model also shows the three different angles for expansion indexes (EI) labelled in blue: EI1, EI2 and EI3 in order to account for bed rotation and maintain true stratal thickness measurement. (c) Map view of the example fault plane (b) showing fault segment centres and tip lines. Measurements of the depth-converted listric fault plane were along strike at fault segment centres and at fault segment lateral tip lines as shown by measurement locations (d). At each measurement location (d), the fault plane is measured down-dip at three distinct intervals of dip angle: (1) upper tip-line to horizon 6 (50–70°); (2) horizon 6 to horizon 4 (38–50°); and (3) horizon 4 to horizon 2 (12–20°). This provides simplified fault plane geometries in order to translate vertical throw into fault plane displacement, by including heave, which is vital in understanding the growth of listric faults that shallow with depth.

(MacDonald *et al.*, 2012a). The latest Santonian–Maastriichtian marks a period of thermal subsidence (basin phase 4) during which the deltaic Hammerhead Supersequence (Fig. 1a), which reaches thicknesses of up to 5000 m in the central Ceduna Sub-Basin, was deposited (Totterdell *et al.*, 2000; Totterdell & Bradshaw, 2004; Macdonald *et al.*, 2013). The Hammerhead Supersequence is divided into three stratigraphic sequences in the Ceduna Sub-Basin, with the two lowermost sequences progradational in nature, and the uppermost being an aggradational sequence (Totterdell *et al.*, 2000). In the central and eastern Ceduna Sub-Basin, the Hammerhead Delta System formed above a detachment at the top of the Tiger Supersequence (Totterdell *et al.*, 2000), with up-dip gravitational extension driving down dip compression (*sensu* King *et al.*, 2009; King & Backé, 2010; Macdonald *et al.*, 2010). A hiatus of 5–7 M.y. separates the Hammerhead Supersequence from the overlying Palaeocene–early Eocene Wobbegong Supersequence of the Eucla Basin (Fig. 1a), which consists of relatively thin, reworked marginal marine to deltaic sandstone and siltstone (Totterdell *et al.*, 2000). This unconformity has created considerable incisions and some canyoning into the top of the Hammerhead Supersequence (Totterdell *et al.*, 2000). This is overlain by the middle Eocene–Pleistocene Dugong Supersequence (Fig. 1a), characterised by a sandstone base transitioning into thick, uniform cool-water carbonates (Totterdell *et al.*, 2000).

DATASET AND METHODOLOGY

Dataset

This study uses a 3D seismic reflection survey (Fig. 1a, b) from the central Ceduna Sub-Basin, which covers a surface area of *ca.* 1245 km² and extends to 9-s two-way-traveltime (TWT). The inline and crossline spacing of the survey are 30 m and 12.5 m, respectively, with the inlines oriented WNW–ESE and crosslines oriented NNE–SSW. The Potoroo-1 well is located 117 km north of the 3D survey, and the Gnarlyknots-1A well is 49 km to the ENE (Fig. 1b). Both wells were tied into the seismic data using two-dimensional (2D) seismic reflection profiles.

Depth conversion and fault plane model

To convert from TWT into metres, we used a simple power function based on the velocity surveys from the Potoroo-1 and Gnarlyknots-1A wells (Fig. 2a). This depth conversion was used to create displacement plots and to estimate fault plane angles in order to translate throw into displacement (Fig. 2b). The velocity and frequency of the 3D seismic dataset is *ca.* 2200 m s⁻¹ and *ca.* 55 Hz, respectively, in the Cenozoic interval and *ca.* 3500 m s⁻¹ and *ca.* 25 Hz, respectively, between the upper and lower depth limits of the top Albian horizon. Therefore, the vertical resolution of the 3D seismic data-

set decreases from *ca.* 10 m in the Cenozoic interval to *ca.* 35 m at the top Albian horizon, where our deepest displacement measurements are made (Fig. 1a).

Constraining fault evolution

The faults analysed in this study are generally listric normal faults. Therefore, the fault plane angle shallows with depth and consequently the heave-to-throw ratio increases. To analyse the evolution of these faults, both throw and heave are accounted for by using fault plane dip-slip displacement. We propose a depth converted and simplified fault plane model (Fig. 3b), where fault plane dip measurements (Fig. 3d) are used to translate throw into dip-slip fault plane displacement (Fig. 3b), which we refer to simply as displacement.

We employ four methods to study the structural evolution of the four major fault systems that are observed within the seismic 3D survey. The first involves displacement–distance (*D*-*x*) graphs and displacement backstripping. Analysis of both the Cenomanian–Santonian and post-Santonian fault systems employs the ‘vertical subtraction method’ (Chapman & Meneilly, 1991; Childs *et al.*, 1993; Dutton & Trudgill, 2009; Jackson & Rotevatn, 2013). This method allows the displacement variation at the time of deposition of a given horizon to be determined by subtracting the displacement of the given horizon from displacement values of deeper horizons (Chapman & Meneilly, 1991; Childs *et al.*, 1993; Dutton & Trudgill, 2009; Jackson & Rotevatn, 2013). While using the ‘vertical subtraction method’, we also include heave to establish absolute displacement. It should be noted that *D*-*x* plots are mainly used to identify large variations in displacement. Smaller displacement minima and maxima cannot be identified due to the arbitrary $\pm 10\%$ displacement error we have allowed for seismic resolution and human error. This provides *ca.* 150 m and *ca.* 970 m of error for the shallowest and deepest measurements respectively. This allows for the 10–35 m of seismic resolution error and the potentially much larger error that can occur through interpretation. We believe this amount of error is sufficiently warranted given the size of fault segments observed in map view (5–15 km), the difficulty in interpretation around fault linkage points, and the high degree of displacement (up to *ca.* 8 km) and bed rotation at the deeper limit of measurements. We also have included this $\pm 10\%$ error for depth measurements and expansion index measurements in the following two methods, based on the same reasoning discussed above. Data maxima and minima are not considered when measurement error bars overlap. The $\pm 10\%$ displacement error for the data is displayed on the graphs as an envelope bordered by the upper and lower limits of error.

The second method employs displacement–depth (*D*-*z*) graphs, which allow vertical segmentation and dip-linkage to be identified (Childs *et al.*, 1996; Mansfield & Cartwright, 1996; Rykkelid & Fossen, 2002; Baudon & Cartwright, 2008; Jackson & Rotevatn, 2013).

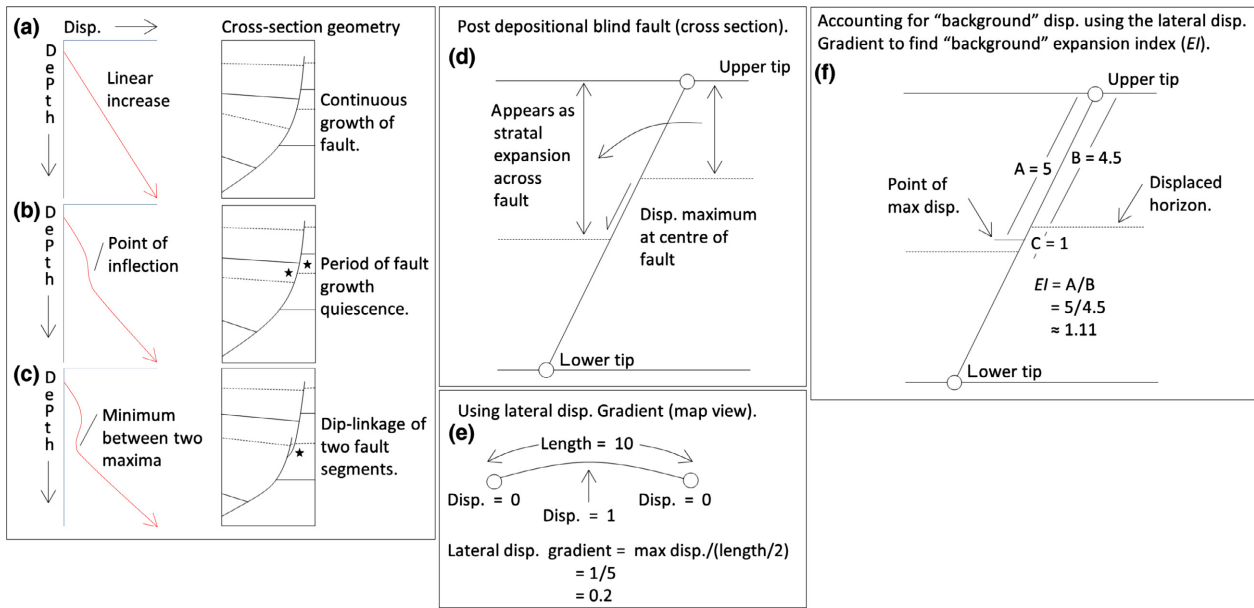


Fig. 3. (a; b; c) Expected patterns on displacement–depth (*D*–*z*) graphs with examples of cross-section geometry for continuous growth and a linear increase in displacement with depth (a), two growth stages of the same fault separated by a period of fault growth quiescence, causing a point of inflection in the graph (b) and dip-linkage of two initially isolated fault segments, creating a displacement minimum between two maxima (c). (d) Schematic diagram of a post-depositional blind fault showing how increasing displacement down a fault plane, from the upper tip, may be mistakenly observed as stratal expansion. (e) Calculation of lateral displacement gradient of a normal fault in map view with a length of 10 units and maximum displacement of 1 unit. (f) Use of lateral displacement in the vertical cross-section as a gauge to ‘calibrate’ against ‘background’ displacement potentially attributed to post-depositional blind faulting. This enables the calculation of the ‘background’ expansion index (*EI*). Any stratal unit which exceeds the background *EI* may be considered as stratal expansion from fault growth.

Measurement of displacement was conducted at fault segment centres, perpendicular to fault strike. The $\pm 10\%$ depth and displacement error range for the data is displayed on the graphs. A linear increase in displacement with depth was interpreted as continuous fault growth (Fig. 3a). A significant upward decrease in displacement, but with no displacement minima, was interpreted as evidence of fault reactivation (Fig. 3b) and displacement minima with error bars that do not overlap with maxima were interpreted as locations of dip-linkage (Fig. 3c). However, the complete interpretation of how the fault systems evolved and interacted takes into account all *D*–*z* profiles, in addition to all other measured data.

The third method uses expansion index (*EI*) graphs. This approach is used to identify intervals of syn-depositional faulting by documenting the thickness variations of stratal units across faults. However, to clearly show the onset of growth faulting and interaction with the free surface, we need to highlight elevated expansion indexes. A post-depositional blind fault can be misinterpreted to have expansion across the fault, when in fact this is simply an increase in displacement towards the centre of the fault (Fig. 3d). To account for any possibility of blind faulting appearing as stratal expansion, we use the highest lateral displacement gradient found in the fault array (see example, Fig. 3e) to propose a ‘background’ displacement gradient, which can be calculated as a ‘background’ *EI* in the vertical section (Fig. 3f). Calculation of the background

EI for this study can be found in the results. We have measured stratal thickness parallel to, and based on calculations from, the fault plane model used for *D*–*x* analysis. Therefore, we are accounting for bed rotation and maintaining true stratal thickness, rather than measuring vertically (see *EI1*, *EI2* and *EI3*, Fig 2b). Stratal units above horizon 6 (late Santonian) were measured using the upper fault plane angle (*EI1*), units between horizon 6 and 4 (top Cenomanian) were measured using the middle fault plane angle (*EI2*) and the lowest (Cenomanian) stratal unit was measured with the lower fault plane angle (*EI3*; Fig 2b).

The fourth method involves isochron mapping, which identifies thickness variations in stratal units in relation to the accommodation space provided through syn-depositional faulting. The dips of the listric faults analysed in this study decrease with depth from as high as 70° to as low as 12° (Fig. 2). Therefore, heave (horizontal displacement) increases with depth, along with an increase in hanging wall bed rotation. Consequently, fault polygons on horizon maps increase in size, with depth and thickness variations due to syn-depositional faulting could not be identified below the top Cenomanian horizon. However, we have performed isochron mapping to study normal fault growth within the post-Cenomanian strata. Burial and post-burial-related compaction of stratal units may result in errors in lateral and vertical displacement analysis (Taylor *et al.*, 2008; Giba *et al.*, 2012). We have

decided not to include any decompaction calculations in this study as our primary interest is in the along-strike variation in displacement on individual fault segments, rather than quantifying the total amount of displacement.

MEASUREMENT OF SYNKINEMATIC STRATA

Present-day geometry of the fault array and the detachment surface

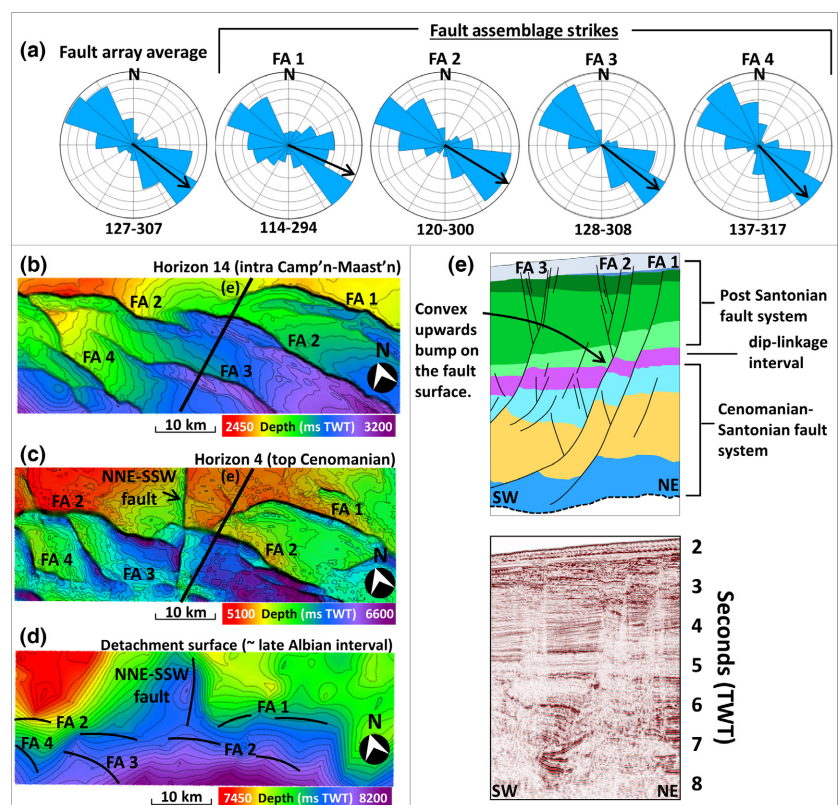
The faults described in this study comprise four along-strike assemblages of linked fault segments, which have an average strike of 127–307° (Fig. 4a). There is a basinward separation of approximately 10 km between the four strike-linked assemblages in the SE of the 3D survey, and this separation decreases towards the NW corner of the 3D survey, where FA2 is linked to FA4 (Fig. 4b–d). The fault assemblages (FA) are termed FA 1, 2, 3 and 4, with FA 1 being the furthest NE (landward) and FA 4 being the furthest SW (basinward). The average strikes of FA 1, 2, 3 and 4 are 114–294°, 120–300°, 128–308° and 137–317°, respectively (Fig. 4a). For the purposes of displacement analysis, we have divided the faults vertically into two geometrically distinct fault systems (Cenomanian–Santonian and post-Santonian), which correspond to the two stacked deltas (Fig. 4e). The vertical separation is based on geometric irregularities in the fault surfaces at the approximately the top Santonian level, with the presence of a convex upwards bump on the fault surface (Fig. 4e).

The Cenomanian–Santonian fault system (Fig. 4e) soles out below horizon 3 (top Cenomanian), with dips of 38–50° decreasing to as low as 12°, giving it a typical listric character. The post-Santonian fault system (Fig. 4e) is much steeper, with fault dips between 50–70°, which do not shallow out with depth. The Cenomanian–Santonian fault system also contains one major NNE–SSW striking fault (Fig. 4c, d) that laterally extends across the entire 3D survey. However, this fault has not been considered in detail in this study, as detailed displacement analysis cannot be performed due to poor seismic imaging of the fault. Post-Santonian faulting with this orientation is not observed in the 3D seismic data, and this is potentially suggestive of a distinct difference in the processes controlling the genesis of the gravity-driven Cenomanian–Santonian fault system in contrast to the more organised fault assemblages of the post-Santonian fault system. The late Albian detachment surface has plateaus in the NW and NE quadrants of the 3D survey, and gently slopes to the SW in the southern half of the survey (Fig. 4d). The four fault assemblages that we have mapped (Fig. 4d) are located on this SW dipping slope, and between the NW and NE plateaus in the central-northern region of the 3D survey, there is a low in the detachment surface.

Displacement-distance analysis

The Cenomanian–Santonian fault system occurs within stratal units 1–4 (Cenomanian–late Santonian; Fig. 1a). Initial displacement is highly variable along strike for all four fault assemblages (Fig. 5a–d). This is indicated by

Fig. 4. Cenomanian–Coniacian and post-Santonian fault geometry revealed through average fault array and individual fault assemblage (FA) strike orientations (a) and intra Campanian–Maastrichtian (b), top Cenomanian (c) and detachment surface (d) depth maps. An interpreted cross-section (e) is also shown to distinguish the nomenclature of vertically isolated ‘fault systems’ from laterally distinct ‘fault assemblages’. Note the convex upwards bump on the fault surface, which vertically separates the ‘fault systems’.



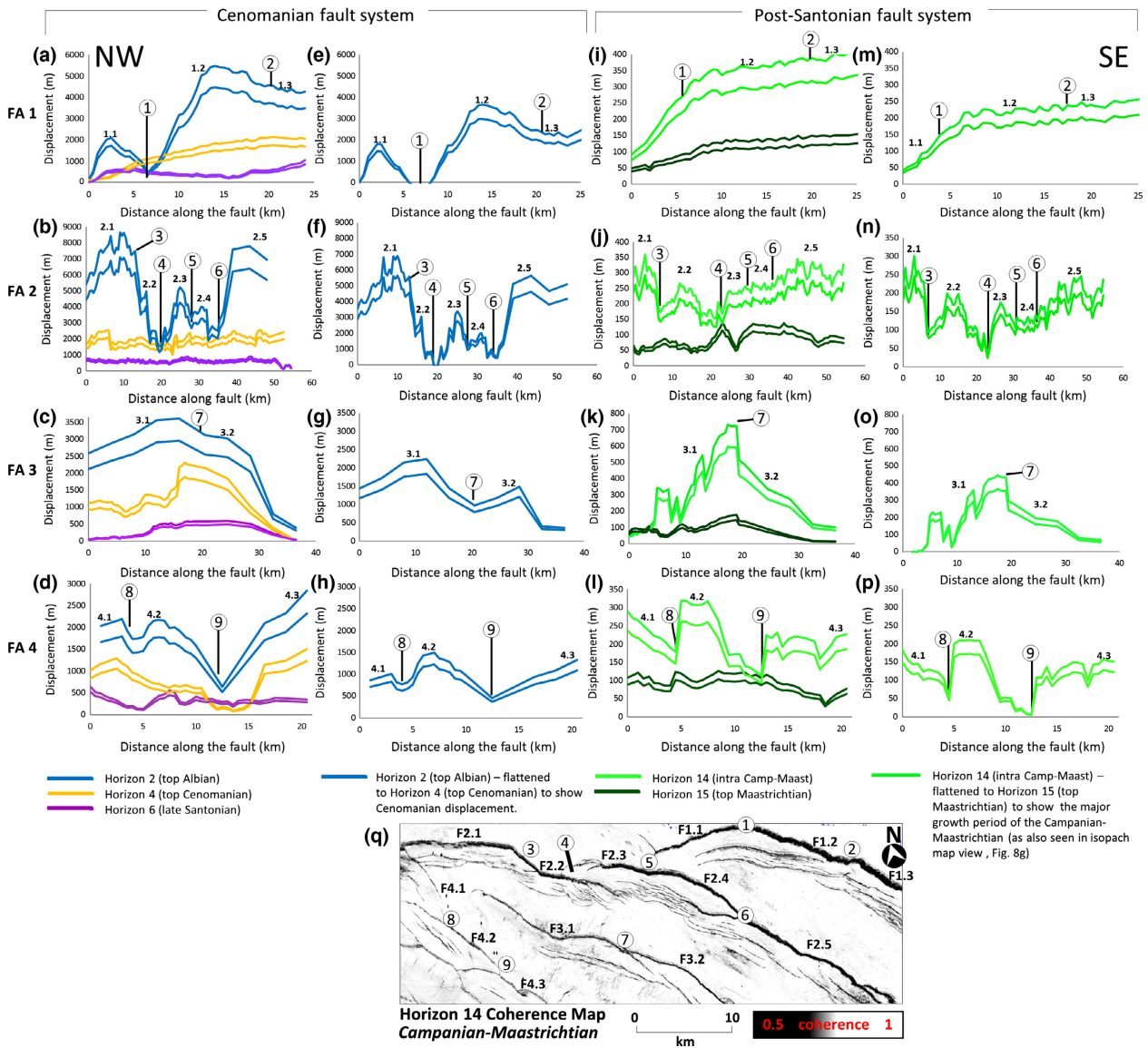


Fig. 5. Displacement–distance (D - x) graphs for the Cenomanian–Santonian (a–d) and post-Santonian (i–l) fault assemblages (FA) 1, 2, 3 and 4. Fault assemblages are along-strike linked normal fault segments as defined in Fig. 2. Cenomanian–Santonian (e–h) and post-Santonian (m–p) graphs have been backstripped to show total displacement during these intervals using the ‘vertical subtraction method’ (Chapman & Meneilly, 1991; Childs *et al.*, 1993; Dutton & Trudgill, 2009; Jackson & Rotevatn, 2013). The $\pm 10\%$ displacement error for the data is displayed on the graphs as an envelope bordered by the upper and lower limits of error. Coherence map (q) shows fault segment centres and linkage points, which correlate to the graphs. See Fig. 1a for colour scheme and horizon correlation with geological ages.

displacement backstripping of the top Cenomanian horizon from the top Albian horizon (Fig. 5e–h). Fault assemblage 1 has three displacement maxima corresponding to the centres of faults 1.1 and 1.2 (1640 m and 3300 m, respectively), with displacement decreasing smoothly from the centre of fault 1.2 to fault 1.3 (2080 m) (Fig. 5e). Cenomanian displacement maxima of faults 1.1 and 1.2 are completely isolated from each other after backstripping (Fig. 5e).

Fault assemblage 2 also exhibits highly variable Cenomanian displacement along strike (Fig. 5f), with maxima occurring at the centre of faults 2.1 (6300 m), 2.3 (3085 m), 2.4 (1850 m) and 2.5 (5150 m). The displace-

ment maximum at the centre of fault 2.2 (2785 m) overlaps with the error range associated with the slight displacement minimum at location 3 (Fig. 5f). Therefore, this is not considered an interpretable displacement maximum. Cenomanian displacement at the centre of faults 2.1 and 2.2 is completely isolated from faults 2.3, 2.4 and 2.5 (Fig. 5f). Displacement along FA 3 (Fig. 5g) is comparatively more homogeneous than along FA 1 and 2 (Fig. 5e, f). The displacement maxima occur at the centre of faults 3.1 and 3.2 (2050 m and 1350 m, respectively), with a localised minimum in between. Similarly, FA 4 has a relatively lower displacement variance (Fig. 5h). However, displacement maxima still occur at the centre of

faults 4.1, 4.2 and 4.3 (925 m, 1370 m and 1214 m, respectively), separated by displacement minima.

The post-Santonian fault system is developed within stratal units 6–9 (Fig. 1a) and it generally displays displacements on the hectometre scale (Fig. 5i–p), as opposed to the kilometre-scale displacement associated with the Cenomanian–Santonian fault system (Fig. 5a–h). Displacements of horizons 14 and 15 along fault assemblages are observed and displayed (Fig. 5i–l), with horizon 14 then backstripped by subtracting horizon 15 (Fig. 5m–p). Horizons 14 and 15 are the upper and lower bounding surfaces to the major post-Santonian growth interval (stratal unit 7).

Displacement during this growth interval is quite variable along strike for fault assemblages 2, 3 and 4 (Fig. 5n–p) but is quite smooth and decreases towards the western tip-line on FA 1 (Fig. 5m). The relative variability in displacement of FA2 is quite similar to that observed in the underlying Cenomanian–Santonian fault system (Fig. 5f), with hectometre-scale displacement maxima occurring at the centre of faults 2.1, 2.2, 2.3, 2.4 and 2.5, which are separated by displacement deficits ranging from *ca.* 230 m to 50 m (Fig. 5n). However, there is also some inter-segment displacement variability along FA 2 on the decimetre scale (Fig. 5n). FA 3 also exhibits hectometre scale variability in displacement (Fig. 5o). However, displacement maxima do not coincide with the centres of faults 3.1 and 3.2 (Fig. 5o). There is high displacement variability west of the centre of fault 3.1 (Fig. 5o). Despite this variability, the overall displacement along FA 3 is a generally bell-shaped, with maximum displacement at the centre of the fault assemblage (Fig. 5o). Fault assemblage 4 (Fig. 5p) exhibits high displacement variability along-strike with maxima observed at the centre of faults 4.2 and 4.3, and displacement of fault 4.1 increasing to the west, where it displays linkage to fault 2.1. Fault 4.3 has decimetre-scale, intra-fault displacement variability, which implies that it may have grown via the linkage of smaller fault segments (Fig. 5p).

Displacement–depth analysis

Continuous growth, fault reactivation and dip-linkage can be discriminated by observations of fault geometry in cross-section (Fig. 6) and the analysis of D - z graphs (Fig. 7; Fig. 3a–c), which display displacement measurements vertically down the fault plane. Continuous growth is manifested by a linear relationship with displacement increasing with depth (Fig. 3a). Fault reactivation will exhibit a significant upward decrease in displacement gradient or an upward steepening of the D - z graph at a point of inflection, between two intervals of increasing displacement with depth (Fig. 3b). Finally, dip-linkage is evident by a D - z graph having two displacement maxima at depth, separated by a displacement minimum (Fig. 3c). Displacement minima occur at the centre of faults 1.2, 2.1, 2.5, 3.1, 3.2, 4.1 and 4.2, most commonly at the late Santonian horizon (F1.2, 2.1, 2.5, 3.1, Fig. 7), but also in

early Campanian strata (F3.2, 4.1, Fig. 7) and at the intra Turonian–Santonian horizon (F4.2 Fig. 7). Faults 1.1, 2.2, 2.3 and 2.4 display a steep D - z profile (point of inflection) between Cenomanian–Santonian and post-Santonian intervals of increasing displacement with depth (Fig. 7).

It appears that faults 1.1, 2.2, 2.3 and 2.4 of the post-Santonian fault system did not grow in vertical isolation, but rather developed due to reactivated growth of the Cenomanian–Santonian fault system. The locations of these reactivated Cenomanian–Santonian faults are quite proximal to one another in the northern central region of the 3D survey, which implies that fault reactivation is not sporadic in terms of location, but rather has occurred in this specific area, where FA 1 is proximal to the centre of fault FA 2. (see coherence map, Fig. 2d).

Expansion index analysis

According to our D - x analyses, the highest lateral displacement gradient observed in the fault array occurs on the SE side of fault 1.1 and the NW side of fault 1.2 (Fig. 5e), with a lateral displacement gradient of 0.56 from the centre of these faults to the displacement deficit in between these faults. A vertical displacement gradient of this magnitude corresponds to an expansion index of *ca.* 1.38 (see Fig. 3f for method). Again, we have included $\pm 10\%$ error when calculating EI for the same reasons outlined in the Methods section. Therefore, any expansion index less than or equal to 1.52 has been considered as potentially indicative of blind faulting, and any expansion index greater than 1.52 has been considered to be indicative of fault growth involving interaction with the free surface.

Down-dip cross sections through the seismic data show thickening of hanging wall sediments towards the fault plane, indicating that the earliest syn-kinematic strata occur within the Cenomanian interval (Fig. 6). Elevated expansion indexes are observed within Cenomanian strata, with indexes ranging from 2.0 to 3.4 on all faults and an array average of 2.4 (Fig. 8). Fault assemblage 2 displays elevated expansion indexes within Turonian–late Santonian strata on all fault segments (Fig. 8c–g). A later stratal expansion is also observed in the latest Cretaceous (stratal unit 7) on faults 1.2, 2.1, 2.2, 2.3, 2.4, 4.1 and 4.2, with expansion indexes ranging from 1.6 to 3.4 (Fig. 8b–f, j, k). Faults 2.5 (Fig. 8g) and 4.2 (Fig. 8k) have elevated expansion indexes of 2.1 and 3.2 in the Cenozoic interval (stratal units 8 and 9).

Isochron mapping

The isochron of stratal unit 3 (*ca.* Turonian?) displays thickening of hanging wall sediments towards each fault, indicating continued growth of the fault assemblages after the Cenomanian (Fig. 9k). Stratal unit 4 is bounded by horizons 5 and 6, which have an unknown absolute age due to lack of well control (Fig. 1a). Therefore, the age of

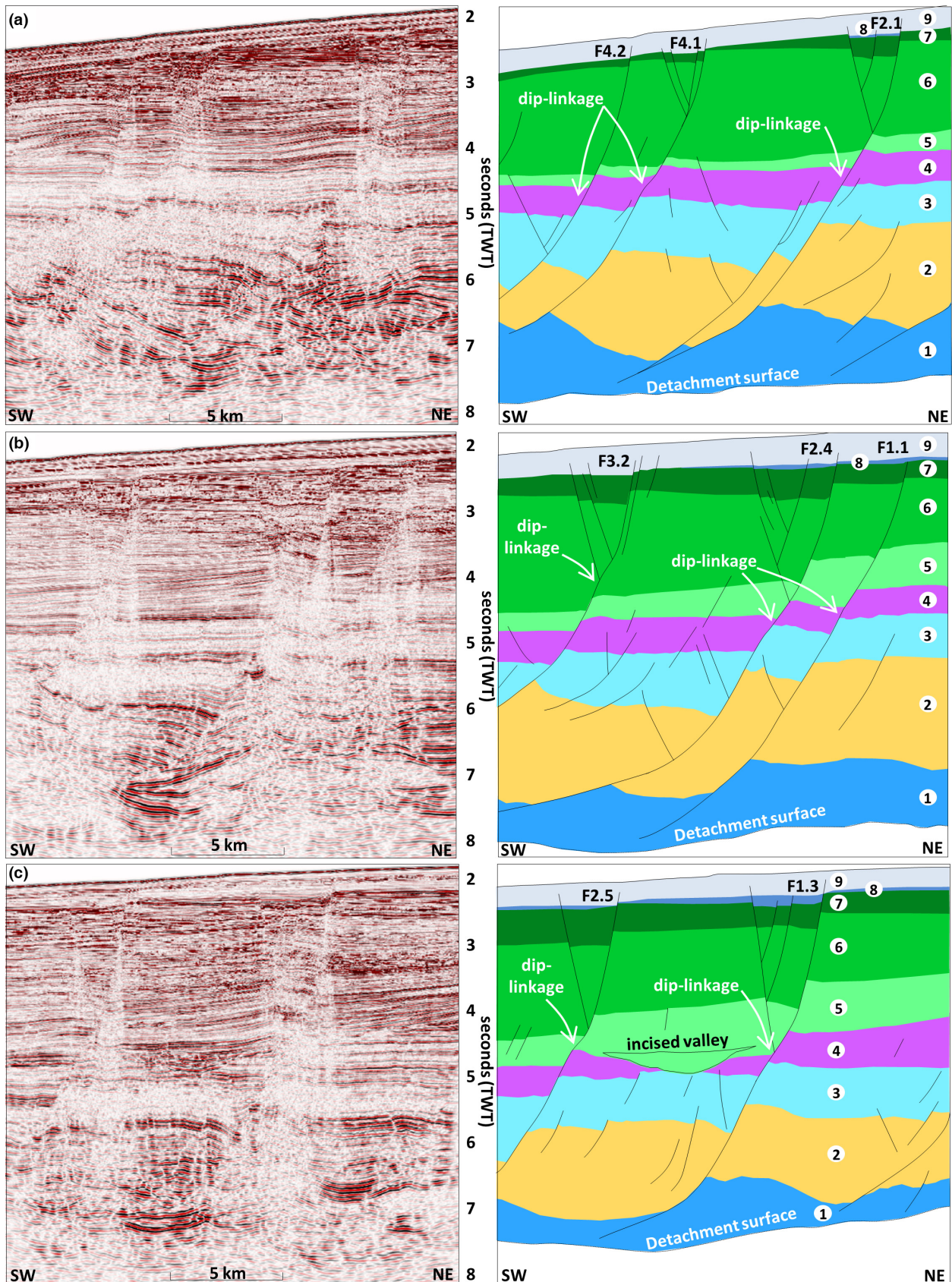


Fig. 6. Seismic cross-sections of down-dip arbitrary lines through the 3D reflection survey (left column) with interpreted cross-sections (right column). Arbitrary lines (a), (b) and (c) and in order from west to east, respectively (See Fig. 3d, for locations of these arbitrary lines). These cross-sections highlight growth strata (stratal units 2, 3, 7, 8 and 9), dip-linkage at the top of stratal unit 4 and the dip-linkage through stratal unit 6 (b). See Fig. 1a for reference to colour scheme and stratal units displayed on cross-sections.

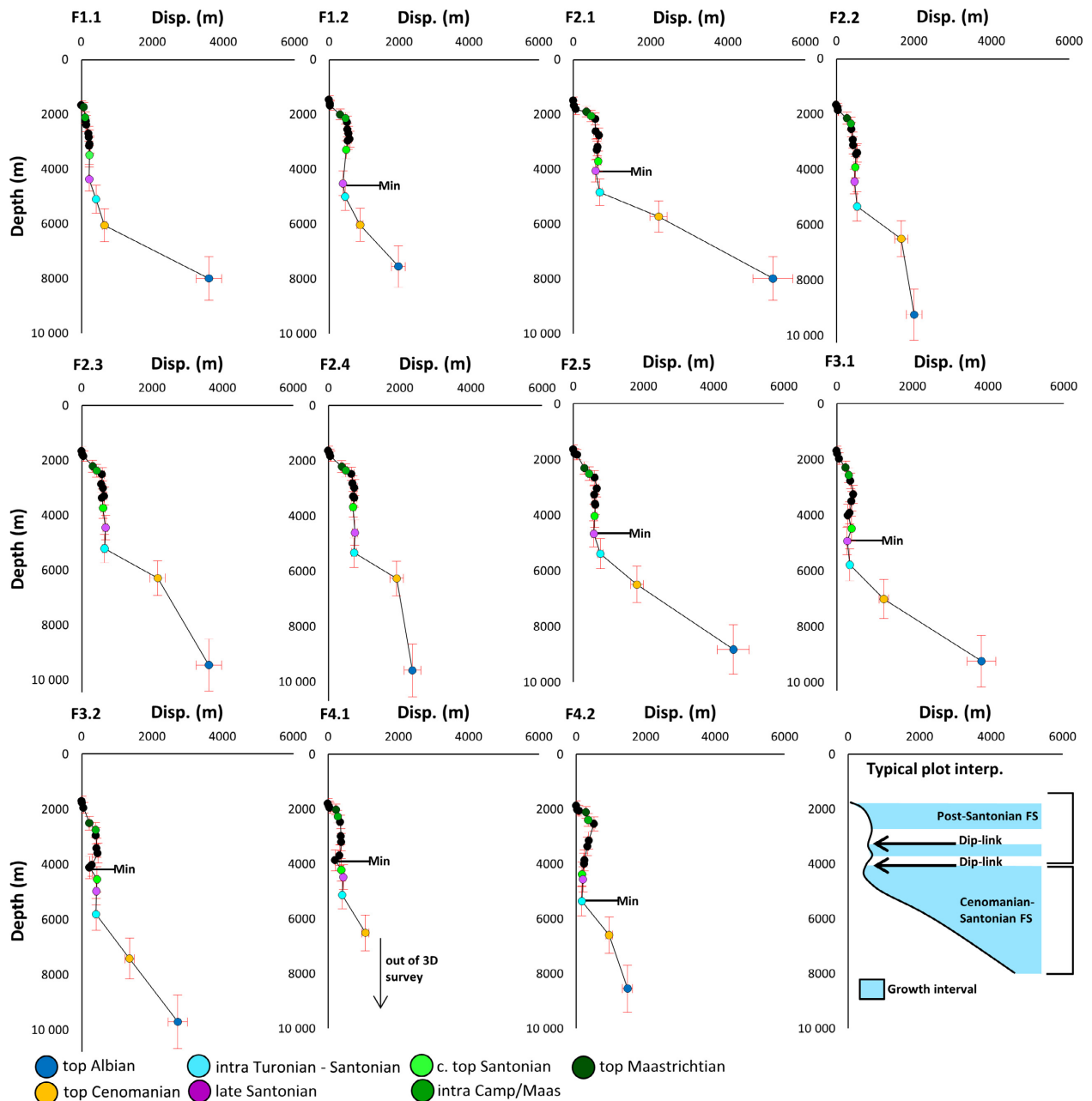


Fig. 7. Displacement-depth ($D-z$) graphs of fault segments 1.1, 1.2, 2.1, 2.2, 2.3, 2.4, 2.5, 3.1, 3.2, 4.1 and 4.2, with a typical plot interpretation (bottom right). Measurements of $D-z$ graphs were at the displacement centre of fault segments. Note the displacement minima occurring at the early Campanian, late Santonian and intra Turonian-Santonian horizons (Min), showing linkage between the Cenomanian-Santonian and post-Santonian fault systems (FS) as outlined in Fig. 2e. We have added 10% y-axis error bars to account for seismic resolution and human error. Interpretation of displacement minima required no overlap of error bars.

stratal unit 4 can only be constrained to intra Turonian-Santonian (Fig. 1a). The isochron map of stratal unit 4 (intra Turonian-Santonian) shows only faults 2.1, 2.2 and potentially 3.2 displaying thickening of hanging wall sediments (Fig. 9j). The top of stratal unit 4 is heavily eroded, with erosion mainly affecting the eastern third of the 3D survey including a 6 km-wide, N-S trending, incised valley (Fig. 9d). The thickness of stratal unit 4 across the study area is relatively homogenous, apart from the incised valley in the far east of the survey, which has completely eroded stratal unit 4 in some areas (Fig. 9j). This

incision is also evident in the isochron map of stratal unit 5 (latest Santonian; Fig. 9i), which exhibits easterly thickening towards this incision. Stratal unit 5 also shows no sign of fault-related thickening (Fig. 9i).

The late Santonian-Maastrichtian deltaic sequence was divided into three distinct seismic stratal units (Fig. 1a). The oldest late Santonian-Maastrichtian stratal unit is Stratal unit 5. This is characterised by an easterly thickening package, which infills the erosional surface (top stratal unit 4) (Figs 6 and 9i). This package is of late Santonian age, with the top Santonian (horizon 7) marking the top

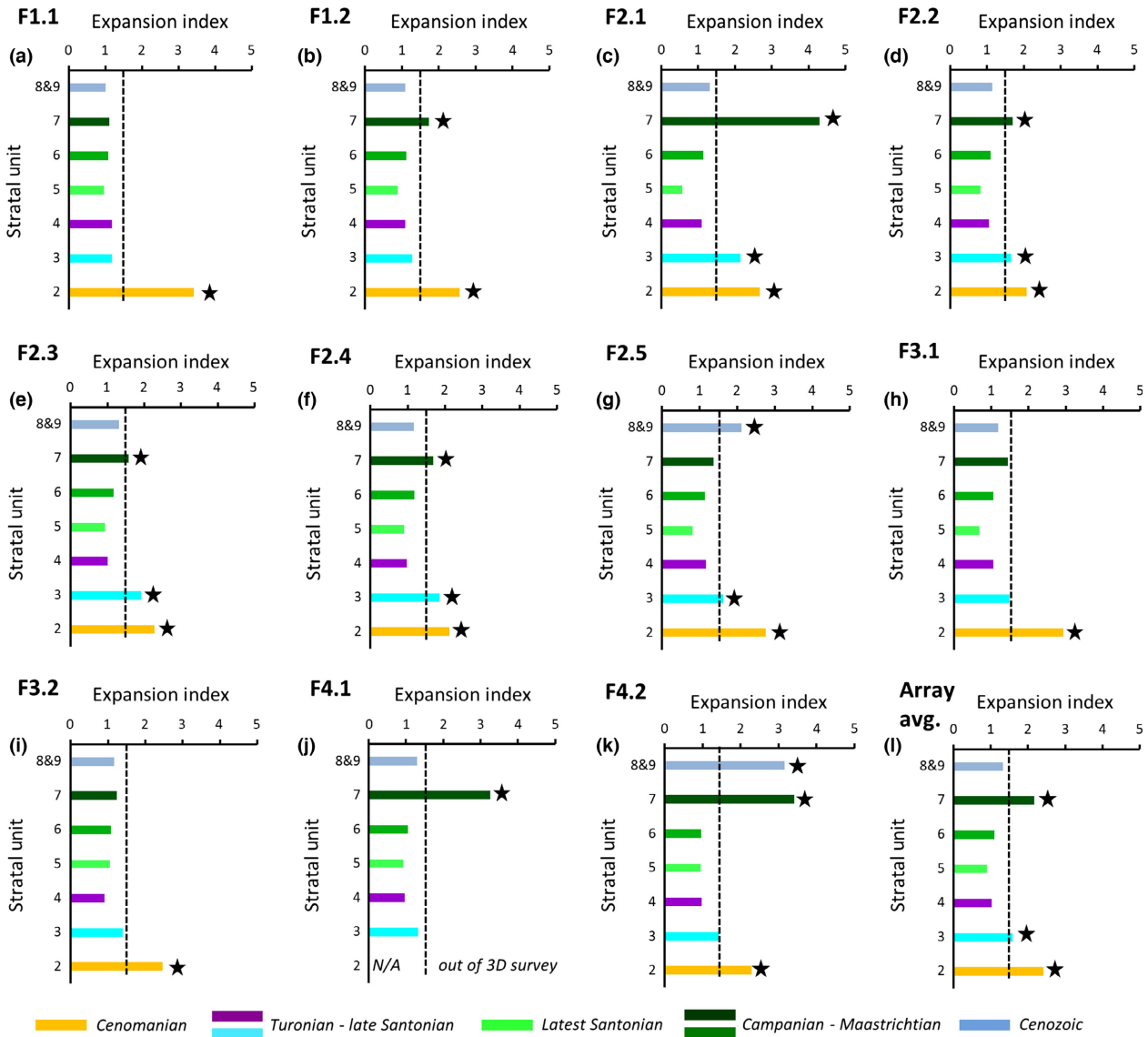


Fig. 8. Expansion index graphs, as employed by Thorsen (1963), measured across the centre of fault segments 1.1, 1.2, 2.1, 2.2, 2.3, 2.4, 2.5, 3.1, 3.2, 4.1 and 4.2 (see Fig. 3d for fault segment locations). The dashed vertical line on each graph indicates a growth index of *ca.* 1.52, revealing values that exceed 1.52 (highlighted by star), which are indicative of syndepositional fault growth. Anything less than 1.52 may be attributed to blind faulting. See expansion index methodology and results for further detail.

of this stratal unit. This is followed by Stratal unit 6, which is of Campanian-Maastrichtian age, and exhibits some minor sediment thickening in the hanging walls of faults (FA 2, fault 1.1 and possibly faults 3.2 and 4.1; Fig. 9h) and has a progressive basinward thickening and a strongly progradational geometry (Totterdell *et al.*, 2000). However, expansion indexes of stratal unit 6 average 1.09 and are not elevated above the potential blind fault range (Fig. 8). Therefore, this time interval is not considered to be a period of fault growth. The final late Santonian-Maastrichtian stratal unit is Stratal unit 7, which is also of Campanian-Maastrichtian age. Isochron mapping shows a major period of fault growth during the deposition of stratal unit 7, with all faults displaying thickening of hanging wall sediments (Fig. 9g). Thickening along all fault assemblages during the deposition of stratal unit 7 appears quite homogenous across fault seg-

ment centres and linkage points, with the exception of faults 2.2 and 2.3, between which there is an unbreached relay ramp (Fig. 9e). The nucleation and growth of antithetic faulting has not been analysed in detail in this study, but isochron mapping of stratal unit 7 (Fig. 9g), indicates that FA 1, 2 and 3 became surface breaching faults during the later stages of late Santonian-Maastrichtian deltaic deposition, evident by synkinematic strata thickening landward across antithetic faults.

EVOLUTION OF THE FAULT ARRAY

Nucleation and growth of the Cenomanian-Santonian fault system

Our detailed mapping suggests that the NW-SE striking Cenomanian-Santonian fault system (Fig. 4)

nucleated during or following the progradation of deltaic sediments over the late Albian interval that consists of ductile marine shales (Totterdell *et al.*, 2000; Totterdell & Bradshaw, 2004). This was a gravity-driven fault system on a gentle, SW-dipping detachment slope (Totterdell & Krassay, 2003). The Cenomanian–Santonian fault system consists of four NW–SE–striking fault assemblages (Fig. 4), totalling 13 fault segments, evident in map view fault geometry (Fig. 2d), with highly variable displacement along strike of all fault assemblages (Fig. 5). Displacement–distance measurements of all four fault assemblages indicate kilometre-scale Cenomanian displacement (Fig. 5e–h) and we also observe an average Cenomanian expansion index of 2.4 across the fault array (Fig. 8l). Based on our interpretation of the seismic data, we cannot determine the timing of fault length establishment, as we would need additional intra-growth package interpretation to provide evidence for the presence or absence of lateral fault propagation through time. Therefore, we cannot establish if these faults grew in accordance with the ‘segmented coherent fault model’ (Walsh *et al.*, 2002, 2003; Childs *et al.*, 2003) or in accordance with the ‘isolated fault model’ (Walsh & Watterson, 1988; Trudgill & Cartwright, 1994; Dawers & Anders, 1995; Huggins *et al.*, 1995; Cartwright *et al.*, 1995; Mansfield & Cartwright, 2001). Therefore, we propose two Cenomanian fault evolution models that encapsulate aspects of our observations that are consistent with both these possible growth models (Fig. 10b, c). The isochron between horizons 4 and 5 (stratal unit 3, likely Turonian–Coniacian) indicates continued growth of all fault assemblages during this period, with fault quiescence occurring during the deposition of stratal unit 4 (likely Santonian) shown by isochron mapping (Fig. 9j).

In summary, the evolution of the Cenomanian–Santonian fault system can be divided into three main stages. The first stage involves Cenomanian nucleation (Fig. 10a) resulting from gravitational instability and growth of fault segments via either: (1) isolated radial propagation and incidental linkage after substantial displacement accumulation in accordance with the ‘isolated fault model’ (Fig. 10b); or (2) rapid length establishment and full linkage of the system, with displacement then accumulating as a kinematically coherent system, in accordance with the ‘segmented coherent fault model’ (Fig. 10c). The second stage involves continued displacement of linked fault assemblages until approximately the end of the Coniacian followed by a period of Santonian fault quiescence, with minor displacement of faults 2.1 and 2.2 (Fig. 10d). The third and final stage is the breakup of Australia and Antarctica in the late Santonian and the initiation of sea floor spreading and regional uplift causing erosion (Totterdell & Bradshaw, 2004; MacDonald *et al.*, 2012a), with a 6 km wide N–S oriented incision and leaving no evidence for any fault growth during this period (Fig. 10e).

Nucleation and growth of the post-Santonian fault system

Following the onset of seafloor spreading at *ca.* 83 Ma (Veevers, 1986; Sayers *et al.*, 2001; Totterdell *et al.*, 2000), an influx and progradation of latest Santonian and Campanian-age deltaic sediments filled the geometric depression created by the late Santonian erosional surface, with easterly thickening of sediments observed within the study area (Fig. 9i). Subsequent thermal subsidence and deltaic loading induced post-Santonian faulting in the central Ceduna Sub-Basin, and the development of a series of growth faults known as the Kowari Fault Family in the SE of the Ceduna Sub-Basin (Totterdell *et al.*, 2000; Totterdell & Bradshaw, 2004; see fig. 18).

The faults analysed in this study generally exhibit displacement minima at the late Santonian horizon (F1.2, 2.1, 2.5, 3.1, Fig. 7), but also in early Campanian strata (F3.2, 4.1, Fig. 7) and at the intra Turonian–Santonian horizon (F4.2 Fig. 7) for faults 1.2, 2.1, 2.5, 3.1, 3.2, 4.1 and 4.2. In addition, we also observe irregularities in the form of a convex upwards bump on the fault surface at approximately the late Santonian level (Fig. 6). Therefore, it would appear plausible that faults 1.2, 2.1, 2.5, 3.1, 3.2, 4.1 and 4.2 of the post-Santonian fault system formed in vertical isolation from, and later dip-linked with, the Cenomanian–Santonian fault system. However, given that the displacement minima are relatively small, the possibility of reactivation and upward propagation of the Cenomanian–Santonian fault system is also conceivable (cf. Childs *et al.*, 1995; Walsh *et al.*, 2002, 2003; Giba *et al.*, 2012; Jackson & Rotevatn, 2013). Four faults (faults 1.1, 2.2, 2.3 and 2.4) have *D*–*z* profiles that are characteristic of fault reactivation, implying that they are the result of reactivation and upward propagation of the underlying Cenomanian–Santonian fault system (Fig. 7).

We have established that the growth of the post-Santonian fault system likely occurred during the latest Cretaceous, supported by elevated growth indexes above the proposed ‘background’ displacement gradient expected for a blind fault (stratal unit 7, Fig. 8). If the post-Santonian fault system nucleated in vertical isolation and later dip-linked with the Cenomanian–Santonian fault system, this may have involved linkage with a Cenomanian–Santonian fault system that was either active or dormant. There is incredibly strong similarity between the along-strike geometries of both fault systems (Fig. 4b, c), and displacement values on the *D*–*z* plots through the zone of dip-linkage display only minor deficits (Fig. 7). This implies that the post-Santonian fault system likely linked with an active Cenomanian–Santonian fault system, agreeing with conclusions from a similar study by Jackson & Rotevatn (2013) in the Suez Rift, Egypt. This particular study examined the interaction of a sub-salt basement fault system with a supra-salt fault system and concluded that coincidental linkage with a lower dormant fault system was unlikely, given the inherited geometry of the upper fault system and non-zero throw in the zone of

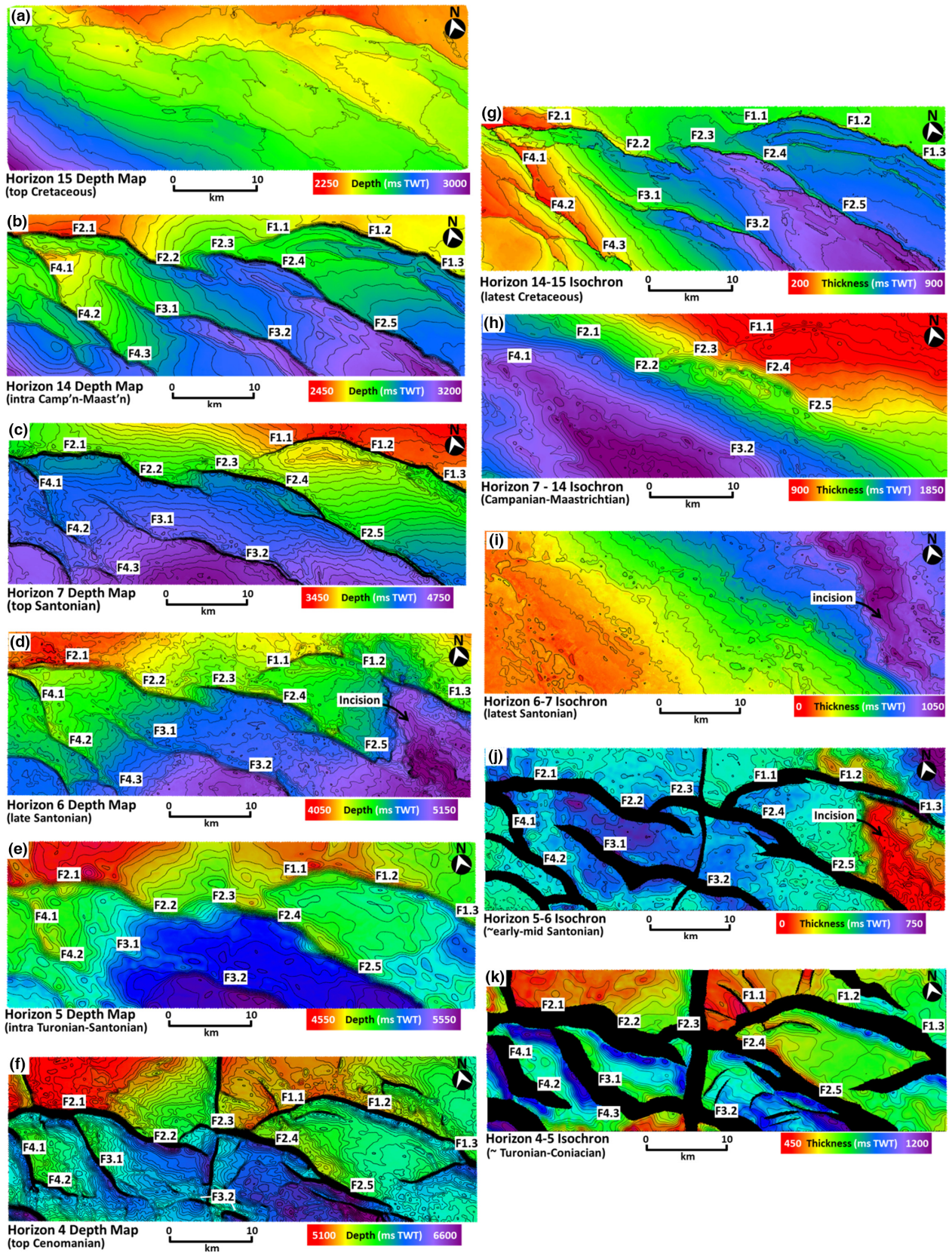


Fig. 9. Depth-structure maps of seismic horizons: H15 (a), H14 (b), H7 (c) H6 (d), H5 (e) and H4 (f). All maps have a contour interval of 50 ms TWT. Isochron maps of key stratal units are show in the right column including stratal unit 7 (g), stratal unit 6 (h), stratal unit 5 (i), stratal unit 4 (j) and stratal unit 3 (k). These isochron maps also have a contour interval of 50 ms TWT. All faults have been labelled on horizon maps and on isochron maps where display control on sediment deposition.

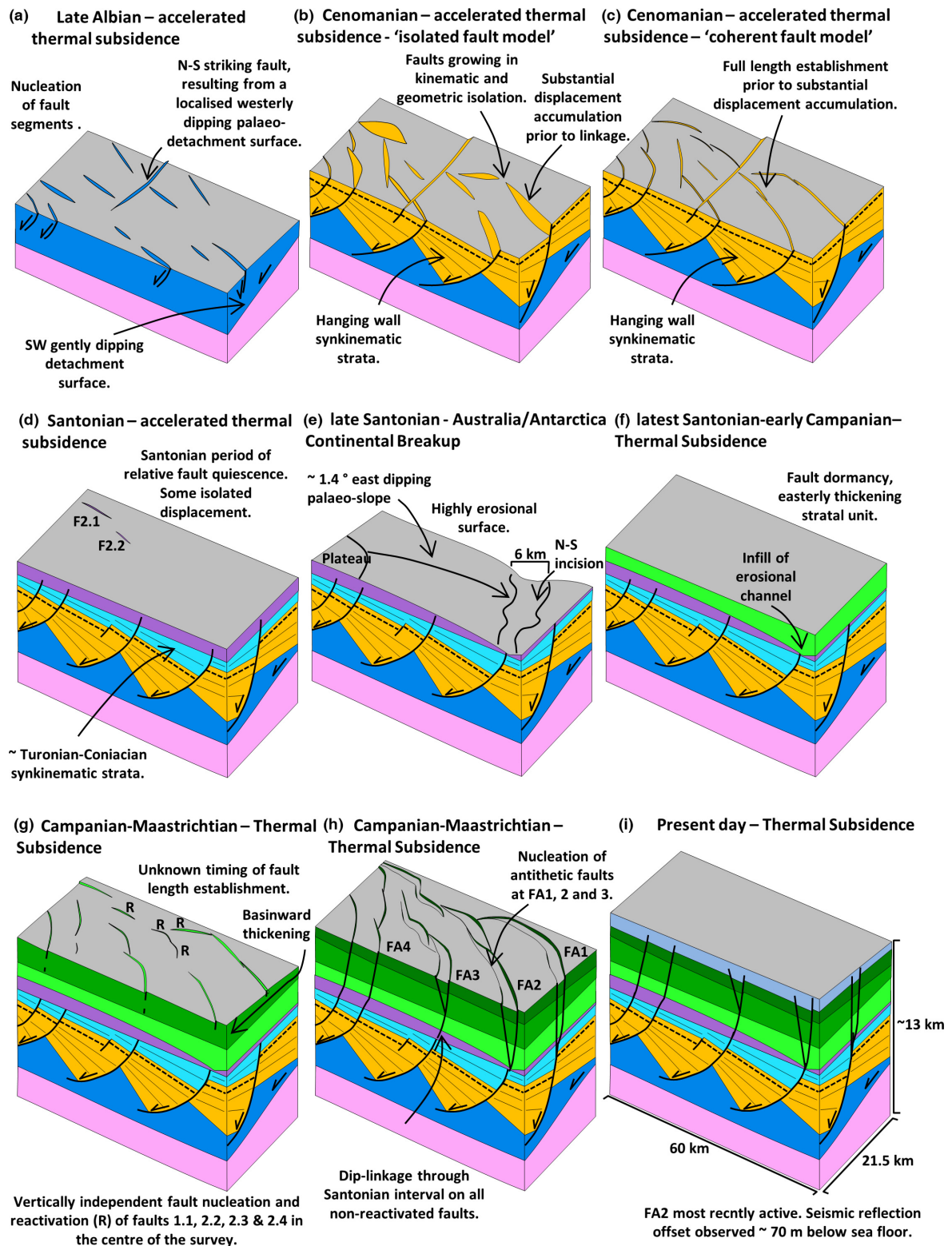


Fig. 10. Structural evolution of the fault array. Stages (a) to (d) exhibit accelerated thermal subsidence, inducing nucleation of isolated fault segments on a SW dipping detachment surface and subsequent kilometre-scale displacement. Erosion during the Australia/Antarctica continental breakup (e) created an easterly dipping palaeoslope towards a 6 km wide, north-south oriented incision in the east of the 3D reflection survey. Latest Santonian-early Campanian fault dormancy followed continental breakup with infill of the erosional surface (f). Campanian-Maastrichtian return to thermal subsidence with nucleation of the post-Santonian fault system and reactivation of the Cenomanian-Santonian fault system (g). Continued Campanian-Maastrichtian thermal subsidence and deltaic loading induced nucleation of antithetic faulting and substantial displacement on major faults, likely creating dip-linkage with the Cenomanian-Santonian fault system during this stage (h). Thermal subsidence until present day has caused continued displacement into the Cenozoic carbonate succession of the Eucla Basin (i).

linkage (Jackson & Rotevatn, 2013). Therefore, we conclude that the Cenomanian–Santonian fault system had a strong control over the development of the post-Santonian fault system.

There is smaller (decimetre) scale, inter-segment displacement variability evident in the post-Santonian fault system, which suggests that this fault system may have grown from smaller-scale fault segments, relative to the Cenomanian–Santonian fault system (Fig. 5m–p). Displacement–distance plots (Fig. 5m–p) for all four fault assemblages indicate hectometre-scale displacement during the latest Cretaceous (stratal unit 7), and we observe an average expansion index of 2.2 across the fault array during this period. (Fig. 8l). The post-Santonian fault system remained active into the Cenozoic, evident by faults propagating into the Cenozoic interval to depths as shallow as *ca.* 70 m below the seafloor (Fig. 6). However, only faults 2.5 and 4.2 show evidence for interaction with the free surface and syn-depositional growth with elevated expansion indexes of 2.1 and 3.2 (Fig. 8g, k). Other displacements observed on all faults within the Cenozoic interval potentially accrued without and interaction with the free surface.

In summary, our interpretation of the growth of the post-Santonian fault system (Fig. 10) can be divided into four stages: (1) early Campanian fault dormancy following continental breakup between Australia and Antarctica (Fig. 10f); (2) Campanian–Maastrichtian (stratal unit 7; Fig. 1a) nucleation of fault segments with unknown timing of fault length establishment and reactivation and upward propagation of Cenomanian–Santonian faults 1.1, 2.2, 2.3, 2.4 (Fig. 10g); (3) full along-strike linkage of the fault assemblages by the end of the Cretaceous, interaction of antithetic faults with the free surface and likely dip-linkage of the post-Santonian fault system with the Cenomanian–Santonian fault system during this stage (Fig. 10h); and (4) Cenozoic growth of faults 2.5 and 4.2 and blind faulting reactivation of all other faults, creating offset of seismic reflections as shallow as *ca.* 70 m below the seafloor (Fig. 10i).

DISCUSSION

Relationship between the Cenomanian–Santonian and post-Santonian fault systems

The aim of this study was to constrain the structural evolution of four Upper Cretaceous–Cenozoic age normal fault assemblages comprising hard-linked fault segments that detach in a shale of late Albian age at an extensional delta top setting. We have demonstrated the segmented growth of these fault assemblages and the interaction of two temporally and spatially isolated delta systems (Fig. 4e). There is a clear spatial relationship between the Cenomanian–Santonian fault system and the post-Santonian fault system. In map view, the geometries of the two fault systems are almost identical (Fig. 4b, c). Furthermore, all faults display either dip-linkage through the

Turonian–early Campanian level, or reactivation of the underlying Cenomanian–Santonian fault system (Fig. 7). This is supported by the concave upwards bump shape of the fault surface observed through the zone of dip-linkage (Fig. 6), which may imply the linkage of two active faults (Rykkeliid & Fossen, 2002), a process described as ‘active’ kinematic linkage, as opposed to static or coincidental ‘inheritance’ (Jackson & Rotevatn, 2013).

Based on these findings, we propose that the post-Santonian fault system nucleated in response to reactivation of the Cenomanian–Santonian fault system, resulting from gravitational instability in post-Santonian sediments. Therefore, the Cenomanian–Santonian fault system controlled the initiation and growth of the post-Santonian fault system. This may imply a vertical kinematically coherent relationship between the two fault systems and potentially greater kinematic coherence within the post-Santonian fault assemblages as they grew over an underlying and reactivating structural framework. Similar growth trends are observed in the Espirito Santo Basin, offshore Brazil, where pre-existing gravity-driven growth faults on the flanks of salt diapirs have reactivated, creating independent nucleation of upper fault segments and eventual dip-linkage (Baudon & Cartwright, 2008). However, dip-linkage along strike is considerably more variable on these salt structures, with reactivation by upward propagation of growth faults commonly occurring (Baudon & Cartwright, 2008).

Fault reactivation was interpreted to have occurred on faults 1.1, 2.2, 2.3 and 2.4, which implies that the Cenomanian–Santonian fault system was highly active during the latest Cretaceous in the central–northern portion of the study area. Fault assemblage 2 (Fig. 4c) also has the highest displacement accumulation (up to *ca.* 7900 m, Fig. 5b) during the Cenomanian–Santonian period, implying that potentially FA 2 maintained the greatest potential for fault displacement from the Cenomanian through to the Maastrichtian compared to other fault assemblages. The reactivation and transference of stress from nearby faults 2.2, 2.3 and 2.4 may have caused the reactivation of fault 1.1.

Implications for normal fault growth and hydrocarbon migration in delta systems

The evolution of normal faults in continental rift basins has been documented in increasing detail using 3D seismic data (Childs *et al.*, 1995; Walsh *et al.*, 1999; Jackson & Larsen, 2009; Kane *et al.*, 2010; Jackson & Rotevatn, 2013; Lewis *et al.*, 2013; Tvedt *et al.*, 2013). However, the detailed three-dimensional evolution of gravity-driven normal faults developed within delta systems on passive margins has not been extensively examined. Gravity-driven extension of sedimentary sequences along passive margins has been relatively well-documented using 2D cross sections and map view geometries (Anderson *et al.*, 2000) and 3D restorations of seismic data (Rouby *et al.*, 2002). Passive margin delta systems analogous to the

Ceduna Sub-Basin, that have been studied extensively, primarily in map view and cross section, include the Niger Delta (Doust & Omatsola, 1989; Morley & Guerin, 1996; Cohen & McClay, 1996; Bilotti & Shaw, 2005; Corredor *et al.*, 2005; Briggs *et al.*, 2006; Cobbold *et al.*, 2009) and the Gulf of Mexico (Buffler *et al.*, 1979; Winker & Edwards, 1983; Wu *et al.*, 1990; Rowan, 1997). These studies illustrate the large-scale structural complexities of deltaic systems, with delta-top extension typically transitioning basinward into a compressional toe thrust zone.

Our study shows that the structural development of the upper delta system is largely controlled by the lower (Cenomanian) delta system, through the reactivation of listric faults within the extensional province of the Cenomanian delta system. Structural control was through either upward propagation of Cenomanian listric faults within the lower delta system, or the nucleation of the upper (post-Santonian) fault system in response to gravitational instability in late Santonian–Maastrichtian sediments, directly above reactivating Cenomanian faults. This variation between upward propagation of listric faults from the lower delta, and dip-linkage of faults from the lower and upper deltas occurs throughout the study area, and highlights the complexity in fault plane development and interaction in stacked delta system settings. The structural control exerted by faults within the lower delta system, and the complex interplay between reactivation and dip-linkage in connecting the two fault systems has implications for the development of normal fault arrays at extensional delta-top settings in other delta systems around the world. This is likely to be especially true for stacked delta systems, such as the Gulf of Mexico (Buffler *et al.*, 1979; Winker & Edwards, 1983; Wu *et al.*, 1990; Rowan, 1997) and the Orange Basin, offshore Namibia (de Vera *et al.*, 2010).

Faults and associated damage zones may be permeable and act as conduits, permitting the vertical migration of hydrocarbons into shallower reservoirs, and/or cross-fault migration between juxtaposed sands (Smith, 1980; Allan, 1989; Hooper, 1991; Anderson *et al.*, 1994). However, faults may also be sealing, allowing for hydrocarbon entrapment and accumulation (e.g. Smith, 1980; Harding & Tuminas, 1989; Bouvier *et al.*, 1989; Jev *et al.*, 1993; Knott, 1993). Therefore, the findings of this study have direct implications for hydrocarbon migration. Cenomanian faults that are interpreted to have reactivated and propagated upwards (faults 1.1, 2.2, 2.3 and 2.4), may have allowed the migration of hydrocarbons from deep sources rocks into shallow reservoirs. However, the independent nucleation of post-Santonian faults, without initial upward propagation of Cenomanian faults, may have inhibited the upward migration of hydrocarbons, and this is a possible interpretation for faults 1.2, 2.1, 2.5, 3.1, 3.2, 4.1 and 4.2. Furthermore, all faults have propagated into the Cenozoic interval, displacing strata as shallow as *ca.* 70 m below the seafloor, with faults 2.5 and 4.2 displaying growth and interaction with the free surface during the

Cenozoic. Therefore, this highlights that recent fault reactivation and potential breach of fault dependent traps located along all fault assemblages analysed in this study represents an important risk to the preservation of hydrocarbons in this basin (MacDonald *et al.*, 2012a).

CONCLUSIONS

We have used 3D seismic reflection data from the Ceduna Sub-Basin, Great Australian Bight, to describe the structural evolution of four Upper Cretaceous–Cenozoic aged, detached normal fault assemblages at an extensional delta top setting. This fault array is unique as it has developed through the influx and interaction of two delta systems of differing structural style. We have identified and constrained the timing of two vertically connected fault systems of Cenomanian–Santonian and post-Santonian age. We show that through a combination of upward propagation of Cenomanian–Santonian listric faults, and dip-linkage of post-Santonian normal faults to Cenomanian–Santonian faults, the Cenomanian–Santonian faults controlled the spatial and temporal development of post-Santonian faults through active kinematic linkage. The observations of segment linkage in map view, highly variable displacement profiles along-strike of fault assemblages and the isolation of faults at depth, leads us to conclude that these fault assemblages formed from the along-strike linkage of fault segments, with individual segments reaching *ca.* 5–15 km in length. We constrain the evolution of the overall fault array into four main stages: (1) Cenomanian–Santonian nucleation and kilometre-scale growth of fault segments, resulting from gravitational instability; (2) Santonian fault growth cessation for a majority of faults; (3) erosion coincident with the continental breakup of Australia and Antarctica (*ca.* 83 Ma); (4) Campanian–Maastrichtian reactivation of the underlying Cenomanian–Santonian fault system, causing upward propagation of some Cenomanian–Santonian faults and inducing the nucleation, growth and consequential dip-linkage of the post-Santonian fault system. Our study contributes to the growing body of research on normal fault growth in the presence of mechanically weak detachments, the structural style of stacked delta systems and the evolution of the Ceduna Sub-Basin, Great Australian Bight.

ACKNOWLEDGEMENTS

This research forms part of a PhD project supported by the ASEG Research Foundation (RF14P04) for which funding is gratefully acknowledged. We would like to thank the Australian Research Council (Discovery Projects DP120101460 and DP160101158) and University of Adelaide for scholarship funding; IHS Kingdom, Move by Midland Valley and Opentect for software use. We

would also like to thank Editor Chris Jackson and Reviewers Craig Magee, Conrad Childs and Atle Rotevatn for their very constructive and extensive reviews of this paper. This forms TRaX record 305.

CONFLICT OF INTEREST

No conflict of interest declared.

REFERENCES

- ALLAN, U.S. (1989) Model for hydrocarbon migration and entrapment within faulted structures. *AAPG Bull.*, **73**(7), 803–811.
- ANDERSON, R.N., FLEMINGS, P., LOSH, S., AUSTIN, J. & WOODHAMS, R. (1994) Gulf of Mexico growth fault drilled, seen as oil, gas migration pathway. *Oil Gas J. (United States)*, **92**(23), 97–104.
- ANDERSON, J.E., CARTWRIGHT, J., DRYSDALL, S.J. & VIVIAN, N. (2000) Controls on turbidite sand deposition during gravity-driven extension of a passive margin: examples from Miocene sediments in Block 4, Angola. *Mar. Pet. Geol.*, **17**(10), 1165–1203.
- BAUDON, C. & CARTWRIGHT, J. (2008) The kinematics of reactivation of normal faults using high resolution throw mapping. *J. Struct. Geol.*, **30**(8), 1072–1084.
- BEIN, J. & TAYLOR, M.L. (1981) The Eyre Sub-basin: recent exploration results. *APPEA J.*, **21**(1), 91–98.
- BILOTTI, F. & SHAW, J.H. (2005) Deep-water Niger Delta fold and thrust belt modelled as a critical taper wedge: the influence of elevated basal fluid pressure on structural styles. *AAPG Bull.*, **89**(11), 1475–1491.
- BOUVIER, J.D., KAARS-SIJPESTEIJN, C.H., KLUESNER, D.F., ONYEJEKWE, C.C. & van der PAL, R.C. (1989) Three-dimensional seismic interpretation and fault sealing investigations, Nun River Field, Nigeria. *AAPG Bull.*, **73**(11), 1397–1414.
- BIGGS, S.E., DAVIES, R.J., CARTWRIGHT, J.A. & MORGAN, R. (2006) Multiple detachment levels and their control on fold styles in the compressional domain of the deepwater west Niger Delta. *Basin Res.*, **18**(4), 435–450.
- BUFFLER, R.T., SHAUB, F.J., WATKINS, J.S. & WORZEL, J.L. (1979) Anatomy of the Mexican ridges, southwestern Gulf of Mexico. *Geological and geophysical investigations of continental margins: AAPG Memoir*, **29**, 319–327.
- CARTWRIGHT, J.A., TRUDGILL, B.D. & MANSFIELD, C.S. (1995) Fault growth by segment linkage: an explanation for scatter in maximum displacement and trace length data from the Canyonslands Grabens of SE Utah. *J. Struct. Geol.*, **17**(9), 1319–1326.
- CHAPMAN, T.J. & MENEILLY, A.W. (1991) The displacement patterns associated with a reverse reactivated, normal growth fault. *Geol. Soc. London Spec. Publ.*, **56**(1), 183–191.
- CHILDS, C., EASTON, S.J., VENDEVILLE, B.C., JACKSON, M.P.A., LIN, S.T., WALSH, J.J. & WATTERSON, J. (1993) Kinematic analysis of faults in a physical model of growth faulting above a viscous salt analogue. *Tectonophysics*, **228**(3), 313–329.
- CHILDS, C., WATTERSON, J. & WALSH, J.J. (1995) Fault overlap zones within developing normal fault systems. *J. Geol. Soc.*, **152**(3), 535–549.
- CHILDS, C., NICOL, A., WALSH, J.J. & WATTERSON, J. (1996) Growth of vertically segmented normal faults. *J. Struct. Geol.*, **18**(12), 1389–1397.
- CHILDS, C., NICOL, A., WALSH, J.J. & WATTERSON, J. (2003) The growth and propagation of synsedimentary faults. *J. Struct. Geol.*, **25**(4), 633–648.
- COBBOLD, P.R., CLARKE, B.J. & LØSETH, H. (2009) Structural consequences of fluid overpressure and seepage forces in the outer thrust belt of the Niger Delta. *Petrol. Geosci.*, **15**(1), 3–15.
- COHEN, H.A. & McCLAY, K. (1996) Sedimentation and shale tectonics of the northwestern Niger Delta front. *Mar. Pet. Geol.*, **13**(3), 313–328.
- CORREDOR, F., SHAW, J.H. & BILOTTI, F. (2005) Structural styles in the deep-water fold and thrust belts of the Niger Delta. *AAPG Bull.*, **89**(6), 753–780.
- DAWERS, N.H. & ANDERS, M.H. (1995) Displacement length scaling and fault linkage. *J. Struct. Geol.*, **17**(5), 607–614.
- DOUST, H. & OMATSOLA, E. (1989) Niger Delta. In: *Divergent/Passive Margin Basins* (Ed. by J.D. Edwards & P.A. Santogrossi) Am. Assoc. Pet. Geol. Mem., **48**, 201–238.
- DUTTON, D.M. & TRUDGILL, B.D. (2009) Four dimensional analysis of the Sembo relay system, offshore Angola: implications for fault growth in salt-detached settings. *AAPG Bull.*, **93**(6), 763–794.
- FRASER, A.R. & TILBURY, L.A. (1979) Structure and stratigraphy of the Ceduna Terrace region. *Great Australian Bight Basin: APEA J.*, **19**, 53–65.
- GIBA, M., WALSH, J.J. & NICOL, A. (2012) Segmentation and growth of an obliquely reactivated normal fault. *J. Struct. Geol.*, **39**, 253–267.
- HARDING, T.P. & TUMINAS, A.C. (1989) Structural interpretation of hydrocarbon traps sealed by basement normal block faults at stable flank of foredeep basins and at rift basins. *AAPG Bull.*, **73**(7), 812–840.
- HILL, A.J. (1995) Bight Basin. In: *The Geology of South Australia, Vol. 2, The Phanerozoic* (Ed. by J.F. Drexel & W.V. Preiss) *Geol. Surv. South Aust. Bull.*, **54**, 133–138.
- HOLFORD, S.P., HILLIS, R.R., DUDDY, I.R., GREEN, P.F., STOKER, M.S., TUITT, A.G., BACKÉ, G., TASSONE, D.R. & MACDONALD, J.D. (2011) Cenozoic post-breakup compressional deformation and exhumation of the southern Australian margin. *APPEA J.*, **51**(1), 613–638.
- HUGGINS, P., WATTERSON, J., WALSH, J.J. & CHILDS, C. (1995) Relay zone geometry and displacement transfer between normal faults recorded in coal-mine plans. *J. Struct. Geol.*, **17**(12), 1741–1755.
- JACKSON, C.L. & LARSEN, E. (2009) Temporal and spatial development of a gravity-driven normal fault array: middle-Upper Jurassic, South Viking Graben, northern North Sea. *J. Struct. Geol.*, **31**(4), 388–402.
- JACKSON, C.A.L. & ROTEVATN, A. (2013) 3D seismic analysis of the structure and evolution of a salt-influenced normal fault zone: a test of competing fault growth models. *J. Struct. Geol.*, **54**, 215–234.
- JAMES, D.M.D. (Ed.) (1984) The geology and hydrocarbon resources of Negara Brunei Darussalam. *Muzium Brunei Brunei Shell Petrol. Company Berhad Spec. Publ.*, **8**, 2–21.
- JEV, B.I., KAARS-SIJPESTEIJN, C.H., PETERS, M.P.A.M., WATTS, N.L. & WILKIE, J.T. (1993) Akaso field, Nigeria: use of integrated 3-D seismic, fault slicing, clay smearing, and RFT pressure data on fault trapping and dynamic leakage. *AAPG Bull.*, **77**(8), 1389–1404.

- KANE, K.E., JACKSON, C.A.L. & LARSEN, E. (2010) Normal fault growth and fault-related folding in a salt influenced rift basin: south Viking Graben, offshore Norway. *J. Struct. Geol.*, **32** (4), 490–506.
- KING, R.C. & BACKÉ, G. (2010) A balanced 2D structural model of the Hammerhead Delta Deepwater Fold-Thrust Belt, Bight Basin, Australia. *Aust. J. Earth Sci.*, **57**(7), 1005–1012.
- KING, R.C., HILLIS, R.R., TINGAY, M.R.P. & MORLEY, C.K. (2009) Present-day stress and neotectonic provinces of the Baram Delta and deep-water fold thrust belt. *J. Geol. Soc.*, **166**, 197–200.
- KING, R.C., BACKÉ, G., MORLEY, C.K., HILLIS, R.R. & TINGAY, M.R. (2010) Balancing deformation in NW Borneo: quantifying plate-scale vs. gravitational tectonics in a Delta and Deepwater Fold-Thrust Belt System. *Mar. Pet. Geol.*, **27**(1), 238–246.
- KNOTT, S.D. (1993) Fault seal analysis in the North Sea. *AAPG Bull.*, **77**(5), 778–792.
- KOOPMAN, A., SCHREURS, J. & ELLENOR, D.W. (1996) The oil and gas resources of Brunei Darussalam—The coastal and offshore oil and gas fields. In: *Geology and Hydrocarbon Resources of Negara Brunei Darussalam (1996 Revision)*, (Ed. by S.T. Sandal), pp. 155–192. Brunei Shell Petroleum/Brunei Museum, Syabas Bandar Seri Begawan, Brunei Darussalam.
- KRASSAY, A.A. & TOTTERDELL, J.M. (2003) Seismic stratigraphy of a large, Cretaceous shelf-margin delta complex, offshore southern Australia. *AAPG Bull.*, **87**(6), 935–963.
- LEWIS, M.M., JACKSON, C.A.L. & GAWTHORPE, R.L. (2013) Salt-influenced normal fault growth and forced folding: the Stavanger Fault System, North Sea. *J. Struct. Geol.*, **54**, 156–173.
- MACDONALD, J.D., KING, R., HILLIS, R.R. & BACKÉ, G. (2010) Structural style of the White Pointer and Hammerhead delta—deepwater fold-thrust belts, Bight Basin, Australia. *Aust. Petrol. Prod. Explor. Assoc. J.*, **50**, 487–510.
- MACDONALD, J.D., BACKÉ, G., KING, R., HOLFORD, S. & HILLIS, R.R. (2012a) Geomechanical modelling of fault reactivation in the Ceduna Sub-Basin, Bight Basin, Australia. In: *Faulting, Fracturing and Igneous Intrusions in the Earth's Crust* (Ed. by D. Healy, R.W.H. Butler, Z.K. Shipton & R.H. Sibson) *Geol. Soc. London Spec. Publ.*, **367**, 71–89.
- MACDONALD, J.D., HOLFORD, S. & KING, R. (2012b) Structure and Prospectivity of the Ceduna Delta Deepwater Fold-Thrust Belt Systems, Bight Basin, Australia. In: *New Understanding of the Petroleum Systems of the Continental Margins of the World* (Ed. by N.C. Rosen) *GCSEPM Foundation Bob F. Perkins Research Conference*, **32**, 779–816.
- MACDONALD, J.D., HOLFORD, S.P., GREEN, P.F., DUDDY, I.R., KING, R.C. & BACKÉ, G. (2013) Detrital zircon data reveal the origin of Australai's largest delta system. *J. Geol. Soc.*, **170**, 3–6.
- MANSFIELD, C.S. & CARTWRIGHT, J.A. (1996) High resolution fault displacement mapping from three-dimensional seismic data: evidence for dip linkage during fault growth. *J. Struct. Geol.*, **18**(2), 249–263.
- MANSFIELD, C. & CARTWRIGHT, J. (2001) Fault growth by linkage: observations and implications from analogue models. *J. Struct. Geol.*, **23**(5), 745–763.
- MARSH, N., IMBER, J., HOLDSWORTH, R.E., BROCKBANK, P. & RINGROSE, P. (2010) The structural evolution of the Halten Terrace, offshore Mid-Norway: extensional fault growth and strain localisation in a multi-layer brittle-ductile system. *Basin Res.*, **22**(2), 195–214.
- MESSENT, B.E.J. (1998) Great Australian Bight: well audit. Australian Geological Survey Organisation Record 1998/37.
- MORLEY, C.K. & GUERIN, G. (1996) Comparison of gravity driven deformation styles and behaviour associated with mobile shales and salt. *Tectonics*, **15**(6), 1154–1170.
- NORVICK, M.S. & SMITH, M.A. (2001) Southeast Australia—Mapping the plate tectonic reconstruction of southern and southeastern Australia and implications for petroleum systems. *APPEA J.*, **41**(1), 15–36.
- PEACOCK, D.C.P. & SANDERSON, D.J. (1991) Displacements, segment linkage and relay ramps in normal fault zones. *J. Struct. Geol.*, **13**(6), 721–733.
- PEEL, F.J. (2014) The engines of gravity-driven movement on passive margins: quantifying the relative contribution of spreading vs. gravity sliding mechanisms. *Tectonophysics*, **633**, 126–142.
- ROUBY, D., RAILLARD, S., GUILLOCHEAU, F., BOUROULLEC, R. & NALPAS, T. (2002) Kinematics of a growth fault/raft system on the West African margin using 3-D restoration. *J. Struct. Geol.*, **24**(4), 783–796.
- ROWAN, M.G. (1997) Three-dimensional geometry and evolution of a segmented detachment fold, Mississippi Fan fold-belt, Gulf of Mexico. *J. Struct. Geol.*, **19**(3), 463–480.
- ROWAN, M.G., HART, B.S., NELSON, S., FLEMINGS, P.B. & TRUDGILL, B.D. (1998) Three-dimensional geometry and evolution of a salt-related growth-fault array: Eugene Island 330 field, offshore Louisiana, Gulf of Mexico. *Mar. Pet. Geol.*, **15**(4), 309–328.
- ROWAN, M.G., JACKSON, M.P.A. & TRUDGILL, B.D. (1999) Salt-related fault families and fault welds in the northern Gulf of Mexico. *AAPG Bull.*, **83**, 1454–1484.
- RYKKELID, E. & FOSSEN, H. (2002) Layer rotation around vertical fault overlap zones: observations from seismic data, field examples, and physical experiments. *Mar. Pet. Geol.*, **19**(2), 181–192.
- SAYERS, J., SYMONDS, P.A., DIREEN, N.G. & BERNARDEL, G. (2001) Nature of the continent-ocean transition on the non-volcanic rifted margin of the central Great Australian Bight. *Geol. Soc. London Spec. Publ.*, **187**(1), 51–76.
- SCHREURS, G. (1997) The petroleum geology of Negara Brunei Darussalam; an update. In: *Proceedings of the IPA Petroleum Systems of SE Asia and Australasia Conference, Jakarta, Indonesia, May 1997* (Ed. by J.V.C. Howes, R.A. Noble), pp. 751–766. Indonesian Petroleum Association, Jakarta.
- SCHULTZ-ELA, D.D. (2001) Excursus on gravity gliding and gravity spreading. *J. Struct. Geol.*, **23**(5), 725–731.
- SMITH, D.A. (1980) Sealing and nonsealing faults in Louisiana Gulf Coast salt basin. *AAPG Bull.*, **64**(2), 145–172.
- STAGG, H.M.J., COCKSHELL, C.D., WILLCOX, J.B., HILL, A.J., NEEDHAM, D.V.C., THOMAS, B., O'BRIEN, G.W. & HOUGH, L.P. (1990) Basins of the Great Australian Bight region—Geology and petroleum potential, Folio 5, Continental Margins Program, Bureau of Mineral Resources, Geology and Geophysics, Canberra, Australia.
- TAPLEY, D., MEE, B.C., KING, S.J., DAVIS, R.C. & LEISCHNER, K.R. (2005) Petroleum potential of the Ceduna Sub-basin: impact of Gnarlyknots-1A. *APPEA J.*, **45**(1), 365–380.
- TAYLOR, S.K., NICOL, A. & WALSH, J.J. (2008) Displacement loss on growth faults due to sediment compaction. *J. Struct. Geol.*, **30**(3), 394–405.
- THORSEN, C.E. (1963) Age of growth faulting in southeast Louisiana. *Gulf Coast Assoc. Geol. Soc. Trans.*, **13**, 103–110.

- TOTTERDELL, J.M. & BRADSHAW, B.E. (2004) The structural framework and tectonic evolution of the Bight Basin. In: *Eastern Australasian Basins Symposium II*, pp. 41–61. Petroleum Exploration Society of Australia, Special Publication.
- TOTTERDELL, J.M. & KRASSAY, A.A. (2003) The role of shale deformation and growth faulting in the Late Cretaceous evolution of the Bight Basin, offshore southern Australia. *Geol. Soc. London Spec. Publ.*, **216**(1), 429–442.
- TOTTERDELL, J.M., BLEVIN, J.E., STRUCKMEYER, H.I.M., BRADSHAW, B.E., COLWELL, J.B. & KENNARD, J.M. (2000) Petroleum frontiers, systems and plays—A new sequence framework for the Great Australian Bight: starting with a clean slate. *APPEA J.*, **40**(1), 95–120.
- TRUDGILL, B. & CARTWRIGHT, J. (1994) Relay-ramp forms and normal-fault linkages, Canyonlands National Park, Utah. *Geol. Soc. Am. Bull.*, **106**(9), 1143–1157.
- TVEDT, A., ROTEVATN, A., JACKSON, C.A.L., FOSSEN, H. & GAWTHORPE, R.L. (2013) Growth of normal faults in multi-layer sequences: a 3D seismic case study from the Egersund Basin, Norwegian North Sea. *J. Struct. Geol.*, **55**, 1–20.
- VEEVERS, J.J. (1986) Breakup of Australia and Antarctica estimated as mid-Cretaceous (95 ± 5 Ma) from magnetic and seismic data at the continental margin. *Earth Planet. Sci. Lett.*, **77**(1), 91–99.
- de VERA, J., GRANADO, P. & McCLAY, K. (2010) Structural evolution of the Orange Basin gravity-driven system, offshore Namibia. *Mar. Pet. Geol.*, **27**(1), 223–237.
- WALSH, J.J. & WATTERSON, J. (1988) Analysis of the relationship between displacements and dimensions of faults. *J. Struct. Geol.*, **10**(3), 239–247.
- WALSH, J.J., WATTERSON, J., BAILEY, W.R. & CHILDS, C. (1999) Fault relays, bends and branch lines. *J. Struct. Geol.*, **21**(8), 1019–1026.
- WALSH, J.J., NICOL, A. & CHILDS, C. (2002) An alternative model for the growth of faults. *J. Struct. Geol.*, **24**(11), 1669–1675.
- WALSH, J.J., BAILEY, W.R., CHILDS, C., NICOL, A. & BONSON, C.G. (2003) Formation of segmented normal faults: a 3-D perspective. *J. Struct. Geol.*, **25**(8), 1251–1262.
- WILLCOX, J.B. & STAGG, H.M.J. (1990) Australia's southern margin: a product of oblique extension. *Tectonophysics*, **173**(1), 269–281.
- WINKER, C.D. & EDWARDS, M.B. (1983) Unstable progradational clastic shelf margins. In: *The Shelfbreak: critical Interface on Continental Margins* (Ed. by D.J. Stanley & G.T. Moore) *SEPM Spec. Publ.* **33**, 139–157.
- WITHJACK, M.O. & CALLAWAY, S. (2000) Active normal faulting beneath a salt layer: an experimental study of deformation patterns in the cover sequence. *AAPG Bull.*, **84**(5), 627–651.
- WITHJACK, M.O., OLSON, J. & PETERSON, E. (1990) Experimental models of extensional forced folds (1). *AAPG Bull.*, **74**(7), 1038–1054.
- WU, S., BALLY, A.W. & CRAMEZ, C. (1990) Allochthonous salt, structure and stratigraphy of the north-Eastern Gulf of Mexico. Part II: structure. *Mar. Pet. Geol.*, **7**(4), 334–370.

Manuscript received 3 March 2015; In revised form 5 February 2016; Manuscript accepted 9 February 2016.

4.2. Paper 2

Robson, A. G., King, R. C., & Holford, S. P. (2016). 3D seismic analysis of gravity-driven and basement influenced normal fault growth in the deepwater Otway Basin, Australia. *Journal of Structural Geology*, 89, 74-87. DOI:10.1016/j.jsg.2016.06.002

Statement of Authorship

Title of Paper	3D seismic analysis of gravity-driven and basement influenced normal fault growth in the deepwater Otway Basin, Australia.
Publication Status	<input checked="" type="checkbox"/> Published <input type="checkbox"/> Accepted for Publication <input type="checkbox"/> Submitted for Publication <input type="checkbox"/> Unpublished and Unsubmitted work written in manuscript style
Publication Details	Robson, A. G., King, R. C., & Holford, S. P. (2016). 3D seismic analysis of gravity-driven and basement influenced normal fault growth in the deepwater Otway Basin, Australia. <i>Journal of Structural Geology</i> , 89, 74-87.

Principal Author

Name of Principal Author (Candidate)	Alexander Robson			
Contribution to the Paper	<ul style="list-style-type: none"> Seismic interpretation fault analysis preparation of manuscript editing manuscript Corresponding author 			
Overall percentage (%)	70%			
Certification:	This paper reports on original research I conducted during the period of my Higher Degree by Research candidature and is not subject to any obligations or contractual agreements with a third party that would constrain its inclusion in this thesis. I am the primary author of this paper.			
Signature	<table border="1" style="width: 100%;"> <tr> <td style="width: 80%;"></td> <td style="width: 20%;">Date</td> <td>6/09/2017</td> </tr> </table>		Date	6/09/2017
	Date	6/09/2017		

Co-Author Contributions

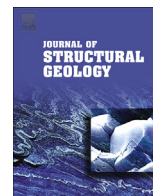
By signing the Statement of Authorship, each author certifies that:

- i. the candidate's stated contribution to the publication is accurate (as detailed above);
- ii. permission is granted for the candidate to include the publication in the thesis; and
- iii. the sum of all co-author contributions is equal to 100% less the candidate's stated contribution.

Name of Co-Author				
Contribution to the Paper	<ul style="list-style-type: none"> Supervised development of work Helped in data interpretation and manuscript evaluation Multiple edits of manuscript during review 			
Signature	<table border="1" style="width: 100%;"> <tr> <td style="width: 80%;"></td> <td style="width: 20%;">Date</td> <td>6/09/2017</td> </tr> </table>		Date	6/09/2017
	Date	6/09/2017		

Name of Co-Author				
Contribution to the Paper	<ul style="list-style-type: none"> Supervised development of work Helped in data interpretation and manuscript evaluation Multiple edits of manuscript during review 			
Signature	<table border="1" style="width: 100%;"> <tr> <td style="width: 80%;"></td> <td style="width: 20%;">Date</td> <td>6/09/2017</td> </tr> </table>		Date	6/09/2017
	Date	6/09/2017		

Please cut and paste additional co-author panels here as required.



3D seismic analysis of gravity-driven and basement influenced normal fault growth in the deepwater Otway Basin, Australia



A.G. Robson ^{a, b, *}, R.C. King ^a, S.P. Holford ^b

^a Centre for Tectonics Resources and Exploration (TRaX), Department of Physical Sciences, University of Adelaide, Adelaide, 5005, South Australia, Australia

^b Australian School of Petroleum, Santos Building, University of Adelaide, Adelaide, 5005, South Australia, Australia

ARTICLE INFO

Article history:

Received 19 November 2015

Received in revised form

30 May 2016

Accepted 2 June 2016

Available online 4 June 2016

Keywords:

Normal fault

Extension

Structural evolution

Otway Basin

Southern margin

3D seismic data

ABSTRACT

We use three-dimensional (3D) seismic reflection data to analyse the structural style and growth of a normal fault array located at the present-day shelf-edge break and into the deepwater province of the Otway Basin, southern Australia. The Otway Basin is a Late Jurassic to Cenozoic, rift-to-passive margin basin. The seismic reflection data images a NW-SE (128–308) striking, normal fault array, located within Upper Cretaceous clastic sediments and which consists of ten fault segments. The fault array contains two hard-linked fault assemblages, separated by only 2 km in the dip direction. The gravity-driven, down-dip fault assemblage is entirely contained within the 3D seismic survey, is located over a basement plateau and displays growth commencing and terminating during the Campanian-Maastrichtian, with up to 1.45 km of accumulated throw (vertical displacement). The up-dip normal fault assemblage penetrates deeper than the base of the seismic survey, but is interpreted to be partially linked along strike at depth to major basement-involved normal faults that can be observed on regional 2D seismic lines. This fault assemblage displays growth initiating in the Turonian-Santonian and has accumulated up to 1.74 km of throw.

Our detailed analysis of the 3D seismic data constraints post-Cenomanian fault growth of both fault assemblages into four evolutionary stages: [1] Turonian-Santonian basement reactivation during crustal extension between Australia and Antarctica. This either caused the upward propagation of basement-involved normal faults or the nucleation of a vertically isolated normal fault array in shallow cover sediments directly above the reactivated basement-involved faults; [2] continued Campanian-Maastrichtian crustal extension and sediment loading eventually created gravitational instability on the basement plateau, nucleating a second, vertically isolated normal fault array in the cover sediments; [3] eventual hard-linkage of fault segments in both fault arrays to form two along-strike, NW-SE striking fault assemblages, and; [4] termination of fault growth in the latest Maastrichtian. We document high variability of throw along-strike and down-dip for both fault assemblages, thereby providing evidence for lateral and vertical segment linkage. Our results highlight the complexities involved in the growth of both gravity-driven normal fault arrays (such as those present in the Niger Delta and Gulf of Mexico) and basement-linked normal fault arrays (such as those present in the North Sea and Suez Rift) with the interaction of an underlying and reactivating basement framework. This study provides an excellent example of spatial variability in growth of two normal fault assemblages over relatively short spatial scales (~2 km separation down-dip).

© 2016 Elsevier Ltd. All rights reserved.

1. Introduction

Normal fault nucleation and growth induced by the gravitational instability of sediment is a complex process. Mechanically weak strata inhibit the propagation of fault tip-lines and instead results in fault-related folding (Rowan, 1997, 1998; Jackson and Larsen, 2009; Kane et al., 2010; Jackson and Rotevatn, 2013; Lewis et al., 2013; Tvedt et al., 2013). The evolution of normal

* Corresponding author. Centre for Tectonics Resources and Exploration (TRaX), Department of Physical Sciences, University of Adelaide, Adelaide, 5005, South Australia, Australia.

E-mail address: Alexander.Robson@adelaide.edu.au (A.G. Robson).

faults becomes even more complex when accounting for the influence of underlying and reactivating basement normal faults under multiple stages of crustal extension (e.g. Kornawan and Morley, 2002; Morley et al., 2004, 2011; Jackson and Rotevatn, 2013; Lewis et al., 2013; Tvedt et al., 2013). Complexities lie in attempting to understand the temporal, geometric and kinematic relationships between reactivation of basement normal faults and the development of shallower normal faults in cover sediments. Three studies using 3D seismic datasets from the North Sea have all concluded a geometric and kinematic relationship between basement normal fault reactivation and supra-salt normal fault development, with basement normal fault reactivation instigating supra-salt extension (Jackson and Rotevatn, 2013; Lewis et al., 2013; Tvedt et al., 2013). Furthermore, studies have also shown that increased tilting, flexure and gravity gliding of cover sediments occurs above basement normal faults, causing the development of sub-parallel striking cover-restricted normal faults (Vendeville et al., 1995; Withjack and Callaway, 2000).

Normal faults have been shown to grow either radially as isolated segments (*isolated fault model*; e.g. Walsh and Watterson, 1988; Trudgill and Cartwright, 1994; Dawers and Anders, 1995) or through geologically instantaneous fault length establishment, followed by displacement accumulation (*coherent fault model*; e.g. Morley, 1999; Walsh et al., 2002; Childs et al., 2003). Furthermore, normal faults may incidentally link by either soft-linkage, where faults overlap but do not have geometric linkage (*sensu* Fig. 10b, Trudgill and Cartwright, 1994), or hard-linkage, where faults are geometrically linked (*sensu* Fig. 10c, Trudgill and Cartwright, 1994).

Normal fault growth resulting from mechanical extension is relatively well studied (e.g. Walsh and Watterson, 1988; Morley, 1999; Childs et al., 1995, 2003; Walsh et al., 2002, 2003). In comparison, gravitationally-driven normal fault growth is relatively understudied (e.g. Rowan, 1997, 1998; Back et al., 2005; Jackson and Larsen, 2009; Kane et al., 2010; Jackson and Rotevatn, 2013; Lewis et al., 2013; Back and Morley, 2016). The linkage of normal faults in map view (driven by either gravitational forces or mechanical extension) can be analysed by the measurement of along-strike displacement variations (Walsh and Watterson, 1988; Peacock and Sanderson, 1991; Childs et al., 1995; Walsh et al., 2003). However, vertical displacement measurements down a fault plane can be used to understand vertical segmentation and, in combination with along strike displacement measurements, these approaches permit fault growth to be studied in three dimensions (e.g. Mansfield and Cartwright, 1996; Kornawan and Morley, 2002; Rykkelid and Fossen, 2002; Morley et al., 2007, 2011; Baudon and Cartwright, 2008). Anomalous down-dip displacement deficits imply segment linkage in the dip direction, a phenomenon known as dip-linkage (Mansfield and Cartwright, 1996).

The aim of this study is to constrain the temporal and spatial evolution of a normal fault array located at the present-day shelf-edge break, bordering on the deepwater province of the Otway Basin, which is situated along the southern Australian rifted-to-passive continental margin (Fig. 1a). The Late Jurassic to Cenozoic aged Otway Basin (Fig. 1a) is a NW-oriented rift basin, which developed into a passive margin basin following the breakup of Australia and Antarctica, and which extends from SE South Australia to offshore NW Tasmania (Moore et al., 2000; Krassay et al., 2004; Stacey et al., 2013; Holford et al., 2014). This study is located at the present-day shelf-edge break, which separates the Inner Otway Basin from the deepwater and frontier Nelson Sub-Basin (Fig. 1a; Moore et al., 2000; Krassay et al., 2004; Stacey et al., 2013).

Using 3D seismic reflection data (the Amrit 3D survey; Fig. 1a) acquired over the present day shelf-edge break of the Otway Basin, Australia, we have identified and individually analysed one isolated

normal fault (Fault 1, Fig. 1c) and one hard-linked (i.e. geometrically linked along strike with breached relay ramps; Fig. 10c, Trudgill and Cartwright, 1994) fault assemblage (Faults 2–6, Fig. 1c) consisting of five normal faults, all of which are also Turonian-Maastrichtian in age. We have also analysed another more distally located hard-linked and gravity-driven fault assemblage consisting of four normal faults that are Campanian-Maastrichtian in age (Fig. 1b; c). The average strike of all faults within the study area is ~NW-SE (128–308) (Fig. 1d). The 3D seismic reflection data (Fig. 1a) enables us to constrain normal fault evolution from measurements and analysis of synkinematic growth strata for fault segments and assemblages in three-dimensions.

Throw-distance, which measures maximum throw variability along strike of a fault, reveals that all fault assemblages are characterized by highly variable throw profiles along strike. This implies that these fault assemblages have grown from the strike-linkage of smaller fault segments. Throw-depth analysis, which evaluates throw variability vertically down the fault plane, highlighted anomalous throw deficits, indicative of vertically segmented fault growth. Greater fault throw and earlier fault nucleation is observed on faults directly above major basement-involved normal faults (fault 1 and fault assemblage 1; Fig. 1c), which eventually dip-link, while faults located over a basement plateau (i.e. on an Early Cretaceous fault block, see Fig. 1e; fault assemblage 2, Fig. 1c), display later and smaller throw accumulation. Our results highlight the complexity of both gravitationally-driven and basement-linked normal fault growth in the presence of mechanically incompetent strata and an underlying and reactivating basement framework. This study also highlights contrasting examples of varying basement influence on normal fault growth by providing analysis of two along-strike fault assemblages proximal to one another in the dip direction.

2. Geological setting of the Otway Basin

The Otway Basin is a NW-oriented rift-to-passive margin basin (Fig. 1a), extending from SE South Australia to NW Tasmania, where it adjoins the Sorell Basin (Moore et al., 2000; see Fig. 7). The Otway Basin contains a Late Jurassic-Cenozoic sedimentary succession of up to ~8 km thick and covers a surface area of 150,000 km², with the majority of the basin (~120,000 km²) lying offshore in water depths up to 3000 m (Moore et al., 2000; Stacey et al., 2013). This study is centered approximately 55 km south of Portland, Victoria, at the present-day outer shelf and slope (Fig. 1a). This region is near the border of the Inner Otway Basin and the deepwater Nelson Sub-Basin (Moore et al., 2000) and is bounded to the west by the Bridgewater High (Fig. 1a) a complex NNE-SSW striking structural high, where Cretaceous-Cenozoic sediments thin to less than 2.5 s two-way-time (TWT) (Moore et al., 2000; Krassay et al., 2004; Stacey et al., 2013). Given the lack of well data basinward of the present-day shelf edge break (Fig. 1), this study uses the well-established sequence stratigraphic framework of Krassay et al. (2004), which is based on basin-scale seismic interpretation.

The Otway Basin formed due to rifting between Australia and Antarctica during the break-up of eastern Gondwana, with rifting commencing in the Tithonian (e.g. Willcox and Stagg, 1990; Moore et al., 2000; Krassay et al., 2004; Norvick, 2005; Holford et al., 2011). Initial rifting during the Tithonian-Barremian created the accommodation space for the deposition of the Crayfish Supersequence, with E-W- to NW-SE striking faults bounding a series of horst and graben structures (Morton et al., 1994; Perincek and Cockshell, 1995; Finlayson et al., 1996; Krassay et al., 2004). Variable orientations of half-graben structures imply that pre-existing Palaeozoic basement structures influenced the development of new normal faults (Finlayson et al., 1996). Regional deep-seismic profiling has

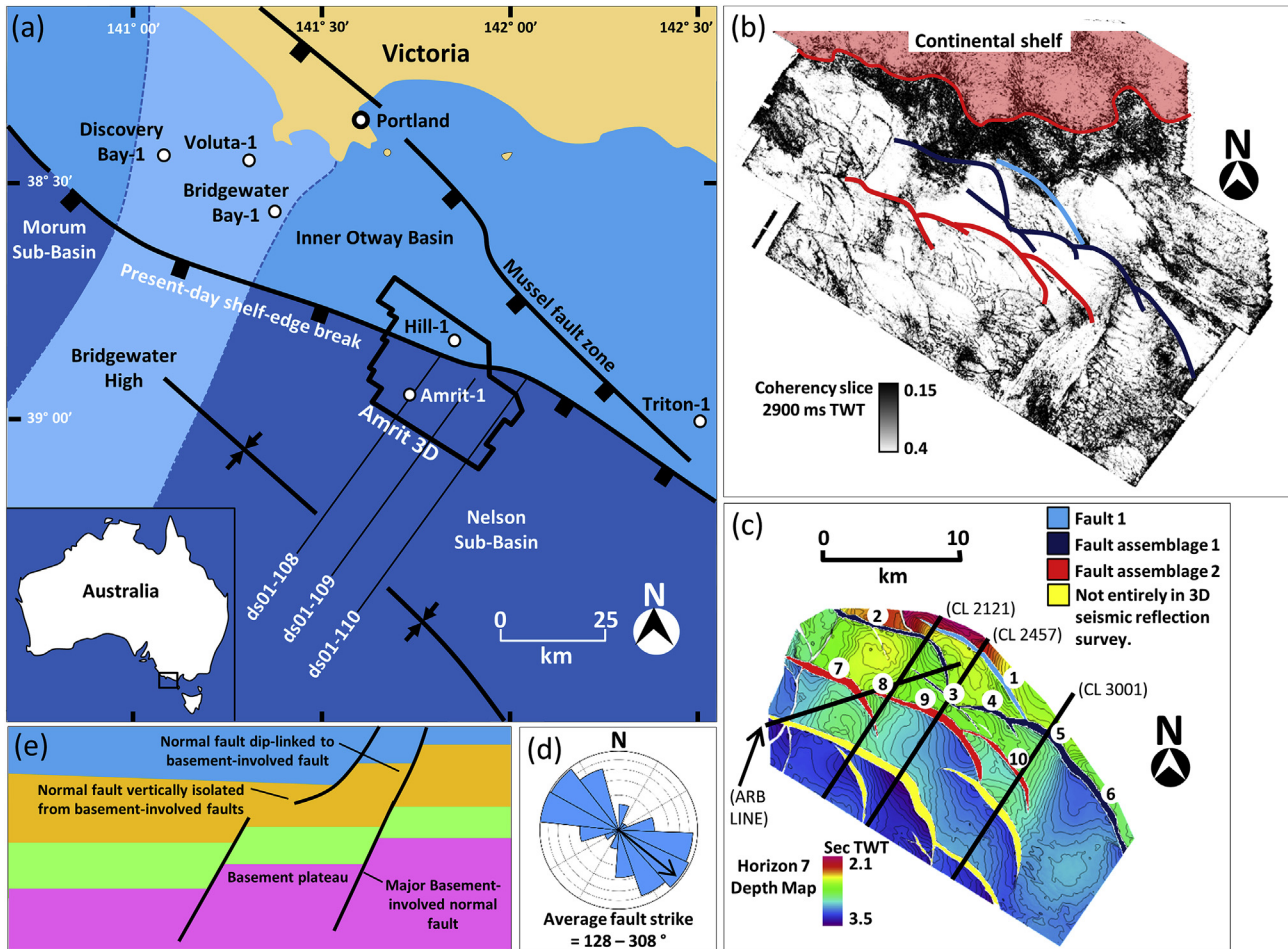


Fig. 1. (a) Location map of the 3D seismic reflection survey, 2D seismic lines ds01-108, ds01-109, ds01-110 and wells Discovery Bay-1, Voluta-1, Bridgewater Bay-1, Hill-1, Amrit-1 and Triton-1 used for this study, relative to the town of Portland, Victoria. The map indicates the deepwater and frontier Nelson Sub-Basin and Morum Sub-Basin, Bridgewater High and the offshore portion of the Inner Otway Basin. Major structural features identified include the Mussel Fault Zone and the present-day shelf edge break, which dissects the 3D seismic reflection survey. (b) Coherency slice (2900 m TWT), highlighting the continental shelf and faults of interest to this study: fault 1 (light blue), fault assemblage 1 (dark blue) and fault assemblage 2 (red). These faults are also shown as fault polygons on the depth (TWT) map of horizon seven (c), with individual fault segments shown for each fault assemblage. Also highlighted on this map are the cross-sections shown in Fig. 3. The average strike of the fault array (d) is NW (128–308°). Need some text to describe (e) – make sure you explain what the different colours are. (For interpretation of the references to colour in this figure legend, the reader is referred to the web version of this article.)

shown that basement-involved rift structures detach at mid-crustal, lower-crustal and even Moho levels (Hill et al., 1995; Finlayson et al., 1996). The Crayfish Supersequence contains organic-rich mudstones, sandstones and some basalts, with maximum thicknesses of up to 5000 m in the northern, onshore Otway Basin (Fig. 2; Ryan et al., 1995; Krassay et al., 2004).

This initial period of rifting was followed by post-rift subsidence during the Aptian-Albian, during which time the westerly and northerly thinning Eumeralla Supersequence was deposited (Fig. 2; Hill et al., 1995; Krassay et al., 2004). The Eumeralla Supersequence is dominated by fluvio-lacustrine strata with a volcanoclastic sediment source (Hill et al., 1995), and is likely the source rock for gas accumulations found in the eastern Otway Basin (Duddy, 1997; Tassone et al., 2014). A major unconformity marks the basal sequence boundary of the Eumeralla Supersequence, with erosion of the Crayfish Supersequence observed in places (Finlayson et al., 1996; Krassay et al., 2004). The Eumeralla Supersequence is ~2.3 km thick at Windermere-2, onshore in Victoria and basin-scale seismic interpretation studies demonstrate a slight southerly thickening of the Eumeralla Supersequence towards the present-day shelf-edge break (Fig. 1a; Krassay et al., 2004; Stacey et al., 2013, Fig. 3.3). These studies also show noticeable thinning of the

Eumeralla Supersequence south beyond the present-day shelf-edge break into deeper water towards the outer edge of the offshore Otway Basin (Krassay et al., 2004; Stacey et al., 2013, Fig. 3.3). A major basin-wide unconformity has been recognized above the Eumeralla Supersequence, with little or no Cenomanian strata preserved (Partridge, 2001; Krassay et al., 2004; Tassone et al., 2014).

Succeeding the Aptian-Albian Eumeralla Supersequence is the Turonian-Santonian Shipwreck Supersequence (Fig. 2), which thickens basinward of the present-day shelf-edge break and Mussel Fault Zone (Fig. 1a), reaching a maximum thickness of 2.5 s TWT (Krassay et al., 2004; O'Brien and Thomas, 2007). The Shipwreck Supersequence can be subdivided into three seismically defined stratal units (Krassay et al., 2004). The oldest, Turonian age, stratal unit is geometrically characterized by syn-kinematic wedge-shaped packages strongly controlled by a vast array of normal faults, whereas the overlying Coniacian-early Santonian age stratal unit displays depositional control by wider spaced faults, evident by more widely spaced syn-kinematic wedge-shaped geometries (Krassay et al., 2004). The youngest late Santonian age stratal unit displays little to no syn-kinematic strata and hence no fault control (Krassay et al., 2004).

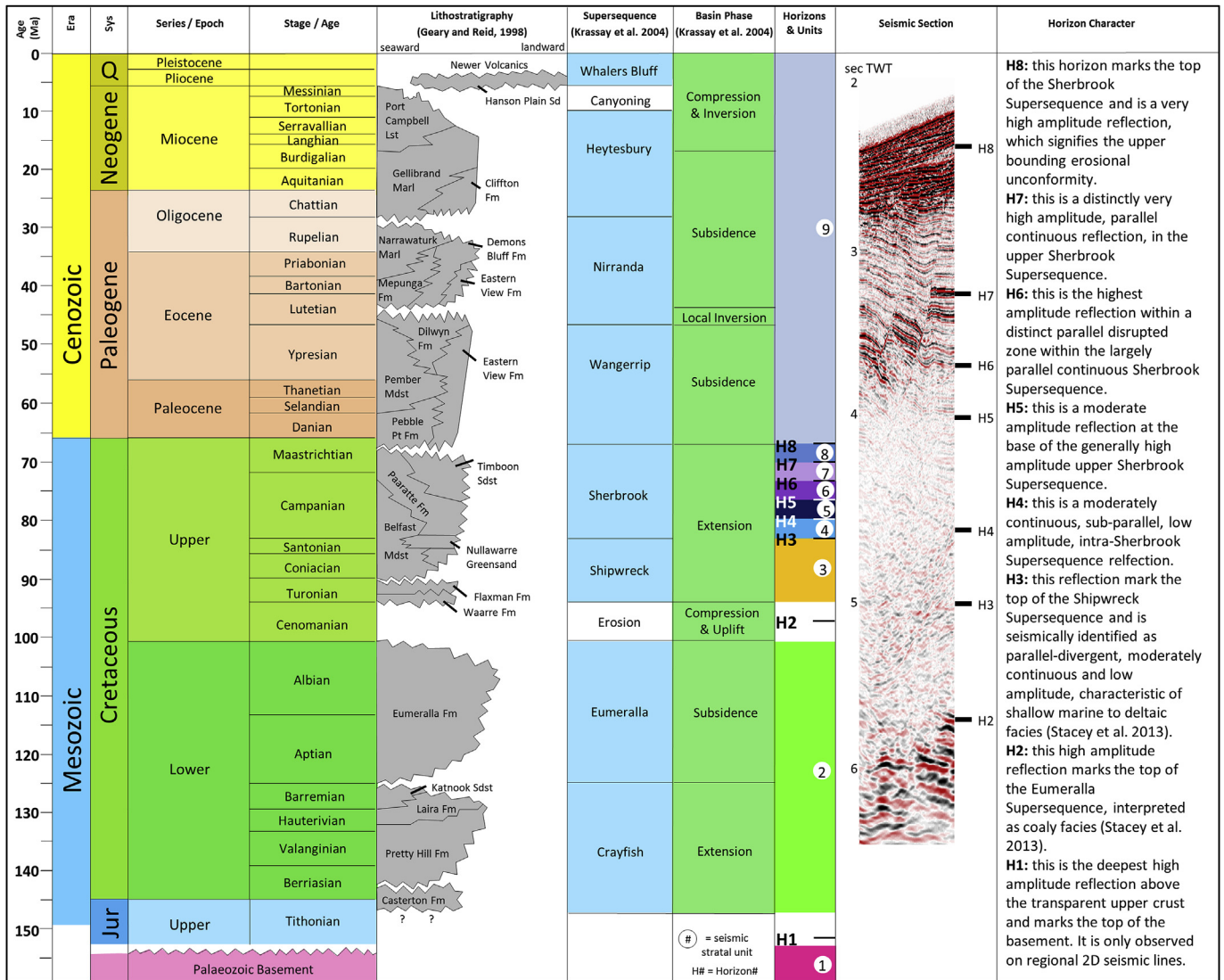


Fig. 2. Otway Basin tectono-stratigraphic framework modified from Krassay et al. (2004) and Geary and Reid (1998), with horizons and seismic stratigraphic units defined for this study. A seismic section has been added to show the seismic character of picked horizons, which are described in the far right column.

The Shipwreck Supersequence is overlain by the Campanian-Maastrichtian Sherbrook Supersequence (Fig. 2), which marks a period of major deltaic deposition and thickens basinward of the present-day shelf-edge break (Fig. 1a), similar to the Shipwreck Supersequence (Partridge, 2001; Krassay et al., 2004; Stacey et al., 2013). During the Campanian-Maastrichtian there is generally less growth of active faults than during the Turonian-Santonian, with the exception of localized growth of the Mussel Fault Zone, resulting from continued mechanical extension prior to the eventual separation of Australia and Antarctica (Krassay et al., 2004; O'Brien and Thomas, 2007). Cenozoic post-rift sedimentation is represented by the latest Maastrichtian to middle Eocene Wangerrip Supersequence, the middle Eocene to early Oligocene Nirranda Supersequence, the Late Oligocene to Late Miocene Heytesbury Supersequence, and the Plio-Pleistocene deposition of the Whalers Bluff Supersequence (Krassay et al., 2004; Holford et al., 2014) (Fig. 2). Sediments of the Paleocene-middle Eocene Wangerrip Supersequence were deposited in coastal plain, deltaic and inner-shelf settings, whilst the younger Nirranda and Heytesbury supersequences developed in open marine conditions, resulting in mixed carbonates/siliciclastic sedimentation (Krassay

et al., 2004; O'Brien and Thomas, 2007). Cenozoic thermal subsidence was intermittently punctuated by periods of inversion and uplift (Holford et al., 2014; Bailey et al., 2014).

The 3D seismic reflection survey (Amrit 3D) used in this study is located at the present-day shelf-edge break, approximately 55 km south of the town of Portland, Victoria. The study area is located at the boundary between the Inner Otway Basin and the deepwater and frontier Nelson Sub-Basin. Syn-depositional fault growth at the shelf-edge break is very clear in the Shipwreck and Sherbrook supersequences at this location (Stacey et al., 2013, Fig. 3.7). Faults are truncated rapidly with erosion of latest fault throw, and appear to have remained dormant into the Cenozoic. Latest Maastrichtian-Cenozoic sediments quite abruptly thin out basinward of the 3D survey. Two wells with minor hydrocarbon shows have been drilled within the confines of 3D survey: Hill-1 and Amrit-1 (Fig. 1a). Both of these wells targeted Paaratte Formation reservoirs (Fig. 2) on tilted fault block closures in water depths of 213 m and 1425 m, respectively, thus making the latter the deepest well drilled in the Otway Basin to date (Department of Resources, Energy and Tourism, 2009).

3. Data and methodology

3.1. 3D seismic reflection data

This study uses the Amrit 3D seismic reflection survey, which was recorded to a depth of 6.5 s TWT. The survey covers an area of ~1120 km² (~43 km along strike and ~26 km in the dip direction) on the present day shelf edge of the offshore Otway Basin. The inline and crossline spacing of the survey are 12.5 m, with the inlines oriented NW-SE and crosslines oriented NE-SW. Water depths within the survey vary between approximately 130 m and 1750 m and all depths discussed herein use sea level as a datum. Between 2 and 6 s two-way-time (TWT) below the sea floor, the vertical resolution of this 3D reflection survey ranges from 19 m to 38 m. This was calculated using the dominant frequency at the upper and lower limits of the TWT interval. This study also uses three two-dimensional (2D) seismic lines (ds01-108, ds01-109 and ds01-110), which all transect the 3D survey (Fig. 1a). Horizon ties for the seismic interpretation were based on well data from Amrit-1 and Hill-1 as well as 2D seismic lines that tie to wells outside the study area (e.g. Bridgewater Bay-1 and Triton-1, Fig. 1a), allowing a chronostratigraphically-constrained seismic-stratigraphic framework to be established. Due to latest Maastrichtian erosion of fault blocks, the youngest periods of growth of these faults cannot be studied, leaving horizon 7 (Fig. 2) as the youngest non-eroded measurement of fault throw.

3.2. Interpretation of 3D seismic data

Interpretation of the 3D seismic reflection survey reveals ten visible normal fault segments, hereafter referred to as F1-F10 (Fig. 1c). Nine of the fault segments (F2-F10, Fig. 1b; c) are arranged in two strike-linked assemblages (hereafter referred to as FA1 and FA2), with one fault (F1) located up-dip from these assemblages. Fault 1 is the most landward fault and is hard-linked on the south-eastern lateral tip line to FA1. Fault assemblage 1 (FA1) is situated immediately down-dip from F1 and consists of F2-F6, which are hard-linked from NW to SE, covering a total strike length of approximately 30 km. Fault assemblage 2 (FA2) is situated immediately down-dip of FA1 and consists of F7-F10, which are hard-linked from NW to SE, respectively, covering a total strike length of approximately 20 km. Of the faults within the study area, F7 is the only fault that cannot be fully analysed as the north-western tip line lies outside of the zone of good quality seismic data. Fault 1 and FA1 continue below the base of the 3D seismic survey, which extends to 6.5 s TWT (Fig. 3). However, FA2 is fully contained within the 3D survey, providing greater confidence in its growth history, in comparison to F1 and FA1 (Fig. 3). To determine the earliest growth and interaction of F1 and FA1, we have also interpreted three 2D seismic reflection profiles that transect the 3D reflection survey and image down to 12 s TWT (Fig. 4). The growth of all ten faults during the latest Cretaceous is difficult to establish, with an erosional surface at the Cretaceous-Cenozoic boundary creating an abrupt termination of fault segment upper tip lines (between stratal units 8 and 9; Fig. 3). The Cenozoic interval is un-faulted, which implies that all ten faults have been dormant since the latest Cretaceous.

3.3. Interpretation of 2D seismic data

Interpretation of the 2D seismic profiles shows that F1-F6 are located directly above, and are linked to major basement-involved faults either via upward tip-line propagation of basement-involved faults or dip-linkage (Fig. 4). Faults 7–10 (FA2) are fully imaged by the 3D survey, with lower tip-lines penetrating only as deep as the Shipwreck Supersequence, and thus are not linked to basement-

involved faults. However, F1-F6 do penetrate down to basement level, displaying linkage to basement-involved faults (Figs. 3 and 4). The basement plateaus (Fig. 1e) are on landward (NE) tilted half-graben fault blocks, which in some places have minor intra-fault block normal faulting (Fig. 4). Major basement-involved normal faults, which offset these fault blocks are generally spaced 1–3 km apart, dip basinward (SW) and typically display upwards of 200 ms TWT of throw (Fig. 4).

3.4. Determining fault growth

We use two techniques to study the evolution of ten normal fault segments that are hard-linked along strike: [1] Throw-distance (*T-x*) graphs and throw backstripping; and [2] throw-depth (*T-z*) analysis. Throw-distance analysis of all fault segments has been conducted displaying throw-distance plots of horizons 2–7 to establish the throw variation along strike of the fault assemblages, and consequently, segment linkage. Throw-depth analysis evaluates downward tip-line propagation and dip-linkage (Mansfield and Cartwright, 1996; Rykkelid and Fossen, 2002; Baudon and Cartwright, 2008; Jackson and Rotevatn, 2013). The degree of differential compaction during or after burial can create errors in the measurement of the vertical and lateral throw analysis used in this study (Taylor et al., 2008; Giba et al., 2012). However, decompaction calculations have not been incorporated into this study as we are primarily interested in the along-strike variation of throw on individual fault segments, rather than trying to quantify the absolute amount of throw. To convert throw values from time to depth we have used a standard Otway Basin power function established from the amalgamation of stacking velocity data for all surveys (up until 2004) across the area (Petkovic, 2004).

4. Fault growth analysis

4.1. Fault 1

Throw-distance analysis of F1 shows a throw profile characteristic of one isolated fault with a maximum throw at location 4 (close to the centre of the fault) of ~1.49 km, and throw decreasing outward to the lateral tip-lines (Fig. 5b). Greater throw accumulation has occurred at a higher stratigraphic level (H6, locations 1, 2, 3, 6, and 7, Fig. 5b) towards the NW and SE lateral tip-lines than at the centre of the fault (H2, locations 4 and 5, Fig. 5b). This suggests that this fault segment has grown laterally while accumulating significant throw. Throw-depth analysis (Fig. 5a) indicates that while constant growth during the deposition of the Turonian-Maastrichtian intervals has occurred at location 5, dip-linkage has occurred on the entire NW half of the fault. This indicates that during the deposition of stratal unit 7, lateral tip-line propagation to the NW occurred, but only at a shallow level, creating vertical isolation of the growth strata from the underlying fault surface (Fig. 5a). Dip-linkage has eventually been achieved following tip-line propagation of fault segments. This fault penetrates below the 3D survey at locations 4 and 5 and may dip-link to major basement-involved faults.

4.2. Fault assemblage 1

Throw-distance analysis of FA1 reveals highly variable throw along strike, with several minor throw maxima separated by local throw minima. A major throw deficit is observed between locations 3 and 4, separating the larger-scale throw maxima near locations 1 and 7 of ~1.62 km and ~1.74 km, respectively (Fig. 6b). This implies that FA1 may have potentially initiated with seven isolated fault

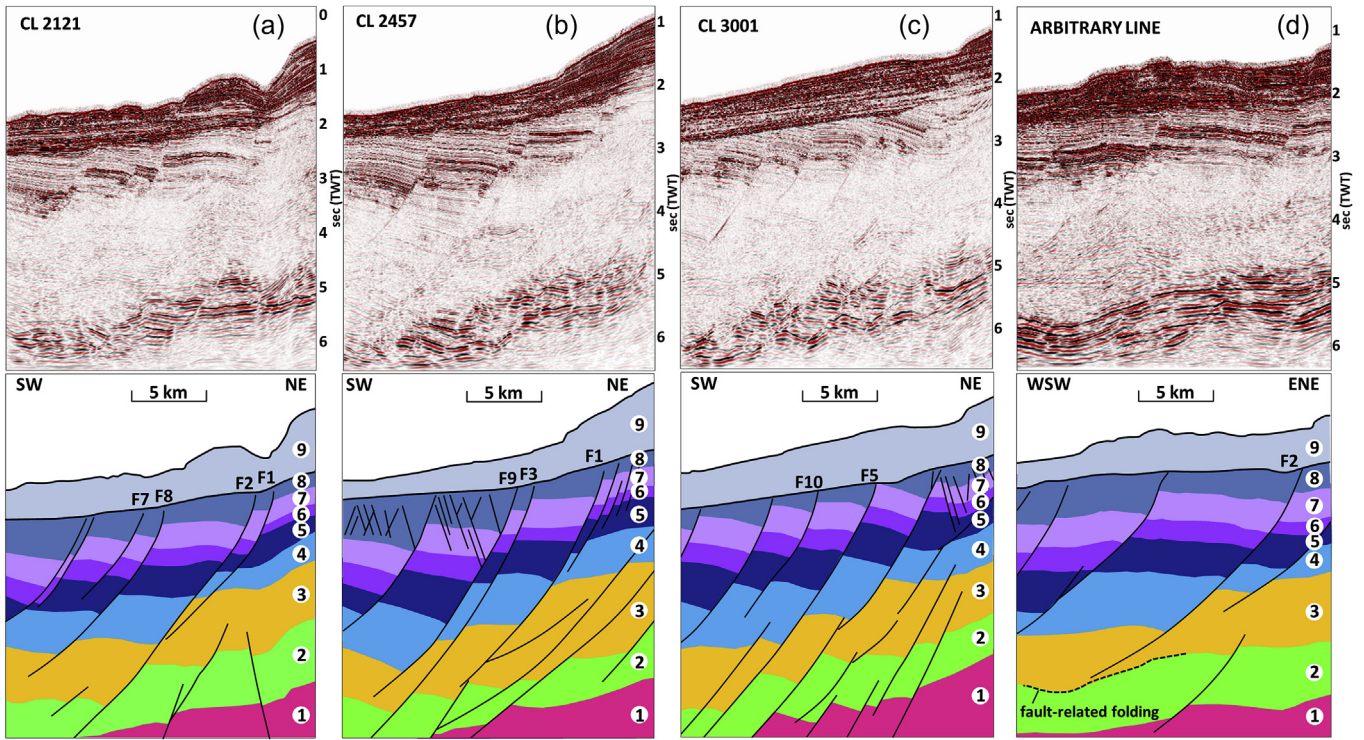


Fig. 3. Seismic crosslines 2121 (a), 2457 (b), 3001 (c) and an arbitrary line (d) from Amrit 3D, with seismic interpretation displayed below, including stratal units and faults used for this study labelled. Note faults 1, 2 and 5 all penetrating deeper than the 3D survey and dip-linking with basement-involved faults and more basinward faults 7, 8, 9 and 10 all contained within the 3D survey, displaying no linkage to basement. Also note the fault-related folding at the top of stratal unit 2 (d). The location of these crosslines is shown in Fig. 1(c).

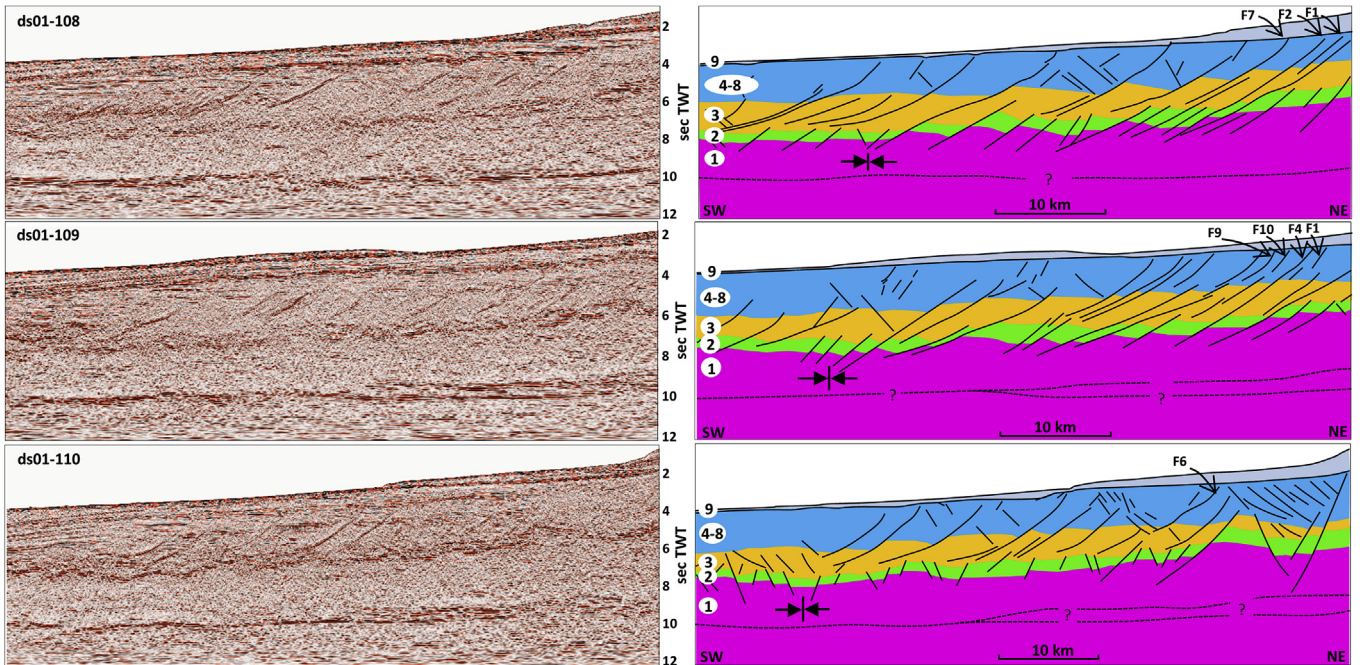


Fig. 4. Two-dimensional (2D) seismic lines ds01-108, ds01-109 and ds01-110 used for this study to show deeper basement structure below the 3D survey. The location of these lines is shown in Fig. 2(a). Note faults 1, 2, 4 and 6 dip-linking to major basement-involved faults and faults 7, 9 and 10 located over basement plateaus (see Fig. 1e) and showing no linkage to basement-involved faults.

segments, which subsequently hard-linked to form a kinematically coherent structure (Fig. 6b). Throw-depth analysis of FA1 indicates that location 1 on F2 has experienced constant growth during the

deposition of Turonian-Maastrichtian sediments (Fig. 6a). However, the SE portions of F2 (locations 2 and 3), F3 and F4 all exhibit vertically segmented (i.e. non constant) growth, creating dip-

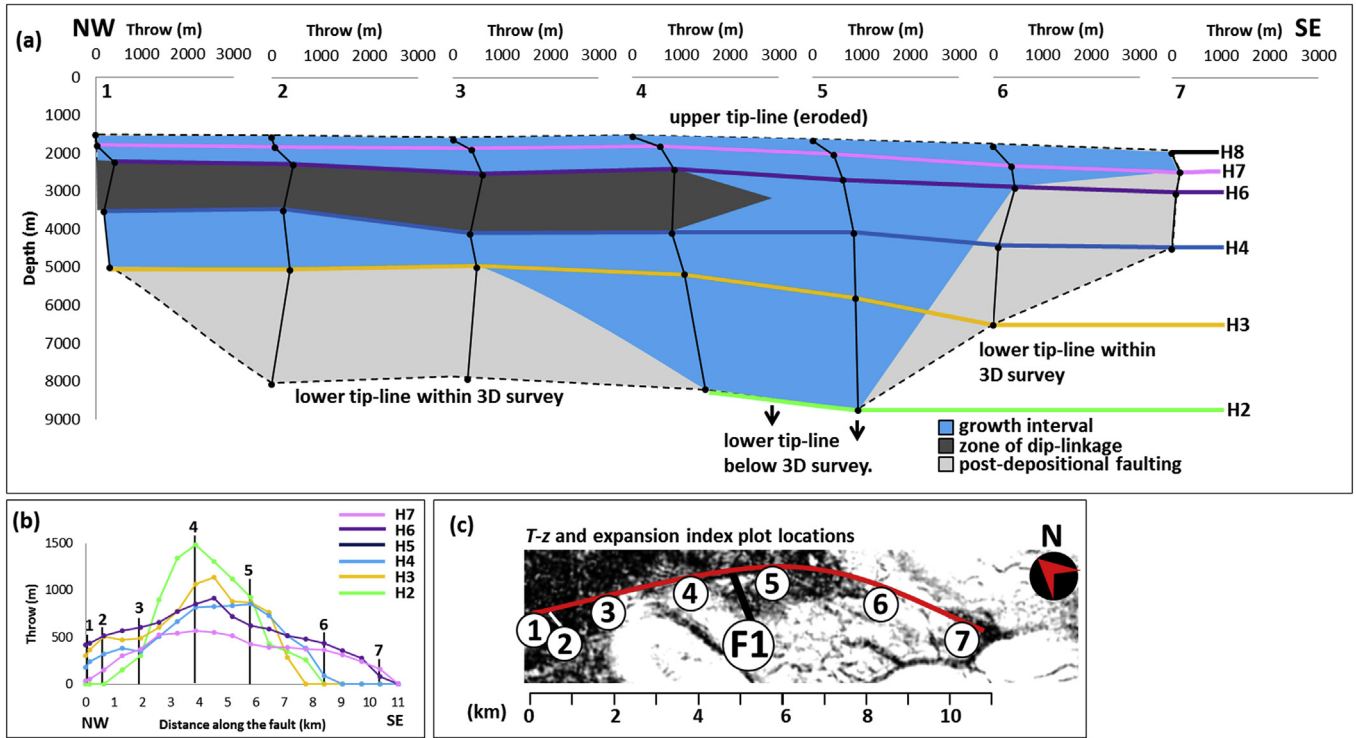


Fig. 5. (a) Throw-depth (*T-z*) analysis along strike from NW (left) to SE (right) of fault 1. The growth intervals are displayed in blue and the tip-line is dashed to show the extent of the fault plane. Note the zone of dip-linkage (dark grey) at locations 1–4. (b) Maximum throw-distance (*T-x*) graph showing the variability of throw along strike of the fault for horizons 2–7. The location of *T-z* plots 1–7 and expansion index (F1) is displayed (c). (For interpretation of the references to colour in this figure legend, the reader is referred to the web version of this article.)

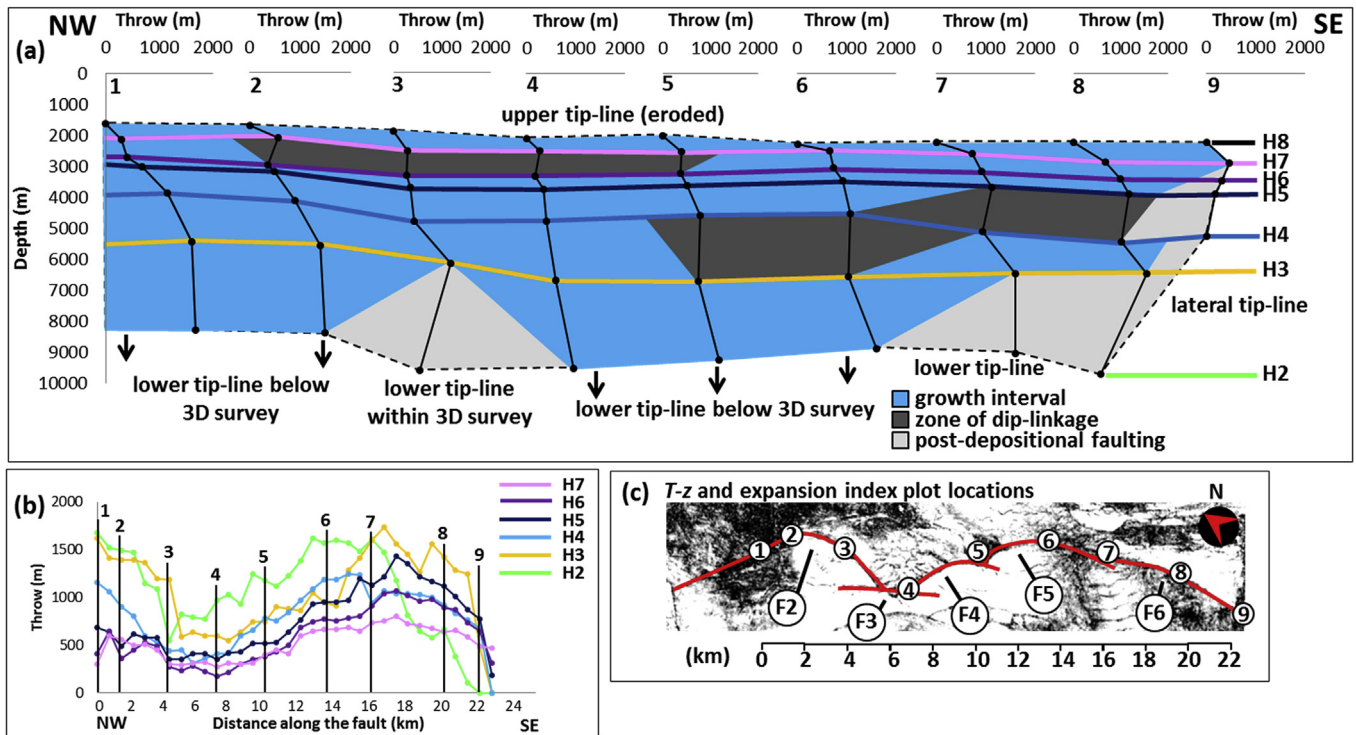


Fig. 6. (a) Throw-depth (*T-z*) analysis along strike from NW (left) to SE (right) of fault assemblage 1, comprised of faults 2–6. The growth intervals are displayed in blue and the tip-line is dashed to show the extent of the fault plane. Note the upper (stratal unit 7) zone of dip-linkage (dark grey) at locations 2–5 and the lower (stratal units 4 and 5) zone at locations 5–8. (b) Maximum throw-distance graph showing the variability of throw along strike of the fault for horizons 2–7. The location of *T-z* plots 1–9 and expansion index (F2–6) is displayed (c). (For interpretation of the references to colour in this figure legend, the reader is referred to the web version of this article.)

linkage through stratal unit 7 (Fig. 6a). Faults 4, 5 and 6 have also experienced vertically segmented growth, creating dip-linkage through stratal unit 4 on F4 and F5 and through stratal unit 5 on F6 (Fig. 6a). Given that there is significant Campanian-Maastrichtian throw accumulation, as evidenced by *T-x* analysis, but no pre-Campanian throw accumulation at location 3, this may indicate that F2 has grown in length to the SE from location 2 to location 3 while accumulating throw (Fig. 6a). However, we observe a relatively high degree of folding of horizon 2 just below the lower tip-line of F2, implying that this is potentially not radial growth, but rather throw accommodated by the ductility of the underlying pre-Cenomanian strata (Fig. 3d). This fault penetrates below the 3D survey at locations 1, 2, 4, 5 and 6, where dip-linkage to major basement-involved faults is observed on 2D seismic lines (e.g. F2 and F4; Fig. 4).

4.3. Fault assemblage 2

Throw-distance analysis of FA2 reveals a highly variable throw profile with three major throw maxima of approximately 1.25 km, 1.10 km and 1.46 km interpreted at locations 1, 2 and 4, respectively, separated by local throw minima (Fig. 7b). This implies that this fault assemblage also has a segmented growth history, with constituent fault segments linking along strike to form a larger, kinematically coherent structure. Throw-depth analysis of FA2 shows the lower tip-line of the fault assemblage fully within the 3D survey and indicates that faults in the assemblage did not nucleate until the Campanian-Maastrichtian, with no throw along the fault assemblage observed prior to the deposition of stratal unit 4 (no growth interval below H3; Fig. 7a). Fault 10 records growth during the deposition of stratal unit 4 and is the only fault active during this stage (location 7; Fig. 7a). Faults 7, 8 and 9 nucleated during the

deposition of stratal unit 5 and all faults display growth (growth interval between H5 and H4; Fig. 7a). Along strike variation of continuous growth and dip-linkage is evident within stratal unit 7 on the NW half of F7, and within stratal unit 6 on F8 and F10 (Fig. 7a).

5. Evolution of the fault array

The use of *T-x* and *T-z* analysis enables us to constrain the timing and style of fault growth and hence interpret the temporal and spatial evolution of the fault array, from its nucleation to attaining its present-day geometry. This allows us to establish the style of fault growth, and identify the factors that potentially influenced its nucleation and growth. Of particular interest to this study is the degree to which reactivation of basement-involved faults influenced fault growth within cover sequences during Upper Cretaceous extension.

5.1. Nucleation of the fault array

The timing of nucleation of F1 and FA1 cannot be determined, as all these structures penetrate deeper than the 3D survey (Figs. 3, 5a and 6a) and link to basement-involved faults, based on interpretation of the 2D seismic data (Fig. 4). The oldest measurable growth strata in the study area are within the Turonian-Santonian Shipwreck Supersequence, which unconformably overlies the Eumeralla Supersequence (Fig. 2). Given that F1-F6 (Fig. 1c) are located directly above basement-involved faults (Fig. 4), it would appear likely that these faults either nucleated as a result of basement fault reactivation during Turonian-Santonian extension or are the result of upward propagation of Early Cretaceous, basement-involved faults. We interpret that F1-F6 nucleated in vertical

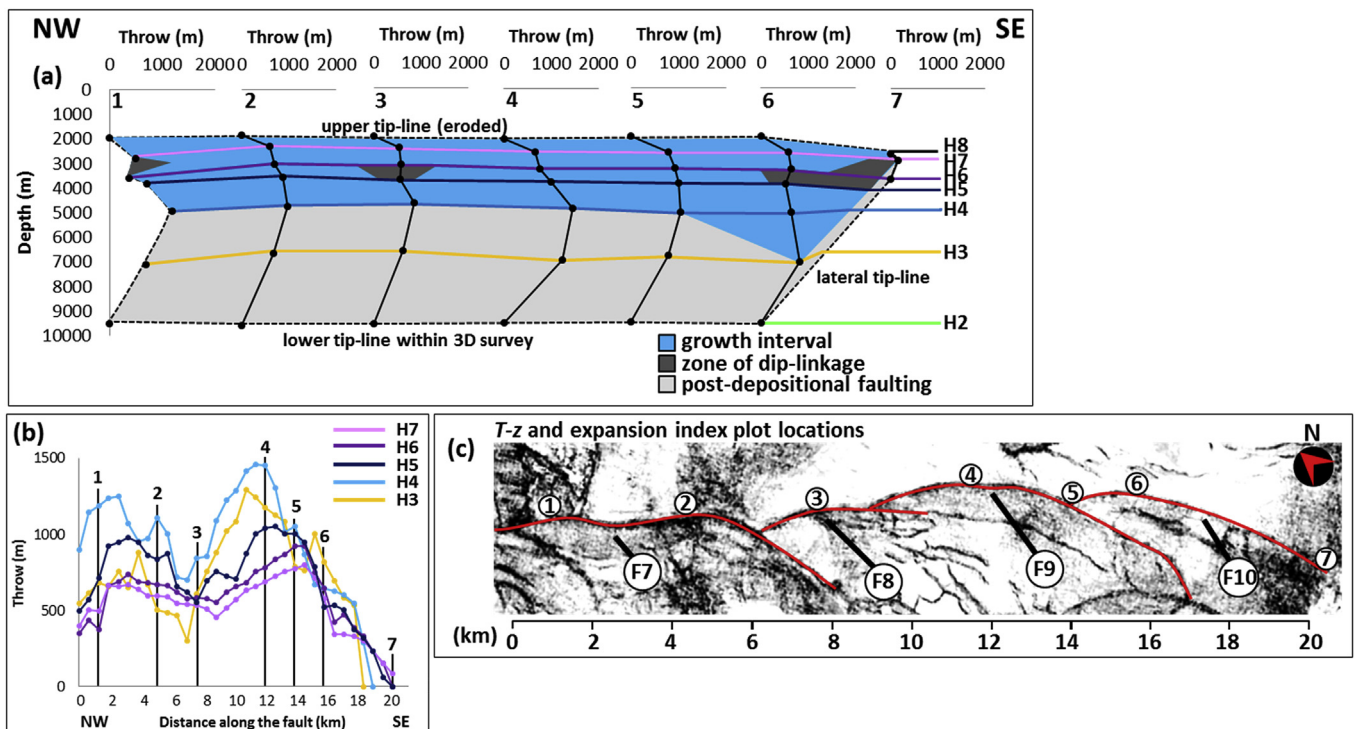


Fig. 7. (a) Throw-depth (*T-z*) analysis along strike from NW (left) to SE (right) of fault assemblage 2, comprised of faults 7–10. The growth intervals are displayed in blue and the tip-line is dashed to show the extent of the fault plane. Note the laterally confined zones of dip-linkage (dark grey) at locations 2, 4, 7 and 8 through stratal unit 6 and 7. (b) Maximum throw-distance graph showing the variability of throw along strike of the fault for horizons 3–7. The location of *T-z* plots 1–8 and expansion index (F7–10) is displayed (c). (For interpretation of the references to colour in this figure legend, the reader is referred to the web version of this article.)

isolation of and later dip-linked to basement-involved faults due to the high variability of throw along strike and the high variability of dip-linkage between the two fault sets. This can be observed where the lower tip-line of F1-F6 is imaged within the 3D survey and does not penetrate down to basement level (Figs. 5a and 6a). Faults 7 to 10 (Fig. 1c) did not nucleate until the earliest Campanian, when plateaus or highs between major basement-involved faults became gravitationally unstable with increasing Campanian-Maastrichtian sediment deposition (Fig. 4).

5.2. Growth of fault 1 and fault assemblage 1

The NW-SE striking F1 (Figs. 1c and 5) nucleated as one fault segment, attaining its final length and a maximum throw profile characteristic of one isolated fault by the deposition of stratal unit 7 (Fig. 8f). Fault 1 displays evidence for kilometre-scale throw prior to establishing its full length (Fig. 5a; b). This implies radial growth for Fault 1, with throw accumulating as it established full length. Throw-depth analysis indicates that the NW portion of F1 was

dormant during the deposition of stratal units 5 and 6, and displays dip-linkage with an upper segment, which nucleated during the deposition of stratal unit 7 (Fig. 5a). This implies that F1 grew through vertical segmentation and eventual linkage of upper and lower fault segments. However, the central region (location 5) of the fault displays continuous growth during these periods (Fig. 5a). In summary, this fault grew as one geometric structure at depth, with the central region displaying continuous fault growth during the Turonian-Maastrichtian and the NW half of the fault displaying vertically segmented growth, indicating the NW half grew with punctuations of fault dormancy.

The NW-SE striking FA1 displays highly variable throw along strike (F2-F6; Figs. 1c and 6). Based on quantitative T - x and T - z analysis of the 3D seismic reflection data (Fig. 6), we interpret that this fault assemblage grew from the nucleation and linkage of smaller fault segments. Homogeneity of throw along strike indicates that the fault assemblage had reached full linkage during or prior to the deposition of stratal unit 6 (Figs. 6c and 8e). Vertically segmented growth is also evident at FA1, with dip-linkage through

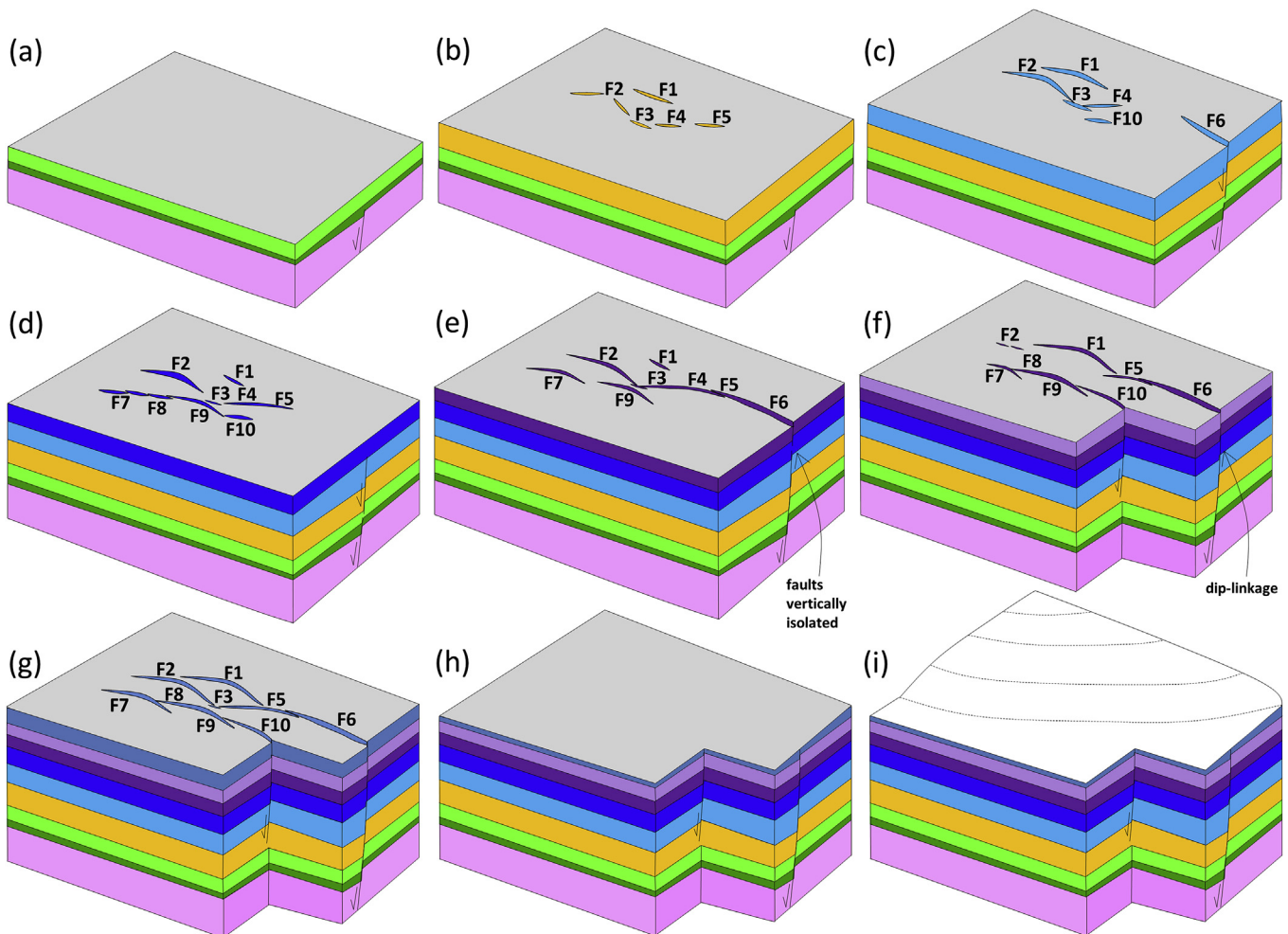


Fig. 8. Structural evolution of the fault array. Stage (a) involves Tithonian-Barremian rifting and syndeposition of the Crayfish Supersequence and Albian-Aptian, post-rift blanketing of the Eumeralla Supersequence (Morton et al., 1994; Hill et al., 1995; Perincek and Cockshell, 1995; Finlayson et al. 1996; Krassay et al., 2004). Stage (b) consists of Turonian-Santonian deposition of the Shipwreck Supersequence during independent nucleation of isolated fault segments (faults 1–5) in response to extensional reactivation of major basement-involved faults. The timing of fault length establishment is unknown. Stages (c) to (h) are progressive Campanian-Maastrichtian stages, which cannot be further distinguished in geological age due to lack of well data. Stage (c) includes continued growth of faults 1–4, dormancy of fault 5 and nucleation of faults 6 and 10. Stage (d) is comprised of the nucleation, and growth of faults 7, 8 and 9, and continued growth of faults 1, 2, 4, 5 and 10. Stage (e) shows continued growth of all 10 faults. Stage (f) includes continued growth of fault assemblage 2 (faults 7–10) and concentrated throw accumulation on fault 1 and the South-eastern end of fault assemblage 1 (faults 5 and 6). Stage (g) is unmeasurable, but simply shows the continued growth of a fully linked fault assemblage, followed by stage (h): erosion of the latest Maastrichtian throw; and stage (i): Cenozoic carbonate ramp build up, with no further fault growth.

stratal unit 4 on F4 and F5 and stratal unit 5 on F6 (Figs. 6a and 8e; f).

5.3. Growth of fault assemblage 2

The NW-SE striking FA2 (Fig. 1c) is completely imaged by the 3D seismic dataset used in this study (Fig. 3). It exhibits no linkage to basement-involved faults (Fig. 4), and displays much later growth in comparison to F1 and FA1, which are both linked to basement (Figs. 1c and 4). Fault assemblage 2 consists of F7-F10 (Fig. 1c), which display highly variable throw along strike (Fig. 7b). Whilst this implies growth via the linkage of smaller fault segments, there is no evidence for lateral tip-line propagation either during or after significant throw accumulation, as described by the 'isolated fault model' (e.g. Walsh and Watterson, 1988; Trudgill and Cartwright, 1994; Dawers and Anders, 1995; Mansfield and Cartwright, 2001). This is because greater throw accumulation at a younger stratigraphic interval, closer to the lateral tip-lines of fault segments is not identified. This would imply that the hanging wall depocentre increased in strike-length over time. Therefore, it is not possible to determine if these faults grew radially, or established their full length early in their growth history and then accumulated throw as a coherent structure, as described by the segmented 'coherent fault model' (e.g. Morley, 1999; Walsh et al., 2002; Childs et al., 2003). Throw-depth analysis indicates dip-linkage through stratal unit 6 at F8 and F10, dip-linkage through stratal unit 7 at the NW half of F7 and continuous growth at F9 (Fig. 7a). This fault assemblage is located over a basement plateau (Figs. 1e and 4) and growth initiated during the Campanian-Maastrichtian deltaic influx of the Sherbrook Supersequence (Fig. 2). Therefore, this fault assemblage may have nucleated and grown in response to either nearby basement reactivation (similar to F1 and FA1), inducing flexure in cover sediments and fault-controlled accommodation (Thorsen, 1963; Bruce, 1983; McCulloh, 1988; Cartwright et al., 1998; Imber et al., 2003; Back et al., 2006; Jackson and Larsen, 2009) or potentially deltaic sediment loading (Lundin, 1992; Damuth, 1994; Corredor et al., 2005), both of which can cause gravitational instability and consequential gravitational collapse (Peel, 2014).

5.4. Summary model for growth of the fault array

The growth of the overall fault array can be summarized into four evolutionary stages:

- [1] Syn-rift deposition of the Crayfish Supersequence during the Tithonian-Barremian (Fig. 2), leading to an underlying basement configuration of depocenters and structural highs, which is then blanketed by the Aptian-Albian Eumeralla Supersequence (Fig. 2) during a period of thermal subsidence and comparative fault dormancy (Fig. 8a; Morton et al., 1994; Hill et al., 1995; Perincek and Cockshell, 1995; Finlayson et al., 1996; Krassay et al., 2004).
- [2] The Turonian-Santonian period of fault growth has two possible interpretations: Either nucleation of F1-6 during the Turonian-Santonian (Fig. 8b), resulting from the reactivation of major basement-involved faults under resumed Upper Cretaceous extension; or reactivation and upward propagation of Early Cretaceous faults into shallow cover sediments. We prefer the first interpretation due to the high variability of throw along strike and the fault sets being only partially dip-linked along strike.
- [3] Nucleation of F7-10 during the Campanian-Maastrichtian (Fig. 8c; d), resulting from increased gravitational instability either from further displacement of underlying basement-involved faults, or sediment loading from the

deltaic Sherbrook Supersequence (Fig. 2). Continued growth during the Campanian-Maastrichtian and hard-linkage of FA1 and FA2 (Fig. 8d-g), and;

- [4] Fault growth termination, with latest Maastrichtian erosion removing evidence for the final stages of fault throw (Fig. 8h), followed by Cenozoic deposition and fault dormancy until the present day (Fig. 8i).

6. Implications for normal fault growth models

The aim of this study was to constrain the evolution of a normal fault array interacting with an active, basement-involved, rift framework. The segmented geometry in map view (Fig. 2b; c), the isolation of faults at depth (Figs. 4 and 5) and throw-distance profiles of this fault array (Figs. 6b, 7b and 8b) demonstrates that the constituent fault assemblages (Fig. 2c) have grown from the nucleation and linkage of smaller fault segments. There is some evidence for radial growth of fault segments. Fault 1 has increased in length in the Campanian-Maastrichtian to the NW while accumulating further throw (Fig. 5a). Location 3 of FA1 also shows significant Campanian-Maastrichtian throw, below which, there is an absence of pre-Campanian throw, which implies that F2 has increased in length to the SE from location 2 to location 3 during the Campanian-Maastrichtian. While greater throw is observed at a younger stratigraphic level on both of these faults, we cannot prove that initial discontinuous (faulting) throw was not transferred into continuous (folding) throw. The observations of a relatively high degree of folding of horizon 2 at location 3, just below the lower tip-line of F2, highlights this notion. This leads us to conclude that throw observed closer to the lateral tip-lines of fault segments, and at a higher stratigraphic interval, may not be indicative of radial growth, and could in fact be a variation along-strike of transference between discontinuous and continuous throw (Fig. 3d). Therefore, we cannot temporally constrain fault length establishment, segment linkage and geometric and kinematic coherence of the fault assemblages within the array. This highlights the difficulty in understanding normal fault growth in the presence of mechanically weak strata that inhibit the propagation of fault tip-lines.

Fault assemblage 1 is located above, and displays clear linkage with, major basement-involved normal faults (Figs. 4 and 9). Fault assemblage 1 has a maximum throw of ~1.74 km (Fig. 6b) and either nucleated during the Turonian-Santonian and subsequently linked with basement-involved normal faults or it is the result of reactivation and upward propagation of the basement-involved normal faults. We interpret the first option as the most likely scenario due to the high variability of throw along strike and that FA1 is only partially dip-linked to basement-involved faults along strike. In comparison, FA2, which is located over a local basement plateau (Fig. 1e), between major basement-involved normal faults, nucleated during the Campanian-Maastrichtian and has a maximum throw along the entire fault assemblage of only ~1.46 km, lower than that observed for FA1 (Fig. 7b). We suggest that major basement-involved normal faults likely reactivated during the Turonian-Santonian under resumed crustal extension (Krassay et al., 2004) and induced the vertically isolated nucleation of FA1 in shallow cover sediment directly above these faults (Fig. 9a and b). We do not rule out the possibility of FA1 nucleating in response to gravitational instability and propagating downwards to link with dormant basement-involved faults. However, FA1 is located directly over the basement-involved fault system and is dip-linked to the basement-involved normal faults along a majority of the fault assemblage. Furthermore, the Late Cretaceous is widely accepted as being a period of mechanical extension in the Otway Basin (Moore et al., 2000; Krassay et al., 2004; Stacey et al., 2013). Therefore, we propose a most likely case scenario that the basement-involved

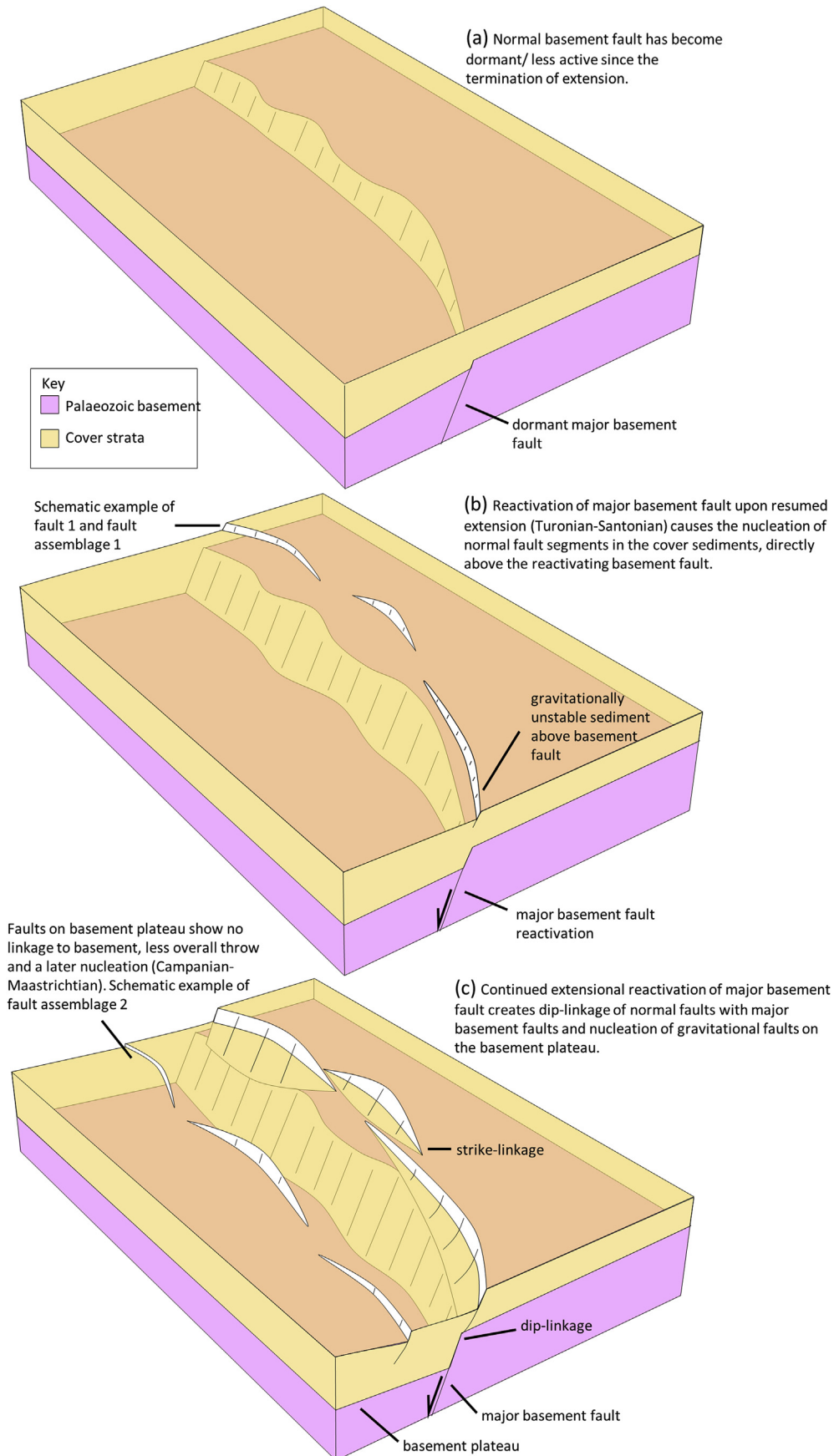


Fig. 9. Three-dimensional (3D) schematic illustration of a dormant extensional basement-involved fault (a), reactivating (b) and inducing the nucleation of normal fault segments in the sediments directly above, with an unknown timing of fault length establishment. With continued mechanical extensional, both the basement-involved and shallower normal faults accumulate further throw and propagate to eventually dip-link. With continued sedimentation and crustal extension, the basement plateau (see Fig. 1e) becomes gravitationally unstable, causing gravitational faults to nucleate in the cover sediments. However, these faults show less overall throw, shallower lower tip line propagation and no interaction with the basement framework, compared to faults directly above basement-involved faults.

normal faults below FA1 were active during the nucleation and growth of FA1, a process described as ‘active’ kinematic linkage, as opposed to static or coincidental ‘inheritance’ (Jackson and Rotevatn, 2013). While gravitational instability is still present over a basement plateau (Fig. 1e), it is of lesser influence compared to sediment overlying a reactivating major basement-involved normal fault, resulting in the later fault nucleation, less overall throw and shallower lower tip-line propagation of FA2 and consequently no linkage to basement (Fig. 9c).

We have interpreted that basement reactivation is the probable cause of nucleation of these shallow normal faults. However, the kinematic coherence between FA1 and the underlying basement-involved normal faults cannot be determined. Therefore, we cannot distinguish between isolated growth and incidental linkage of FA1 to basement-involved normal faults or the development of a Cretaceous aged kinematically coherent fault system (Walsh and Watterson, 1991; Childs et al., 1995, 2003; Giba et al., 2012; Jackson and Rotevatn, 2013). There is no 3D seismic data coverage of the underlying basement sequence, and hence it is not possible to determine: [1] the exact orientation and geometry of the basement framework (previously determined regional W to NW trend; Moore et al., 2000; Teasdale et al., 2003; Krassay et al., 2004; Boulton et al., 2008; Gibson et al., 2013); [2] the along-strike continuity of basement-involved normal faults observed on 2D seismic lines, and; [3] the variations of throw, along-strike, of the basement-involved normal faults. Given these uncertainties, we cannot determine the along-strike continuity of basement influence over the Upper Cretaceous fault development of FA1.

The Upper Jurassic-Cenozoic Ceduna Sub-Basin, Great Australian Bight, which is also situated along Australia’s southern margin and formed during the break-up of Australia and Antarctica, contains a record of Campanian-Maastrichtian deltaic deposition, similar to that represented by the Sherbrook Supersequence of the Otway Basin. However, the Ceduna Sub-Basin also hosts a Cenomanian delta system and an associated late Albian shale detachment, with thermal subsidence initiating in the Early Cretaceous (Totterdell et al., 2000; Totterdell and Bradshaw, 2004). Despite these differences, evidence from the Ceduna Sub-Basin shows similar structural style and spatial constraints to FA2 in this study, by showing little to no influence or interaction of basement framework on gravity-driven normal fault growth, high variability of throw/displacement along strike and the linkage of smaller fault segments to form larger fault assemblages (Robson et al., 2016). This study, at the present-day shelf-edge break of the Otway Basin, highlights the difficulty in constraining normal fault growth for gravity-driven fault arrays in the presence of mechanically weak strata and interacting with a rifting basement framework. The interpretation of the Amrit 3D seismic reflection data shows evidence for high variability of throw along-strike and down-dip of fault assemblages and consequently provides an example of laterally and vertically segmented normal fault growth to form larger fault assemblages.

Detailed normal fault growth studies using 3D seismic data have been relatively well-documented in rift basins (e.g. Kornsawan and Morley, 2002; Morley et al., 2007; Jackson and Larsen, 2009; Kane et al., 2010; Giba et al., 2012; Jackson and Rotevatn, 2013). Normal fault growth has been studied to a lesser degree within the predominantly gravity-driven, post-rift strata of passive margin basins (Koledoye, Aydin and May, 2003; Khani and Back, 2012; Robson et al., 2016). This study represents an advance on previous work in that it provides detailed temporal and spatial constraints on the growth of gravity-driven normal faults that were also influenced by basement-involved normal fault reactivation during continued rifting. This study also compares two normal fault assemblages that developed during a period of crustal extension, one of which has

direct geometric linkage to basement-involved faults and the other having no linkage to basement-involved faults. Therefore, the findings of this study not only have an impact on our understanding of the growth of normal fault arrays, such as those present in the Gulf of Mexico (Buffler et al., 1979; Winker and Edwards, 1983; Wu et al., 1990; Rowan, 1997), Niger Delta (Doust and Omatsola, 1990; Morley and Guerin, 1996; Cohen and McClay, 1996; Bilotti and Shaw, 2005; Corredor et al., 2005; Briggs et al., 2006; Cobbold et al., 2009) and Baram Delta (James, 1984; Koopman et al., 1996; Schreurs, 1997; King et al., 2010), but also on rift basins, where the basement framework has a large influence over shallow faulting in the cover, such as the North Sea, the Suez Rift and the Gulf of Thailand (Morley et al., 2004; Jackson and Larsen, 2009; Kane et al., 2010; Jackson and Rotevatn, 2013; Lewis et al., 2013). The results of this study also highlight short-wavelength variability in fault growth with clear geometric and temporal differences between two along-strike fault assemblages, located as little as 2 km apart in the dip direction. Margin and basin-scale studies proximal to this location include the evolution of the entire southern margin of Australia (Willcox and Stagg, 1990; Sayers et al., 2001; Holford et al., 2011; Totterdell et al., 2011), the tectono-stratigraphic framework of the Otway Basin (Hill et al., 1995; Finlayson et al., 1996; Geary and Reid, 1998; Moore et al., 2000; Krassay et al., 2004), and the structure and petroleum prospectivity of the deep-water Otway Basin (Moore et al., 2000; Stacey et al., 2013). This study contributes to this body of research by providing detailed constraints on the growth of a normal fault array at the present-day shelf-edge break, which divides the relatively well-explored Inner Otway Basin from the frontier deepwater parts of the basin.

7. Conclusions

We used 2D and 3D seismic reflection data from the present-day shelf-edge break of the Otway Basin, Australia, to establish temporal and spatial constraints for the structural evolution of a normal fault array. In this study we have analysed the growth of two fault assemblages, one of which is a vertically independent gravity-driven fault assemblage over a basement plateau and the other has clear linkage to basement-involved normal faults, which have heavily influenced growth. Thus, comparison of the structural style of normal fault growth on fault assemblages in close proximity to one another, but with distinctly different levels of interaction with the underlying rifted basement is possible. It is established in this study that both fault assemblages display highly variable along-strike and vertical throw patterns, providing evidence for growth via lateral and vertical segment linkage. It is also established that the fault assemblage linked to basement-involved normal faults displays earlier growth and greater overall throw, due to the earlier initiation of faults above reactivating basement-involved normal faults during Upper Cretaceous rifting. The initial kinematic and geometric coherence and the along-strike continuity of interaction between the basement-involved normal faults and the shallower normal faults cannot be constrained. This is due to the lack of information on the geometry, orientation and throw trends of the underlying basement-involved normal faults. This study highlights the complexity of gravity-driven normal fault growth in the presence of mechanically weak strata and the interaction of basement-involved normal faults with shallower normal faults developed in cover sediments. Furthermore, this study provides new constraints on the structural evolution of the under-explored, deepwater Otway Basin, by highlighting kilometre-scale, intermittent, Turonian-Maastrichtian normal fault growth at the present-day shelf edge break.

Acknowledgments

This research forms part of a PhD project supported by the ASEG Research Foundation (RF14P04) for which funding is gratefully acknowledged. We would also like to thank the Australian Research Council (DP120101460, DP160101158) and University of Adelaide for scholarship funding; IHS (Kingdom) DownUnder Geosolutions (DUG Insight) and Midland Valley (Move) for software use. This forms TRaX record 354.

References

- Back, S., Höcker, C., Brundiers, M.B., Kukla, P.A., 2006. Three-dimensional-seismic coherency signature of Niger Delta growth faults: integrating sedimentology and tectonics. *Basin Res.* 18, 323–337.
- Back, S., Tioe, H.J., Thang, T.X., Morley, C.K., 2005. Stratigraphic development of synkinematic deposits in a large growth-fault system, onshore Brunei Darussalam. *J. Geol. Soc.* 162 (2), 243–257.
- Back, S., Morley, C.K., 2016. Growth faults above shale—Seismic-scale outcrop analogues from the Makran foreland, SW Pakistan. *Mar. Pet. Geol.* 70, 144–162.
- Bailey, A., King, R., Holford, S., Sage, J., Backe, G., Hand, M., 2014. Remote sensing of subsurface fractures in the Otway Basin, South Australia. *J. Geophys. Res. Solid Earth* 119 (8), 6591–6612.
- Baudon, C., Cartwright, J., 2008. The kinematics of reactivation of normal faults using high resolution throw mapping. *J. Struct. Geol.* 30 (8), 1072–1084.
- Bilotti, F., Shaw, J.H., 2005. Deep-water Niger Delta fold and thrust belt modeled as a critical taper wedge: the influence of elevated basal fluid pressure on structural styles. *AAPG Bull.* 89 (11), 1475–1491.
- Boult, P., Freeman, B., Yielding, G., Menpes, S., Diekmann, L.J., 2008. A minimum-strain approach to reducing the structural uncertainty in poor 2D seismic data, Gambier Embayment, Otway Basin, Australia. In: Blevin, J.E., Bradshaw, B.E., Uruski, C. (Eds.), *Eastern Australian Basins Symposium III*, Petroleum Exploration Society of Australia, pp. 109–118. Special Publication.
- Briggs, S.E., Davies, R.J., Cartwright, J.A., Morgan, R., 2006. Multiple detachment levels and their control on fold styles in the compressional domain of the deepwater west Niger Delta. *Basin Res.* 18 (4), 435–450.
- Bruce, C., 1983. Shale tectonics, Texas coastal area growth faults. In: Bally, A.W. (Ed.), *Seismic Expression of Structural Styles: American Association of Petroleum Geologists Studies in Geology*, vol. 15, 2.3.1–2.3.1-6.
- Buffler, R.T., Shaub, F.J., Watkins, J.S., Worzel, J.L., 1979. Anatomy of the Mexican ridges, southwestern Gulf of Mexico. *Geol. Geophys. Investig. Cont. Margins AAPG Mem.* 29, 319–327.
- Cartwright, J.A., Bouroulllec, R., James, D., Johnson, H.D., 1998. Polycyclic motion history of Gulf Coast Growth Faults from high resolution kinematic analysis. *Geology* 26, 819–822.
- Childs, C., Nicol, A., Walsh, J.J., Watterson, J., 2003. The growth and propagation of syndimentary faults. *J. Struct. Geol.* 25 (4), 633–648.
- Childs, C., Watterson, J., Walsh, J.J., 1995. Fault overlap zones within developing normal fault systems. *J. Geol. Soc.* 152 (3), 535–549.
- Cobbold, P.R., Clarke, B.J., Løseth, H., 2009. Structural consequences of fluid overpressure and seepage forces in the outer thrust belt of the Niger Delta. *Pet. Geosci.* 15 (1), 3–15.
- Cohen, H.A., McClay, K., 1996. Sedimentation and shale tectonics of the northwestern Niger Delta front. *Mar. Pet. Geol.* 13 (3), 313–328.
- Corredor, F., Shaw, J.H., Bilotti, F., 2005. Structural styles in the deep-water fold and thrust belts of the Niger Delta. *AAPG Bull.* 89 (6), 753–780.
- Damuth, J.E., 1994. Neogene gravity tectonics and depositional processes on the deep Niger Delta continental margin. *Mar. Pet. Geol.* 11, 321–346.
- Dawers, N.H., Anders, M.H., 1995. Displacement length scaling and fault linkage. *J. Struct. Geol.* 17 (5), 607–614.
- Department of Resources, Energy and Tourism, 2009. Release Areas V09-1, V09-2, V09-3 and V09-4, Central Otway Basin, Victoria. <http://www.petroleum-creage.gov.au/>.
- Doust, H., Omatsola, E., 1990. Niger Delta. In: Edwards, J.D., Santogrossi, P.A. (Eds.), *Divergent/Passive Margin Basins*, vol. 48. American Association of Petroleum Geologists Memoir, pp. 201–238.
- Duddy, I.R., 1997. Focusing exploration in the Otway Basin: Understanding timing of source rock maturation. *APPEA J.* 35, 178–1491.
- Finlayson, D.M., Johnstone, D.W., Owen, A.J., Wake-Dyster, K.D., 1996. Deep seismic images and the tectonic framework of early rifting in the Otway Basin, Australian southern margin. *Tectonophysics* 264 (1), 137–152.
- Geary, G.C., Reid, I.S.A., 1998. Hydrocarbon Prospectivity of the Offshore Eastern Otway Basin, Victoria for the 1998 Acreage Release. Victorian Initiative for Minerals and Petroleum Report 55. Department of Natural Resources and Environment.
- Giba, M., Walsh, J.J., Nicol, A., 2012. Segmentation and growth of an obliquely reactivated normal fault. *J. Struct. Geol.* 39, 253–267.
- Gibson, G.M., Totterdell, J.M., White, L.T., Mitchell, C.H., Stacey, A.R., Morse, M.P., Whitaker, A., 2013. Pre-existing basement structure and its influence on continental rifting and fracture zone development along Australia's southern rifted margin. *J. Geol. Soc.* 170 (2), 365–377.
- Hill, K.A., Finlayson, D.M., Hill, K.C., Cooper, G.T., 1995. Mesozoic tectonics of the Otway Basin: the legacy of Gondwana and the active Pacific margin— a review and ongoing research. *APPEA J.* 35 (1), 467–493.
- Holford, S.P., Hillis, R.R., Duddy, I.R., Green, P.F., Stoker, M.S., Tuitt, A.G., Backé, G., Tassone, D.R., Macdonald, J.D., 2011. Cenozoic post-breakup compressional deformation and exhumation of the southern Australian margin. *APPEA J.* 51 (1), 613–638.
- Holford, S.P., Tuitt, A.K., Hillis, R.R., Green, P.F., Stoker, M.S., Duddy, I.R., Tassone, D.R., 2014. Cenozoic deformation in the Otway Basin, southern Australian margin: implications for the origin and nature of post-breakup compression at rifted margins. *Basin Res.* 26 (1), 10–37.
- Imber, J., Childs, C., Nell, P.A.R., Walsh, J.J., Hodgetts, D., Flint, S.S., 2003. Hanging wall fault kinematics and footwall collapse in listric growth fault systems. *J. Struct. Geol.* 25, 197–208.
- Jackson, C.L., Larsen, E., 2009. Temporal and spatial development of a gravity-driven normal fault array: middle–upper Jurassic, South Viking graben, northern North Sea. *J. Struct. Geol.* 31 (4), 388–402.
- Jackson, C.A.L., Rotevatn, A., 2013. 3D seismic analysis of the structure and evolution of a salt-influenced normal fault zone: a test of competing fault growth models. *J. Struct. Geol.* 54, 215–234.
- James, D.M.D. (Ed.), 1984. *The Geology and Hydrocarbon Resources of Negara Brunei Darussalam*, vol. 8. Muzium Brunei and Brunei Shell Petroleum Company Berhad, pp. 2–21. Special Publication.
- Kane, K.E., Jackson, C.A.L., Larsen, E., 2010. Normal fault growth and fault-related folding in a salt influenced rift basin: South Viking Graben, offshore Norway. *J. Struct. Geol.* 32 (4), 490–506.
- Khani, H.F., Back, S., 2012. Temporal and lateral variation in the development of growth faults and growth strata in western Niger Delta, Nigeria. *AAPG Bull.* 96 (4), 595–614.
- King, R.C., Backé, G., Morley, C.K., Hillis, R.R., Tingay, M.R., 2010. Balancing deformation in NW Borneo: quantifying plate-scale vs. gravitational tectonics in a delta and deepwater fold-thrust belt system. *Mar. Pet. Geol.* 27 (1), 238–246.
- Koledoye, B.A., Aydin, A., May, E., 2003. A new process-based methodology for analysis of shale smear along normal faults in the Niger Delta. *AAPG Bull.* 87 (3), 445–463.
- Koopman, A., Schreurs, J., Ellenor, D.W., 1996. The oil and gas resources of Brunei Darussalam— The coastal and offshore oil and gas fields. In: Sandal, S.T. (Ed.), *Geology and Hydrocarbon Resources of Negara Brunei Darussalam*, pp. 155–192.
- Kornsawan, A., Morley, C.K., 2002. The origin and evolution of complex transfer zones (graben shifts) in conjugate fault systems around the Funan Field, Pattani Basin, Gulf of Thailand. *J. Struct. Geol.* 24 (3), 435–449.
- Krassay, A.A., Cathro, D.L., Ryan, D.J., 2004. A regional tectonostratigraphic framework for the Otway Basin. In: Boult, P.J., Johns, D.R., Lang, S.C. (Eds.), *Eastern Australian Basins Symposium II*. Petroleum Exploration Society of Australia, pp. 97–116. Special Publication.
- Lewis, M.M., Jackson, C.A.L., Gawthorpe, R.L., 2013. Salt-influenced normal fault growth and forced folding: the Stavanger fault system, North Sea. *J. Struct. Geol.* 54, 156–173.
- Lundin, E.R., 1992. Thin-skinned extensional tectonics on a salt detachment, northern Kwanza Basin, Angola. *Mar. Pet. Geol.* 9, 405–411.
- Mansfield, C.S., Cartwright, J.A., 1996. High resolution fault displacement mapping from three-dimensional seismic data: evidence for dip linkage during fault growth. *J. Struct. Geol.* 18 (2), 249–263.
- Mansfield, C., Cartwright, J., 2001. Fault growth by linkage: observations and implications from analogue models. *J. Struct. Geol.* 23 (5), 745–763.
- McCulloch, R.P., 1988. Differential fault-related early Miocene sedimentation, Bayou Herbert area, southwestern Louisiana. *Am. Assoc. Pet. Geol. Bull.* 72, 477–492.
- Moore, A.M.G., Stagg, H.M.J., Norvick, M.S., 2000. Deep-water Otway Basin: a new assessment of the tectonics and hydrocarbon prospectivity. *APPEA J.* 32 (1), 66–85.
- Morley, C.K., Guerin, G., 1996. Comparison of gravity driven deformation styles and behaviour associated with mobile shales and salt. *Tectonics* 15 (6), 1154–1170.
- Morley, C.K., 1999. Patterns of displacement along large normal faults: implications for basin evolution and fault propagation, based on examples from east Africa. *AAPG Bull.* 83 (4), 613–634.
- Morley, C.K., Haranya, C., Phoosongsee, W., Pongwapee, S., Kornsawan, A., Wonganan, N., 2004. Activation of rift oblique and rift parallel pre-existing fabrics during extension and their effect on deformation style: examples from the rifts of Thailand. *J. Struct. Geol.* 26 (10), 1803–1829.
- Morley, C.K., Gabdi, S., Seusutthiya, K., 2007. Fault superimposition and linkage resulting from stress changes during rifting: examples from 3D seismic data, Phitsanulok Basin, Thailand. *J. Struct. Geol.* 29 (4), 646–663.
- Morley, C.K., Charusiri, P., Watkinson, I., 2011. Structural geology of Thailand during the Cenozoic. In: Ridd, M.F., Barber, A.J., Crow, M.J. (Eds.), *Geology of Thailand*. Geological Society, London, pp. 273–334.
- Morton, J.G.G., Hill, A.J., Parker, G., Tabassi, A., 1994. Towards a unified stratigraphy for the Otway Basin (abs.). In: Finlayson, D.M. (Ed.), *Extended abstracts. Australian Geological Survey Organisation, Record 1994/14. NGMA/PESA Otway Basin Symposium*, Melbourne, pp. 7–12.
- Norvick, M.S., 2005. Plate Tectonic Reconstructions of Australia's Southern Margins. *Geoscience Australia, Record 2005/07*.
- Department of Primary Industries O'Brien, G.W., Thomas, J.H., 2007. A Technical Assessment of yet-to-find Hydrocarbon Resources Inventory, Offshore and Onshore Otway Basin. *GeoScience Victoria, Victoria, Australia*.

- Partridge, A.D., 2001. Revised stratigraphy of the Sherbrook group, Otway Basin. In: Hill, K.C., Bernecker, T. (Eds.), Eastern Australasian Basins Symposium, a Refocused Energy Perspective for the Future, Petroleum Exploration Society of Australia, pp. 455–465. Special Publication.
- Peacock, D.C.P., Sanderson, D.J., 1991. Displacements, segment linkage and relay ramps in normal fault zones. *J. Struct. Geol.* 13 (6), 721–733.
- Peel, F.J., 2014. The engines of gravity-driven movement on passive margins: quantifying the relative contribution of spreading vs. gravity sliding mechanisms. *Tectonophysics* 633, 126–142.
- Perincek, D., Cockshell, C.D., 1995. The Otway Basin: Early Cretaceous rifting to Neogene inversion. *APPEA J.* 35, 451–466.
- Petkovic, P., 2004. Geoscience Australia. Time-depth functions for the Otway Basin (2004/02).
- Robson, A.G., King, R.C., Holford, S.P., 2016. Structural evolution of a gravitationally detached normal fault array: analysis of 3D seismic data from the Ceduna Sub-Basin, Great Australian Bight. *Basin Res.* <http://dx.doi.org/10.1111/bre.12191>.
- Rowan, M.G., 1997. Three-dimensional geometry and evolution of a segmented detachment fold, Mississippi Fan foldbelt, Gulf of Mexico. *J. Struct. Geol.* 19 (3), 463–480.
- Rowan, M.G., Hart, B.S., Nelson, S., Flemings, P.B., Trudgill, B.D., 1998. Three-dimensional geometry and evolution of a salt-related growth-fault array: Eugene Island 330 field, offshore Louisiana, Gulf of Mexico. *Mar. Pet. Geol.* 15 (4), 309–328.
- Ryan, S.M., Knight, L.A., Parker, G.J., 1995. The Stratigraphy and Structure of the Tyrendarra Embayment. Geological Survey of Victoria, Otway Basin, Victoria. VIMP report 15.
- Rykkelid, E., Fossen, H., 2002. Layer rotation around vertical fault overlap zones: observations from seismic data, field examples, and physical experiments. *Mar. Pet. Geol.* 19 (2), 181–192.
- Sayers, J., Symonds, P.A., Direen, N.G., Bernardel, G., 2001. Nature of the continent-ocean transition on the non-volcanic rifted margin of the central Great Australian Bight. *Geol. Soc. Lond. Spec. Publ.* 187 (1), 51–76.
- Schreurs, G., 1997. The petroleum geology of Negara Brunei Darussalam; an update. In: Howes, J.V.C., Noble, R.A. (Eds.), Proceedings of the IPA Petroleum Systems of SE Asia and Australasia Conference, Jakarta, Indonesia, May, 1997. Indonesian Petroleum Association, Jakarta, pp. 751–766.
- Stacey, A.R., Mitchell, C.H., Struckmeyer, H.I.M., Totterdell, J.M., 2013. Geology and Hydrocarbon Prospectivity of the Deepwater Otway and Sorell Basins, Offshore Southeastern Australia. Record 2013/02. Geoscience Australia, Canberra.
- Tassone, D.R., Holford, S.P., Duddy, I.R., Green, P.F., Hillis, R.R., 2014. Quantifying Cretaceous Cenozoic exhumation in the Otway Basin, southeastern Australia, using sonic transit time data: implications for conventional and unconventional hydrocarbon prospectivity. *AAPG Bull.* 98 (1), 67–117.
- Taylor, S.K., Nicol, A., Walsh, J.J., 2008. Displacement loss on growth faults due to sediment compaction. *J. Struct. Geol.* 30 (3), 394–405.
- Teasdale, J.P., Pryer, L.L., Stuart-Smith, P.G., Romine, K.K., Etheridge, M.A., Loutit, T.S., Kyan, D.M., 2003. Structural framework and basin evolution of Australia's southern margin. *APPEA J.* 43 (1), 13–37.
- Thorsen, C.E., 1963. Age of growth faulting in southeast Louisiana. *Gulf Coast Assoc. Geol. Soc. Trans.* 13, 103–110.
- Totterdell, J.M., Gibson, G.M., Stacey, A.R., Mitchell, C.H., Morse, M.P., Nayak, G.K., Kuszniir, N.J., 2011. Structural architecture of Australia's 4000 km-long southern rifted continental margin. In: EGU General Assembly 2011. Geophysical Research Abstracts, 13. EGU2011-1427-1.
- Totterdell, J.M., Blevin, J.E., Struckmeyer, H.I.M., Bradshaw, B.E., Colwell, J.B., Kennard, J.M., 2000. Petroleum frontiers, systems and plays-A new sequence framework for the Great Australian Bight: starting with a clean slate. *APPEA J.* 40 (1), 95–120.
- Totterdell, J.M., Bradshaw, B.E., 2004. The structural framework and tectonic evolution of the Bight Basin. In: Eastern Australasian Basins Symposium II. Petroleum Exploration Society of Australia, pp. 41–61. Special Publication.
- Trudgill, B., Cartwright, J., 1994. Relay-ramp forms and normal-fault linkages, Canyonlands National Park, Utah. *Geol. Soc. Am. Bull.* 106 (9), 1143–1157.
- Tvedt, A., Rotevatn, A., Jackson, C.A.L., Fossen, H., Gawthorpe, R.L., 2013. Growth of normal faults in multilayer sequences: a 3D seismic case study from the Egersund Basin, Norwegian North Sea. *J. Struct. Geol.* 55, 1–20.
- Vendeville, B.C., Ge, H., Jackson, M.P.A., 1995. Scale models of salt tectonics during basement-involved extension. *Petrol. Geosci.* 1 (2), 179–183.
- Walsh, J.J., Watterson, J., 1988. Analysis of the relationship between displacements and dimensions of faults. *J. Struct. Geol.* 10 (3), 239–247.
- Walsh, J.J., Watterson, J., 1991. Geometric and kinematic coherence and scale effects in normal fault systems. *Geol. Soc. Lond. Spec. Publ.* 56 (1), 193–203.
- Walsh, J.J., Nicol, A., Childs, C., 2002. An alternative model for the growth of faults. *J. Struct. Geol.* 24 (11), 1669–1675.
- Walsh, J.J., Bailey, W.R., Childs, C., Nicol, A., Bonson, C.G., 2003. Formation of segmented normal faults: a 3-D perspective. *J. Struct. Geol.* 25 (8), 1251–1262.
- Willcox, J.B., Stagg, H.M.J., 1990. Australia's southern margin: a product of oblique extension. *Tectonophysics* 173 (1), 269–281.
- Winker, C.D., Edwards, M.B., 1983. Unstable progradational clastic shelf margins. In: Stanley, D.J., Moore, G.T. (Eds.), *The Shelfbreak: Critical Interface on Continental Margins*. Society of Economic Paleontologists and Mineralogists, Special Publication, 33, pp. 139–157.
- Withjack, M.O., Callaway, S., 2000. Active normal faulting beneath a salt layer: an experimental study of deformation patterns in the cover sequence. *AAPG Bull.* 84 (5), 627–651.
- Wu, S., Bally, A.W., Cramez, C., 1990. Allochthonous salt, structure and stratigraphy of the north- Eastern Gulf of Mexico. Part II. *Struct. Mar. Pet. Geol.* 7 (4), 334–370.

4.3 Paper 3

Robson, A. G., Holford, S. P., & King R. C. (2017). Structural evolution of a normal fault array in the

Gambier Embayment, offshore Otway Basin, South Australia: insights from 3D seismic data.

Australian Journal of Earth Sciences, 64(5), 611-624. DOI:10.1080/08120099.2017.1324822

Statement of Authorship

Title of Paper	Structural evolution of a normal fault array in the Gambier Embayment, offshore Otway Basin, South Australia: insights from 3D seismic data.
Publication Status	<input checked="" type="checkbox"/> Published <input type="checkbox"/> Accepted for Publication <input type="checkbox"/> Submitted for Publication <input type="checkbox"/> Unpublished and Unsubmitted work written in manuscript style
Publication Details	Robson, A. G., Holford, S. P., & King R. C. (2017). Structural evolution of a normal fault array in the Gambier Embayment, offshore Otway Basin, South Australia: insights from 3D seismic data. Australian Journal of Earth Sciences, 64(5), 611-624. DOI:10.1080/08120099.2017.1324822

Principal Author

Name of Principal Author (Candidate)	Alexander Robson				
Contribution to the Paper	<ul style="list-style-type: none"> Seismic interpretation fault analysis preparation of manuscript editing manuscript Corresponding author 				
Overall percentage (%)	70%				
Certification:	This paper reports on original research I conducted during the period of my Higher Degree by Research candidature and is not subject to any obligations or contractual agreements with a third party that would constrain its inclusion in this thesis. I am the primary author of this paper.				
Signature	<table border="1"> <tr> <td>_____</td> <td>_____</td> <td>Date</td> <td>6/09/2017</td> </tr> </table>	_____	_____	Date	6/09/2017
_____	_____	Date	6/09/2017		

Co-Author Contributions

By signing the Statement of Authorship, each author certifies that:

- the candidate's stated contribution to the publication is accurate (as detailed above);
- permission is granted for the candidate to include the publication in the thesis; and
- the sum of all co-author contributions is equal to 100% less the candidate's stated contribution.

Name of Co-Author					
Contribution to the Paper	<ul style="list-style-type: none"> Supervised development of work Helped in data interpretation and manuscript evaluation Multiple edits of manuscript during review 				
Signature	<table border="1"> <tr> <td>_____</td> <td>_____</td> <td>Date</td> <td>6/09/2017</td> </tr> </table>	_____	_____	Date	6/09/2017
_____	_____	Date	6/09/2017		

Name of Co-Author					
Contribution to the Paper	<ul style="list-style-type: none"> Supervised development of work Helped in data interpretation and manuscript evaluation Multiple edits of manuscript during review 				
Signature	<table border="1"> <tr> <td>_____</td> <td>_____</td> <td>Date</td> <td>6/09/2017</td> </tr> </table>	_____	_____	Date	6/09/2017
_____	_____	Date	6/09/2017		

Please cut and paste additional co-author panels here as required.

Structural evolution of a normal fault array in the Gambier Embayment, offshore Otway Basin, South Australia: insights from 3D seismic data

A. G. Robson^{a,b}, S. P. Holford^b and R. C. King^a

^aCentre for Tectonics Resources and Exploration (TRaX), Department of Physical Sciences, University of Adelaide, Adelaide, 5005, South Australia, Australia; ^bAustralian School of Petroleum, Santos Building, University of Adelaide, Adelaide, 5005, South Australia, Australia

ABSTRACT

This study was undertaken to determine the structural evolution of a normal fault array using detailed kinematic analysis of normal fault tip propagation and linkage, adding to the growing pool of research on normal fault growth. In addition, we aim to provide further insight into the evolution of the offshore Otway Basin, Australia. We use three-dimensional (3D) seismic reflection data to analyse the temporal and spatial evolution of a Late Cretaceous–Cenozoic age normal fault array located in the Gambier Embayment of the offshore Otway Basin, South Australia. The seismic reflection data cover a NW–SE-oriented normal fault array consisting of six faults, which have grown from the linkage of numerous, smaller segments. This fault array overlies and has partial dip-linkage to E–W-striking, basement-involved faults that formed during the initial Tithonian–Barremian rifting event in the Otway Basin. Fault displacement analysis suggests four key stages in the post-Cenomanian growth history of the upper array: (1) nucleation of the majority of faults resulting from resumed crustal extension during the early Late Cretaceous; (2) an intra-Late Cretaceous period of general fault dormancy, with the nucleation of only one newly formed fault; (3) latest Cretaceous nucleation of another newly formed fault and further growth of all other faults; and (4) continued growth of all faults, leading to the formation of the Cenozoic Gambier Sub-basin in the Otway Basin. Our analysis also demonstrates that Late Cretaceous faults, which are located above and dip-link to basement-involved faults, display earlier nucleation and greater overall throw and length, compared with those which do not link to basement-involved faults. This is likely attributed to increased rift-related stress concentrations in cover sediments above the upper tips of basement faults. This study improves our understanding of the geological evolution of the presently under-explored Gambier Embayment, offshore Otway Basin, South Australia by documenting the segmented growth style of a Late Cretaceous normal fault array that is located over, and interacts with, a reactivated basement framework.

ARTICLE HISTORY

Received 10 May 2016
Accepted 24 April 2017

KEYWORDS

Normal fault; extension; fault growth; segmentation; Otway Basin; southern margin; Gambier Embayment; 3D seismic data

Introduction

Normal faults evolve through geological time through the growth of fault surfaces, and the mechanical interaction and physical linkage of discrete fault segments (e.g. Childs, Watterson, & Walsh, 1995; Freeman, Boulton, Yielding, & Menpes, 2010; Walsh & Watterson, 1988; Walsh, Bailey, Childs, Nicol, & Bonson, 2003). Therefore, interpretation of faults must be physically plausible in terms of wall-rock strain distribution and magnitude (Figure 1; Freeman et al., 2010; Walsh et al., 2003). A fault should have a reasonably smooth displacement variation in three dimensions across the fault surface, with displacement decreasing from a maximum at the fault centre to the tip-lines and thus minimising strain in the faulted rock volume (Boulton, Freeman, Yielding, Menpes, & Diekmann, 2008; Freeman et al., 2010; Peacock & Sanderson, 1991, 1994; Walsh & Watterson, 1988).

Constraining and understanding the growth of normal faults requires the measurement and analysis of growth

strata, in addition to displacement patterns across the fault surface to establish how the fault geometrically and kinematically evolved (e.g. Cartwright, Trudgill, & Mansfield, 1995; Huggins, Watterson, Walsh, & Childs, 1995; Mansfield & Cartwright, 1996, 2001; Walsh et al., 2003; Walsh, Nicol, & Childs, 2002). Early models of normal fault growth suggest linkage of structures that nucleated and propagated independently, incidentally overlapped and geometrically linked through relay ramp breaching and this is referred to as the ‘isolated fault model’ (Figure 1a–c; Dawers & Anders, 1995; Peacock & Sanderson, 1991; Stewart & Hancock, 1991; Trudgill & Cartwright, 1994; Walsh & Watterson, 1988). However, more recent models indicate that some faults, which appear segmented in map view, may have grown through the upward propagation of a single structure at depth, bifurcating and forming ‘branch lines’ in cover sediments (Figure 1g; Childs et al., 1995; Childs, Nicol, Walsh, & Watterson, 2003; Giba, Walsh, & Nicol, 2012; Walsh & Watterson, 1991). These structures have been shown to be

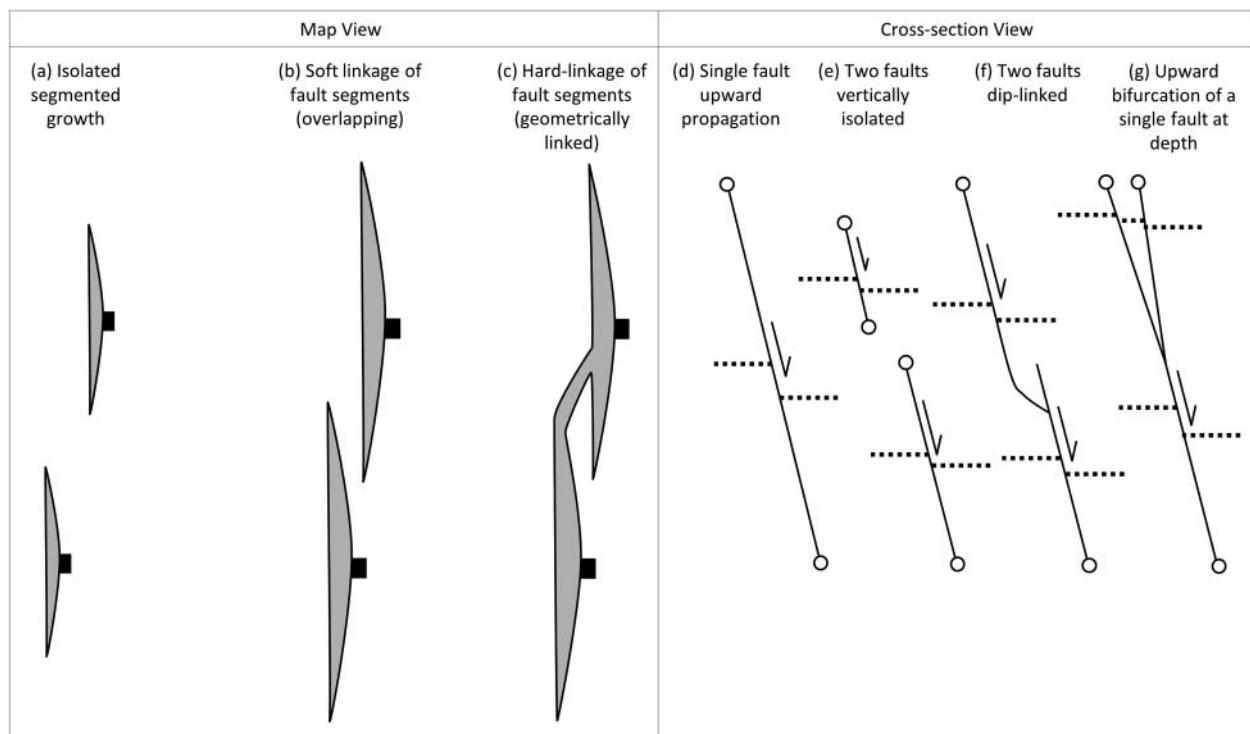


Figure 1. Schematic diagram showing the map view evolution of normal fault segments: (a) isolated segmented growth; (b) overlapping interaction, where faults may be kinematically linked, but not geometrically linked; and (c) hard-linkage (geometric and kinematic linkage) of fault segments to form one 'master' fault with a relic fault tip. Cross-section views show the appearance of: (d) a single fault, which has propagated upwards during growth; (e) two faults, which are vertically isolated, similar to faults growing in isolation in map view (a); (f) the hard dip-linkage of two initially vertically isolated faults; and (g) a normal fault, which has bifurcated during upward propagation, to appear segmented in shallow strata, but in fact it is linked to one structure at depth.

kinematically coherent from their initiation (i.e. multiple fault segments, which may be geometrically isolated, but have a cumulative displacement variation that is similar to that of a single isolated fault; Childs et al., 1995, 2003; Walsh & Watterson, 1991; Walsh et al., 2003). In cross-section, upward bifurcating faults will be physically and kinematically connected to one structure at depth (Figure 1g; Jackson & Rotevatn, 2013, figure 1b). This difference in growth style between upward bifurcation and segment isolation highlights the necessity of detailed cross-section analysis and displacement profiling of faults to constrain the variation of along-strike displacement and consequently establish the kinematic and spatial evolution of a fault.

Segment linkage has been shown to occur not only along strike, but also vertically, with local displacement deficits implying the linkage of segments in the dip direction, a phenomenon known as dip-linkage (Figure 1e, f; Baudon & Cartwright, 2008; Childs, Nicol, Walsh, & Watterson, 1996; Mansfield & Cartwright, 1996; Robson, King, & Holford, 2016a; Rotevatn & Jackson, 2014). Therefore, to understand the kinematic and geometric evolution of a fault array, we must analyse growth strata, in addition to displacement patterns across fault surfaces and fault geometry, both along-strike and vertically down a fault plane to constrain this process in three dimensions.

The purpose of this study is to analyse the growth of a normal fault array from the Gambier Embayment, offshore Otway Basin, in order to further our understanding of how normal

faults grow during polyphase extension with an underlying fault array striking 45° to the fault array of interest (Figure 2a). We aim to determine whether the fault array grew via upward bifurcation of the basement-involved faults or whether they nucleated independently in the cover and propagated downward to link with the basement-involved faults. Furthermore, we aim to document the length-displacement accumulation of individual fault segments through time and interpret the kinematic and geometric growth history.

The Otway Basin (Figure 2a) is a Late Jurassic to Cenozoic, NW-oriented rift/passive margin basin, extending from SE South Australia to NW offshore Tasmania (Holford et al., 2014; Krassay, Cathro, & Ryan, 2004; Moore, Stagg, & Norvick, 2000; Stacey, Mitchell, Struckmeyer, & Totterdell, 2013). The Otway Basin is divided into five main depocentres: the primarily onshore Inner Otway Basin, the eastern Torquay Sub-basin and the Morum, Nelson and Hunter sub-basins, which are all located in the deep-water province, seaward of the Tartwaup-Mussel Fault Zone (Figure 2a; Krassay et al., 2004; Moore et al., 2000; Stacey et al., 2013). Our study area is located 7–30 km offshore within the Gambier Embayment, which is a Cenozoic sub-basin (also referred to as the Gambier Sub-basin; Alley & Lindsay, 1995) located in the larger Otway Basin. The study area is bounded to the north and east by a major NW-striking fault system called the Tartwaup Hinge Zone (Figure 2a).

Using good-quality 3D seismic reflection data (Carpenter 3D; Figure 1a), we have identified and analysed six 5–16 km-long NW–SE-striking, Late Cretaceous normal faults, to

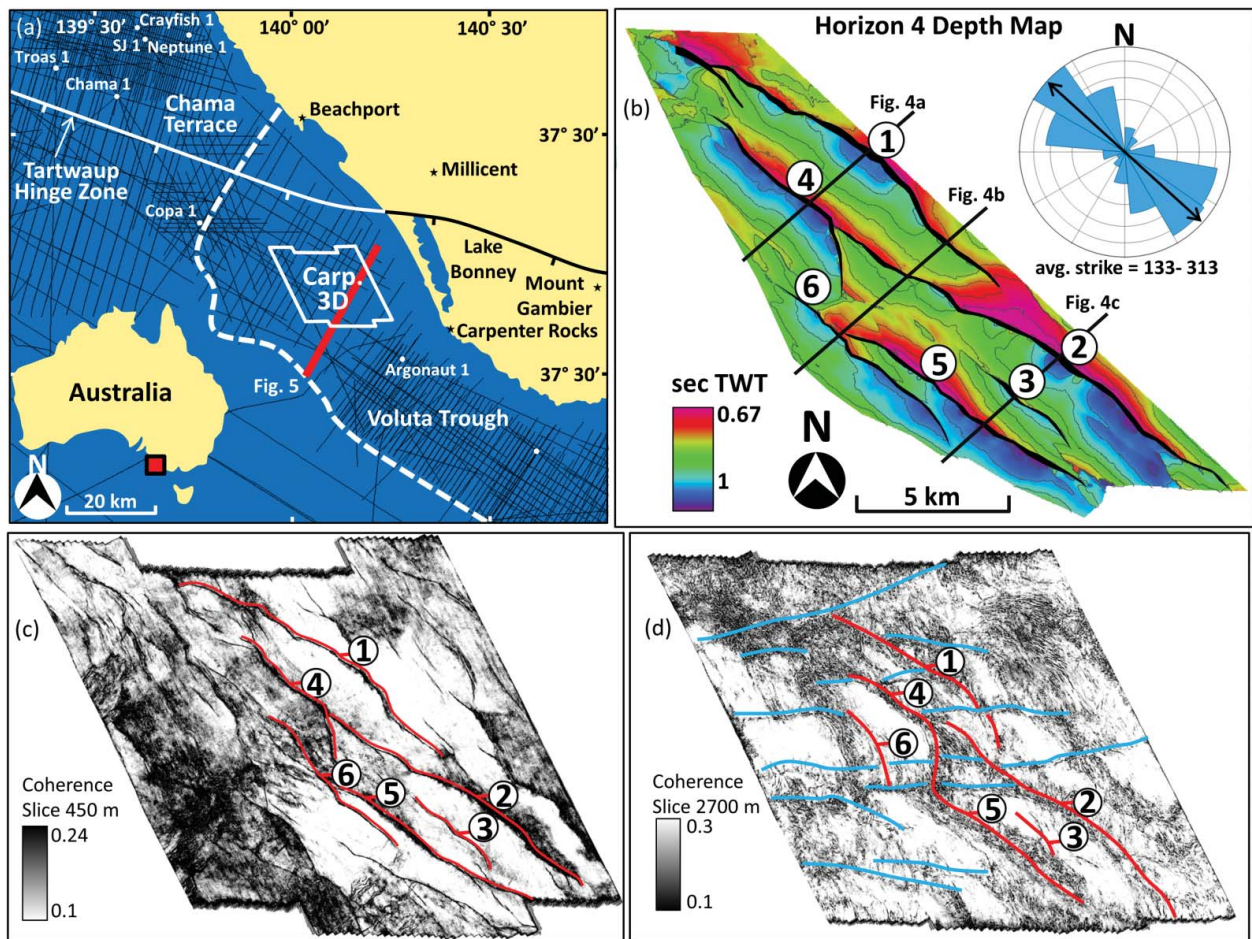


Figure 2. (a) Location map of the 3D seismic reflection survey (Carpenter 3D) used for this study and 2D seismic reflection data (black lines) and offshore nearby wells (white dots), relative to nearby SE South Australian towns. The map indicates the major structural features of the area: the Voluta Trough, Tartwaup Hinge Zone and the Chama Terrace. (b) Horizon 4 depth map (TWT) showing faults 1–6 analysed in this study and seismic cross-sections displayed in Figure 4. The average strike of the fault array is also shown here as NW (133–313°). (c) Coherence slice (~450 m), highlighting faults 1–6 analysed in this study at a shallow level (Cenozoic strata), with surrounding faults also revealed. (d) Coherence (~2700 m), highlighting faults 1–6 at depth and the interpreted E–W-striking basement framework (blue lines), as observed by Boulton et al. (2008).

constrain their temporal and spatial evolution through detailed analysis of syndepositional growth strata and fault displacements.

High to moderate displacement variation along these faults indicates they initially comprised multiple fault segments that subsequently linked to form larger structures. These Late Cretaceous faults are located above, and in some cases dip-linked to, major basement faults. The faults that are physically linked to deeper faults display earlier (likely Turonian) nucleation and greater overall throw and length compared with faults that are spatially isolated from the basement faults. Our results are consistent with, and provide further evidence for, Tithonian–Barremian and Late Cretaceous rifting events in the Otway Basin, with the continued growth of normal faults into the Cenozoic, to ultimately form the Gambier Sub-basin.

Geological setting

The Otway Basin covers an area of 150 000 km², most of which (~120 000 km²) is located offshore in South Australia,

Victoria and Tasmania, in water depths that reach up to 3000 m (Stacey et al., 2013). This study is located approximately 7–30 km offshore of the Gambier Embayment, South Australia on the present-day continental shelf, in water depths of 35–150 m (Figure 2a). The study area is situated within the Voluta Trough, which is bordered to the north and east by the Tartwaup Hinge Zone (a major NW–SE-striking extensional fault zone of the Otway Basin), to the SE by the Bridgewater High and to the SW by the present-day shelf edge break and the deep-water province of the Otway Basin (Krassay et al., 2004; Moore et al., 2000; Pollock, 2003; Stacey et al., 2013).

Rifting between Australia and Antarctica led to the formation of the southern margin of Australia (and thus the Otway Basin) during breakup of eastern Gondwana (Holford et al., 2011; Krassay et al., 2004; Moore et al., 2000; Norvick, 2005; Totterdell et al., 2011; Willcox & Stagg, 1990). The oldest known stratigraphic units within the Otway Basin (Figure 3) form part of the Tithonian–Barremian Crayfish Supersequence, and are found within E–W- to NW–SE-trending horst and graben structures (Finlayson, Johnstone, Owen, & Wake-Dyster, 1996; Krassay et al., 2004; Morton, Hill, Parker, &

Tabassi, 1994; Perincek & Cockshell, 1995). Pre-existing Paleozoic structures exerted a strong influence on local extension during this period, leading to variably oriented (NE–SW-, E–W and NW–SE-striking) Tithonian–Barremian half graben (Finlayson et al., 1996). The Crayfish Supersequence (Figure 3) is characterised by organic-rich mudstones, sandstones and basalts, which reach thicknesses of up to 5000 m in the northern, onshore Otway Basin region (Krassay et al., 2004; Ryan, Knight, & Parker, 1995). Deposition of the Crayfish Supersequence was strongly controlled by latest Jurassic to Early Cretaceous rifting, which occurred in the northern onshore region of the Otway Basin. Owing to a lack of well data and relatively poor seismic imaging at depth, the Crayfish Supersequence thickness is unknown in the study area.

Cessation of rifting by the Aptian–Albian was superseded by thermal subsidence and deposition of the post-rift Eumeralla Supersequence (Figure 3; Hill, Finlayson, Hill, & Cooper, 1995; Krassay et al., 2004). This supersequence is characterised by fluvio-lacustrine deposits with evident volcanoclastic influence (Bryan et al., 1997; Hill et al., 1995; Krassay et al., 2004)

and is suggested to be the source rock for gas accumulations that occur in the eastern Otway Basin (Duddy, 1997; Tassone, Holford, Duddy, Green, & Hillis, 2014). Erosion of the Crayfish Supersequence resulted in the formation of a major unconformity at the base of the Eumeralla Supersequence (Finlayson et al., 1996; Krassay et al., 2004). Southerly thickening trend (to a maximum of ~4 s two-way-time (TWT)) of the Eumeralla Supersequence occurs up to the present-day shelf break, with thinning basinward from this point into the deep-water province (Krassay et al., 2004; Stacey et al., 2013, see figure 3.3). Owing to compression and uplift, little or no Cenomanian strata is preserved above the Eumeralla Supersequence, with the top of this unit marking a regional unconformity (Krassay et al., 2004; Partridge, 2001).

The Turonian–Santonian Shipwreck Supersequence (Figure 3) was deposited during renewed rifting in the Otway Basin, with basinward thickening (up to 2.5 s TWT) observed beyond the Tartwaup and Mussel fault zones and the present-day shelf break (Figure 2a; Krassay et al., 2004). The Campanian–Maastrichtian is characterised by a period of deltaic

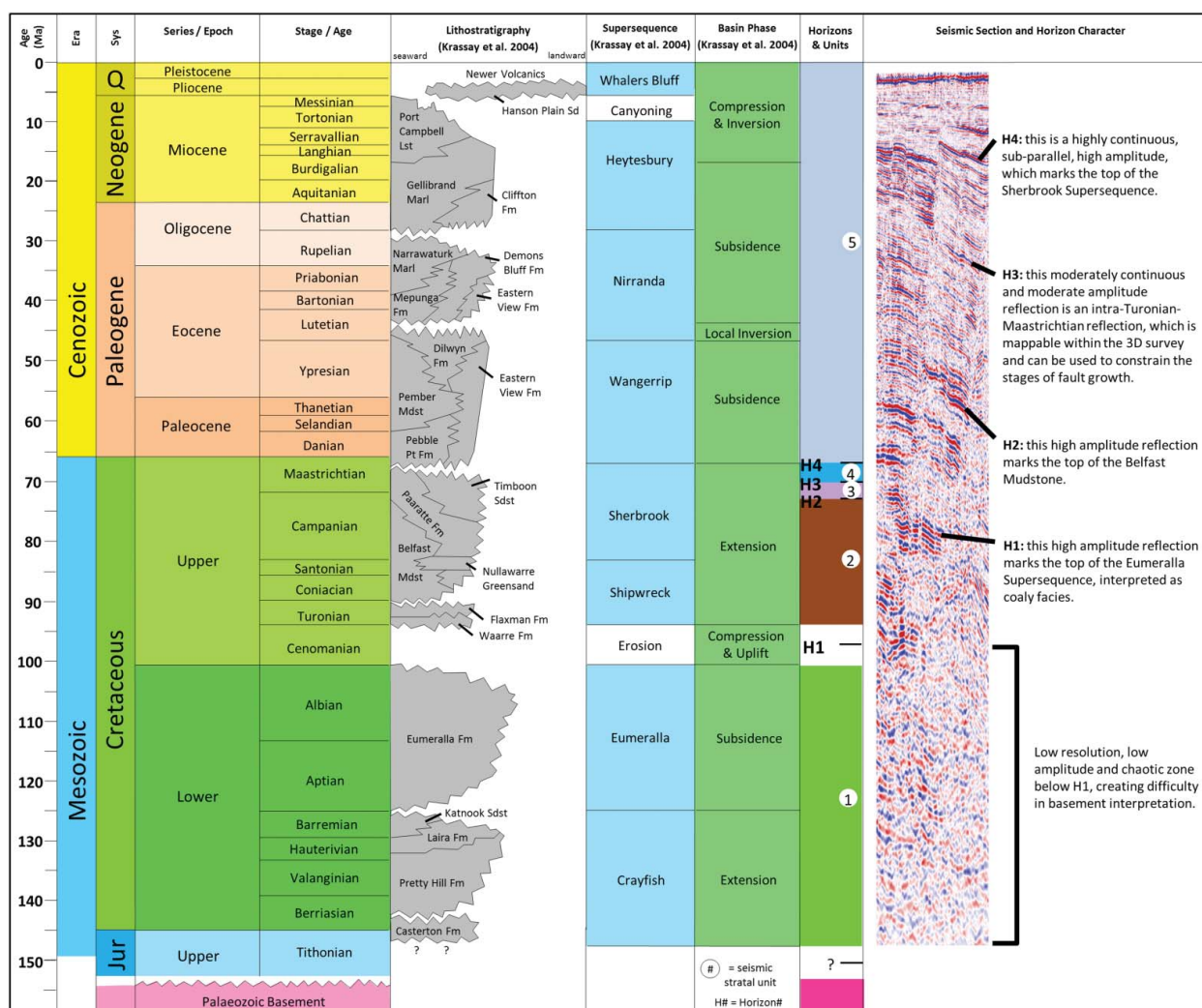


Figure 3. Tectono-stratigraphic framework of the Otway Basin, modified from Krassay et al. (2004) and Geary and Reid (1998), with seismic stratal units and horizons defined for this study and horizon seismic character displayed in the last two columns.

deposition, defined as the Sherbrook Supersequence (Figure 3). The Sherbrook Supersequence thickens to the south, basinward of the present-day shelf break, showing a thickness distribution similar to the Shipwreck Supersequence (Krassay et al., 2004; Partridge, 2001; Stacey et al., 2013). Campanian–Maastrichtian syndepositional strata on the hanging wall of the Tartwaup and Mussel fault zone (Figure 2a) signifies further accrued displacement, resulting from continued rifting in the Otway Basin (Krassay et al., 2004). Thermal subsidence controlled deposition during the Cenozoic, although subsidence was sporadically interrupted by some localised inversion and uplift (Holford et al., 2014; Krassay et al., 2004; Figure 3). The Cenozoic interval is defined by the deposition of the latest Maastrichtian to middle Eocene Wangerrip Supersequence, the middle Eocene to lower Oligocene Nirranda Supersequence, the upper Oligocene to upper Miocene Heytesbury Supersequence and the Plio-Pleistocene Whalers Bluff Supersequence (Krassay et al., 2004; O'Brien & Thomas, 2007; Figure 3).

Basement faults trending E–W to WNW–ESE have previously been observed in surrounding parts of the Otway Basin, namely the Penola Trough (Chantraprasert, McClay, & Elders, 2001) and Robe Trough (Perincek & Cockshell, 1995). Chantraprasert et al. (2001) interpret normal faults imaged in the Haselgrove 3D survey in the Penola Trough that displace the top Crayfish Supersequence horizon (Figure 3). By comparison with physical models of rift fault systems (McClay, Dooley, Whitehouse, & Mills, 2002), which show that most normal faults form at high angles to the extensional direction, Chantraprasert et al. (2001) conclude these faults would have been formed in response to NNE–SSW extension. They also observe and conclude in their evolutionary model that E–W-striking basement faults are present in the Penola Trough and are likely controlled by mechanical interactions between surrounding major basement faults under a NNE–SSW extensional regime (Chantraprasert et al., 2001). An E–W to WNW–ESE-striking Crayfish Supersequence (Figure 3) depocentre has also been observed in the nearby Robe Trough, which has been interpreted to have formed under N–S to NNE–SSW extension (Perincek & Cockshell, 1995). Therefore, an underlying E–W to WNW–ESE basement fabric is potentially influencing the growth of NW–SE-trending Late Cretaceous normal fault systems in Otway Basin depocentres surrounding the Gambier Embayment.

Data and methodology

Data set

This study uses a time-migrated 3D seismic reflection survey (Carpenter 3D) acquired in 2002 covering $\sim 380 \text{ km}^2$ ($\sim 22 \text{ km}$ in a NNW–SSE orientation and $\sim 20 \text{ km}$ in an ENE–WSW orientation) and imaging down to 6 s TWT. The survey covers a portion of the continental shelf, 7–30 km offshore of the Gambier Embayment (Figure 2a). The inline and crossline spacing of the survey are 14 m and 12.5 m, respectively, with the inlines oriented NNW and crosslines oriented ENE. The water depth

over the survey area ranges from approximately 35 to 150 m, and all depths discussed hereafter are from sea-level. The velocity and frequency of the 3D seismic dataset are $\sim 2300 \text{ m s}^{-1}$ and $\sim 19 \text{ Hz}$, respectively, in the Cenozoic interval and $\sim 3200 \text{ m s}^{-1}$ and $\sim 16 \text{ Hz}$, respectively, between the upper and lower depth limits of the top Albian horizon. Therefore, the vertical resolution of the 3D reflection survey ranges from 30 to 51 m through the interval of throw measurements (~ 100 – 4350 m subsea). The top Eumeralla Supersequence (H1) and top Sherbrook Supersequence (H4) horizons were tied to wells Argonaut-1A and Copa-1 along a NW–SE-oriented 2D seismic line (oh91-402). Two more Upper Cretaceous horizons (H2 and H3) were used to constrain throw variations, although a lack of age constraints, beyond them being Upper Cretaceous, meant that they could not provide any further temporal constraint. It should be noted that when we use the term basement, we are referring to interpreted acoustic basement as we have no direct evidence of its composition.

Determining fault growth

We use two methods to study the kinematics of six normal faults imaged in the 3D survey. The first technique is throw–distance (T – x) analysis, which is used to establish the variability of throw along strike for the faults analysed in this study. For faults 1, 2, 4 and 5 we display horizons 1 (top Albian), 3 (intra-Campanian–Maastrichtian) and 4 (top Cretaceous). This is because horizons 3 and 4 show the distribution of throw on the upper fault segments and horizon 1 shows the distribution of throw on the lower segments. These fault segments are dip-linked at horizon 2 (top Santonian). For fault 3 we have displayed horizons 2 (top Santonian), 3 and 4, as no displacement was accumulated at horizon 1. For fault 6 we only show horizons 3 and 4, as these horizons have the greatest throw accumulation. Note that a regional unconformity, and possible erosion of previously accumulated throw at the horizon 1 level, means that the horizon 1 throw measurement is a minimum estimation of throw. The second technique used was throw–depth (T – z) plots; these display the vertical variation in throw down the fault plane. This technique is used to identify cross-fault stratal expansion by an increase in T – z gradient through a stratal unit, which constrains growth packages. This technique also analyses vertical segmentation and dip-linkage processes (Baudon & Cartwright, 2008; Giba et al., 2012; Jackson & Rotevatn, 2013; Robson et al., 2016a; Rykkelid & Fossen, 2002). For these graphs we have plotted throw on horizons 1–4 and the depth of the upper tip-line at various along-strike locations. The two techniques outlined above can be affected by the degree of differential compaction during or after burial (Giba et al., 2012; Taylor, Nicol, & Walsh, 2008). However, we have decided not to include decompaction calculations, as the main objective of this study are to determine the along-strike throw variations of faults, as opposed to quantifying absolute throw.

Depth conversion of throw measurements and 3D seismic cross-sections has been done using a standard Otway Basin

power function established from the amalgamation of stacking velocity data for all surveys across the area (Petkovic, 2004).

Seismic interpretation

Interpretation of the 3D seismic reflection survey has revealed six large normal faults, whose lengths vary from 6 km to over 15 km (Figure 2a–d). Most faults are separated by relay ramps, meaning they are soft-linked (Figure 1b). The fault array strikes to the NW (133–313) (Figure 2b; c). However, a coherence slice from greater depths (~2700 m; Figure 2d) reveals an E–W-striking basement fabric, as previously observed by Boulton et al. (2008). Coherence is a seismic attribute used to identify lateral variations in the seismic amplitude caused by changes in lithology, porosity, fluid and in this case, structure (Marfurt, Kirilin, Farmer, & Bahorich, 1998). This E–W fault set is a basement trend observed in potential field data throughout southern Australia (Boulton et al., 2008). Poor seismic imaging below the top Eumeralla Supersequence horizon (H1; Figure 3) causes difficulty in establishing the lower tip-line of faults and pre-Turonian throw accumulation. However, good-quality seismic imaging above the Eumeralla Supersequence allows us to constrain the growth of the Aptian–Cenozoic fault array.

Fault analysis

Fault 1

Fault 1 is the most landward fault in the array (Figure 2b) and has been observed to link to basement faults at single point locations, given their ~45° difference in strike orientation, as observed in map view coherence slices (i.e. Figure 2d). Throw–distance analysis of fault 1 reveals a highly variable throw profile, with four local throw maxima defined on horizon 3 (intra-Campanian–Maastrichtian) (Figure 6b). Top Cretaceous throw is relatively more homogenous along strike (Figure 6b), with only two significant throw maxima observed. Throw–depth analysis shows a throw minimum occurring at horizon 2 (top Santonian) at locations 1–5 (Figure 6a). The distribution of throw along-strike for fault 1 is broadly consistent within the latest Cretaceous and Cenozoic intervals (stratal units 4 and 5), except for location 7, which displays zero throw during the latest Cretaceous (stratal unit 4; Figure 6a).

Fault 2

Fault 2 is the second most landward fault and is located immediately south of fault 1 (Figure 2b). Fault 2 partially links downward with major basement faults at single point locations, given their ~45° difference in strike orientation (Figures 2c and 4b, c). Throw–distance analysis of fault 2 reveals a moderately variable throw profile along strike, with a maximum throw of ~940 m at location 3 (horizon 1; Figure 7b). The variability of throw along strike shows as many as six maxima, separated by minima with only minor throw deficits (<70 m deficits) (Figure 7b). Throw

measurements are not possible to SE of location 4, because the quality of the 3D seismic data diminishes. Throw–depth analysis indicates a throw minima occurring at horizon 2 (top Santonian) at locations 3 and 4, whereas location 2 shows no such minimum and instead exhibits continuous Late Cretaceous growth (Figure 7a).

Fault 3

Fault 3 is located approximately 3 km basinward of fault 2 (Figure 2b) and appears to have no linkage to basement faults (Figure 4c). Throw–distance analysis of fault 3 reveals moderately variable throw along strike, with several throw maxima and a local throw minimum being observed (Figure 7e). Throw–depth analysis indicates throw minima occurring along horizon 3 at locations 3, 4 and 5, whereas location 2 shows no such minimum and instead exhibits continuous Late Cretaceous growth (Figure 7d).

Faults 4 and 5

Faults 4 and 5 are located immediately basinward of faults 1–3, with fault 4 located to the NW of fault 5 (Figure 2b). Faults 4 and 5 partly link to major basement faults at single point locations, given their ~45° difference in strike orientation, with fault 5 only being linked at its NW end (Figures 2c, 4a, b, c and 8). Throw–distance analysis of faults 4 and 5 reveals two scales of throw variability along strike. Locations 2 (~830 m) and 8 (~580 m) mark the throw maxima on faults 4 and 5, respectively, which occur at horizon 1 (top Albian), with location 5 (~160 m) being the throw minima between these faults (Figure 8b). However, there is still high variability within each major fault segment (up to ~190 m of throw fluctuation; Figure 8b). Faults 4 (locations 1–5) and 5 (locations 5–12) display eight and five local throw maxima, respectively, implying that these faults, at this level of investigation, formed from the linkage of smaller segments (Figure 8b). The top Cretaceous horizon *T*–*x* profile of faults 4 and 5 displays two throw maxima, separated by a zone of zero throw near location 5 (horizon 4; Figure 8b). This is also exhibited in the coherence slice at ~450 m, which shows that faults 4 and 5 are isolated in the cover (Figure 8d, e). However, *T*–*x* analysis shows a non-zero top Albian (horizon 1) throw measurement from locations 1 to 10, inferring these faults are linked at depth (Figure 8b). Throw–depth analysis shows several throw minima along horizon 2 (top Santonian), similar to faults 1 and 2 (Figure 8a). At location 11 and 12, growth strata are observed within stratal units 4 and 5, suggesting fault 5 was growing during the latest Cretaceous and Cenozoic.

Fault 6

Fault 6 is located immediately basinward of faults 4 and 5, and is the most basinward of the faults analysed in this study (Figure 2b). Fault 6 does not link to a basement-involved fault and is restricted to shallow (Upper Cretaceous) strata (Figure 4c). Throw–distance analysis of fault 6 reveals a highly

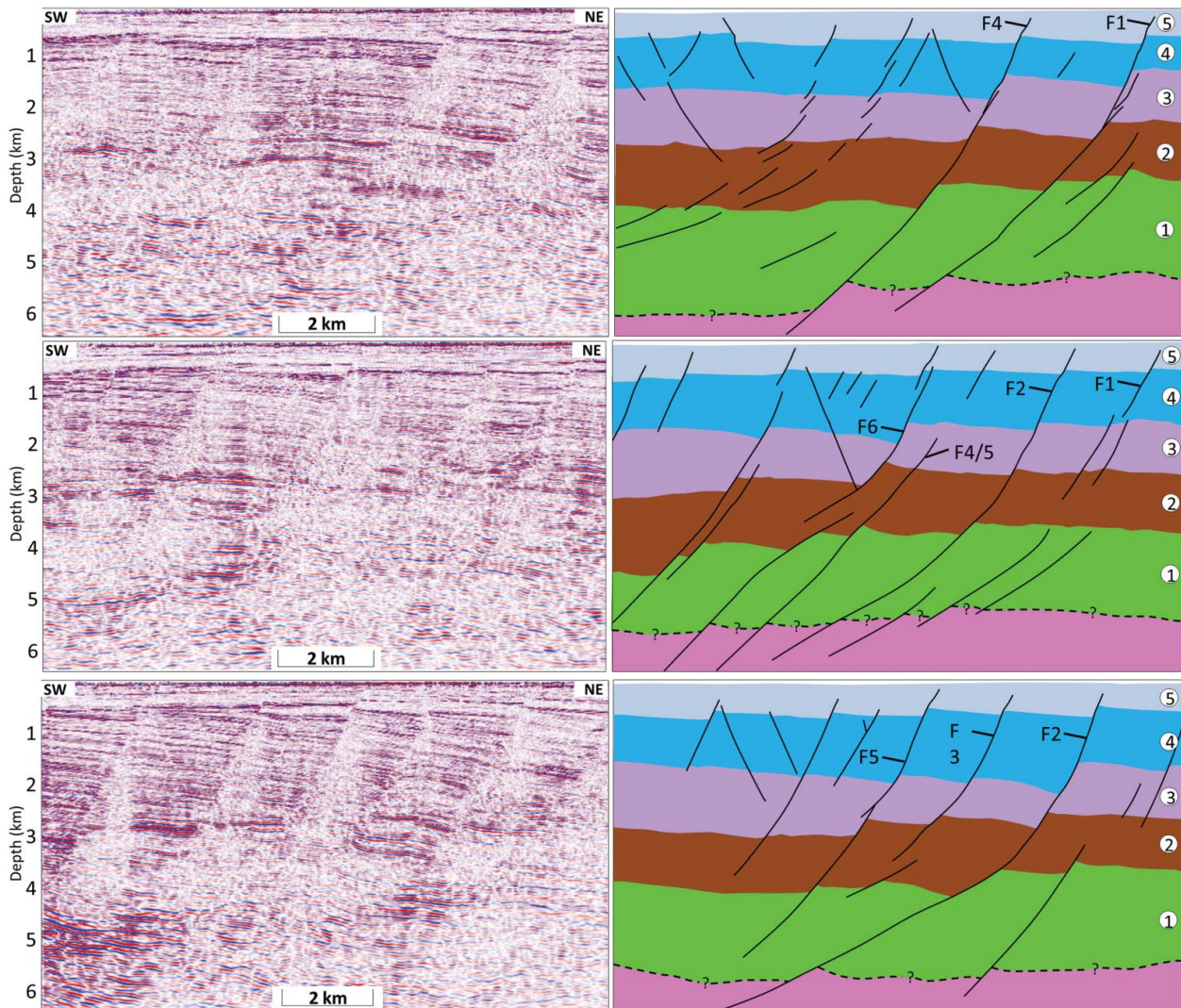


Figure 4. Seismic cross-sections (a), (b) and (c) from Carpenter 3D, oriented NE-SW, with seismic interpretation displayed in the right-hand column, including stratal units and faults used for this study labelled. Note the planar nature of the fault array, with fault 2 highlighting the dip-linkage point in stratal unit 2, where an upper steep fault has dip-linked to a lower and shallower dipping fault. Note that while the top basement horizon has been interpreted on these cross-sections, the confidence in this interpretation is reasonably low and should only be used as a possible geometry. The locations of cross-sections (a), (b) and (c) are shown in Figure 2b.

variable throw profile of horizon 3 (intra-Campanian–Maastrichtian), with throw maxima at locations 2 (~380 m), 4 (~160 m) and 6 (~160 m) separated by local throw minima at locations 3 (~80 m) and 5 (~50 m) (Figure 9b). Horizon 4 (top Cretaceous) shows a smoother throw profile, with throw decreasing towards the lateral tip-lines of the fault (Figure 9b). Throw–depth analysis shows stratal unit expansion at locations 2, 4 and 6, during the deposition of stratal unit 4, and continuous along-strike growth at all locations during the Cenozoic (Figure 9a). Throw–depth profiles along fault 6 show no evidence for throw minima occurring down the fault plane (Figure 9a).

Evolution of the fault array

We have constrained throw patterns on six kilometre-scale faults located in the Gambier Embayment, offshore South

Australia. All faults are characterised by moderately to highly variable throw along strike, with faults 1, 2, 4 and 5 at least partly linking downward with major basement-involved faults. In contrast, faults 3 and 6 are cover restricted. Furthermore, T - z analysis has highlighted sub-horizontal throw minima occurring on faults 1–5, with fault 6 having no such minima.

Fault array nucleation

The Otway Basin initiated with Upper Jurassic–uppermost Cretaceous synrift deposition of the Crayfish Supersequence and Lower Cretaceous blanketing of the Eumeralla Supersequence, during a period of post-rift thermal subsidence (Figure 3; Finlayson et al., 1996; Hill et al., 1995; Krassay et al., 2004; Morton et al., 1994; Perincek & Cockshell, 1995). Our detailed mapping suggests that the six faults analysed in this

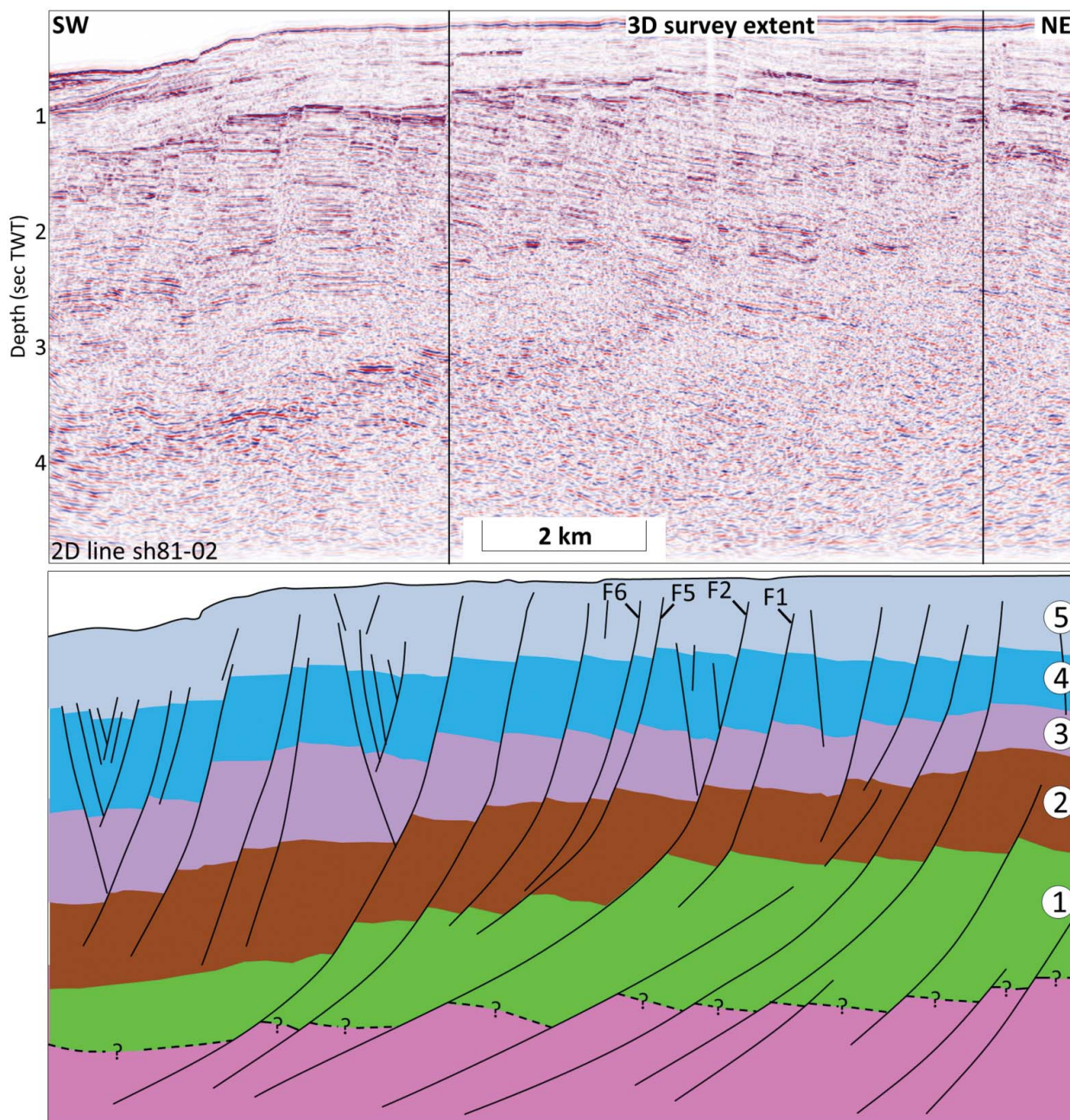


Figure 5. Two-dimensional (2D) seismic line sh81-02 oriented NE–SW, which intersects the 3D survey as shown. This interpretation shows the structure of the 3D survey in the context of further up-dip and down-dip structures. Given that this seismic line is displayed in TWT, the shallow dip of deeper basement faults is likely exaggerated. However, shallower dipping basement structures are also observed in the depth converted 3D reflection survey as noted in Figure 4. The location of this lines is shown in Figure 2a.

study nucleated during the Late Cretaceous, during a second phase of crustal extension in the Otway Basin.

The timing of nucleation of individual faults during the Late Cretaceous is quite variable. The NW half of fault 1 and faults 2, 4 and 5 all display growth during the deposition of stratal unit 2 (Turonian–Santonian). These four faults may have either: (1) formed from reactivation and upward bifurcation of a deeper E–W-striking basement fault; or (2) nucleated independently in the cover as new segments, with a NW-strike orientation, and subsequently dip-linked to the E–

W-striking basement faults. Given the 45° change in strike orientation between the basement faults and the cover faults and no observations of helicoid or non-cylindrical geometry as seen by Giba et al. (2012), we propose the latter scenario as the most likely case. In contrast, faults 3 and 6 display complete geometric isolation from the basement framework. Growth packages indicate that fault 3 nucleated later during deposition of stratal unit 3 (Campanian–Maastrichtian), whereas fault 6 and fault 1 nucleated later still during the latest Cretaceous (Maastrichtian; stratal unit 4) (Figures 6–9).

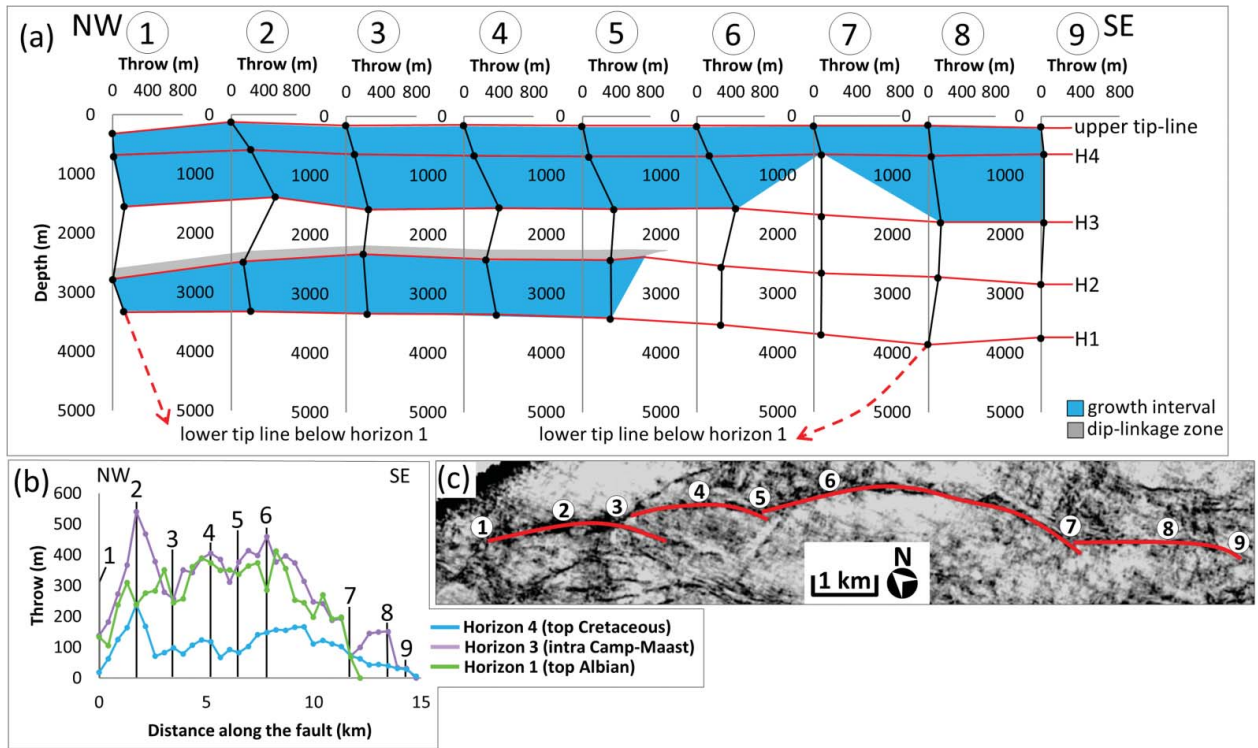


Figure 6. (a) Throw-depth ($T-z$) analysis along strike from NW (left) to SE (right) of fault 1. The growth intervals are displayed in blue and the tip-line is dashed in red to show the extent of the fault plane. Note the NW zone of dip-linkage (dark grey) at locations 1–5 through stratal unit 3. Throw–distance ($T-x$) graphs (b) display maximum throw and Cenozoic throw along strike of the fault. Four local throw maxima are defined on horizon 3 (intra-Campanian–Maastrichtian) at locations 2 (~540 m), 4 (~400 m), 6 (~460 m) and 8 (~150 m), separated by throw minima at locations 3 (~260 m), 5 (~380 m) and 7 (~80 m). Two significant throw maxima along horizon 4 are observed between locations 6 and 7 (166 m) and at location 2 (238 m). The locations of $T-z$ plots are displayed (c).

Late Cretaceous fault growth

The NW–SE-striking faults 1, 2, 4 and 5 nucleated and display growth during the Turonian–Santonian, with highly variable $T-x$ profiles (stratal unit 2; Figures 2b, c, 6, 7a–c and 8).

Subsequent growth during the Campanian–Maastrichtian (stratal unit 3) occurred on faults 2 (location 2; Figure 7a), 4 and 5 (Figure 8a), with fault 3 nucleating at this stage (Figure 7d). Throw–depth analysis of fault 1 shows a

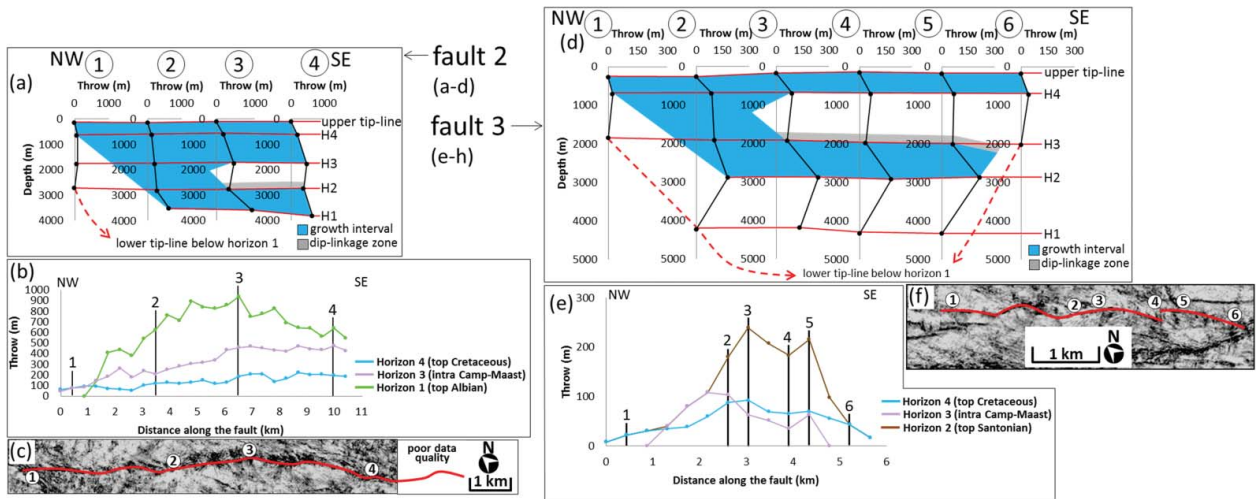


Figure 7. (a, d) Throw-depth ($T-z$) analysis along strike from NW (left) to SE (right) of faults 2 and 3, respectively. The growth intervals are displayed in blue and the tip-line is dashed in red to show the extent of the fault plane. Note the zones of dip-linkage (dark grey) at locations 3 and 4 on fault 2 through stratal unit 3 and locations 3, 4, 5 and 6 through stratal unit 4 on fault 3. Throw–distance ($T-x$) graphs (b, e) display maximum throw and Cenozoic throw along strike of faults 2 and 3, respectively. The location of $T-z$ plots are displayed (c, f) for faults 2 and 3, respectively.

Downloaded by [UNIVERSITY OF ADELAIDE LIBRARIES] at 17:22 07 September 2017

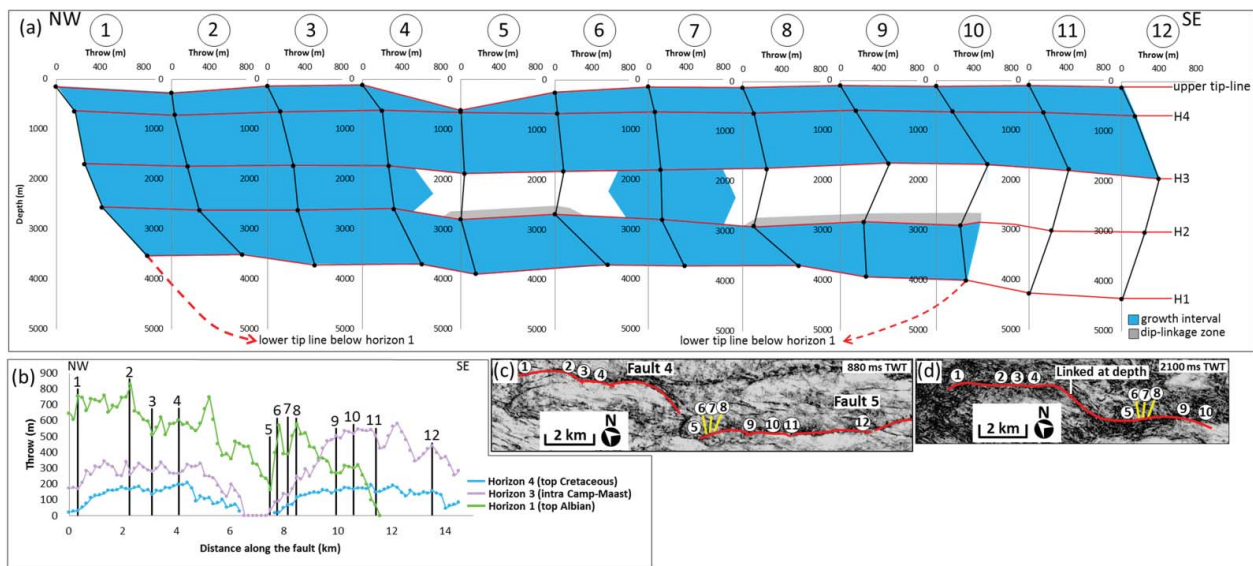


Figure 8. (a) Throw–depth (T - z) analysis along strike from NW (left) to SE (right) of faults 4 and 5. The growth intervals are displayed in blue and the tip-line is dashed in red to show the extent of the fault plane. Note the laterally confined zones of dip-linkage (dark grey) at locations 5, 6, 8, 9 and 10 through stratal unit 3. Throw–distance (T - x) graphs (b) display maximum throw and Cenozoic throw along strike of the fault. Note continuous maximum throw at depth, implying linkage of faults 4 and 5 and the isolated Cenozoic throw accumulations, implying no linkage in the shallow strata. The locations of T - z plots are displayed at 880 ms TWT (c) and 2100 ms TWT (d).

downward reduction in throw through this interval of strata, which implies a period of fault dormancy (Figure 6a).

Latest Cretaceous and Cenozoic fault growth

Latest Cretaceous (stratal unit 4) growth is evident on all faults, including the nucleation and growth of fault 6, which formed from the strike-linkage of three fault segments (Figure 9). This is evident by a highly variable T - x profile containing three maxima along horizon 3 and at a younger stratigraphic level (horizon 4) a smooth profile exists (Figure 9). The T - x profile along horizon 4 is similar to that of one isolated fault and the linkage points display greater throw at a younger stratigraphic level (horizon 4), inferring the fault segment lengths have increased to the point of relay breaching and linkage during the Cenozoic (stratal unit 5).

During the latest Cretaceous, fault 1 resumed growth at locations 1–5, grew in length to the SE to location 6 and the furthest SE segment (locations 8 and 9) nucleated (Figure 6). Fault 2 continued to grow during the latest Cretaceous and Cenozoic, extending to the NW, establishing its full length at some stage during the Cenozoic, evident by the Cenozoic throw accumulated at location 1 (Figure 7a, b). Latest Cretaceous and Cenozoic growth on the SE half of fault 2 was only at a shallow level, creating vertical isolation of an upper segment from the deeper segment, which eventually dip-linked, evident from throw minima occurring at horizon 2 (Figure 7a).

Fault 3 displays very minor growth (only at location 2) during the latest Cretaceous (Figure 7d). However, fault 3 extended to the NW, creating full fault length establishment during the Cenozoic, evident by only Cenozoic throw accumulated at location 1 (Figure 7d).

Faults 4 and 5 display growth along the entire fault length during the latest Cretaceous (Figure 8a). However, Cenozoic

throw is absent at location 5 (between the faults), which is likely the result of preferential fault reactivation on NW–SE-striking portions of the fault and not at the N–S-striking linkage point (see location 5; Figure 8a, b).

Dip-linkage and fault dip angles

Dip-linkage occurs at the top Santonian level (horizon 2) on faults 1, 2, 4 and 5 (see zone of dip-linkage and throw minima at horizon 2; Figures 6a, 7a and 8a); at approximately this same level fault dip increases into shallower strata (see stratal unit 3; Figures 6 and 7). This is not a gradual steepening, which is more characteristic of a listric fault, but rather an abrupt change from ~ 30 – 45° within stratal unit 2 to ~ 52 – 60° above stratal unit 3 (Figure 4). We infer this is potentially caused by dip-linkage of an upper, steep-dipping segment with a lower, more gently dipping fault segment. Faults 1 and 2 exemplify this abrupt change in fault dip with depth (Figure 4). However, the 2D seismic cross-section exaggerates this feature as it has not been depth converted (Figure 5).

Summary of fault growth

The growth of the fault array can be summarised into five evolutionary stages: (1) Tithonian–Barremian synrift deposition of the Crayfish Supersequence (Figure 3) forming the underlying E–W-striking basement framework, followed by Aptian–Albian deposition of the Eumeralla Supersequence (Figure 3) during a period of post-rift/intra-rift subsidence (Figure 10a; Finlayson et al., 1996; Hill et al., 1995; Krassay et al., 2004; Morton et al., 1994; Perincek & Cockshell, 1995); (2) nucleation and initial growth of faults 1, 2, 4 and 5 during subsequent crustal extension through the Turonian–Santonian (Figure 10b). Faults 1, 2, 4 and 5 comprise smaller

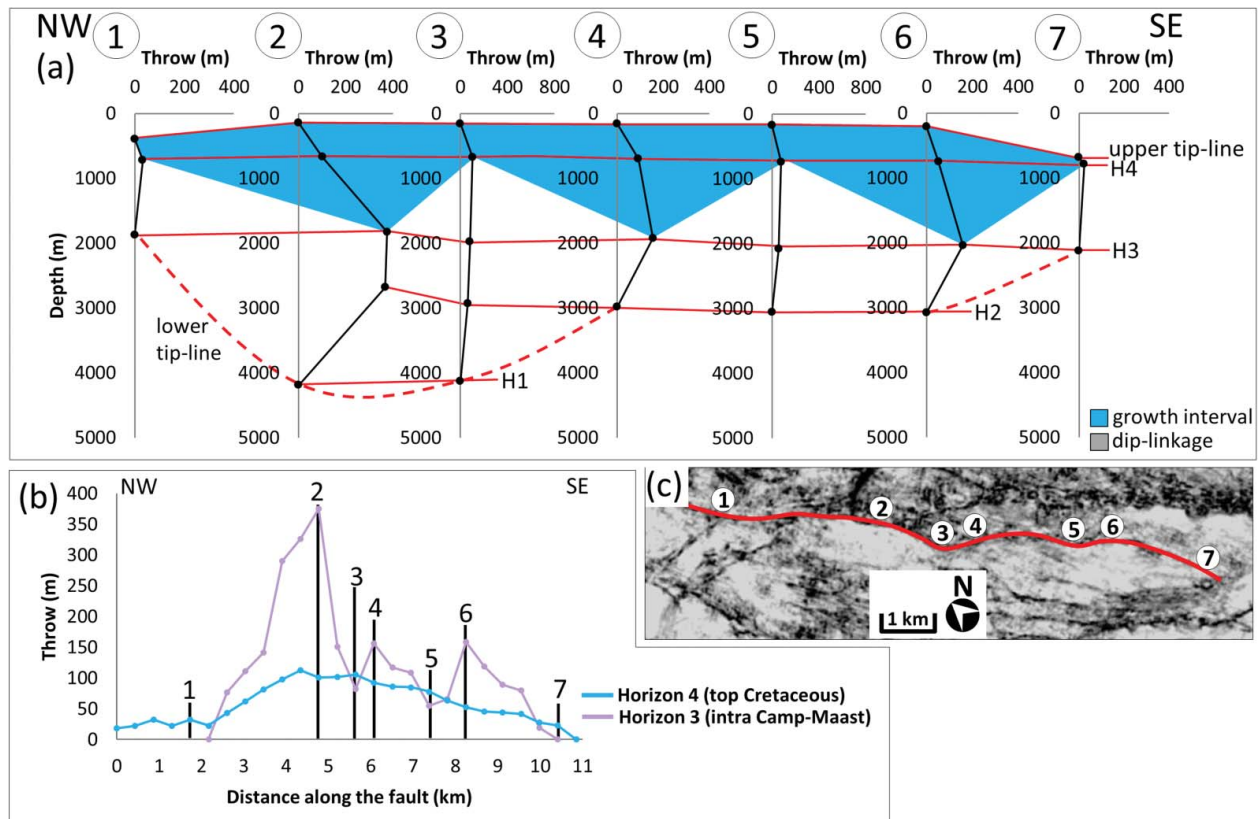


Figure 9. (a) Throw–depth ($T-z$) analysis along strike from NW (left) to SE (right) of fault 6. The growth intervals are displayed in blue and the tip-line is dashed in red to show the extent of the fault plane. Throw–distance ($T-x$) graphs (b) display maximum throw and Cenozoic throw along strike of the fault. The locations of $T-z$ plots are displayed (c).

fault segments, which eventually linked to form larger, throughgoing faults (Figure 10b); (3) nucleation of fault 3 during the Campanian–Maastrichtian (stratal unit 3) as two fault segments, which later linked. The NW ends of faults 2, 4 and 5 continued to grow during this period (Figure 10c); (4) latest Cretaceous (stratal unit 4) nucleation of fault 6, with resumed growth of fault 1 and further growth of faults 2, 4 and 5 and the NW half of fault 3, through an along-strike variation of either continued growth of lower cover fault segments or dip-linkage of upper and lower cover fault segments at the top Santonian level (Figure 10d). Faults 1, 2, 4 and 5 all at least partially dip-linked to E–W-striking basement faults at some stage during growth, whereas fault 3 and 6 remained isolated in the cover; and (5) continued growth of all faults until intra-Cenozoic termination of growth, creating the Cenozoic Gambier Sub-basin of the Otway Basin (Figure 10e, f).

Implications for normal fault growth and development of Australia’s southern margin

Regional implications

The aim of this study was to use 3D seismic data to establish constraints on the structural evolution of a normal fault array located in the Gambier Embayment, offshore Otway Basin, South Australia (Figure 2). In map view these faults are reasonably linear and sub-parallel (Figure 2b, c). However, the observation of minor variations in along-strike fault plane

orientation (Figure 2b, c), and highly to moderately variable throw–distance profiles of all faults (Figures 6b, 7b, 7e, 8b and 9b), indicates that all six faults grew from the linkage of multiple smaller fault segments.

Faults 1, 2, 4 and 5 (Figures 6–8) display growth during the deposition of stratal unit 2 (Upper Cretaceous) and display much greater total throw accumulation, lower tip-line depth and fault length in comparison with faults 3 and 6 (Figures 7 and 9), which nucleated later during deposition of stratal units 3 and 4 (uppermost Cretaceous), respectively. Despite these differences, all six faults are sub-parallel and strike NW–SE (Figure 2b–d). This implies that the orientation of stress that led to the nucleation of these faults was reasonably consistent in the study area during much of the Late Cretaceous. The basement framework is interpreted to have an E–W-strike orientation and thus to have formed in response to N–S extension (Figure 2d). This implies either a perturbation of stress orientation prior to or during the Cenomanian, also recognised by Boulton et al. (2008), or that the E–W-basement fabric was formed owing to NW–SE-oblique extension above an even deeper structural fabric.

Faults 1, 2, 4 and 5 have been interpreted to penetrate down to basement level and likely have at least partly linked to the E–W-basement structures (Figures 4 and 5). These faults display significantly more overall throw than faults 3 and 6, which do not penetrate down to basement level (Figures 4 and 5). There is a change in structural orientation from E–W-striking in the basement framework (Figure 2d) to the NW–

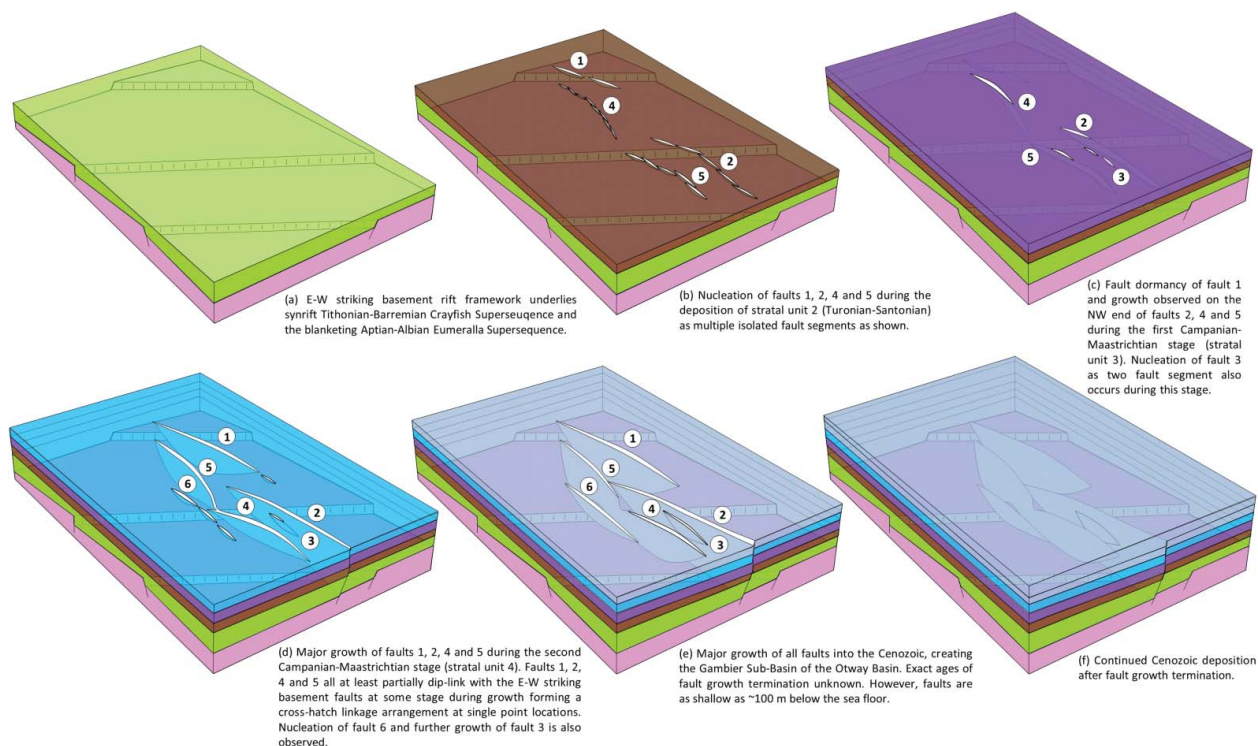


Figure 10. Structural evolution of the normal fault array through the 3D reflection survey discussed in stages from the latest Albian to the Cenozoic.

SE-striking Late Cretaceous faults analysed in this study (Figure 2b, c). Furthermore, vertical throw minima are observed between the E–W-striking basement faults and the NW–SE-striking Late Cretaceous faults. Therefore, we interpret that all faults nucleated independently as spatially isolated segments, which were not initially linked to the basement framework at depth. However, there are locations where throw minima do not occur, potentially implying some upward propagation of the underlying basement faults in restricted locations (see faults 2–5; Figures 7 and 8).

Data from the present-day shelf break of the Otway Basin, located 55 km south of Portland, Victoria, and bordering the Inner Otway Basin and deep-water Morum Sub-basin, demonstrate the influence and complexity of a reactivating basement framework during polyphase extension (Robson, King, & Holford, 2016b). The study by Robson et al. (2016b) analysed two NW–SE-oriented fault sets, comprising smaller, linked fault segments, that are geometrically similar to the six faults analysed in this study. One fault set is located above major basement-involved faults, whereas the other is located 2 km down-dip above a basement plateau. The fault set overlying and partly linked to the basement faults initiated in the Turonian–Santonian and has relatively large throws (Robson et al., 2016b). In contrast, the fault set overlying the basement plateau nucleated later in the Campanian–Maastrichtian, has less throw and does not penetrate down to basement level (Robson et al., 2016b).

Our findings demonstrate similarities to the study by Robson et al. (2016b), given that faults 1, 2, 4 and 5 penetrate down to basement level, display an earlier (~Turonian) growth strata and greater throw, and have attained greater

fault length compared with faults 3 and 6. Together, these studies collectively imply that faults that grew during the Late Cretaceous phase of extension in the Otway Basin, and which were located above major basement faults, generally nucleate earlier and have greater throw and basement linkage. In addition, the temporal and spatial constraints on fault growth in these two studies are highly comparable, both of which highlight a Late Cretaceous period of fault growth punctuated by intervals of fault quiescence and consequent periods of vertically segmented fault growth. Furthermore, our study demonstrates that fault growth continued into the Cenozoic, leading to the formation of the Gambier Sub-basin of the Otway Basin.

Implications for petroleum exploration

Vertical migration of hydrocarbons may occur through faults and their associated damage zones (Allan, 1989; Anderson, Flemings, Losh, Austin, & Woodhams, 1994; Hooper, 1991; Smith, 1980). Therefore, faults analysed in this study, which display greater interaction with basement-involved faults, may represent areas of enhanced vertical migration from deep source rocks into shallow reservoirs. Furthermore, these faults have been active through the Late Cretaceous and into the Cenozoic, leaving a broad window for potential vertical hydrocarbon migration. In contrast, fault-dependent trapping mechanisms may be breached as a result of the Late Cretaceous–Cenozoic slip, resulting in further vertical hydrocarbon migration and/or cross-fault migration between juxtaposed reservoirs. With a good understanding of the regional and local structural evolution, these findings may highlight more

prospective areas for petroleum exploration in the Otway Basin and Australia's southern margin.

Implications for normal fault growth

Based on the scale of our measurements, we have identified two key findings with implications towards normal fault growth models. The first finding is the growth style of fault 6, which has grown from the linkage of three individual fault segments. Fault 6 has highly variable throw along strike with the three throw maxima occurring along horizon 3 (intra-Campanian–Maastrichtian) at fault segment centres. However, significant throw minima are observed along horizon 3 at segment linkage points. Furthermore, greater throw accumulation is observed at a younger stratigraphic level (horizon 4—top Cretaceous) at segment linkage points, inferring these segments increased in length while accumulating throw and eventually linked. This finding supports early models of normal fault growth, whereby structures nucleated and propagated independently, incidentally overlapped and geometrically linked through relay ramp breaching, referred to as the 'isolated fault model' (Figure 1a–c; Dawers & Anders, 1995; Peacock & Sanderson, 1991; Stewart & Hancock, 1991; Trudgill & Cartwright, 1994; Walsh & Watterson, 1988). The second finding is that fault 2 displays a varying growth style along strike over a relatively minimal distance, with continuous growth observed on the NW end (location 2) and dip-linkage of upper and lower segments on the SE end (locations 3 and 4), only ~3 km apart. Dip-linkage has been documented many times previously (Figure 1e, f; Baudon & Cartwright, 2008; Childs et al., 1996; Mansfield & Cartwright, 1996; Robson et al., 2016a; Rotevatn & Jackson, 2014). However, our findings show that dip-linkage and reactivation and upward propagation can occur along-strike of the same fault over relatively short distances.

Conclusions

We have constrained the growth of a normal fault array consisting of six faults, using 3D seismic reflection data from the Gambier Embayment, offshore Otway Basin, South Australia. We have established that each of the six faults analysed in this study grew from the nucleation and linkage of multiple smaller fault segments. This study is unique because we have analysed the growth of a normal fault array, overlying and partially dip-linking to a basement framework displaying a different strike orientation (E–W) to the fault array analysed (NW–SE). We observe variations across the fault array in the timing of fault nucleation, the overall fault length and throw, and linkage to basement. We show that faults that display linkage to basement have greater overall throw and an earlier nucleation than faults that are spatially isolated from the basement framework. This study provides further knowledge to the presently under-explored Gambier Embayment, offshore Otway Basin, South Australia, by highlighting hectometre scale Turonian–Cenozoic segmented growth of normal faults.

Acknowledgements

This research forms part of a PhD project supported by the ASEG Research Foundation (RF14P04) for which funding is gratefully acknowledged. We would like to thank Chris Jackson for his extensive review of this manuscript. We would also like to thank the Australian Research Council and University of Adelaide for scholarship funding, IHS Kingdom, DownUnder Geosolutions (DUG Insight) and Move by Midland Valley for software use. This forms TRaX record 373.

Disclosure statement

No potential conflict of interest was reported by the authors.

Funding

This work was supported by Australian Society of Exploration Geophysicists Research Foundation [grant number RF14P04].

References

- Allan, U. S. (1989). Model for hydrocarbon migration and entrapment within faulted structures. *AAPG Bulletin*, 73(7), 803–811.
- Alley, N. F., & Lindsay, J. M. (1995). Tertiary. In: J. F. Drexel & W. V. Preiss (Eds.), *The geology of South Australia, Vol. 2, The Phanerozoic* (pp. 151–215). Adelaide, SA: Geological Survey of South Australia Bulletin, 54.
- Anderson, R. N., Flemings, P., Losh, S., Austin, J., & Woodhams, R. (1994). Gulf of Mexico growth fault drilled, seen as oil, gas migration pathway. *Oil Gas Journal (United States)*, 92(23), 97–104.
- Baudon, C., & Cartwright, J. (2008). The kinematics of reactivation of normal faults using high resolution throw mapping. *Journal of Structural Geology*, 30(8), 1072–1084.
- Boult, P., Freeman, B., Yielding, G., Menpes, S., & Diekman, L. J. (2008). A minimum-strain approach to reducing the structural uncertainty in poor 2D seismic data, Gambier Embayment, Otway Basin, Australia. *PESA Eastern Australian Basins Symposium, III*, 109–118.
- Bryan, S. E., Constantine, A. E., Stephens, C. J., Ewart, A., Schon, R. W., & Parianos, J. (1997). Early Cretaceous volcano-sedimentary successions along the eastern Australian continental margin: Implications for the break-up of eastern Gondwana. *Earth and Planetary Science Letters*, 153, 85–102.
- Cartwright, J. A., Trudgill, B. D., & Mansfield, C. S. (1995). Fault growth by segment linkage: An explanation for scatter in maximum displacement and trace length data from the Canyonlands Grabens of SE Utah. *Journal of Structural Geology*, 17(9), 1319–1326.
- Chantrapraser, S., McClay, K. R., & Elders, C. (2001). 3D rift fault systems of the western Otway Basin, SE Australia. In K. C. Hill & T. Bernecker (Eds.), *Eastern Australasian basins symposium, a refocused energy perspective for the future* (pp. 435–445). Melbourne: Petroleum Exploration Society of Australia Special Publication.
- Childs, C., Nicol, A., Walsh, J. J., & Watterson, J. (1996). Growth of vertically segmented normal faults. *Journal of Structural Geology*, 18(12), 1389–1397.
- Childs, C., Nicol, A., Walsh, J. J., & Watterson, J. (2003). The growth and propagation of synsedimentary faults. *Journal of Structural Geology*, 25(4), 633–648.
- Childs, C., Watterson, J., & Walsh, J. J. (1995). Fault overlap zones within developing normal fault systems. *Journal of the Geological Society*, 152(3), 535–549.
- Dawers, N. H., & Anders, M. H. (1995). Displacement length scaling and fault linkage. *Journal of Structural Geology*, 17(5), 607–614.
- Duddy, I. R. (1997). Focussing exploration in the Otway Basin: Understanding timing of source rock maturation. *APPEA Journal-Australian Petroleum Production and Exploration Association*, 37(1), 178–191.
- Finlayson, D. M., Johnstone, D. W., Owen, A. J., & Wake-Dyster, K. D. (1996). Deep seismic images and the tectonic framework of early rifting in

- the Otway Basin, Australian southern margin. *Tectonophysics*, 264(1), 137–152.
- Freeman, B., Boulton, P. J., Yielding, G., & Menpes, S. (2010). Using empirical geological rules to reduce structural uncertainty in seismic interpretation of faults. *Journal of Structural Geology*, 32(11), 1668–1676.
- Geary, G. C., & Reid, I. S. A. (1998). Hydrocarbon prospectivity of the offshore eastern Otway Basin, Victoria for the 1998 Acreage Release. *Victorian initiative for minerals and petroleum report 55*. Melbourne, Vic: Department of Natural Resources and Environment.
- Giba, M., Walsh, J. J., & Nicol, A. (2012). Segmentation and growth of an obliquely reactivated normal fault. *Journal of Structural Geology*, 39, 253–267.
- Hill, K. A., Finlayson, D. M., Hill, K. C., & Cooper, G. T. (1995). Mesozoic tectonics of the Otway Basin: The legacy of Gondwana and the active Pacific margin—a review and ongoing research. *The APPEA Journal*, 35(1), 467–493.
- Holford, S. P., Hillis, R. R., Duddy, I. R., Green, P. F., Stoker, M. S., Tuitt, A. G., ... Macdonald, J. D. (2011). Cenozoic post-breakup compressional deformation and exhumation of the southern Australian margin. *APPEA Journal—Australian Petroleum Production and Exploration Association*, 51(1), 613–638.
- Holford, S. P., Tuitt, A. K., Hillis, R. R., Green, P. F., Stoker, M. S., Duddy, I. R., & Tassone, D. R. (2014). Cenozoic deformation in the Otway Basin, southern Australian margin: Implications for the origin and nature of post-breakup compression at rifted margins. *Basin Research*, 26(1), 10–37.
- Hooper, E. C. D. (1991). Fluid migration along growth faults in compacting sediments. *Journal of Petroleum Geology*, 14(S1), 161–180.
- Huggins, P., Watterson, J., Walsh, J. J., & Childs, C. (1995). Relay zone geometry and displacement transfer between normal faults recorded in coal-mine plans. *Journal of Structural Geology*, 17(12), 1741–1755.
- Jackson, C. A. L., & Rotevatn, A. (2013). 3D seismic analysis of the structure and evolution of a salt-influenced normal fault zone: A test of competing fault growth models. *Journal of Structural Geology*, 54, 215–234.
- Krassay, A. A., Cathro, D. L., & Ryan, D. J. (2004). A regional tectonostratigraphic framework for the Otway Basin. In P. J. Boulton, D. R. Johns, & S. C. Lang (Eds.), *Eastern Australasian basins symposium II* (pp. 97–116). Adelaide: Petroleum Exploration Society of Australia, Special Publication.
- Mansfield, C. S., & Cartwright, J. A. (1996). High resolution fault displacement mapping from three-dimensional seismic data: Evidence for dip linkage during fault growth. *Journal of Structural Geology*, 18(2), 249–263.
- Mansfield, C., & Cartwright, J. (2001). Fault growth by linkage: Observations and implications from analogue models. *Journal of Structural Geology*, 23(5), 745–763.
- Marfurt, K. J., Kirilin, R. L., Farmer, S. L., & Bahorich, M. S. (1998). 3-D seismic attributes using a semblance-based coherency algorithm. *Geophysics*, 63(4), 1150–1165.
- McClay, K. R., Dooley, T., Whitehouse, P., & Mills, M. (2002). 4-D evolution of rift systems: Insights from scaled physical models. *AAPG Bulletin*, 86(6), 935–960.
- Moore, A. M. G., Stagg, H. M. J., & Norvick, M. S. (2000). Deep-water Otway Basin: A new assessment of the tectonics and hydrocarbon prospectivity. *The APPEA Journal*, 32(1), 66–85.
- Morton, J. G. G., Hill, A. J., Parker, G., & Tabassi, A. (1994). Towards a unified stratigraphy for the Otway Basin (abs.). In D. M. Finlayson (Compiler), *NGMA/PESA Otway basin symposium, Melbourne, 1994. Extended abstracts* (pp. 7–12). Canberra ACT: Australian Geological Survey Organisation, Record 1994/14.
- Norvick, M. S. (2005). *Plate tectonic reconstructions of Australia's southern margins*. Canberra, ACT: Geoscience Australia, Record 2005/07.
- O'Brien, G. W., & Thomas, J. H., (2007). *A technical assessment of yet-to-find hydrocarbon resources inventory, offshore and onshore Otway Basin, Victoria, Australia*. Melbourne Vic: Victorian Department of Primary Industries.
- Partridge, A. D. (2001). Revised stratigraphy of the Sherbrook Group, Otway Basin. In K. C. Hill & T. Bernecker (Eds), *Eastern Australasian basins symposium, a refocused energy perspective for the future* (pp. 455–465). Melbourne, Vic.: Petroleum Exploraton Society of Australia, Special Publication.
- Peacock, D. C. P., & Sanderson, D. J. (1991). Displacements, segment linkage and relay ramps in normal fault zones. *Journal of Structural Geology*, 13(6), 721–733.
- Peacock, D. C. P., & Sanderson, D. J. (1994). Geometry and development of relay ramps in normal fault systems. *AAPG Bulletin*, 78(2), 147–165.
- Perincek, D., & Cockshell, C. D. (1995). The Otway Basin: Early Cretaceous rifting to Neogene inversion. *The APPEA Journal*, 35, 451–466.
- Petkovic, P. (2004). Geoscience Australia. Time–depth functions for the Otway Basin, (2004/02).
- Pollock, R. M. (2003). *Sequence stratigraphy of the Paleocene to Miocene Gambier Sub-basin, southern Australia* (Doctoral dissertation). University of Adelaide, Adelaide SA.
- Robson, A. G., King, R. C., & Holford, S. P. (2016a). Structural evolution of a gravitationally detached normal fault array: Analysis of 3D seismic data from the Ceduna Sub–Basin, Great Australian Bight. *Basin Research* (In press). doi: 10.1111/bre.12191
- Robson, A. G., King, R. C., & Holford, S. P. (2016b). 3D seismic analysis of gravity-driven and basement influenced normal fault growth in the deepwater Otway Basin, Australia. *Journal of Structural Geology*, 89, 74–87.
- Rotevatn, A., & Jackson, C. A. L. (2014). 3D structure and evolution of folds during normal fault dip linkage. *Journal of the Geological Society*, 171(6), 821–829.
- Ryan, S. M., Knight, L. A., & Parker, G. J. (1995). *The stratigraphy and structure of the Tyrendarra Embayment, Otway Basin, Victoria*. Melbourne, Vic: Geological Survey of Victoria, VIMP Report 15.
- Rykkelid, E., & Fossen, H. (2002). Layer rotation around vertical fault overlap zones: Observations from seismic data, field examples, and physical experiments. *Marine and Petroleum Geology*, 19(2), 181–192.
- Smith, D. A. (1980). Sealing and nonsealing faults in Louisiana Gulf Coast salt basin. *AAPG Bulletin*, 64(2), 145–172.
- Stacey, A. R., Mitchell, C. H., Struckmeyer, H. I. M., & Totterdell, J. M. (2013). *Geology and hydrocarbon prospectivity of the deepwater Otway and Sorell basins, offshore southeastern Australia* (Record 2013/02). Canberra ACT: Geoscience Australia.
- Stewart, I. S., & Hancock, P. L. (1991). Scales of structural heterogeneity within neotectonic normal fault zones in the Aegean region. *Journal of Structural Geology*, 13(2), 191–204.
- Tassone, D. R., Holford, S. P., Duddy, I. R., Green, P. F., & Hillis, R. R. (2014). Quantifying Cretaceous Cenozoic exhumation in the Otway Basin, southeastern Australia, using sonic transit time data: Implications for conventional and unconventional hydrocarbon prospectivity. *AAPG Bulletin*, 98(1), 67–117.
- Taylor, S. K., Nicol, A., & Walsh, J. J. (2008). Displacement loss on growth faults due to sediment compaction. *Journal of Structural Geology*, 30(3), 394–405.
- Totterdell, J. M., Gibson, G. M., Stacey, A. R., Mitchell, C. H., Morse, M. P., Nayak, G. K., & Kuszniir, N. J. (2011). Structural architecture of Australia's 4000 km-long southern rifted continental margin. EGU General Assembly 2011. *Geophysical Research Abstracts*, 13, EGU2011–1427–1421.
- Trudgill, B., & Cartwright, J. (1994). Relay-ramp forms and normal-fault linkages, Canyonlands National Park, Utah. *Geological Society of America Bulletin*, 106(9), 1143–1157.
- Walsh, J. J., & Watterson, J. (1988). Analysis of the relationship between displacements and dimensions of faults. *Journal of Structural Geology*, 10(3), 239–247.
- Walsh, J. J., & Watterson, J. (1991). Geometric and kinematic coherence and scale effects in normal fault systems. In A. M. Roberts, G. Yielding, & B. Freeman (Eds.), *The geometry of normal faults* (pp. 193–203). London, UK: Geological Society, London, Special Publications, 56 (1).
- Walsh, J. J., Nicol, A., & Childs, C. (2002). An alternative model for the growth of faults. *Journal of Structural Geology*, 24(11), 1669–1675.
- Walsh, J. J., Bailey, W. R., Childs, C., Nicol, A., & Bonson, C. G. (2003). Formation of segmented normal faults: A 3-D perspective. *Journal of Structural Geology*, 25(8), 1251–1262.
- Willcox, J. B., & Stagg, H. M. J. (1990). Australia's southern margin: A product of oblique extension. *Tectonophysics*, 173(1), 269–228

4.4 Paper 4

Robson, A. G., Holford, S. P., King R. C., Kulikowski, D., (2018). Structural evolution of horst and half-graben structures proximal to a transtensional fault system using a 3D seismic dataset from the Shipwreck Trough, offshore Otway Basin, Australia. *Marine and Petroleum Geology*, 89, 615-634, DOI: 10.1016/j.marpetgeo.2017.10.028.

Statement of Authorship

Title of Paper	Structural evolution of horst and half-graben structures proximal to a transtensional fault system determined using 3D seismic data from the Shipwreck Trough, offshore Otway Basin, Australia.
Publication Status	<input checked="" type="checkbox"/> Published <input type="checkbox"/> Accepted for Publication <input type="checkbox"/> Submitted for Publication <input type="checkbox"/> Unpublished and Unsubmitted work written in manuscript style
Publication Details	Robson, A.G., Holford, S.P., King, R.C., & Kulikowski, D. (2018). Structural evolution of horst and half-graben structures proximal to a transtensional fault system determined using 3D seismic data from the Shipwreck Trough, offshore Otway Basin, Australia. <i>Marine and Petroleum Geology</i> , 89, 615-634.

Principal Author

Name of Principal Author (Candidate)	Alexander Robson			
Contribution to the Paper	<ul style="list-style-type: none"> Seismic interpretation fault analysis preparation of manuscript editing manuscript Corresponding author 			
Overall percentage (%)	70%			
Certification:	This paper reports on original research I conducted during the period of my Higher Degree by Research candidature and is not subject to any obligations or contractual agreements with a third party that would constrain its inclusion in this thesis. I am the primary author of this paper.			
Signature	<table border="1" style="width: 100%;"> <tr> <td style="width: 80%;"></td> <td style="width: 20%;">Date</td> <td>6/09/2017</td> </tr> </table>		Date	6/09/2017
	Date	6/09/2017		

Co-Author Contributions

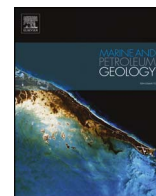
By signing the Statement of Authorship, each author certifies that:

- i. the candidate's stated contribution to the publication is accurate (as detailed above);
- ii. permission is granted for the candidate to include the publication in the thesis; and
- iii. the sum of all co-author contributions is equal to 100% less the candidate's stated contribution.

Name of Co-Author	Simon Holford			
Contribution to the Paper	<ul style="list-style-type: none"> Supervised development of work Helped in data interpretation and manuscript evaluation Multiple edits of manuscript during review 			
Signature	<table border="1" style="width: 100%;"> <tr> <td style="width: 80%;"></td> <td style="width: 20%;">Date</td> <td>6/09/2017</td> </tr> </table>		Date	6/09/2017
	Date	6/09/2017		

Name of Co-Author	Rosalind King			
Contribution to the Paper	<ul style="list-style-type: none"> Supervised development of work Helped in data interpretation and manuscript evaluation Multiple edits of manuscript during review 			
Signature	<table border="1" style="width: 100%;"> <tr> <td style="width: 80%;"></td> <td style="width: 20%;">Date</td> <td>6/09/2017</td> </tr> </table>		Date	6/09/2017
	Date	6/09/2017		

Name of Co-Author	David Kulikowski			
Contribution to the Paper	<ul style="list-style-type: none"> Depth conversion of seismic data Helped in data interpretation and manuscript evaluation Multiple edits of manuscript during review 			
Signature	<table border="1" style="width: 100%;"> <tr> <td style="width: 80%;"></td> <td style="width: 20%;">Date</td> <td>6/09/2017</td> </tr> </table>		Date	6/09/2017
	Date	6/09/2017		



Research paper

Structural evolution of horst and half-graben structures proximal to a transtensional fault system determined using 3D seismic data from the Shipwreck Trough, offshore Otway Basin, Australia

A.G. Robson^{a,b,*}, S.P. Holford^b, R.C. King^a, D. Kulikowski^b^a Centre for Tectonics Resources and Exploration (TRaX), Department of Physical Sciences, University of Adelaide, Adelaide, 5005, South Australia, Australia^b Australian School of Petroleum, Santos Building, University of Adelaide, Adelaide, 5005, South Australia, Australia

ARTICLE INFO

Keywords:

Transform
Normal fault
Listric
Extension
Fault growth
Otway Basin
Southern margin
3D seismic data
Investigator

ABSTRACT

Using a three-dimensional (3D) seismic reflection dataset from the Shipwreck Trough, offshore Otway Basin, southern Australia, we aim to characterise and understand the structural evolution of the Shipwreck Fault Zone (SFZ) and associated extensional structures. The SFZ is a key structural element of the Otway Basin, which is a NW striking, Upper Jurassic-Cenozoic, rift-to-passive margin basin that formed due to the breakup of Australia and Antarctica. The SFZ marks the transition from the major southern margin rift system to the west and the oceanic-continental transform margin to the SE. The SFZ formed and bounds the Shipwreck Trough on the eastern side and is interpreted as a N–S striking transtensional fault zone, representing the northern *en echelon* extension of the transform margin to the south. The Shipwreck Trough is the downward thrown (western) side of the SFZ and is host to an array of horst and half-graben structures, two of which contain the producing Geographe and Thylacine gas fields. The Shipwreck Trough and SFZ are imaged by the Investigator 3D seismic dataset, which has previously been studied to conduct 2D restorations and interpret the timing, magnitude, orientation and nature of the structural events of the Shipwreck Trough. Our study adds to this previous research by using spectral decomposition and coherence volumes to further characterise the SFZ (and associated igneous features), basement structural elements and Late Cretaceous horst and half-graben structures. We have identified examples of releasing bend, releasing jog and restraining jog structures along the SFZ that are indicative of sinistral transtensional deformation and have highlighted areas of increased basement fault block relief, which have driven extensional faulting in the cover. We have also conducted throw-distance and throw-depth analysis on four horst and half-graben structures and shown that the associated normal faults have had continuous Late Cretaceous growth with the structures being formed through incidental linkage of normal fault segments. Finally, our two-way-time (TWT) and isochronal mapping of the entire 3D survey shows the development of the Late Cretaceous rifting event in the Shipwreck Trough and highlights numerous other structural closures similar to (and with close vicinity of) the Thylacine and Geographe gas fields, providing implications for prospectivity.

1. Introduction

The process of normal fault growth located near the furthest extent of a rift or rift compartment may increase in complexity due to the interaction with transfer zones, rift-oblique lineaments and continental transforms. The offshore eastern Otway Basin, Australia, is a relatively understudied petroleum province, with structural complexities due to the transition from an extensional setting to the west to a N–S oriented transform margin to the south (Fig. 1b; Stacey et al., 2013). The Shipwreck Trough (Fig. 1a) is located ~60 km offshore of Port Campbell, Victoria, and is a key geological feature of the offshore Otway Basin,

marking abrupt change from the NW-SE striking southern rifted continental margin to the west (Fig. 1b) to a transitional zone, containing N–S striking transtensional fault systems. One of these fault systems is the Shipwreck Fault Zone (SFZ; Fig. 1a), which formed and bounds the Shipwreck Trough on the eastern side (Palmowski et al., 2004). The Shipwreck Trough and SFZ have previously been studied by Palmowski et al. (2004) and they interpreted the timing, magnitude, orientation and nature of the structural events of the Shipwreck Trough by conducting a 2D restoration of inlines and crosslines from the Investigator 3D seismic survey (Fig. 1a). Palmowski et al. (2004) showed that ~1.12 km of lateral offset occurred along the SFZ from the Coniacian to

* Corresponding author. Centre for Tectonics Resources and Exploration (TRaX), Department of Physical Sciences, University of Adelaide, Adelaide, 5005, South Australia, Australia.
E-mail address: Alexander.Robson@adelaide.edu.au (A.G. Robson).

<http://dx.doi.org/10.1016/j.marpetgeo.2017.10.028>

Received 18 July 2017; Received in revised form 25 October 2017; Accepted 29 October 2017

Available online 03 November 2017

0264-8172/ © 2017 Elsevier Ltd. All rights reserved.

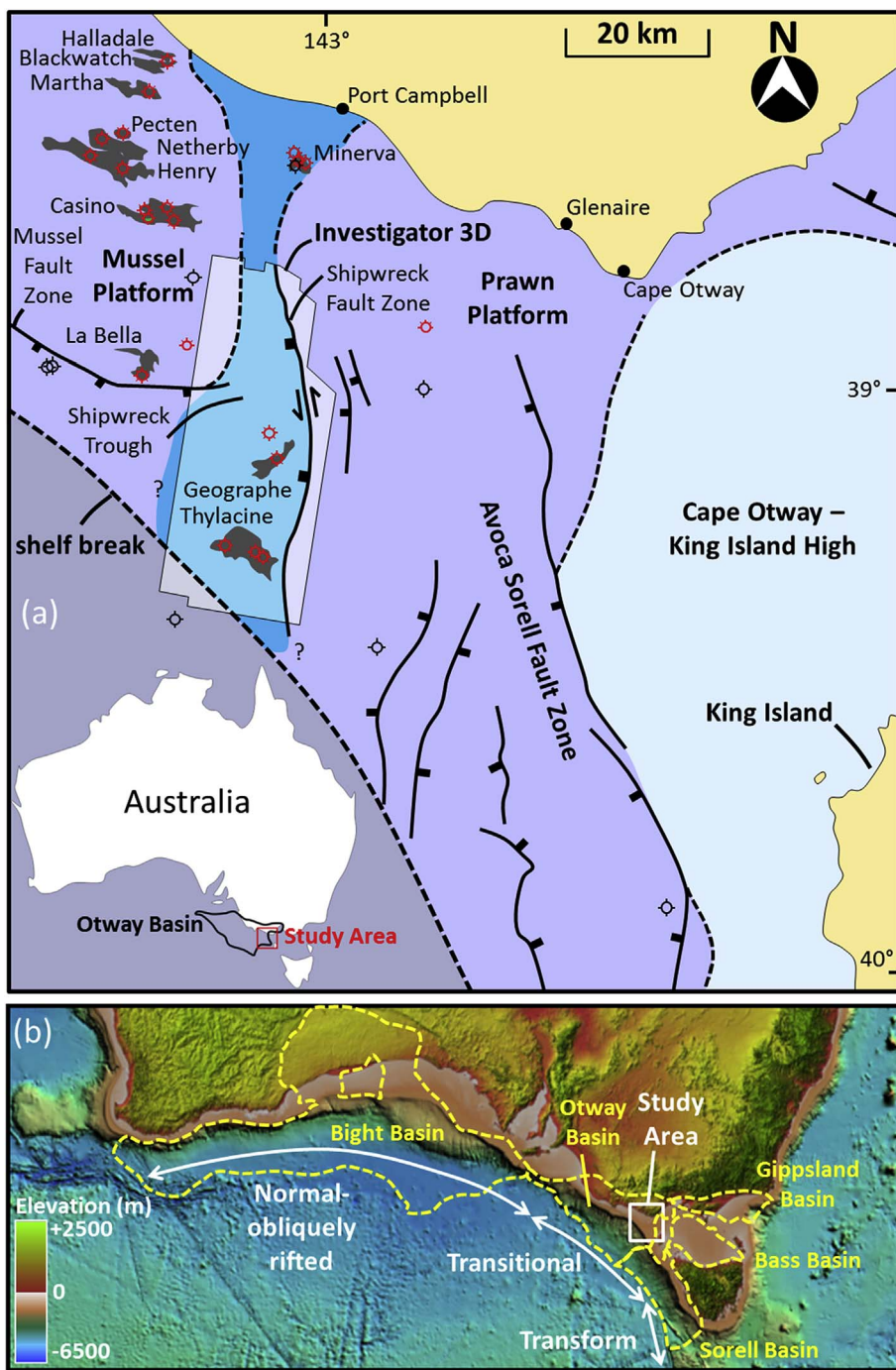


Fig. 1. (a). Location map of the 3D seismic reflection survey (Investigator 3D) relative to coastal Victorian towns Port Campbell, Glenaire and Cape Otway. Surrounding offshore gas fields are labeled and shown in grey, with associated well locations also displayed. Broad scale structural features are shown on the map, including the location of the transtensional Shipwreck Fault Zone, which borders the eastern side of the Shipwreck Trough. (b) Digital elevation map showing the location of the Bight, Otway, Gippsland, Bass and Sorell basins in relation to the study area and the broader southern margin tectonic elements (modified from Totterdell et al., 2012; Stacey et al., 2013).

the Early Eocene and proposed that the SFZ is the northern en echelon extension of the transform margin to the south (Fig. 1b). The SFZ (Fig. 1a) is characterised by a negative flower structure, which formed during Late Cretaceous rifting in the Otway Basin and accommodated greater south-southwest directed extension on the western side (~1.91 km) compared to the east (~0.79 km) from the Coniacian-Early Eocene (Palmowski et al., 2004).

The Shipwreck Trough contains several horst and half-graben structures imaged by the Investigator 3D seismic survey, two of which are host to the Thylacine and Geographe gas fields (Fig. 1a). Furthermore, the Investigator 3D seismic survey provides a wealth of information on the development of extensional structures proximal to a transtensional fault system. This, in addition to the proven gas discoveries in the Shipwreck Trough, is the reason we are aiming to further

the understanding of the structural evolution of the Shipwreck Trough (Fig. 1a). Our study adds to previous research on the Shipwreck Trough (Palmowski et al., 2004) by using spectral decomposition and coherence volumes to characterise the SFZ (and associated volcanics), basement structural elements and Late Cretaceous horst and half-graben structures. We also conduct throw-distance and throw-depth analysis of the four major horst and half-graben structures and two-way-time (TWT) and isochronal mapping of the entire 3D survey to constrain the structural evolution of the Shipwreck Trough and SFZ (Fig. 1a).

Our interpretation of the 3D seismic survey documents a basement plateau, or high, in the north of the survey, with at least three kilometer-scale basement horsts in the central region and an isolated basement high in the southern portion of the survey. We observe

greater Cenomanian-Turonian development of horst and half-graben structures that formed above the basement highs which have larger relief, in the central and southern portions of the survey. In contrast, we observe more consistent growth across all horst and half-graben structures and the SFZ (Fig. 1a) during the Coniacian-Maastrichtian, implying this was a major period of extension/transension in the region. Our TWT and isochronal maps highlight numerous other structural closures, similar to (and with close vicinity of) the Thylacine and Geographe gas fields (Fig. 1a), providing implications for prospectivity and Late Cretaceous play development within the Shipwreck Trough for future exploration. Furthermore, our study describes in detail two structurally distinct domains; the transtensional SFZ and the Shipwreck Trough, characterised by extensional horst and half-graben structures (Fig. 1a). Finally, our isochronal mapping, throw profiling and volcanic interpretation has provided further evidence to support the timing and structural style of the structural evolution of the Shipwreck Trough and the broader southern margin of Australia (Fig. 1b).

2. Geological setting of the Otway Basin and Shipwreck Trough

The Otway Basin (Fig. 1b) is a NW oriented rift-to-passive margin basin, which extends from SE South Australia to NW Tasmania, where it is contiguous with the Sorell Basin (Fig. 1b; see Fig. 7, Moore et al., 2000; Krassay et al., 2004; Stacey et al., 2013; Holford et al., 2014). The Otway Basin (Fig. 1b) covers a surface area of 150,000 km², with ~120,000 km² located offshore of South Australia and Victoria in up to 3000 m of water depth (Stacey et al., 2013). This study is located in the Shipwreck Trough of the eastern Otway Basin, centered approximately 45 km SSW of Port Campbell, Victoria (Fig. 1a). The Shipwreck Trough is a broadly N–S striking graben sub-parallel to and slightly north of a transform margin (Fig. 1b). It is separated from the failed rift Bass Basin to the east by the Prawn Platform, which is bounded to the west by the SFZ, which is studied in detail in this paper (Fig. 1a and b).

The formation of the Otway Basin relates to rifting between Australia and Antarctica during the Early Cretaceous break-up of East Gondwana (Johnson et al., 1980; Li et al., 1996; Bryan et al., 1997; Gibbons et al., 2013), probably situated at a triple junction between the Bight Basin to the west, the Bass Basin to the east and the Sorell Basin to the south (Fig. 1b; Willcox and Stagg, 1990; Moore et al., 2000; Krassay et al., 2004; Palmowski et al., 2004; Norvick, 2005; Holford et al., 2011; Totterdell et al., 2012). Tithonian-Barremian rifting led to the creation of accommodation space, resulting in the deposition of the Crayfish Supersequence (Fig. 2), with E-W to NW-SE striking horst and graben structures (Morton et al., 1994; Perincek and Cockshell, 1995; Finlayson et al., 1996; Krassay et al., 2004). A variation in half-graben orientations (NE-SW, E-W and NW-SE) under a N–S extensional stress regime implies that NW-SE and N–S pre-existing Palaeozoic structure impacted on the development of Tithonian-Barremian normal faults (Finlayson et al., 1996). Organic-rich mudstones, sandstones and basalts characterise the Crayfish Supersequence (Fig. 2), which reaches a maximum thicknesses of up to 5000 m in the northern, onshore Otway Basin (Ryan et al., 1995; Krassay et al., 2004).

The initial rift phase was followed by an Aptian-Albian period of thermal subsidence, resulting in further accommodation space for the deposition of the westerly and northerly thinning Eumeralla Supersequence (Fig. 2; Hill et al., 1995; Krassay et al., 2004). Fluvio-lacustrine shales, thin coal measures and feldspathic sandstones with apparent volcanoclastic influence dominate the Eumeralla Supersequence (Hill et al., 1995; Duddy et al., 2003; Krassay et al., 2004). These coals are thought to be the source rock for gas accumulations located in the study area, such as the Thylacine, Geographe, Minerva and La Bella gas fields (Fig. 1a; Duddy, 1997; Tassone et al., 2014). The base of the Eumeralla Supersequence is marked by a major unconformity, with erosion of the Crayfish Supersequence in some areas (Finlayson et al., 1996; Krassay et al., 2004). Interpretation of regional data sets suggests the Eumeralla Supersequence (Fig. 2) thickens in a

southerly direction towards the shelf edge (Fig. 1a), beyond which it thins into the deeper water (Krassay et al., 2004; Stacey et al., 2013; see Fig. 3.3). Little or no preserved Cenomanian strata has been recognized above the Eumeralla Supersequence, the top of which is marked by a major regional unconformity. This can be observed as a high amplitude seismic reflection below the Upper Cretaceous syn-rift strata (Partridge, 2001; Krassay et al., 2004; Palmowski et al., 2004; Tassone et al., 2014). However, regional seismic interpretation shows that Cenomanian sediments are likely preserved in growth wedges in the hanging wall of normal faults below wells Conan-1 and Mussel-1, which are both proximal to the study area (Krassay et al., 2004, Fig. 8).

Following the post-rift deposition of the Aptian-Albian Eumeralla Supersequence, the Cenomanian-Santonian Shipwreck Supersequence (Fig. 2) and the Campanian-Maastrichtian Sherbrook Supersequence (Fig. 2) were deposited (Krassay et al., 2004). Both of these supersequences thicken basinward of the present-day shelf break and Mussel Fault Zone (Fig. 1a) as a result of renewed rifting in the Otway Basin during the Late Cretaceous (Krassay et al., 2004; O'Brien and Thomas, 2007). The Shipwreck and Sherbrook supersequences are comprised of the Cenomanian-Turonian Waarre and Flaxman formations, the Coniacian-Santonian Belfast Mudstone and the Campanian-Maastrichtian Paaratte Formation (Fig. 2). The Cenomanian-Turonian syn-rift Waarre and Flaxman formations (Fig. 2) show a distinct coarsening upwards seismic character from transparent to high amplitude reflectivity (Krassay et al., 2004; Palmowski et al., 2004). The Waarre and Flaxman formations are characterised in two wells within the study area (Geographe-1 and Thylacine-1; Fig. 1a) by thick non-marine, interbedded sands, silts and shales, with rare coal measures, which transition upwards into a blocky, fluvial to marginal marine sand interval (Krassay et al., 2004; Cliff et al., 2004). These formations are overlain by the Coniacian-Santonian Belfast Mudstone (Fig. 2). The Belfast Mudstone is represented in the Victorian portion of the Otway Basin by an abrupt change from the underlying Turonian sandstones to a marine mudstone interval, signifying a marine flooding event, which is easily identified by a strong seismic reflection (Krassay et al., 2004). The Coniacian-early Santonian interval of the Belfast Mudstone highlights growth of major structures within the study area, with strong evidence for growth wedges in the hanging wall of normal faults and hectometer scale cross-fault thickening (Krassay et al., 2004; Palmowski et al., 2004). However, the late Santonian interval shows a cessation of fault growth across the Shipwreck Trough (Fig. 1; Krassay et al., 2004). The Campanian-Maastrichtian period witnessed the deposition of the near-shore marine Paaratte Formation (Fig. 2) through the study area (Krassay et al., 2004; Moore et al., 2000; Palmowski et al., 2004). However, the Paaratte Formation is relatively thin (less than 300 ms TWT) over the Shipwreck Trough (Krassay et al., 2004; Palmowski et al., 2004) and displays very little thickening across faults, with fault growth generally restricted to the southern portion of the study area (Palmowski et al., 2004). During the Campanian-Maastrichtian there is generally reduced fault growth observed in the Otway Basin compared to the Turonian-Santonian period, with the exemption of continued Turonian-Santonian displacement accumulation of the Mussel Fault Zone (Fig. 1a), prior to the latest Maastrichtian separation of Australia and Antarctica in the Otway Basin (Krassay et al., 2004; O'Brien and Thomas, 2007).

Post-continental breakup deposition is represented by the latest Maastrichtian to Middle Eocene Wangerrip Supersequence, the middle Eocene to early Oligocene Nirranda Supersequence, the late Oligocene to late Miocene Heytesbury Supersequence, and the Plio-Pleistocene Whalers Bluff Supersequence (Fig. 2; Krassay et al., 2004; Holford et al., 2014). Coastal plain, deltaic and inner shelf depositional environments characterise the Paleocene-middle Eocene Wangerrip Supersequence, which transitions into open marine conditions that represent the younger Nirranda and Heytesbury supersequences and create mixed carbonates/siliciclastic sedimentation (Fig. 2; Krassay et al., 2004; O'Brien and Thomas, 2007). Episodes of inversion and uplift intermittently punctuated Cenozoic thermal subsidence (Holford et al.,

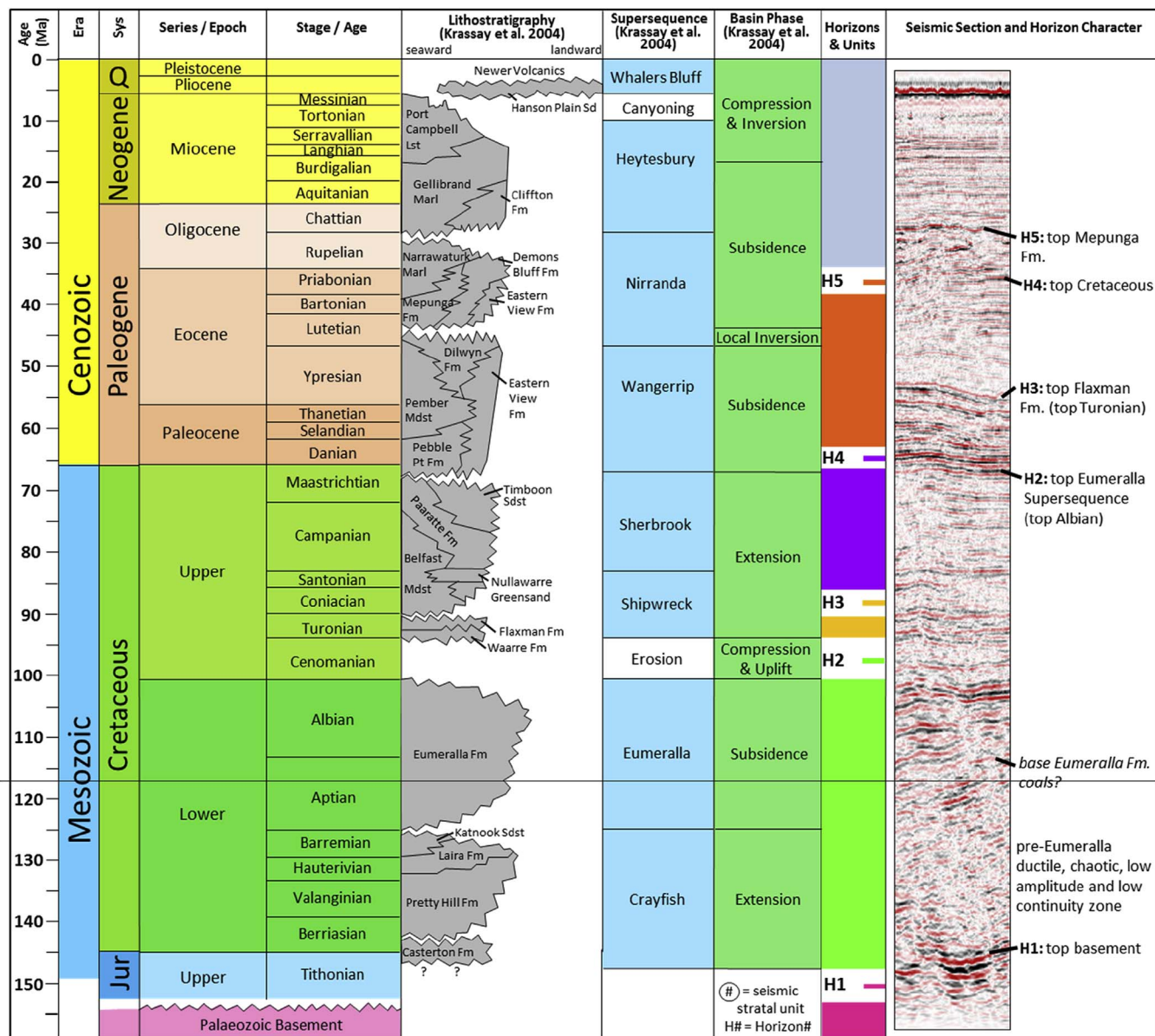


Fig. 2. Otway Basin tectono-stratigraphic framework modified from Krassay et al. (2004) and Geary and Reid (1998), with horizons defined for this study. Added in the far right column is a seismic section to show the seismic character of picked horizons.

2014; Bailey et al., 2014).

3. Data and methodology

3.1. 3D seismic reflection data

The 3D seismic reflection survey used for this study (Investigator 3D, Fig. 1a) covers an area of c. 986 km² (c. 22 km along strike and c. 52 km in the dip direction), has a maximum penetration of 4.6 s two-way-time (TWT) and covers a portion of the continental shelf and shelf break, centered 45 km offshore of Port Campbell, Victoria (Fig. 1a). The Investigator 3D seismic survey covers the Thylacine and Geographe gas fields and is located just to the west of the La Bella and Minerva gas fields (Fig. 1a). The inline and crossline spacing of the survey are both 12.5 m, with the inlines oriented NNE and crosslines oriented WNW. Water depth over the survey ranges from approximately 39–203 m and all depths discussed herein are from sea level. The vertical resolution of the 3D reflection survey ranges from ~35 to 53 m through the interval of throw measurements (~1–7.5 km Subsea). Horizons 3, 4 and 5 (top

Turonian, top Cretaceous and top Mepunga Formation, respectively; Fig. 2) were tied to wells Geographe-1, Geographe North-1, Thylacine-1 and Thylacine-2, which are all located within the 3D survey (Fig. 1a). Horizons 1 and 2 are deeper than the wells within the study area and were tied to regional interpretation by Geoscience Australia.

3.2. Frequency decomposition volumes and colour blending

The seismic reflection survey has been interpreted using a standard amplitude volume, and also using frequency decomposition volumes, which helped to detect (decametre scale) horst and half-graben bounding faulting as well as deeper (kilometer scale) basement structures. Standard frequency decomposition (standard FD) and high definition frequency decomposition (HDFD) volumes were generated using a commercial software package. The frequency decomposition volumes allow the user to investigate the seismic response within a frequency band. These volumes can then be combined using red-green-blue (RGB) colour blending to understand the subtle interaction of low, mid and high frequency responses. Using this method avoids limitations of the

human eye in terms of colour perception, and allows us to express a range of structural features that might not be simultaneously imaged by a single attribute. The standard FD uses a method based on a Fast Fourier Transform and delivers the greatest frequency resolution, providing the greatest variation in the data. Therefore, the standard FD volume was used for highlighting the main structural features (including the basement framework) in map view. The HDFD uses a method based on Matching Pursuit algorithm and maintains a better vertical resolution when decomposing the signal, preserving structural subtleties within subsurface strata. Therefore, the HDFD volume was used for highlighting the main structural features and basement framework in cross-section. Red-green-blue colour blending was used on each volume as a screening tool until an optimum bandwidth colour balance was achieved to highlight necessary structures.

3.3. Determining fault growth

Two techniques have been used to analyse the growth history of two horst structures and two half-graben bounding normal fault arrays identified within the 3D survey: [1] Throw-distance (*T-x*) profiles. Throw of either the top Turonian (yellow) or top Albian (green) horizons have been displayed along-strike of faults, depending on which horizon displays the greatest throw along the fault being analysed. In some cases, both horizons have been displayed where the maximum throw occurs on different horizons along-strike. It should be noted that *T-x* plots are mainly used to identify large variations in throw. Smaller throw minima and maxima cannot be identified due to the 5% throw error we have ascribed to compensate for seismic resolution and human error. Therefore maxima and minima are not considered when vertical error bars (throw measurement error) overlap; [2] Throw-depth (*T-z*) analysis. This involves the analysis of downward tip-line propagation and dip-linkage, by highlighting throw deficits down the fault plane (Mansfield and Cartwright, 1996; Rykkeliid and Fossen, 2002; Baudon and Cartwright, 2008; Jackson and Rotevatn, 2013; Robson et al., 2016a, 2016b).

We have also calculated and analysed the fault throw deficit percentage (Fig. 3) of all localised throw minima and provided a throw deficit percentage average for the faults bounding each of the four horst and half-graben structures analysed with *T-x* and *T-z* analysis. This is a new approach (illustrated in detail in Fig. 3) which we believe adequately represents the variability of maximum throw along strike of a fault or fault system. This calculation was used to analyse the difference in throw variability along each of the normal faults to see if there is a correlation between fault throw variability and the variability of fault strike orientation. The measurement of vertical and lateral throw used can be affected by the extent of differential compaction during or after burial (Taylor et al., 2008; Giba et al., 2012). However, as we are primarily concerned in the along-strike variance of throw on fault assemblages, rather than quantifying the absolute amount of throw, decompaction calculations have not been incorporated into this study. Throw values have been depth converted using a standard Otway Basin velocity-depth relationship, calculated from the analysis and amalgamation of stacking velocity data for all surveys across the area (Petkovic, 2004).

4. Interpretation of the 3D seismic dataset

4.1. Horst and half-graben structures

To help identify and interpret structures within the 3D seismic reflection dataset (Fig. 1a) a frequency spectral decomposition volume was generated. Interpretation of the frequency spectral decomposition volume reveals four normal fault arrays bounding horst and half-graben structures. From herein these four horst and half-graben structures will be referred to as structures 1, 2, 3 and 4 from north to south in the 3D survey (Fig. 4). Horst structures 1 and 4 (Fig. 4a, d) are bound by hard-linked, basinward and landward dipping, NNW-SSE to WNW-ESE striking normal fault assemblages. Structure 1 (Fig. 4a) is furthest to the north and is 'diamond-shaped' in planform, ~5 km in length (NW-SE) and ~1.6 km wide (NE-SW). Structure 4 (Fig. 4d) is the most southerly

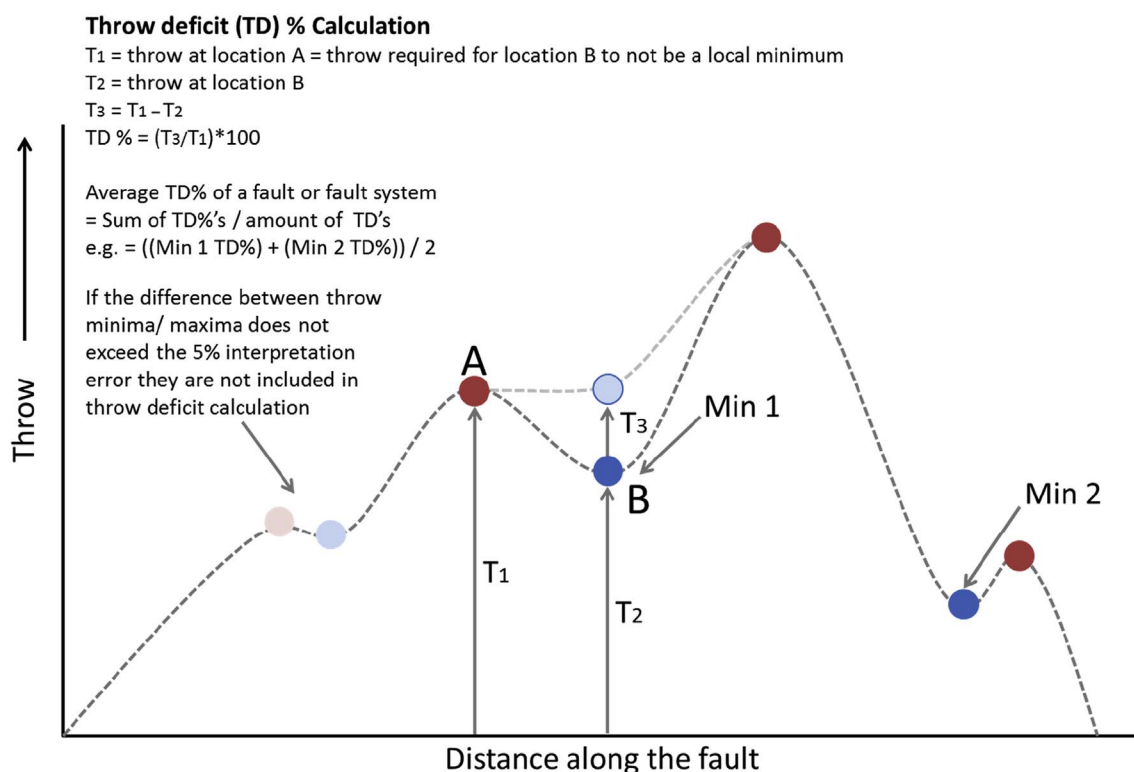


Fig. 3. Diagram showing the new method used for the throw deficit calculation of a throw-distance graph, as shown above.

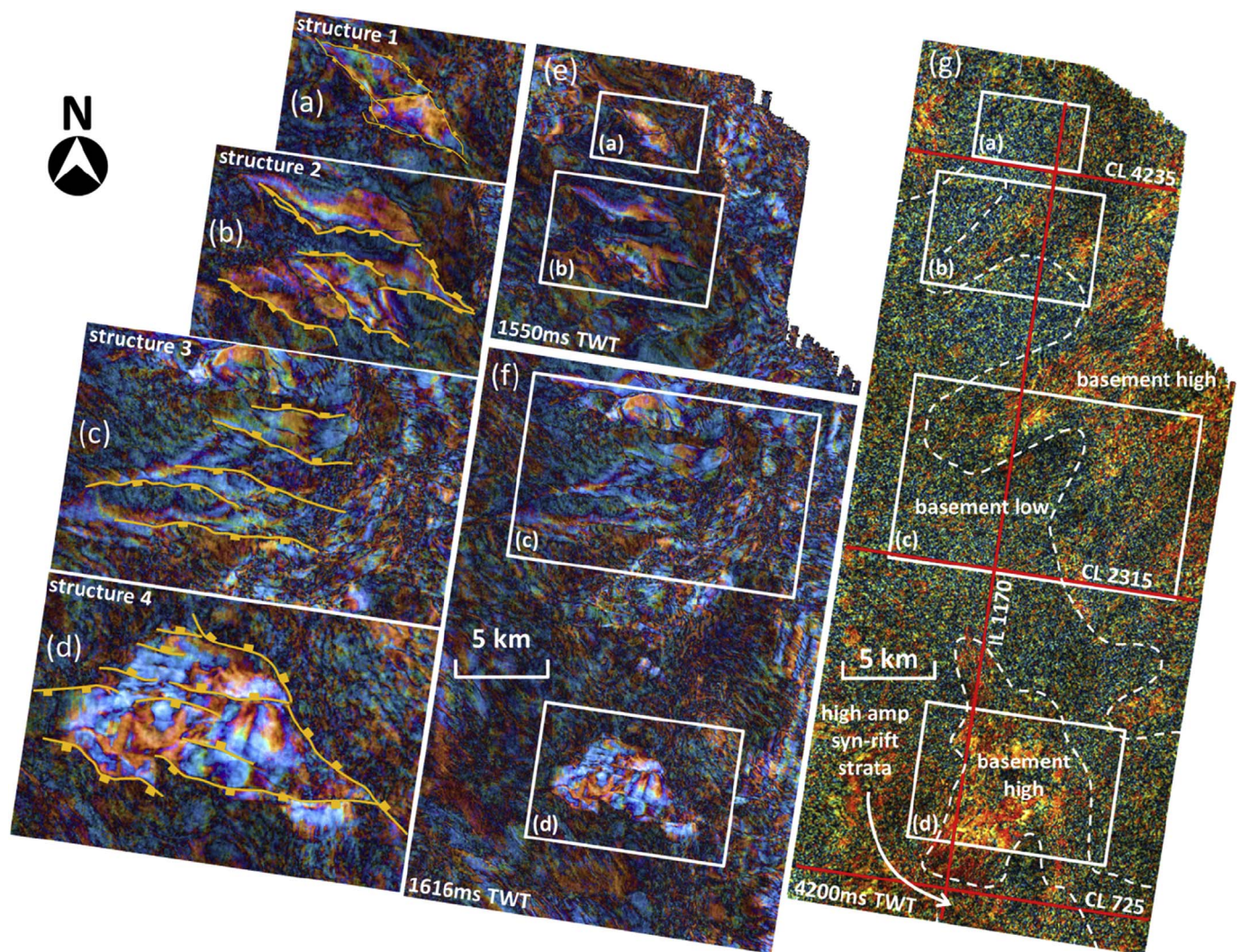


Fig. 4. Structures 1 (a), 2 (b), 3 (c) and 4 (d) highlighted by standard frequency decomposition slices of the 3D reflection survey at 1550 ms TWT (e) and 1616 ms TWT (f) using a method based on the Fast Fourier Transform. A high definition frequency decomposition slice of the 3D reflection survey at 4200 ms TWT (g) using a method based on the Matching Pursuit algorithm is also displayed to highlight basement highs (likely horst structures) and basement lows (likely graben structures). These ‘flame red’ colours highlighting the basement framework can also be seen in cross-section (Fig. 5; 11). Note that the ‘flame red’ colour in the far SW of the survey corresponds to high amplitude syn-rift strata. The locations of crosslines 4235, 2315 and 725 (Fig. 4) and inline 1270 (Fig. 5) overlay the map. (For interpretation of the references to colour in this figure legend, the reader is referred to the web version of this article.)

structure and is ‘V-shaped’, with two bounding normal fault assemblages meeting at the eastern tip of the structure, giving the structure a total length of ~8 km (NW-SE) and a maximum width at the western side of ~4 km. Half-graben structures 2 and 3 (Fig. 4b and c) are located in between structures 1 and 4. The SW-SSW dipping normal fault arrays that constitute structures 2 and 3 (Fig. 4b and c) have a NW-SE to WNW-ESE strike orientation and are typically down-dip from one another, which forms the series of half-graben structures. These faults, which constitute structures 2 and 3, vary in length from ~4 to 8 km (structure 2) and ~5.5–8.5 km (structure 3).

All normal faults that form structures 1, 2 and 3 have planar geometries (Fig. 5), which transitions to listric normal faults in the south of the survey (SSW side of structure 4, Fig. 5), agreeing with observations of cross-sectional geometries in previous studies (Palmowski et al., 2004; see Fig. 14). The faults analysed in this study mostly do not penetrate down to basement level (Fig. 5) and display hectometer to kilometer scale late Cretaceous hanging wall growth strata and fault block rotation (15–25°, Palmowski et al., 2004). Previous studies have suggested that because there is 15–25 degrees of Upper Cretaceous fault block rotation and little/no basement fault block rotation, a detachment exists between the rotated strata and the basement horst and graben

structures (Palmowski et al., 2004). However, we do observe some degree of rotation of basement fault blocks (Fig. 5) and we have found no direct evidence in the seismic dataset of a detachment surface.

4.2. Highlighting basement framework using frequency decomposition

Frequency decomposition has proven useful in determining basement structural trends. The basement structure is visible in a majority of the survey, except where grabens, developed during the Cretaceous rifting, appear to be faulted down below the coverage of the 3D survey in the central-western portions (Fig. 4g). Interpretations of basement structure can be made along inlines and crosslines using the reflectivity volume. A generalised basement framework was further aided by time-slices through the frequency spectral decomposition volume at basement depths (Fig. 4g). Using this data, at least three kilometer-scale basement horsts, and the basement plateau to the east of the SFZ, are easily visible in the north and eastern portions of the survey (red/orange colours), as well as an isolated basement high in the SW of the survey (Fig. 4g). This leaves much of the central-western area interpreted to be a basement low (green/blue colours, Fig. 4g), where the Crayfish Supersequence (Fig. 2) is likely to have accumulated during

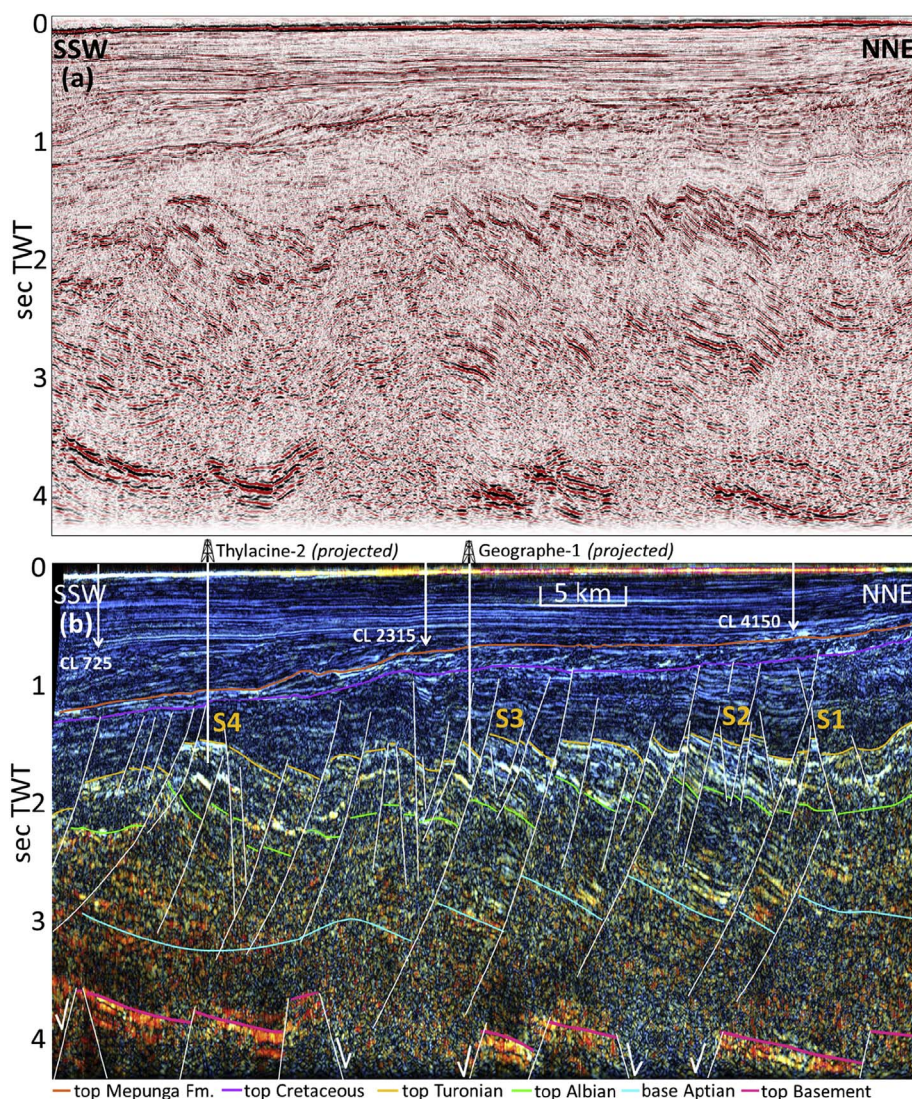


Fig. 5. (a) High definition (HD) frequency decomposition and (b) amplitude seismic inline 1170 showing the down-dip structure of the Shipwreck Trough covered by the Investigator 3D seismic survey. The high definition frequency decomposition volume of the seismic survey, generated using Geo Teric, is displayed. Note the homogenous thickness of the Waarre and Flaxman formations (top Albian-top Turonian) in the NNE, which thicken across faults in the SSW and the Belfast Mudstone and Paaratte Formation (top Turonian-top Cretaceous), which display syn-kinematic strata across all Upper Cretaceous faults. Wells Thylacine-2 and Geographe-1 have been strike projected onto the seismic line to show their generalised location. The location of crosslines 725, 2315 and 4150 from Fig. 11 are displayed on the section. Also displayed, are the locations of structures 1 (S1), 2 (S2), 3 (S3) and 4 (S4). For the location of this inline refer to Fig. 4 (map view) and Fig. 11 (crossline intersection).

the early Cretaceous rifting event.

5. Normal fault growth analysis of the horst and half-graben structures

5.1. Throw analysis of structure 1

Structure 1 (Figs. 4a, 6) is a horst structure, and has previously been identified as a potential hydrocarbon prospect known informally as the Roebuck lead (Origin Energy Australia, 2002). Structure 1 is a diamond-shaped horst bounded by planar normal faults, which strike NNW-SSE to NW-SE. A normal fault that strikes ~ E-W dissects the centre of the horst block (Fig. 6a). Throw has been measured incrementally along bounding faults with location numbers provided in the corresponding figure (Fig. 6) at throw maxima and minima for reference. The fault that bounds the NE side of the horst (locations 1–10) displays a highly variable maximum throw profile, with three significant throw maxima occurring at locations 1, 5 and 7, separated by localised throw minima (Fig. 6b). Minor throw maxima are observed at locations 3 and 9 (Fig. 6b). However, these maxima do not create a deficit with localised throw minima greater than the 5% error range allowed for interpretation. Therefore, these are not considered throw maxima. Throw-depth measurement at location 5 reveals that the maximum throw occurs at the top Turonian horizon (Fig. 6c). The E-W fault which dissects the horst structure (locations 11–13) displays a

throw maximum at location 12, with throw decreasing outwards towards locations 11 and 13 (Fig. 6b). Throw-depth profiling shows that the throw maximum at location 12 occurs at the top Turonian horizon (Fig. 6c). Throw towards the fault tips, beyond locations 11 and 13, is unreliable due to poor imaging in fault shadows of the larger bounding faults, likely caused by velocity differences on opposite sides of a fault (Fig. 6b). The SW side of the horst structure (locations 14–20) displays a highly variable throw profile with three throw maxima at locations 15, 17 and 19, separated by localised throw minima (Fig. 6b). In contrast to all other faults bounding and dissecting this horst structure, the SW bounding fault has a maximum throw observed at the top Albian horizon at location 17 (Fig. 6c). However, T-z profiling at location 19 shows that maximum throw of this fault segment is observed at the top Turonian horizon (Fig. 6c). The average throw deficit percentage of structure 1 is 39% (Fig. 6b; refer to Fig. 3 for methodology).

5.2. Throw analysis of structure 2

Structure 2 comprises an array of NW-SE to WNW-ESE striking and basinward dipping (SW/SSW), tilted half-grabens, with one fault that dips landward (NNE), creating a small horst structure at the centre of the fault array (Fig. 4b,7a). Maximum throw profiling of the northern most fault (locations 1–13) reveals a moderately variable throw profile, with throw maxima at locations 2, 4, 8 and 10, separated by only minor throw deficits (Fig. 7b). Throw maxima at locations 6 and 12 are below

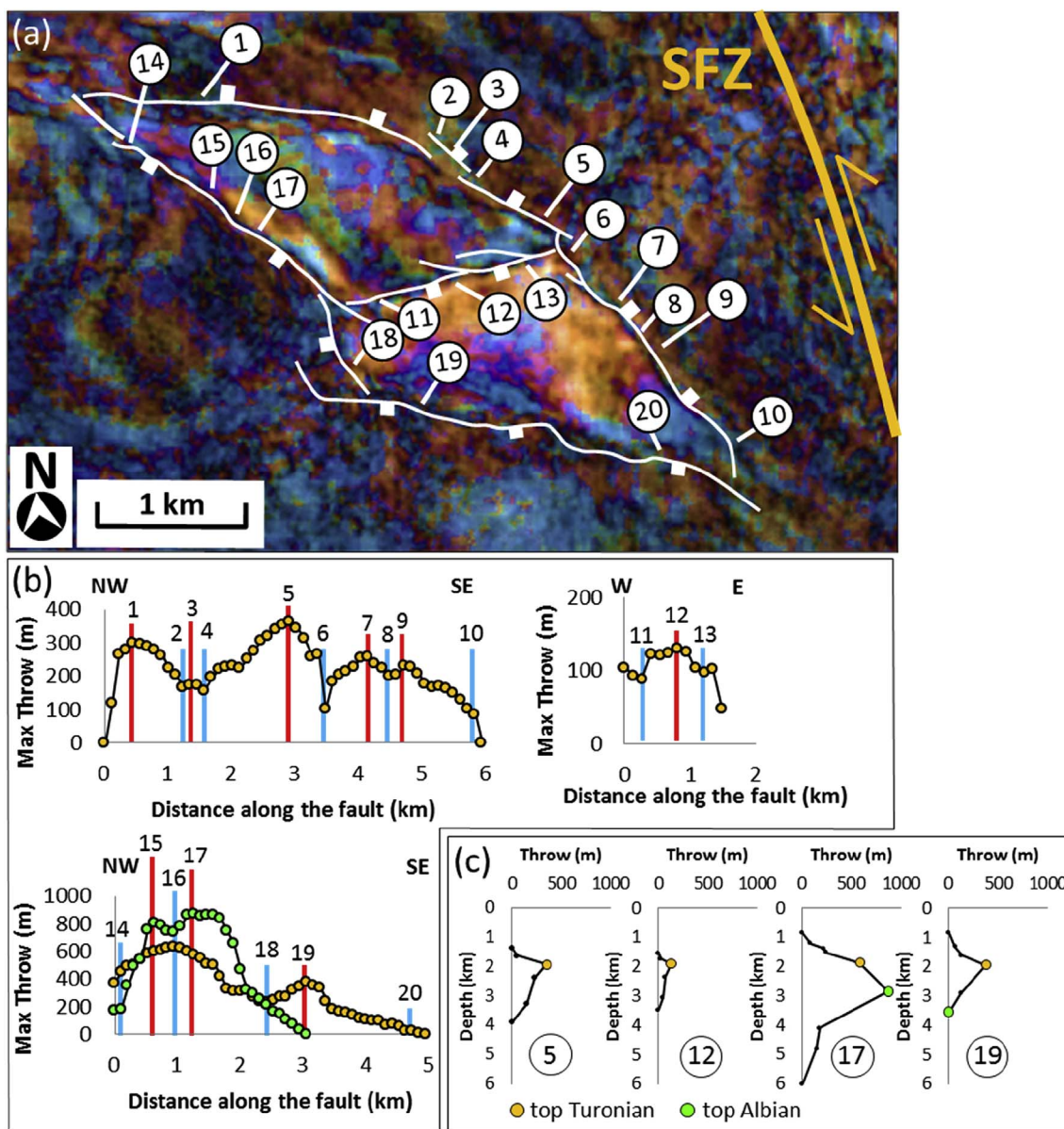


Fig. 6. (a) Structure 1 highlighted by standard frequency decomposition slices of the 3D reflection survey at 1550 ms TWT using a method based on the Fast Fourier Transform. Locations 1–20 are shown on the map, which correspond to the numbers on the graphs below (b; c). (b) Maximum throw-distance (*T-x*) graphs showing the variability of throw along strike of the fault assemblages in (a). (c) Throw-depth (*T-z*) analysis at locations 5, 12, 17 and 19.

the 5% error range allowed for interpretation error and cannot be considered throw maxima in this study (Fig. 7b). Throw-depth profiling at location 10 (Fig. 7c) shows that the maximum throw occurs at the top Turonian horizon (Fig. 2). Maximum throw profiling of the landward (NNE) dipping fault (locations 14–18) also shows a moderately variable throw profile, with throw maxima at locations 14 and 18, separated by only minor throw deficits (Fig. 7b). The throw maximum at location 16 is below the error range of 5% and cannot be considered a throw maximum in this study (Fig. 7b). Throw-depth profiling at location 18 (Fig. 7c) shows that the maximum throw occurs at the top Turonian horizon (Fig. 2).

The eastern most fault (location 19) displays a very smooth throw profile with throw decreasing outward from the centre to the tip-line (Fig. 7b). In addition, this fault does not have any rapid strike orientation variations. Throw-depth *T-z* profiling at location 19 (Fig. 7c) shows that the maximum throw occurs at the top Albian horizon (Fig. 2). Slightly further south, we observe another basinward (SW) dipping fault (locations 20–28), which shows a moderately variable

maximum throw profile along strike, with five throw maxima occurring at locations 20, 22, 24, 26 and 28, separated by minor throw deficits (Fig. 7b). Throw-depth profiling at location 26 (Fig. 7c) shows that maximum throw occurs at the top Albian horizon, with a rapid shallowing of the *T-z* slope between the top Turonian and top Albian horizons (see location 26, Fig. 7c). The southernmost fault (locations 29–33) has two throw maxima along strike, found at locations 29 and 31 (Fig. 7b). A throw maximum occurs at location 33, which is below the error range of 5% allowed for interpretation error and cannot be considered a throw maximum in this study (Fig. 7b). Throw-depth profiling at location 31 shows a maximum throw at the top Albian horizon (Fig. 7c). The average throw deficit percentage of structure 2 is 19% (Fig. 7b).

5.3. Throw analysis of structure 3

Structure 3 is a NW-SE to WNW-ESE striking fault array, with a landward (NW) dipping normal fault in the north and 3 basinward

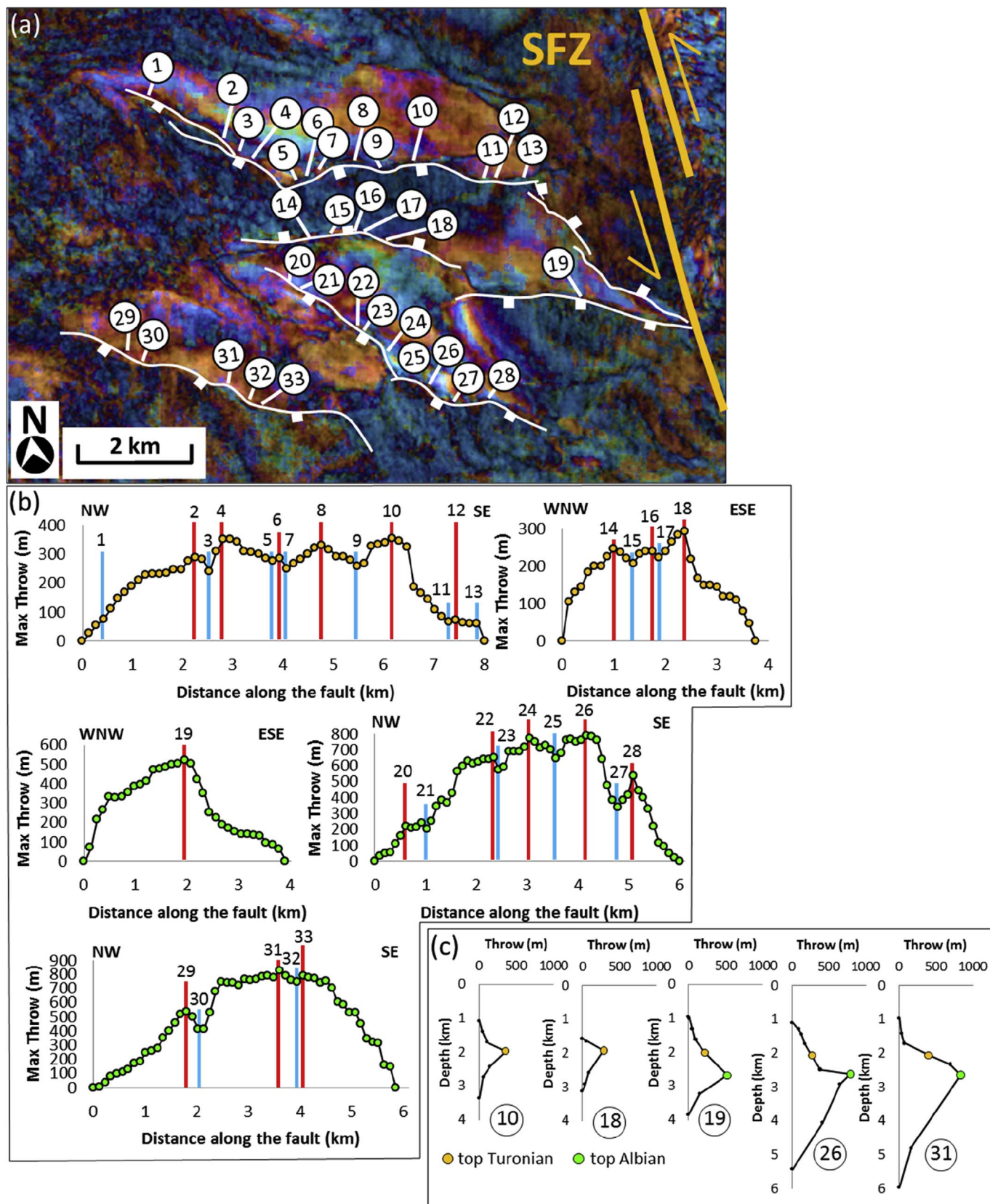


Fig. 7. (a) Structure 2 highlighted by standard frequency decomposition slices of the 3D reflection survey at 1550 ms TWT using a method based on the Fast Fourier Transform. Locations 1–33 are shown on the map, which correspond to the numbers below (b); (c). (b) Maximum throw-distance (T-x) graphs showing the variability of throw along strike of the fault assemblages in (a). (c) Throw-depth (T-z) analysis at locations 10, 18, 19, 26 and 31.

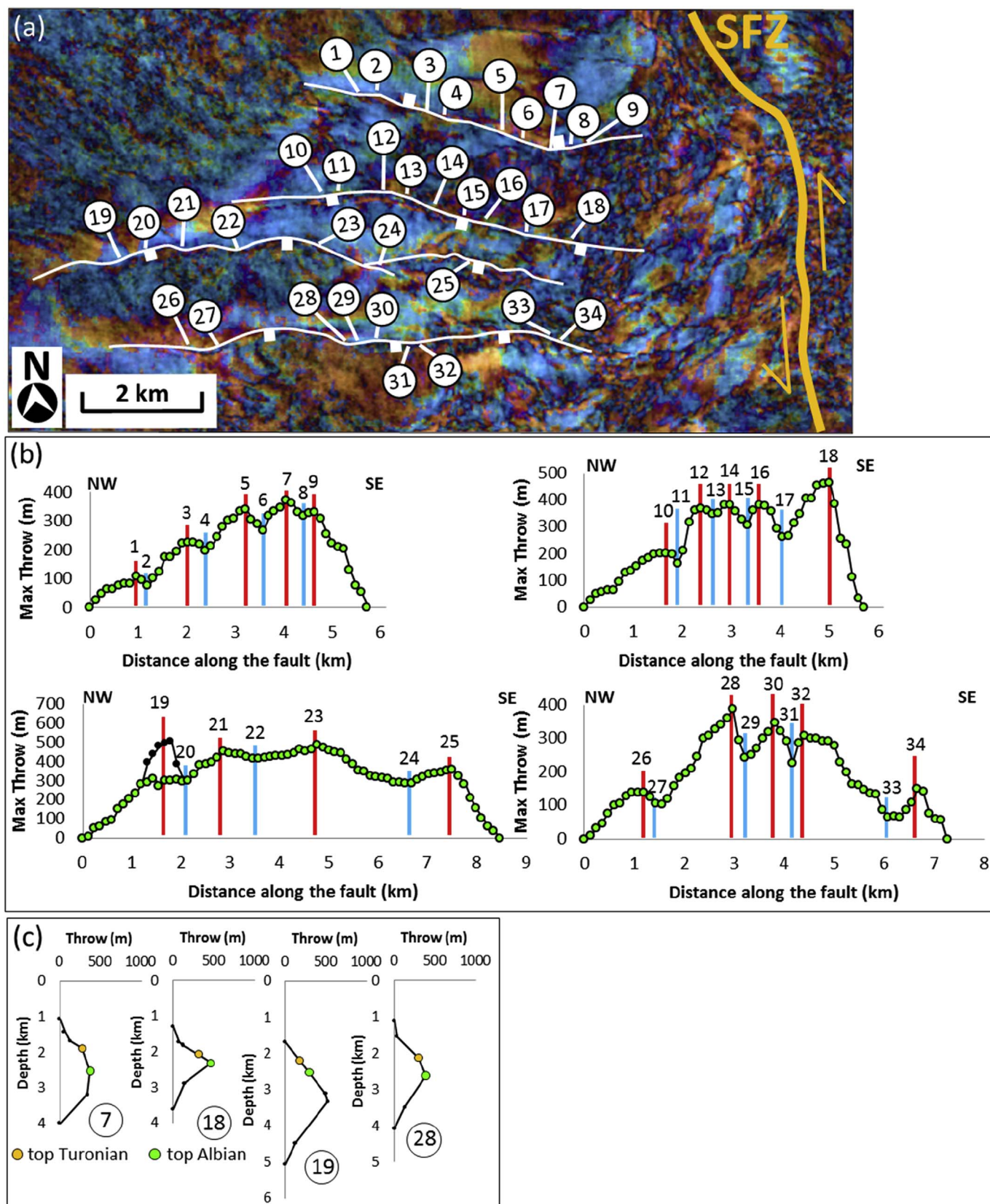


Fig. 8. (a) Structure 3 highlighted by standard frequency decomposition slices of the 3D reflection survey at 1616 ms TWT using a method based on the Fast Fourier Transform. Locations 1–34 are shown on the map, which correspond to the numbers on the graphs below (b; c). (b) Maximum throw-distance (T-x) graphs showing the variability of throw along strike of the fault assemblages in (a). (c) Throw-depth (T-z) analysis at locations 7, 18, 19 and 28.

(SSW) dipping normal faults in the south. This fault structure creates a horst structure in the north and three tilted half-grabens in the south (Fig. 4c,8a). The landward (NW) dipping fault in the north (locations 1–9) displays a moderately variable maximum throw profile, with throw maxima at locations 1, 3, 5 and 7 separated by localised throw minima (Fig. 8b). The throw maximum at locations 9 is below the 5% error range allowed for interpretation error and cannot be considered a throw maximum in this study (Fig. 8b). The northernmost, basinward dipping (SSW) normal fault (locations 10–18) displays a highly variable maximum throw profile, with throw maxima occurring at locations 10, 14, 16 and 18, separated by localised throw deficits (Fig. 8b). The throw maximum at location 12 is below the 5% error range allowed for interpretation and cannot be considered a throw maximum in this study (Fig. 8b).

The central half-graben bounding fault (locations 19–25) displays a highly variable throw profile, with throw maxima occurring at locations 19, 21, 23 and 25, separated by localised throw deficits (Fig. 8b). The southernmost normal fault (locations 26–34) also displays a highly variable maximum throw profile, with throw maxima occurring at locations 26, 28, 30, 32 and 34, separated by localised throw minima (Fig. 8b). Throw-depth profiling at locations 7, 18, 19 and 28 (Fig. 8c) reveals that the maximum throw occurs at the top Albian horizon for all faults, except the central half-graben fault (locations 19–25), which displays a maximum throw below the top Albian horizon (see T-z plot of location 19, Fig. 8c). The average throw deficit percentage of structure 3 is 25% (Fig. 8b).

5.4. Throw analysis of structure 4

Structure 4 is a horst structure, which is roughly triangular in shape, with a NW-SE striking, landward (NE) dipping, listric normal fault assemblage bounding the NE side, and a WNW-ESE striking, basinward (SSW) dipping, listric normal fault assemblage bounding the southern side (Figs. 4d,9a). The top of the Thylacine gas field (Fig. 1) is located near the eastern most tip of the horst structure, where these two fault assemblages intersect (Origin Energy Australia, 2002). The NE bounding fault assemblage (locations 1–11) displays highly variable maximum throw along strike, with six throw maxima observed at locations 1, 3, 5, 7, 9 and 11, separated by localised throw deficits (Fig. 9b). The southern bounding fault assemblage shows only moderate variability of maximum throw along strike, with throw maxima observed at locations 12, 16 and 18, separated by localised throw minima (Fig. 9b). The insignificant throw maximum at locations 14 is below the 5% error range and cannot be interpreted (Fig. 9b). Throw-depth profiling at locations 7 and 16 shows that maximum throw occurs at the top Albian horizon for both of these fault assemblages (Fig. 9c). The average throw variability of structure 4, measured as a percentage throw deficit from adjacent throw maxima is 21%.

5.5. Horizon and isochronal mapping of the 3D seismic survey

Horizon (Fig. 10a; b; c) and isochronal (Fig. 10d; e) mapping was interpreted for the entire 3D seismic survey. The horizons mapped were the top Cretaceous, top Turonian and top Albian horizons (Fig. 10a; b; c). The presence of the SFZ (Fig. 1a) is visible on all three two-way-time (TWT) maps (Fig. 10a; b; c) as a N–S oriented fault system in the north-eastern portion of the survey, with the greatest amount of faulting and fault throw observed on the top Turonian TWT map (Fig. 10b). Closer spaced normal faulting across the entire survey is observed on the top Turonian TWT map (Fig. 10b) in comparison to the top Albian TWT map (Fig. 10c), indicating that structures are generally larger and more continuous at the top Albian level (deeper) and more heavily faulted and compartmentalized at the top Turonian level (shallower). Numerous fault dependent and independent structural closures can be observed on the top Turonian and top Albian TWT maps (Fig. 10b; c). The top Turonian map (Fig. 10b) is equivalent in age to the top

reservoir for the Thylacine and Geographe gas fields (Fig. 1a). Therefore, this indicates that there are potentially numerous other analogous petroleum prospects in close vicinity to the Thylacine and Geographe gas fields (Fig. 1a). However, these potential structural closures should be mapped in detail with an accurate depth conversion to assess the future petroleum prospectivity of the area.

Larger throw of normal faults in the southern portions of the 3D survey is observed on the top Albian TWT map, compared to the top Turonian TWT map (Fig. 10b; c). This agrees with the detailed T-x and T-z analysis, showing that the greatest throw occurs at the top Albian horizon for the three most southern normal faults bounding structure 2 and all normal faults bounding structures 3 and 4 (Figs. 7–9). The Cenomanian-Turonian isochron map (Fig. 10e) confirms this finding with observations of thickening in the hanging wall of normal faults, located in the middle and south of the survey. Syn-rift depocentres are less well developed in the north during this time interval. This implies that the faults in the middle and southern portions of the 3D survey experienced greater Cenomanian-Turonian growth. The Coniacian-Maastrichtian isochron map shows highly variable thickness over the entire survey, including across the SFZ (Fig. 10d). Thickening is occurring in the hanging wall of normal faults and on the western side of the SFZ, with no portion of the survey showing greater thickness variations (Fig. 10d). This indicates that this was a major growth period for normal faults across the entire survey and was the major period of growth of the SFZ.

6. Structural characterisation of the Shipwreck Fault Zone

The Shipwreck Fault Zone (SFZ) is a N–S oriented, sinistral trans-tensional fault zone which borders the eastern side of, and provides accommodation space for, the Shipwreck Trough sediments (Fig. 1a; Origin Energy Australia, 2002; Palmowski et al., 2004). The SFZ is located immediately (less than 5 km) to the east of the horst and half-graben structures 1–4, previously discussed in this paper. The SFZ has previously been interpreted as a negative flower structure, which accommodated greater extension on the western side (~1.91 km) than on the eastern side (~0.79 km), from the Coniacian to Early Eocene, with ~1.12 km of sinistral movement (Palmowski et al., 2004). The SFZ is described as a concentration of 50–70° dipping, low displacement, normal faults located over one or two 80–90° dipping normal faults (Palmowski et al., 2004), with the fault system broadening to the south, in conjunction with a shallowing of normal fault dips. Hence, Palmowski et al. (2004) interpretation of a negative flower structure, as outlined in Harding (1983). Palmowski et al. (2004) also propose that the SFZ is the northern en echelon extension of the transform margin to the south (Fig. 1b).

Basin asymmetry has been shown to develop in rift-oblique sedimentary basins, which are bound on one side by a continental transform (Harding et al., 1985; Ben-Avraham, 1985; Ben-Avraham and Zoback, 1992), due to displacement along the transform fault system controlling the basin subsidence (Harding et al., 1985). A rift-oblique structural setting is markedly different to a pull-apart basin (Christie-Blick and Biddle, 1985), which is bounded on either side by transform faults, forming the borders of an extensional basin within. This structural setting also differs from transfer zones and accommodation zones in a typical rift basin where these zones purely exist to conserve regional extensional strain between en echelon normal fault systems, such as the East African Rift, Red Sea rift in the Gulf of Suez and the Faroe-Shetland Basin (Morley et al., 1990; Younes and McClay, 2002; Moy and Imber, 2009).

The Shipwreck Trough (Fig. 1a) is asymmetrical from east to west (Fig. 11), with thicker Upper Cretaceous sediments abutting the SFZ and thinning of these sediments to the west, up onto the Mussel Platform (Figs. 1,11; also see Palmowski et al., 2004, Fig. 11). The Shipwreck Trough is also located between a rift/oblique-rift setting to the west (Bight Basin and western Otway Basin) and a transform margin to

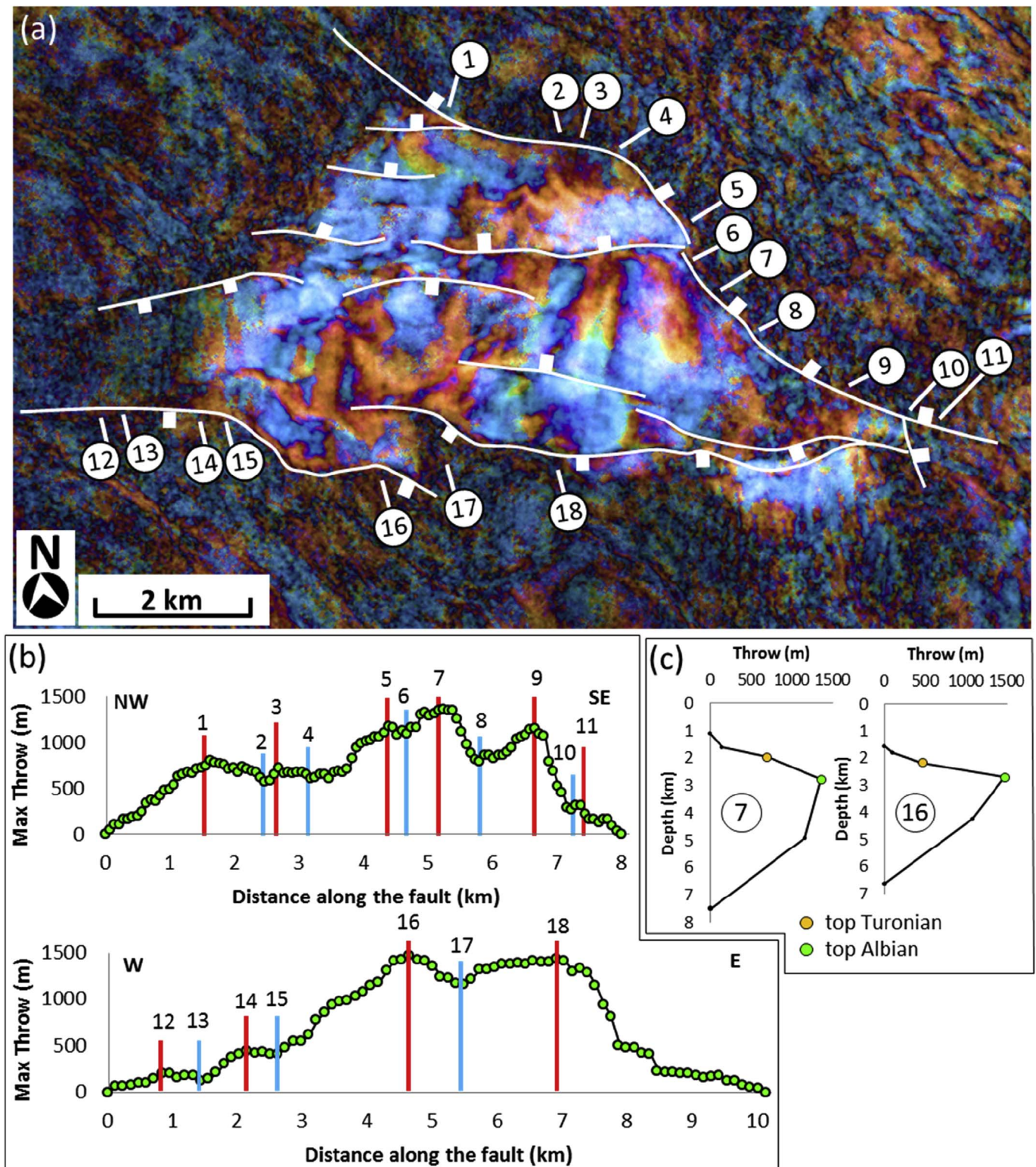


Fig. 9. (a) Structure 3 highlighted by standard frequency decomposition slices of the 3D reflection survey at 1616 ms TWT using a method based on the Fast Fourier Transform. Locations 1–18 are shown on the map, which correspond to the numbers on the graphs below (b; c). (b) Maximum throw-distance (*T-x*) graphs showing the variability of throw along strike of the fault assemblages in (a). (c) Thrown-depth (*T-z*) analysis at locations 7 and 16.

the south (Fig. 1b). Sinistral movement of the SFZ created the asymmetrical accommodation space of the Shipwreck Trough (Fig. 11). Therefore, the SFZ does not exist purely to conserve regional extensional strain. It is a primary structural feature of the Otway Basin, showing characteristics of a negative flower structure, with ~1.12 km of sinistral movement recorded during the Otway Basin Late Cretaceous

ripping event (Palmowski et al., 2004). It is also sub-parallel and in close proximity to the N–S oriented transform margin to the south (Fig. 1b). Therefore, the proposed model by Palmowski et al. (2004), suggesting that the SFZ is the northern en echelon extension of the transform margin, is highly plausible. While the Upper Cretaceous faulting along the SFZ does not always penetrate down to basement level and

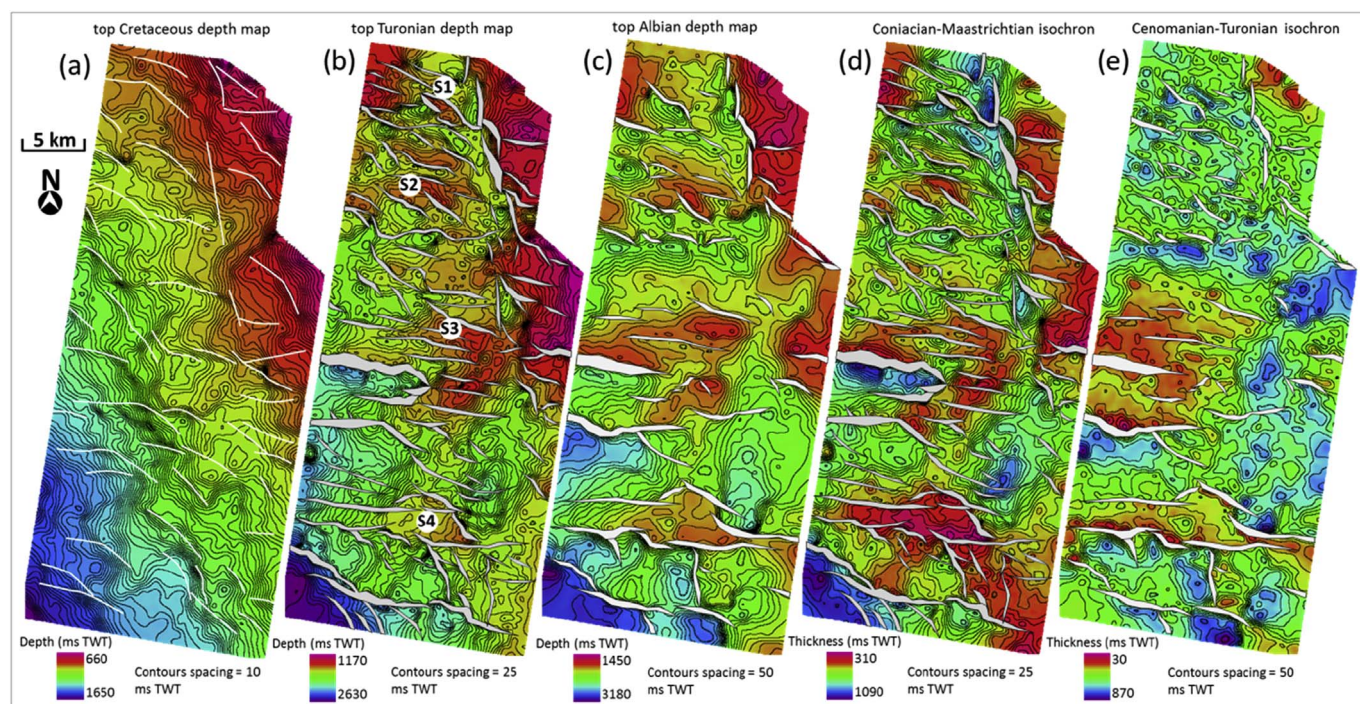


Fig. 10. Depth maps (ms TWT) of the top Cretaceous (a), top Turonian (b) and top Albian (c) surfaces, with major fault polygons tied to the top Turonian (b) and top Albian (c) surfaces. Fault traces were used for the top Cretaceous (a) surfaces as heave in map view is extremely minimal. Isochronal maps (ms TWT) of the Coniacian-Maastrichtian (d) and Cenomanian-Turonian (e) intervals are also displayed with fault polygons from the top Turonian (b) and top Albian (c) depth maps respectively, overlaid to highlight any potential syn-depositional faulting during those periods. Note the syn-depositional faulting present in the south of the survey during the Cenomanian-Turonian (e) and over the entire survey during the Coniacian-Maastrichtian (d). The locations of structures 1 (S1), 2 (S2), 3 (S3) and 4 (S4) as defined in Fig. 4 are shown on the isochron maps.

therefore is not geometrically linked to basement-involved faults, it is most likely kinematically linked. This is evident by the SFZ (Fig. 1a) aligning well with the edge of the basement high along the eastern side of the survey area (Fig. 4g). This N–S orientation of the basement high and the SFZ is likely the result of Paleozoic structure which has previously been interpreted to have impacted the development of Tithonian-Barremian normal faults (Finlayson et al., 1996).

The Shipwreck Trough is thought to have been initiated during the Cenomanian-Turonian deposition of the Waarre and Flaxman formations (Fig. 2), with minor thickening of Cenomanian-Turonian strata into the trough from 500 m to east of the fault, on the Prawn Platform, to 550 m on the downthrown western side (see Fig. 11, Palmowski et al., 2004). However, transtensional movement along the SFZ continued to provide significant accommodation space throughout the Coniacian-Maastrichtian deposition of the Belfast Mudstone and Paaratte Formation (Fig. 2), which is considered to be the major period of fault movement (Origin Energy Australia, 2002; Palmowski et al., 2004). Isochronal mapping of the 3D seismic survey further substantiates this model, with the Cenomanian-Turonian interval (Fig. 10e) showing minor thickening across the SFZ. Furthermore, the Coniacian-Maastrichtian isochronal map (Fig. 10d) shows major thickening across the fault zone by as much as 600 ms TWT (also see cross sections, Fig. 11).

Further evidence for transtensional character of the SFZ is visible through coherence volume slices (Fig. 12). In the north of the 3D survey, the SFZ displays structures typical of transtensional kinematics, such as a ~1 km wide, left stepping, releasing jog, with a sinistral sense of shear, observed at 1200 ms TWT (Fig. 12c), which at the same location, but in shallower strata (990 ms TWT) has become a releasing bend (Fig. 12b). This may imply greater kinematic coherence of the SFZ in shallower strata through linkage of transtensional fault segments. A ~300 m wide restraining jog is observed to the north of the previous location (Fig. 12d) and a much larger restraining jog is visible to the south, both of which have a sinistral sense of shear (Fig. 12e). In

addition, normal faults surrounding these restraining jogs appear to have rotated strike orientation from NW-SE to E-W, striking perpendicular to the SFZ the more proximal to the restraining jog they become (Fig. 12b; d).

Cessation of transtensional movement of the SFZ is evident through little to no variability in post Cretaceous thickness across the fault zone (Fig. 11). However, further evidence is also available from a previously identified sill (Holford et al., 2012) related to the SFZ, which appears to feed a shallower extrusive lava flow (Fig. 13). With the aid of a frequency decomposition volume, we can easily identify a slightly saucer shaped sill (Planke et al., 2005, see Fig. 8, Table 1), which cross-cuts stratigraphy on its NE side, just below the top Cretaceous horizon (Fig. 13d). We also interpret an extrusive lava flow related to this sill, which has flowed to the SW, downslope on the palaeosurface (Fig. 13b; c; d). This sill and related extrusive lava flow appears in map view to not have been laterally offset in by the SFZ (Fig. 13b). However, in cross section antithetic faulting may have vertically offset this sill (Fig. 13a; d). Given the sill and extrusive flow has no lateral offset, this potentially constrains the latest lateral movement of this portion of the SFZ by the end of the Cretaceous. However, we do observe normal faults associated with the SFZ penetrating the top Cretaceous horizon in other portions of the 3D seismic survey (Fig. 11). None of these faults penetrate the top Mepunga Formation horizon (Fig. 11), which implies termination of faulting by the early/mid Eocene, agreeing with previous studies (Palmowski et al., 2004).

7. Evolution of extensional structures proximal to a transtensional fault system

The style and timing of fault growth can be constrained using throw-distance and throw-depth analysis (Mansfield and Cartwright, 1996; Rykkelid and Fossen, 2002; Jackson and Rotevatn, 2013; Robson et al., 2017; Jackson et al., 2017) and this enables us to interpret the temporal and spatial evolution of the four horst and half-graben structures

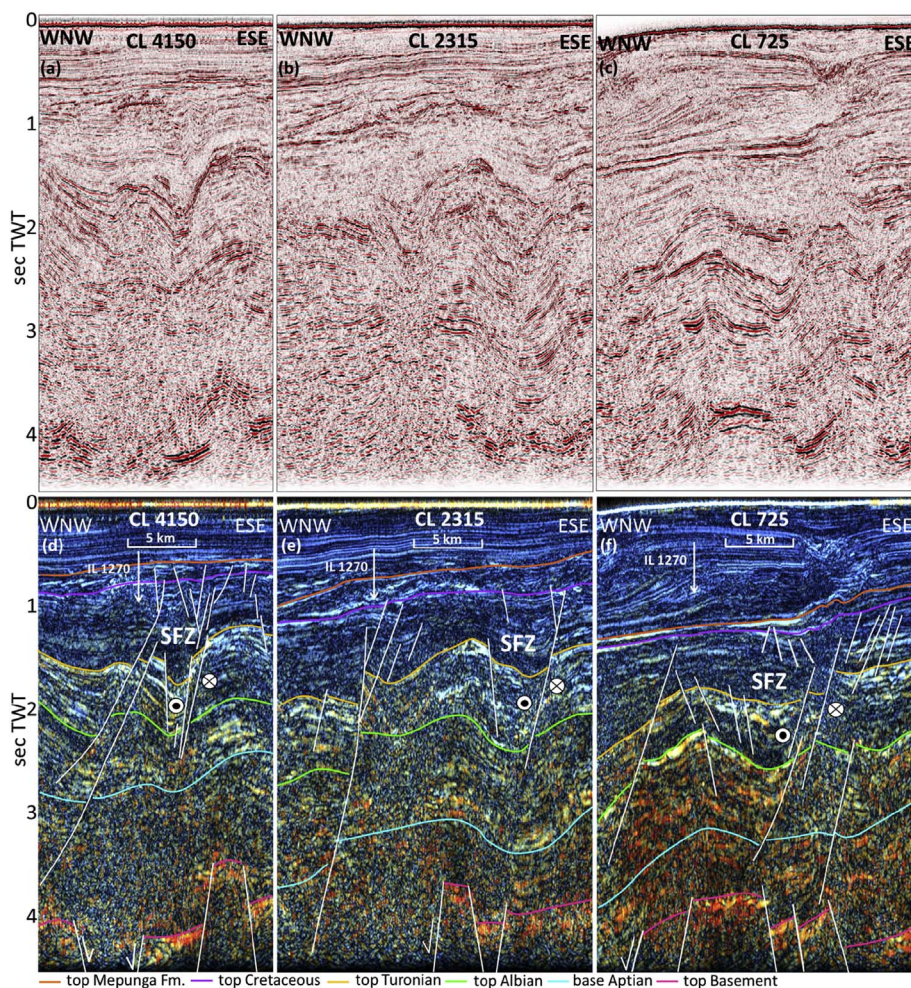


Fig. 11. (a; b; c) amplitude and (d; e; f) high definition frequency decomposition seismic crosslines from north to south: 4150, 2315 and 725 from Investigator 3D high definition frequency decomposition volume, with seismic interpretation overlaid, with faults in white and horizon colours labelled below. Note the relatively homogeneous thickness of the Waarre and Flaxman Formations (top Albian-top Turonian) across the Shipwreck Fault Zone (SFZ) and the westerly thickening of the Belfast Mudstone and Paaratte Formation (top Turonian-top Cretaceous) across the SFZ. Also note that the SFZ is narrow and steeply faulted in the north and broad with shallower dipping faults in the south. For crossline locations refer to Fig. 4 (map view) and Fig. 5 (inline intersection). (For interpretation of the references to colour in this figure legend, the reader is referred to the web version of this article.)

analysed in this study, from their nucleation to their present day geometries. Our main objectives for this section of the study are: [1] to establish the timing of the nucleation and major growth periods for all structures; [2] understand how the faults bounding all four horst and half-graben structures developed spatially and kinematically; and [3] to compare and contrast the structural style of these structures with the SFZ.

7.1. Nucleation of extensional structures

Previous studies interpret that the normal faults that bound the four structures that we analysed do not penetrate down to basement level and have significant fault block rotation, compared to the un-rotated basement horst and graben structures (Palmowski et al., 2004). They have also implied from this interpretation that a detachment exists between the Upper Cretaceous syn-rift strata, and the basement; likely in the Crayfish Supersequence strata (Fig. 2; Palmowski et al., 2004). We agree that this is a plausible interpretation. However, based on the data quality, we cannot be sure that this is the only possible interpretation. Furthermore, there are some faults which may penetrate down to basement level and there are basement fault blocks that do appear to have some degree of rotation, similar to the horst and half-graben structures analysed in this study (Fig. 5). Finally, we do not see any direct evidence within the study area of a detachment surface in the Eumeralla or Crayfish supersequences (Fig. 2), between the Upper Cretaceous faults and the top basement horizon (H1, Fig. 2). Therefore, we believe it is inconclusive as to whether these four structures and associated normal faults have nucleated and grown in response to mechanical extension, gravitational instability or a combination of

both, across the study area.

Nucleation of fault segments generally occurred during the deposition of the Waarre and Flaxman formations (Cenomanian-Turonian, Fig. 2) or the Belfast Mudstone (Coniacian-Santonian, Fig. 2). However, one fault (see location 19, structure 3, Fig. 8) displays evidence for an earlier timing of nucleation at some stage prior to the Cenomanian and likely during the deposition of the Eumeralla Supersequence (Fig. 2). This is consistent with previous studies, suggesting that the Early Cretaceous rifting event continued into the Aptian-Albian in some areas of the Otway Basin (Cooper, 1995; Palmowski et al., 2004).

Isochronal mapping and T-z analysis show that normal faults bounding structures in the central and southern portions of the study area (southern faults of structure 2, structure 3 and structure 4, see Figs. 4,7–9) nucleated in the Cenomanian-Turonian. This correlates well with basement structure, highlighted by the standard frequency decomposition slice, which shows that large basement lows exist between basement highs in the central region, under structures 2 and 3 (Fig. 4g). Furthermore, in the southern region, structure 4 is located over an isolated structural high, which drops off to basement lows in all directions (Fig. 4g). This basement high can also be seen under structure 4 in cross section (Fig. 5). Isochronal mapping and T-z analysis also shows that normal faults bounding the northern structures (structure 1 and northern faults of structure 2, see Figs. 4,6,7) nucleated later, during the Coniacian-Santonian. The location of the structural highs in the Cretaceous section correlate with basement highs (Fig. 4g), indicating some level of basement control on the cover sequences.

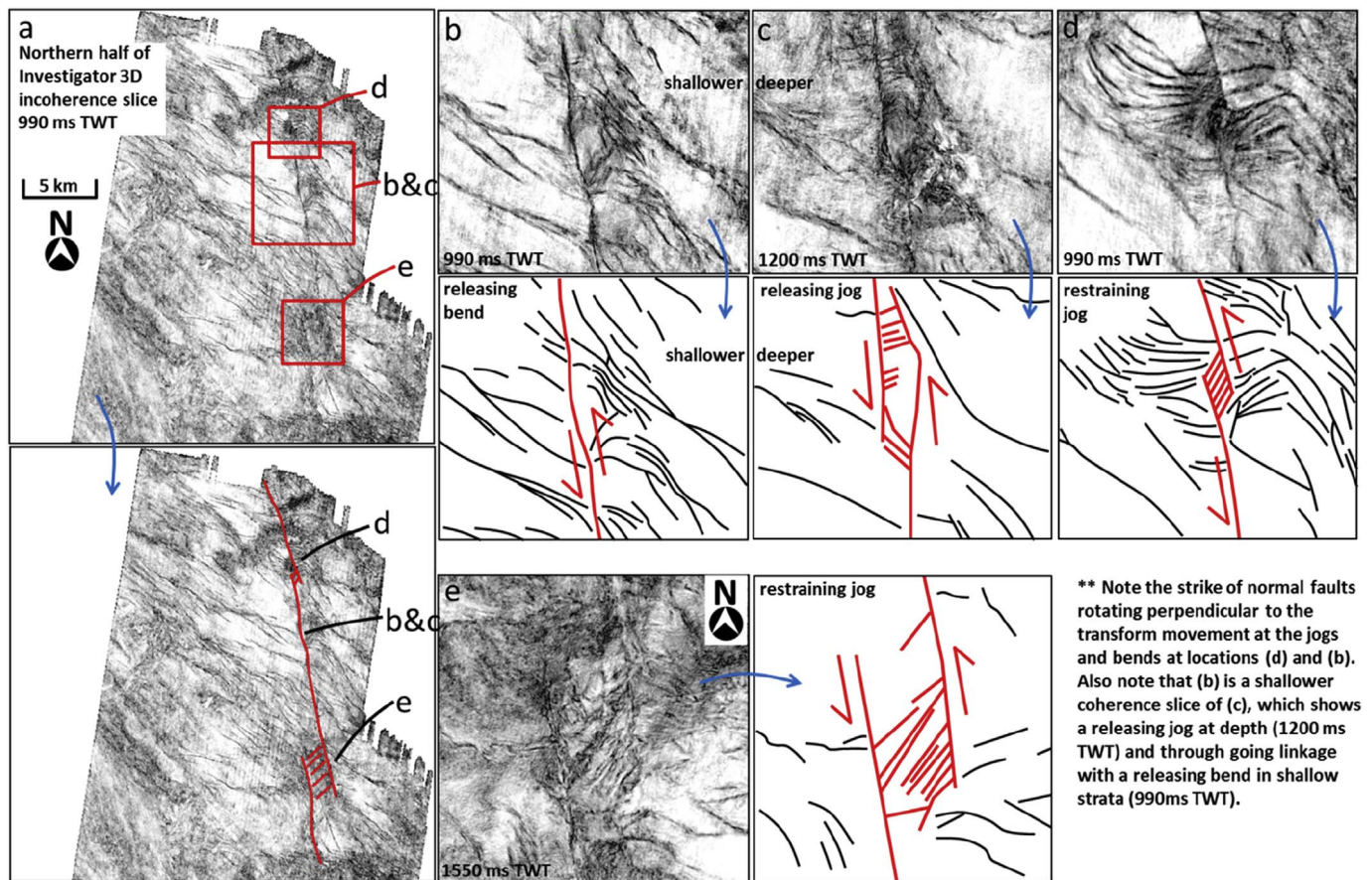


Fig. 12. (a) Incoherence slice at 990 ms TWT of the northern half of Investigator 3D overlaid with interpretation of the Shipwreck Fault Zone and the locations of (b), (c), (d) and (e). (b) Incoherence slice at 990 ms TWT highlighting an interpreted releasing bend. (c) Incoherence slice at 1200 ms TWT highlighting an interpreted releasing jog, which is located directly above (b). Incoherence slices at 990 ms TWT (d) and 1550 ms TWT (e) highlighting interpreted restraining jogs. Major strike-slip faults are shown in red and minor normal faults are shown in black. Note the change in orientation of minor normal faults rotating to perpendicular in close proximity to the major strike-slip faults (b; d). (For interpretation of the references to colour in this figure legend, the reader is referred to the web version of this article.)

7.2. Growth of extensional structures

All fault assemblages analysed in this study have displayed highly to moderately variable throw profiles along strike, with throw maxima separated by localised throw deficits (Figs. 6–9). This implies that all of these fault assemblages have grown from multiple fault segments, which eventually form strike linkages and ultimately kinematically and geometrically coherent fault arrays that bound horst and half-graben structures.

7.2.1. Growth of structure 1

Structure 1 (Figs. 4a,6) initiated as two fault segments on the SW side, nucleating during the Cenomanian-Turonian (Figs. 6b,14b). All other segments on the SW side (three in total), the NE side (four segments) and the central E-W dissecting fault (up to three segments) nucleated during the Coniacian-Maastrichtian (Figs. 6b,14c). All fault segments have accumulated over 100 m of throw and have incidentally linked to form a ‘diamond shaped’ horst structure oriented NW-SE (Fig. 14d). Growth continued on all faults into the Cenozoic, as upper-tip-lines reach slightly above the top Cretaceous horizon. No faults have been interpreted to propagate shallower than the top Mepunga Formation horizon (Fig. 5), suggesting that fault growth cessation occurred during the Paleocene-Eocene.

7.2.2. Growth of structure 2

The three southern normal fault assemblages of structure 2 (see locations 19–33, Fig. 7) nucleated during the Cenomanian-Turonian as multiple fault segments, which linked to form half-graben bounding

normal faults (Fig. 14b). The two northern fault assemblages of structure 2 (see locations 1–18, Fig. 7) nucleated and grew during the Coniacian-Maastrichtian, creating horst bounding normal faults (Fig. 14c). This was concurrent with continued growth of the southern fault assemblages (see locations 19–33, Fig. 7). A longer period of fault development (post-Cenomanian) is likely why the southern faults have accumulated maximum throws of up to ~520–825 m (locations 1–18, Fig. 7b), compared to the later nucleated (post-Turonian) northern faults accumulating maximum throws of only ~290–350 m (locations 19–33, Fig. 7b). Growth of structure 2 continued until the latest Maastrichtian, with no evident growth above the top Cretaceous horizon (Fig. 5).

7.2.3. Growth of structure 3

All normal fault assemblages forming the half-grabens of structure 3 (Figs. 4c,8) nucleated during the Cenomanian-Turonian, except for the far western segment of the central half-graben fault assemblage (see location 19, Fig. 8). This far western segment (see location 19, Fig. 8) had a pre-Cenomanian nucleation (Fig. 14a), likely during the deposition of the Aptian-Albian Eumeralla Supersequence (Fig. 2). This conclusion was drawn based on previous work (Palmowski et al., 2004) on the growth of half-grabens bordering the western limit of the 3D survey coverage, which highlighted Eumeralla Supersequence growth strata in hanging walls (see red normal faults, Fig. 14). These western half-graben faults (Palmowski et al., 2004) have not been analysed in detail in this study and the spatial evolution of these faults in map view (Fig. 14) is only conceptual. Cenomanian-Turonian growth of the normal fault assemblages bounding structure 3 involved the nucleation

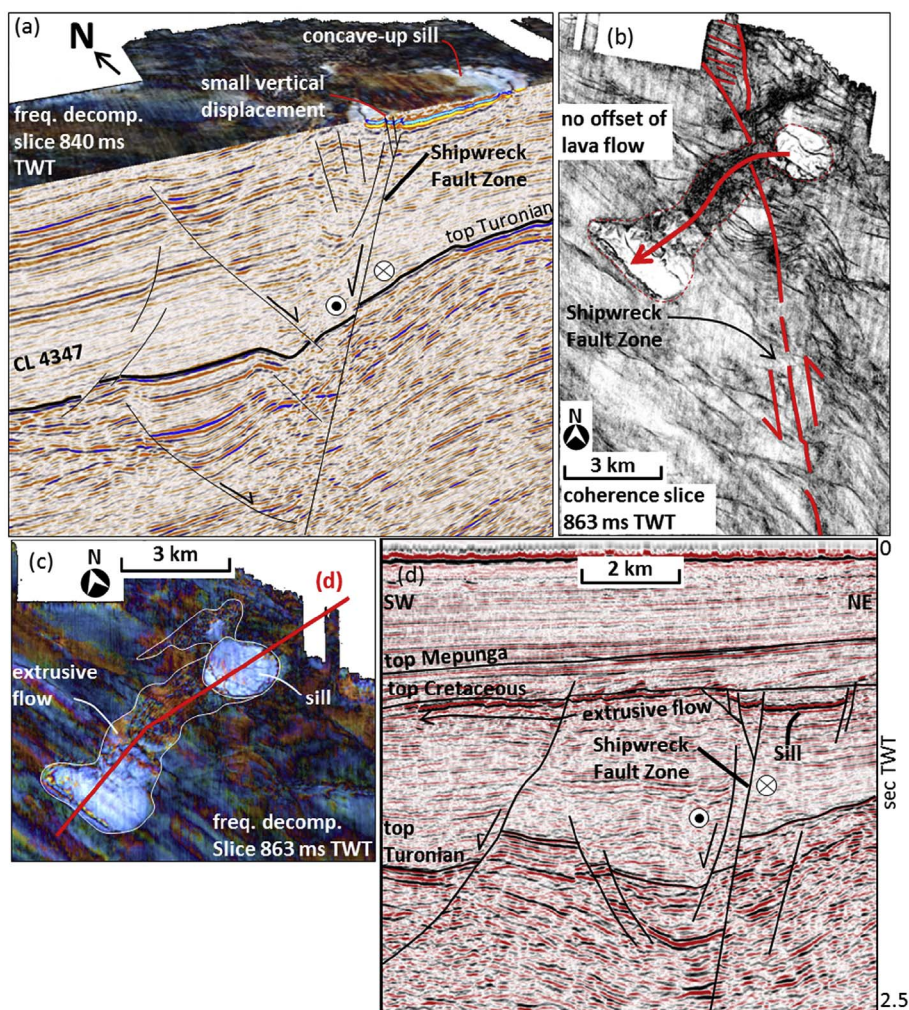


Fig. 13. (a) Three-dimensional perspective view of a volcanic sill located in the north of the 3D seismic reflection survey. The 840 ms TWT time slice displayed is a standard frequency decomposition slices of the 3D survey using a method based on the Fast Fourier Transform and the vertical section is crossline 4347. Note the concave up 'slight saucer shape' of the volcanic sill, which has potentially been vertically displaced by the Shipwreck Fault Zone. (b) Incoherence slice at 863 ms TWT highlighting the volcanic sill and the Shipwreck Fault Zone in map view. Note the extrusive flow from the sill has not been offset by the transtensional Shipwreck Fault Zone. (c) Standard frequency decomposition slice at 863 ms TWT of the 3D survey using a method based on the Fast Fourier Transform. This visually highlights the sill and extrusive flow in much more detail than incoherence. Note the location of cross-section (d) found in (c). (d) Arbitrary line through the 3D survey to show the sill and extrusive flow in cross-section relative to the Shipwreck Fault Zone.

of at least 21 fault segments (Fig. 14b), which linked to form four master faults. Fault growth continued during the Cenomanian-Maastrichtian with cessation of fault growth for this structure appearing to be at approximately the latest Maastrichtian-earliest Cenozoic.

7.2.4. Growth of structure 4

The bounding faults of structure 4 (Figs. 4d,9) nucleated in the Cenomanian-Turonian as multiple fault segments (Fig. 14b), which have subsequently linked to bound the present-day horst structure. Growth continued into the Coniacian-Maastrichtian (Fig. 14d) and terminated in the latest Maastrichtian-early Cenozoic (Fig. 5). However exact termination of faulting is hard to establish, given that the sagging of the top Cretaceous horizon above the structure could be attributed to continued blind faulting or differential compaction. The faults bounding structure 4 have achieved significant post-Albian throw accumulation and display the greatest throw of the fault analysed (up to ~1500 m).

7.2.5. Throw variability of normal faults bounding structures 1-4

A common finding with regards to the fault assemblages of structures 2, 3 and 4 is that all faults have relatively minor throw deficits between throw maxima in comparison to the maximum throw of the entire fault assemblage. This is shown by average throw variabilities of 19%, 25% and 21%, respectively (Fig. 7b,8b,9b). This contrasts with structure 1, which displays more significant throw deficits between throw maxima, reaching an average throw variability of 39% (Fig. 6b). Significant throw deficits along strike of the bounding faults of

structure 1 are located where the bounding faults strike orientation changes at linkage points (locations 2, 6 and 18, Fig. 6). Therefore, the degree of throw variability could be attributed to the degree of fault strike orientation variance. This is potentially why we observed a lower throw variance on the more linear fault assemblages of structures 2, 3 and 4. The notion that throw variability may be the result of fault strike orientation variability could be applicable to other segmented fault assemblages, in order to predict the along-strike throw variability of an assemblage based on map-view geometry.

7.3. Summary growth model for the Shipwreck Fault Zone and horst and half-graben structures

The spatial and temporal evolution of the four structures analysed in this study, in combination with known regional tectonic events, can be summarised as follows: [1] Tithonian-Barremian rifting of the basement framework coinciding with deposition of the Crayfish Supersequence (Fig. 2) establishing the Lower Cretaceous depocenters and structural highs (Fig. 4g), succeeded by Aptian-Albian blanketing of the Eumeralla Supersequence (Fig. 2) through thermal subsidence (Morton et al., 1994; Hill et al., 1995; Perincek and Cockshell, 1995; Finlayson et al., 1996; Krassay et al., 2004). The Aptian-Albian period is considered regionally as a time of relative tectonic quiescence (see references above). However, we observe one fault segment (see location 17, Figs. 7,14a), which does exhibit growth during this time and agrees with previous findings of Aptian-Albian fault growth from the same 3D dataset (Palmowski et al., 2004) and the Torquay Sub-Basin (Cooper,

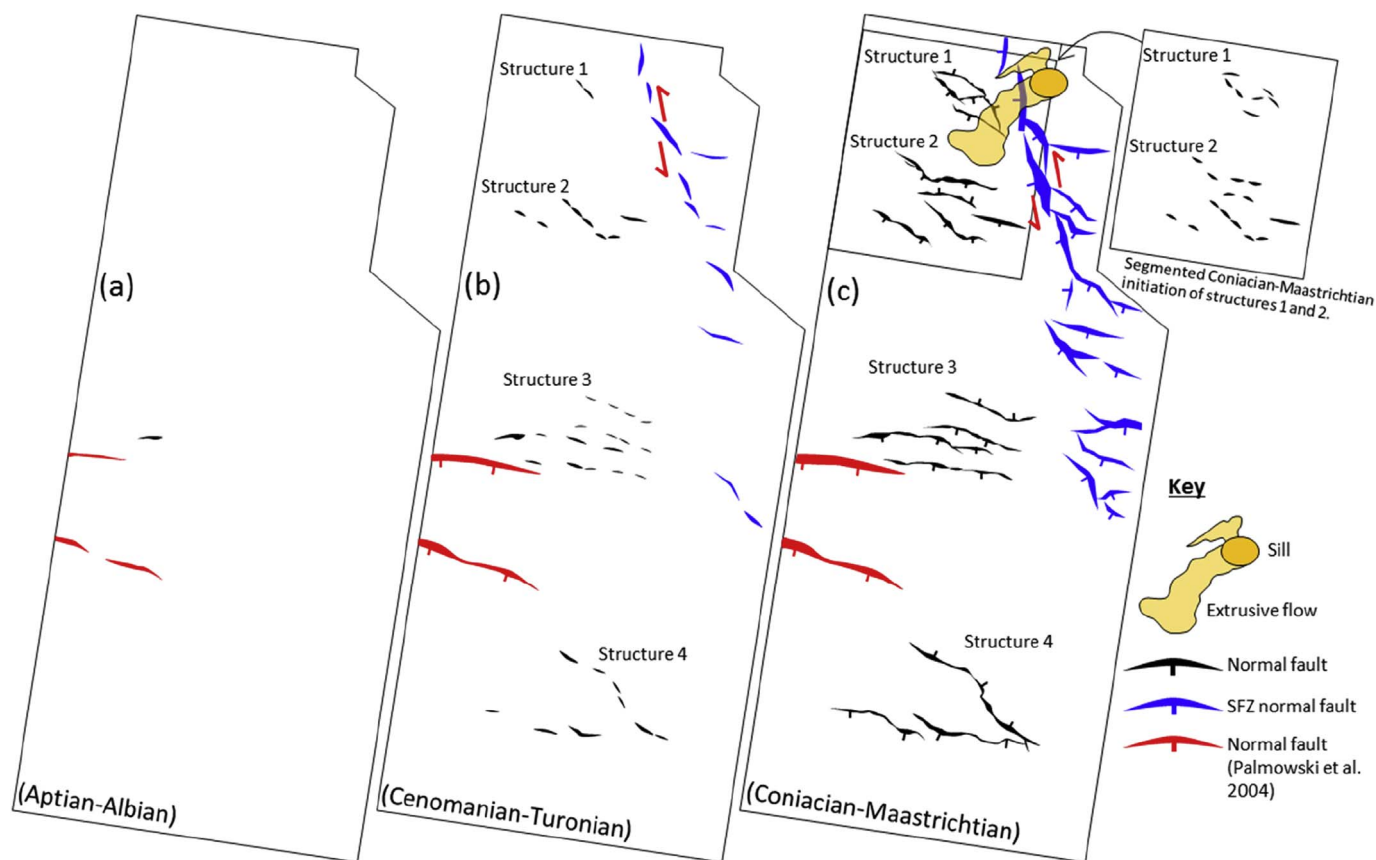


Fig. 14. Map view of the area covered by the 3D seismic reflection survey showing the growth of structures 1, 2, 3 and 4 (black), the Shipwreck Fault Zone (SFZ; blue) and half graben faults (red) analysed from a previous study (Palmowski et al., 2004), with assumed segmented initiation, based on the findings of this study. Growth has been divided into three stages: (a) Aptian-Albian deposition of the Eumeralla Supersequence; (b) Cenomanian-Turonian deposition of the Waarre and Flaxman formations; and (c) Coniacian-Maastrichtian deposition of the Belfast Mudstone and Paaratte Formation. Some of the faults bounding structures 1 and 2 nucleated as smaller segments during the Coniacian-Maastrichtian (c) as shown by the top right insert. This figure is a schematic figure only and fault heaves in map view should not be considered precise. Rather, this figure highlights segment linkage and the timing of growth of structures 1, 2, 3 and 4 which have been studied using throw-distance (T-x) and throw-depth (T-z) analysis. Stage (b) shows the nucleation of the Shipwreck Fault Zone and these segments have been interpreted from the Cenomanian-Turonian isochronal map (Fig. 9e), but have not been analysed using T-x and T-z analysis. Also note the timing (d) of the sill and extrusive flow (orange) related to the Shipwreck Fault Zone in the north of the survey. (For interpretation of the references to colour in this figure legend, the reader is referred to the web version of this article.)

1995); [2] Cenomanian-Turonian deposition of the Waarre and Flaxman formations (Fig. 2) and nucleation of fault segments, initiating growth of all structures, with greater growth observed in the south of the study area (e.g. southern portion of structure 2 and structures 3 and 4; Figs. 10e,14b). During this time, nucleation and minor growth is observed across the SFZ, signifying the initiation of sinistral movement (Figs. 10e,14b); [3] Coniacian-Maastrichtian deposition of the Belfast Mudstone and Paaratte Formation and accelerated growth of all structures (Figs. 10d,14c,d). Major growth is observed across the SFZ during this period, with all faults displaying extensional offset, creating a southward broadening negative flower structure (Figs. 10d,14d; Palmowski et al., 2004); [4] fault growth cessation in the early Cenozoic (Paleocene/Eocene), with no faults propagating through the top Mepunga horizon (Fig. 5). This timing coincides with the end of the wrenching phase on the Tasmanian margin (~42 Ma, see Table 1; Willcox and Stagg, 1990); and [5] continued Cenozoic deposition, punctuated by periods of inversion and uplift (Holford et al., 2014; Bailey et al., 2014).

8. Implications for regional geology, normal fault growth and petroleum exploration

8.1. Regional implications for the offshore Otway Basin

The aim of this study was to temporally and spatially constrain the

evolution of two horst structures and two half-graben fault arrays (structures 1–4, Fig. 4), located proximal to the Shipwreck Fault Zone (SFZ) in the Shipwreck Trough of the Otway Basin, Australia (Fig. 1a). Previous interpretation by Palmowski et al. (2004) suggests that the SFZ is the northern *en echelon* extension of the transform margin to the south (Fig. 1b) and has the characteristics of a southward broadening negative flower structure. Our interpretation of the 3D reflection survey shows a distinct separation of transtensional and extensional domains. The SFZ displays characteristics of a N–S oriented, sinistral, transtensional fault zone (Figs. 11,12) whereas the extensional domain is characterised by generally NW-SE oriented horst structures and half-graben arrays (Fig. 4). We have also shown evidence of releasing bends, releasing jogs and restraining jogs along the SFZ, which all have a sinistral sense of shear (Fig. 12). Based on this evidence and the strong basin asymmetry from east to west (Fig. 11), typical of a rift-oblique sedimentary basin bounded by a continental transform on the eastern side (Harding et al., 1985; Ben-Avraham, 1985; Ben-Avraham and Zoback, 1992), we propose that the transtensional SFZ is a primary structural feature of the offshore Otway Basin, which formed the Shipwreck Trough. Therefore, we agree with Palmowski et al. (2004) that the SFZ may be the most northern extent of the transform margin to the south (Totterdell et al., 2012; Stacey et al., 2013) and denotes the boundary between the normal-obliquely rifted zone (Bight Basin) and transitional zone (Otway Basin) to the west and the transform zone to the south (Sorell Basin; Fig. 1b). This model accounts for the sharp

transition between the two structurally distinct domains observed in this study, from generally NW-SE extensional horst structures and half-graben arrays (Fig. 4a; b; c; d), to a N-S oriented left-lateral transtensional fault system (Fig. 12). However, further work could be undertaken around this 3D seismic survey, using regional 2D seismic data, to understand how this local structural model fits into the regional model.

Our interpretation of the 3D seismic survey documents a basement plateau in the north of the survey, with at least three kilometer-scale basement horsts in the central region and an isolated basement high in the southern portion of the survey (Fig. 4g). Using throw profiling (Figs. 6–9) and isochronal maps (Fig. 10d; e) we have identified that the normal faults bounding the horst structures and half-graben arrays that are located in the central and southern portions of the survey display Cenomanian-Turonian growth. We have also observed greater Cenomanian-Turonian development of horst and half-graben structures that formed above the basement highs (Fig. 4g) which have larger relief (southern fault assemblages of structure 2, structures 3 and 4; Fig. 4b; c; d), in the central and southern portions of the survey. This is in contrast to those structures located on the basement plateau (structure 1 and northern fault assemblages of structure 2; Fig. 4a; b) in the northern portions of the survey, which generally show later growth (Coniacian-Maastrichtian). We also observe that growth of normal faults across the entire 3D survey and development of the SFZ is present during the Coniacian-Maastrichtian, indicating a major period of extension/transension in the Shipwreck Trough. This observation of Late Cretaceous rifting in the Shipwreck Trough supports the findings of Palmowski et al. (2004) and the regional tectono-stratigraphic framework (Morton et al., 1994; Krassay et al., 2004; Stacey et al., 2013; Totterdell et al., 2012).

8.2. Implications for normal fault growth

The faults bounding these horst and half-graben structures display isolation at depth, segmented geometry in map view and highly to moderately variable along-strike throw profiles (Figs. 6–9). All of these observations imply that the formation of these faults is the result of small-scale fault segment nucleation within the Upper Cretaceous section with lateral propagation and linkage to form bounding faults on horst structures and along-strike fault assemblages creating half-graben structures (Fig. 14). Maximum throw values occurring at the top Albian and top Turonian horizons (Figs. 6–9), along with isochronal mapping of the Cenomanian-Turonian (Fig. 10e) and Coniacian-Maastrichtian (Fig. 10d) strata, show evidence for Cenomanian-Turonian nucleation and growth of all structures. The same data also shows that Cenomanian-Turonian fault growth was concentrated on the southern portion of the survey. Growth on all structures followed during the Coniacian-Maastrichtian (Fig. 14), with fault growth termination by the early Cenozoic (Paleocene-Eocene). Based on the scale of interpreted horizons, the faults analysed in this study show no evidence for vertically segmented fault growth (Figs. 6–9). Instead, fault growth was continuous throughout the Upper Cretaceous period, with termination of fault growth occurring in the early Cenozoic (Paleocene/Eocene).

We have demonstrated that there is a correlation in our data between along-strike throw variability and fault strike orientation variability, whereby faults that display greater map view orientation variations are shown to display greater throw variability between segment centres and linkage points (see Fig. 3 for method). This may imply less kinematic coherence between fault segments that do not share similar strike orientations (e.g. Structure 1, Fig. 6b), compared to an organised along-strike fault segment assemblage (e.g. Structure 2, Fig. 7b). However, this has not been extensively examined as we have only analysed four structures within one geological province.

8.3. Implications for petroleum exploration

The Shipwreck Trough hosts a proven petroleum system with two producing gas fields (Thylacine and Geographe Gas Fields; Fig. 1a) located within the study area. These two gas accumulations are both laterally fault bound traps sealed above by the overlying Belfast Mudstone (Origin Energy Australia, 2002). Several other fault dependent and independent structural closures are present on the top Turonian and top Albian TWT maps (Fig. 10b; c). The top Turonian map (Fig. 10b) is equivalent in age to the top reservoir for the Thylacine and Geographe gas fields (Fig. 1a; Origin Energy Australia, 2002). Therefore, with an accurate depth conversion applied, these structural closures may be analogous to, and within close vicinity of, the Thylacine and Geographe gas fields (Fig. 1a). These findings provide implications for prospectivity and Late Cretaceous play development within the Shipwreck Trough for future exploration.

The main period of fault growth occurred during the Coniacian-Maastrichtian, coeval with deposition of the Belfast Mudstone and Paaratte Formation (Fig. 2), with the Belfast Mudstone considered a regional seal in the area (Origin Energy Australia, 2002; Palmowski et al., 2004). Permeable faults and associated damage zones may act as vertical conduits, providing a migration pathway from deep source rocks into shallower reservoirs (Smith, 1980; Allan, 1989; Anderson et al., 1994). The continuous growth and lack of vertical segmentation of these faults may have significantly contributed to the migration potential of these structures, given that two producing hydrocarbon fields are located within horst structures 3 (Geographe gas field) and 4 (Thylacine gas field). However, fault zones may also be sealing, inhibiting the vertical and cross-fault migration of hydrocarbons, thus providing hydrocarbon entrapment and accumulation (Smith, 1980; Harding and Tuminas, 1989; Bouvier et al., 1989; Jev et al., 1993; Knott, 1993). Therefore, with the Belfast Mudstone (Fig. 2) providing good vertical and lateral seal (by fault juxtaposition) and no evidence for any further fault reactivation since the early Cenozoic (Paleocene/Eocene), this provides greater confidence in the sealing integrity of these fault zones. Given that producing gas fields are bound by the faults analysed in this study, understanding the evolution of these structures is crucial to uncovering the hydrocarbon potential of the Shipwreck trough and the wider Otway basin.

9. Conclusions

We used a 3D seismic reflection dataset from the Shipwreck Trough, offshore Otway Basin, Australia to establish the structural evolution of horst and half-graben structures proximal to a transtensional fault zone, known as the Shipwreck Fault Zone (SFZ). We have analysed and interpreted spectral decomposition and coherence volumes to characterise the SFZ (and associated volcanics), basement structural elements and Late Cretaceous horst structures and half-graben arrays. We have also conducted throw-distance and throw-depth analysis of the four major horst and half-graben bounding normal faults and two-way-time (TWT) and isochronal mapping of the entire 3D survey to establish the structural evolution of the Shipwreck Trough and SFZ. We show that the Shipwreck Trough has strong basin asymmetry from east to west, with the thickest Upper Cretaceous sediments abutting the N-S oriented SFZ, which bounds the eastern side of the trough. It is evident from isochronal mapping that transtensional movement of the SFZ, and consequently the downthrown western side of the fault zone is the primary cause of the formation of the Shipwreck Trough. This evidence is characteristic of a rift-oblique sedimentary basin bounded by a continental transform on the eastern side and supports previous studies, suggesting that the SFZ is the furthest northern, sub-parallel, extent of the transform margin to the south. We also show that the generally NW-SE oriented horst structures and half-graben arrays, abutting the western side of the SFZ, have developed via continuous growth and along-strike segment linkage of normal fault segments during the Late

Cretaceous, with termination of growth in the Paleocene-Eocene. Furthermore, we have documented numerous structural closures which are analogous to, and within close vicinity of, the Thylacine and Geographe gas fields, providing implications for future petroleum exploration in the Shipwreck Trough.

Acknowledgments

This research forms part of a PhD project supported by the ASEG Research Foundation (RF14P04) for which funding is gratefully acknowledged. We would also like to thank the Australian Research Council and University of Adelaide for scholarship funding; GeoTeric from ffa, IHS (Kingdom), DownUnder GeoSolutions (DUG) for software use. In particular, we would like to thank Jacob Smith from Geo Teric for his contribution to this study. This forms TRaX record 389.

References

- Allan, U.S., 1989. Model for hydrocarbon migration and entrapment within faulted structures. *AAPG Bull.* 73 (7), 803–811.
- Anderson, R.N., Flemings, P., Losh, S., Austin, J., Woodhams, R., 1994. Gulf of Mexico growth fault drilled, seen as oil, gas migration pathway. *Oil Gas J. (United States)* 92 (23), 97–104.
- Bailey, A., King, R., Holford, S., Sage, J., Backe, G., Hand, M., 2014. Remote sensing of subsurface fractures in the Otway Basin, south Australia. *J. Geophys. Res. Solid Earth* 119 (8), 6591–6612.
- Baudon, C., Cartwright, J., 2008. The kinematics of reactivation of normal faults using high resolution throw mapping. *J. Struct. Geol.* 30 (8), 1072–1084.
- Ben-Avraham, Z., 1985. Structural framework of the gulf of Elat (Aqaba), northern Red sea. *J. Geophys. Res. Solid Earth* 90 (B1), 703–726.
- Ben-Avraham, Z., Zoback, M.D., 1992. Transform-normal extension and asymmetric basins: an alternative to pull-apart models. *Geology* 20 (5), 423–426.
- Bouvier, J.D., Kaars-Sijpesteijn, C.H., Kluesner, D.F., Onyejekwe, C.C., van der Pal, R.C., 1989. Three-dimensional seismic interpretation and fault sealing investigations, Nun River Field, Nigeria. *AAPG Bull.* 73 (11), 1397–1414.
- Bryan, S.E., Constantine, A.E., Stephens, C.J., Ewart, A., Schön, R.W., Parianos, J., 1997. Early Cretaceous volcano-sedimentary successions along the eastern Australian continental margin: implications for the break-up of eastern Gondwana. *Earth Planet. Sci. Lett.* 153 (1), 85–102.
- Christie-Blick, N., Biddle, K.T., 1985. Deformation and Basin Formation along Strike-slip Faults, vol. 37. pp. 1–34 SEPM (Society for Sedimentary Geology) Special publication.
- Cliff, D.C.B., Tye, S.C., Taylor, R., 2004. The Thylacine and Geographe gas discoveries, offshore eastern Otway Basin. *APPEA J.* 441–461. v. 44.
- Cooper, G.T., 1995. Seismic structure and extensional development of the eastern Otway Basin- Torquay Embayment. *APPEA J.* 35 (1), 436–450.
- Duddy, I.R., 1997. Focussing exploration in the Otway Basin: understanding timing of source rock maturation. *APPEA J.* 37 (1), 178–191.
- Duddy, I.R., Erout, B., Green, P.F., Crowhurst, P.V., Boulton, P.J., 2003. Timing constraints on the structural history of the western Otway Basin and implications for hydrocarbon prospectivity around the Morum High, South Australia. *APPEA J.* 43 (1), 59–83.
- Finlayson, D.M., Johnstone, D.W., Owen, A.J., Wake-Dyster, K.D., 1996. Deep seismic images and the tectonic framework of early rifting in the Otway Basin, Australian southern margin. *Tectonophysics* 264 (1), 137–152.
- Geary, G.C., Reid, I.S.A., 1998. Hydrocarbon Prospectivity of the Offshore Eastern Otway Basin, Victoria for the 1998 Acreage Release. Department of Natural Resources and Environment Victorian Initiative for Minerals and Petroleum Report 55.
- Giba, M., Walsh, J.J., Nicol, A., 2012. Segmentation and growth of an obliquely reactivated normal fault. *J. Struct. Geol.* 39, 253–267.
- Gibbons, A.D., Whittaker, J.M., Müller, R.D., 2013. The breakup of East Gondwana: assimilating constraints from Cretaceous ocean basins around India into a best-fit tectonic model. *J. Geophys. Res. Solid Earth* 118 (3), 808–822.
- Harding, T.P., 1983. Divergent wrench fault and negative flower structure, Andaman Sea. *Seismic Expr. Struct. Styles* 3, 4–12.
- Harding, T.P., Vierbuchen, R.C., Christie-Blick, N., 1985. Structural styles, plate-tectonic settings, and hydrocarbon traps of divergent (transtensional) wrench faults. In: Biddle, K.T., Christie-Blick, N. (Eds.), *Strike-slip Deformation, Basin Formation, and Sedimentation*, pp. 51–77 Society of Economic Paleontologists and Mineralogists Special Publication 37.
- Harding, T.P., Tuminas, A.C., 1989. Structural interpretation of hydrocarbon traps sealed by basement normal block faults at stable flank of foredeep basins and at rift basins. *AAPG Bull.* 73 (7), 812–840.
- Hill, K.A., Finlayson, D.M., Hill, K.C., Cooper, G.T., 1995. Mesozoic tectonics of the Otway Basin: the legacy of Gondwana and the active Pacific margin- a review and ongoing research. *APPEA J.* 35 (1), 467–493.
- Holford, S.P., Hillis, R.R., Duddy, I.R., Green, P.F., Stoker, M.S., Tuitt, A.G., Backé, G., Tassone, D.R., Macdonald, J.D., 2011. Cenozoic post-breakup compressional deformation and exhumation of the southern Australian margin. *APPEA J. Austr. Pet. Prod. Explor. Assoc.* 51 (1), 613–638.
- Holford, S.P., Schofield, N., Macdonald, J.D., Duddy, L.R., Green, P.F., 2012. Seismic analysis of igneous systems in sedimentary basins and their impacts on hydrocarbon prospectivity: examples from the southern Australian margin. *APPEA J.* 52, 229–252.
- Holford, S.P., Tuitt, A.K., Hillis, R.R., Green, P.F., Stoker, M.S., Duddy, I.R., Tassone, D.R., 2014. Cenozoic deformation in the Otway Basin, southern Australian margin: implications for the origin and nature of post-breakup compression at rifted margins. *Basin Res.* 26 (1), 10–37.
- Jackson, C.A.L., Rotevatn, A., 2013. 3D seismic analysis of the structure and evolution of a salt-influenced normal fault zone: a test of competing fault growth models. *J. Struct. Geol.* 54, 215–234.
- Jackson, C.A.L., Bell, R.E., Rotevatn, A., Tvedt, A.B., 2017. Techniques to Determine the Kinematics of Synsedimentary Normal Faults and Implications for Fault Growth Models 439 Geological Society, London Special Publications, SP439–22.
- Jev, B.I., Kaars-Sijpesteijn, C.H., Peters, M.P.A.M., Watts, N.L., Wilkie, J.T., 1993. Akaso field, Nigeria: use of integrated 3-D seismic, fault slicing, clay smearing, and RFT pressure data on fault trapping and dynamic leakage. *AAPG Bull.* 77 (8), 1389–1404.
- Johnson, B.D., Powell, C.M., Veivers, J.J., 1980. Early spreading history of the Indian Ocean between India and Australia. *Earth Planet. Sci. Lett.* 47 (1), 131–143.
- Knott, S.D., 1993. Fault seal analysis in the North sea. *AAPG Bull.* 77 (5), 778–792.
- Krassay, A.A., Cathro, D.L., Ryan, D.J., 2004. A regional tectonostratigraphic framework for the Otway Basin. In: Boulton, P.J., Johns, D.R., Lang, S.C. (Eds.), *Eastern Australasian Basins Symposium II. Petroleum Exploration Society of Australia*, pp. 97–116 Special Publication.
- Li, Z.X., Metcalfe, I., Powell, C.M., 1996. Breakup of Rodinia and Gondwanaland and assembly of Asia-introduction. *Aust. J. Earth Sci.* 43 (6), 591–592.
- Mansfield, C.S., Cartwright, J.A., 1996. High resolution fault displacement mapping from three-dimensional seismic data: evidence for dip linkage during fault growth. *J. Struct. Geol.* 18 (2), 249–263.
- Moore, A.M.G., Stagg, H.M.J., Norvick, M.S., 2000. Deep-water Otway Basin: a new assessment of the tectonics and hydrocarbon prospectivity. *APPEA J.* 32 (1), 66–85.
- Morley, C.K., Nelson, R.A., Patton, T.L., Munn, S.G., 1990. Transfer zones in the East African Rift System and their relevance to hydrocarbon exploration in rifts. *AAPG Bull.* 74, 1234–1253.
- Morton, J.G.G., Hill, A.J., Parker, G., Tabassi, A., 1994. Towards a unified stratigraphy for the Otway Basin. In: Finlayson, D.M. (Ed.), *NGMA/Petroleum Exploration Society of Australia Otway Basin Symposium*, Melbourne. vol. 20. pp. 7–12.
- Moy, D.J., Imber, J., 2009. A critical analysis of the structure and tectonic significance of rift-oblique lineaments ('transfer zones') in the Mesozoic–Cenozoic succession of the Faroe–Shetland Basin, NE Atlantic margin. *J. Geol. Soc.* 166 (5), 831–844.
- Norvick, M.S., 2005. Plate Tectonic Reconstructions of Australia's Southern Margins. *Geoscience Australia Record* 2005/07.
- O'Brien, G.W., Thomas, J.H., 2007. Department of primary industries. A Technical Assessment of yet-To-find Hydrocarbon Resources Inventory, Offshore and Onshore Otway Basin, Victoria, Australia.
- Origin Energy Australia, 2002. Investigator 3D & 2D Seismic Interpretation Report. Victoria/Tasmanian. Department of Primary Industries Seismic Interpretation Report (unpublished).
- Palmowski, D., Hill, K.C., Hoffman, N., 2004. Structure and hydrocarbons in the Shipwreck Trough, Otway Basin: half-graben gas fields abutting a continental transform. *APPEA J.* 44, 417–440.
- Partridge, A.D., 2001. Revised stratigraphy of the Sherbrook Group, Otway Basin. In: Hill, K.C., Bernecker, T. (Eds.), *Eastern Australasian Basins Symposium, a Refocused Energy Perspective for the Future*. PESA, pp. 455–465 Special Publication.
- Perincek, D., Cockshell, C.D., 1995. The Otway Basin: Early cretaceous rifting to neogene inversion. *APPEA J.* 35, 451–466.
- Petkovic, P., 2004. Time-depth Functions for the Otway Basin, (2004/02). *Geoscience Australia*.
- Planke, S., Rasmussen, T., Rey, S.S., Myklebust, R., 2005. Seismic characteristics and distribution of volcanic intrusions and hydrothermal vent complexes in the Vøring and Møre basins. In: Geological Society, London, Petroleum Geology Conference series, vol. 6. Geological Society of London, pp. 833–844 No. 1.
- Robson, A.G., King, R.C., Holford, S.P., 2016a. Structural evolution of a gravitationally detached normal fault array: analysis of 3D seismic data from the Ceduna Sub-Basin, Great Australian Bight. *Basin Res.* <http://dx.doi.org/10.1111/bre.12191>.
- Robson, A.G., King, R.C., Holford, S.P., 2016b. 3D seismic analysis of gravity-driven and basement influenced normal fault growth in the deepwater Otway Basin, Australia. *J. Struct. Geol.* 89, 74–87.
- Robson, A.G., King, R.C., Holford, S.P., 2017. Structural evolution of a normal fault array in the Gambier Embayment, offshore Otway Basin, South Australia: insights from 3D seismic data. *Aust. J. Earth Sci.* 64 (5), 611–624.
- Ryan, S.M., Knight, L.A., Parker, G.J., 1995. In: *The Stratigraphy and Structure of the Tyrendarra Embayment, Otway Basin, Victoria*. Geological Survey of Victoria VIMP report 15.
- Rykkelid, E., Fossen, H., 2002. Layer rotation around vertical fault overlap zones: observations from seismic data, field examples, and physical experiments. *Mar. Pet. Geol.* 19 (2), 181–192.
- Smith, D.A., 1980. Sealing and nonsealing faults in Louisiana Gulf Coast salt basin. *AAPG Bull.* 64 (2), 145–172.
- Stacey, A.R., Mitchell, C.H., Struckmeyer, H.I.M., Totterdell, J.M., 2013. In: *Geology and Hydrocarbon Prospectivity of the Deepwater Otway and Sorell Basins, Offshore Southeastern Australia*. Geoscience Australia, Canberra Record 2013/02.
- Tassone, D.R., Holford, S.P., Duddy, I.R., Green, P.F., Hillis, R.R., 2014. Quantifying Cretaceous Cenozoic exhumation in the Otway Basin, southeastern Australia, using sonic transit time data: implications for conventional and unconventional hydrocarbon prospectivity. *AAPG Bull.* 98 (1), 67–117.
- Taylor, S.K., Nicol, A., Walsh, J.J., 2008. Displacement loss on growth faults due to

- sediment compaction. *J. Struct. Geol.* 30 (3), 394–405.
- Totterdell, J.M., Gibson, G.M., Stacey, A.R., Mitchell, C.H., Morse, M.P., Nayak, G.K., Kuszniir, N.J., 2012. The structure of Australia's southern rifted margin: basement architecture, rifting processes and basin development. In: *Proceedings of the 34th International Geological Congress 2012, Brisbane, Australia.*
- Willcox, J.B., Stagg, H.M.J., 1990. Australia's southern margin: a product of oblique extension. *Tectonophysics* 173 (1), 269–281.
- Younes, A.I., McClay, K., 2002. Development of accommodation zones in the gulf of Suez–Red sea rift, Egypt. *AAPG Bull.* 86, 1003–1026.

5. Discussion: Controls on normal fault growth along Australia's rifted-to-passive southern margin

This chapter is a discussion on the normal fault growth and segmentation along Australia's southern margin and is a summary of the four previous chapters (papers). We give a detailed summary of normal fault growth in each of the four locations studied (sections 5.1-5.4), followed by a section detailing the contributions to the regional geology of Australia's rifted-to-passive southern margin (section 5.5) and finally a section on the implications for normal fault growth and exploration (section 5.6).

5.1 Normal fault growth in the Ceduna Sub-basin

This thesis presented the spatial and kinematic growth of a detached, listric fault array from the Ceduna Sub-basin, Great Australian Bight (*paper 1*). Prior to this study, the detailed three-dimensional evolution of gravity-driven normal faults developed within a delta system on a passive margin had not been extensively examined. Detailed throw-distance, throw-depth, expansion index and isochronal mapping showed that the fault array consists of two vertically (dip) linked fault arrays, associated with the two temporally and spatially isolated delta systems (Tab. 1; Fig. 1a). We have shown that there is a complex relationship between faults associated with the underlying Cenomanian-Santonian delta system and the overlying post-Santonian fault system, with evidence for both dip-linkage of the fault systems and complete reactivation and upward propagation of the Cenomanian-Santonian fault system into post-Santonian strata. On faults which have dip-linked, it is clear that reactivation of the Cenomanian-Santonian fault system induced the nucleation and growth of the post-Santonian fault system. Therefore, with these two models of growth development present, it is clear that the underlying fault system has controlled the nucleation and growth of the upper fault system. Furthermore, the post-Santonian fault system displays much more kinematically coherent growth of strike linked fault segments, indicating that fault length was established relatively early in fault growth history, without substantial displacement accumulation. Therefore, our findings show that: [1] In stacked delta system settings (i.e. Gulf of Mexico and Orange Basin,

offshore Namibia), faults associated with the lower delta system will likely have a large control over the development of faults in the upper delta system, and consequently the delta system itself, with growth faults controlling sediment dispersal; and [2] more kinematic coherence, in the form of rapid fault length establishment, is likely to be present in faults associated with the upper delta system, which have formed over an underlying and reactivating structural framework. Faults growing via rapid fault length establishment would induce an earlier overlapping geometry with relay ramp establishment, giving greater fault control over earlier stages of sediment dispersal, than faults which take a much greater amount of time to overlap and link.

A larger scale (and very recent) study agrees with our findings, showing that dip-linkage occurs on listric faults located in the basinward (south-western) portion of the central Ceduna Sub-basin (Ryan et al., 2017). However, Ryan et al., (2017) also shows that listric faults located up-dip in the very centre of the Ceduna Sub-basin display continuous propagation and even further up-dip in the landward (north-eastern) portion of the central Ceduna Sub-basin is a set of reactivated listric faults (Ryan et al., 2017). This study concluded that the style of fault growth (dip-linked, continuous or reactivated) was most likely controlled by the variations in host rock (tiger Supersequence and lower Hammerhead Supersequence) composition, in which dip-linkage and reactivation has occurred (Ryan et al., 2017). This is because the mudstone content in the tiger Supersequence and lower Hammerhead Supersequence would most probably increase basinward, typical of a delta system, likely reducing the mechanical competency of the rock. This reduced mechanical competency would hinder fault tip propagation, creating a vertically segmented fault array. Therefore, not only is the reactivation of the lower fault array controlling the growth of the upper fault array, but the competency of the rock between the fault arrays is controlling their geometric and kinematic interaction.

Our findings also have implications towards hydrocarbon migration, given that faults and associated damage zones may act as vertical conduits. Faults which have developed through reactivation and

upward propagation of the underlying Cenomanian-Santonian fault system are likely to act as migration pathways from deep source rocks to shallower reservoirs, whereas independent nucleation of upper faults likely hindered the upward migration in comparison. Our results also showed that all faults have penetrated into the Cenozoic interval, displacing strata as shallow as 70m below the seafloor. This shows that reactivation of these faults occurred extremely recently, with a high potential for fault seal breach of fault dependent traps located along the faults analysed in this study, which presents an important risk to the preservation of hydrocarbons.

5.2 Normal fault growth at the present-day shelf edge break and deepwater Otway Basin

This study analysed the growth of a fault assemblage which shows clear linkage to basement-involved faults that have heavily influenced its growth, and another fault assemblage, located only 2km further basinward over a basement plateau, which is vertically independent and gravity driven (Tab. 1; Fig. 1c). The normal fault assemblage which is linked to the basement –involved faults displays earlier nucleation and greater overall fault throw than the vertically independent and gravity driven fault assemblage. This is due to the influence of the underlying and reactivating basement-involved faults, during Upper Cretaceous rifting; a process known as ‘active’ kinematic linkage. These findings show that in an active rift setting, newly formed faults in cover sediments are: [1] more likely to initiate earlier above a reactivating basement-involved normal fault, where increased flexure of cover sediments occurs; and [2] these faults will generally display greater overall fault throw, given the pre-existing and underlying faults are influencing their development.

5.3 Normal fault growth in the Gambier Embayment of the Otway Basin

In this study we have showed that the depocentre created by the growth of a normal fault has laterally increased in size through geological time, which implies this fault increased in length while accumulating significant amounts of throw until eventual linkage. This finding supports early models of normal fault growth, whereby structures nucleated and propagated independently, incidentally

overlapped and geometrically linked through relay ramp breaching, referred to as the 'isolated fault model' (Walsh & Watterson 1988; Cartwright et al. 1995; Dawers & Anders 1995). Both the process of dip-linkage and upward propagation of normal faults have previously been documented many times (Childs et al. 1996; Mansfield and Cartwright, 1996; Rykkelid and Fossen, 2002; Baudon and Cartwright, 2008; Jackson and Rotevatn, 2013). However, in this study we have highlighted that dip-linkage of fault segments and reactivation and upward propagation of fault segments can occur on the same fault over relatively short distance (~3 km), directly showing the complexities of normal fault growth (Tab. 1; Fig. 1b).

5.4 Normal fault growth in the Shipwreck Trough of the Otway Basin

We have also analysed horst and half-graben bounding normal fault arrays that are proximal to a transtensional fault system (Shipwreck Fault Zone), which is likely the northern extent of a transform margin to the south of the study area (Tab. 1; Fig. 1d). These faults show direct evidence for growth via hectometre-scale segment linkage. The variations in throw along-strike of fault assemblages is on a much smaller-scale (hectometre-scale) in comparison to the three previous fault assemblages analysed (kilometre-scale) and potentially this is due to their proximity to a transtensional fault system, creating much more complex growth history involving both extension and wrenching.

We have created a new method for calculating throw variance as a single value to characterise a fault system, which previously had not been conducted. Using this innovative method, we have demonstrated a correlation between fault strike orientation variability and along-strike throw variability. This finding implies that faults which display greater orientation variations in map view display greater throw variability between segment centres and linkage points. This may imply greater kinematic coherence between faults that have similar strike orientations. However the amount of data used was quite limiting to how applicable this finding may be for other fault arrays. Furthermore, unlike the three previously studied fault arrays, these faults do not display vertically segmented fault growth and perhaps this is testament to the severe compartmentalisation of the

Shipwreck Trough, through the basin asymmetry, created by transtensional movement of the Shipwreck Fault Zone. This transtensional movement created a very large accommodation space and consequently a thick Upper Cretaceous syn-rift deposition. This sediment loading may have contributed significantly to the continued growth of this normal fault array, whereas the three previous studies displayed a period of late Santonian fault dormancy.

5.5 Contributions to the regional geology of Australia's rifted-to-passive southern margin

Previous research along Australia's southern margin has been mostly focussed on margin and basin scale evolution. We have provided a detailed structural evolution model for the growth of normal faults in the Ceduna Sub-basin and the Gambier Embayment, Deepwater province and Shipwreck Trough of the Otway Basin. Our findings from the Ceduna Sub-basin show that: [1] the underlying faults associated with the lower Cenomanian-Santonian delta system heavily control the growth of the upper, post-Santonian fault system through fault reactivation; [2] the post-Santonian faults have been very recently active, with displacement evident as shallow as 70 m below the seafloor; [3] growth of the fault assemblages has been via large-scale (10 km scale) along-strike segment linkage; [4] most faults are vertically segmented with dip-linkage occurring at the top-Santonian level, which coincides with the timing of continental breakup and wide scale erosion through the study area.

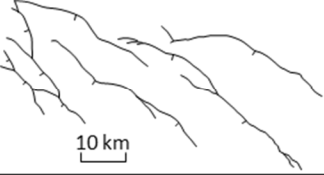
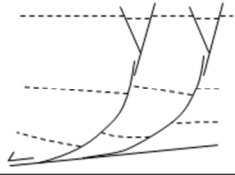

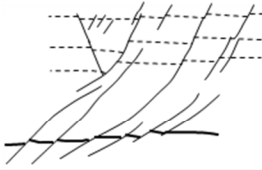

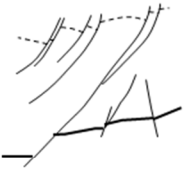

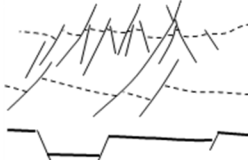
Our findings at the present-day shelf edge break and deepwater province of the Otway Basin show that: [1] Upper Cretaceous faults in the Otway Basin, which are located above major basement-involved normal faults are likely to have nucleated earlier and have greater overall throw and linkage to the basement-involved faults than normal faults which are located over a basement Plateau; [2] these faults have grown via kilometre-scale along strike segment linkage; [3] these faults display vertical segmentation, with dip-linkage occurring at the top Santonian level. Our findings in the Gambier Embayment of the Otway Basin show that [1] the orientation of stress that led to the nucleation of these faults analysed was fairly consistent during the Upper Cretaceous; [2] there was a perturbation of stress from N-S extension to NE-SW extension prior to or during the Cenomanian,

or the E-W orientation of the basement fabric in the Gambier Embayment was formed owing to NW-SE oblique extension above an even deeper basement fabric; [3] a confirmation of a previous finding from the deepwater province of the Otway Basin that Upper Cretaceous faults that developed above major basement faults, generally nucleate earlier and have greater throw and basement linkage; [4] faults continued to grow well into the Cenozoic in the Gambier Embayment of the Otway Basin; and [5] vertically segmented normal fault growth also occurs in the Gambier Embayment with dip-linkage of segments generally at the top Santonian level.

Our findings from the Shipwreck Trough of the Otway basin have: [1] further characterised the Shipwreck Fault Zone, through isochronal analysis, highlighting transtensional structures (releasing and restraining jogs and bends) and analysis of a volcanic sill, providing more evidence for the timing of cessation of transtensional movement; [2] consolidated previous research, showing that the Shipwreck Fault Zone is likely the northern most extension of the transform margin to the south; [3] highlighted the basement structure using spectral decomposition, creating better visualisation of the horst and graben structures developed through Cretaceous rifting; [4] confirmed, using different techniques, that earlier nucleation and growth of normal faults occurs in the central and southern portions of the Shipwreck Trough, compared to the north; [5] showed that segment linkage of normal faults is generally on the hectometre-scale in the Shipwreck Trough, compared to kilometre-scale in other areas of the Otway Basin and 10 km scale in the Ceduna Sub-Basin.

Together, these four studies have showed that: [1] the late Santonian continental breakup in the western portions of the southern margin (Bight Basin) had a large influence over normal fault growth in the Ceduna Sub-basin and western and central portions of the Otway Basin, with some degree of fault growth dormancy observed in all three locations at this stage; [2] Continental breakup during the late Santonian did not have a large effect on normal fault growth in the eastern portion of the Otway Basin (Shipwreck Trough), likely due to the distal proximity to the breakup location, transtensional movement, basin compartmentalisation and sediment loading; and [3] the

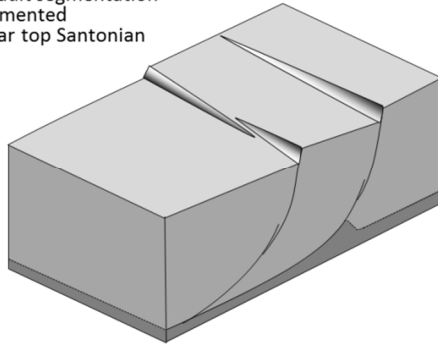
along-strike segment linkage of normal faults reduces easterly, from 10 km scale in the Ceduna Sub-basin, to kilometre-scale in the western and central portions of the Otway Basin, to hectometre-scale in the Shipwreck Trough. This may be due to the transition from normal-oblique (and purely gravity driven) extension in the Ceduna Sub-basin, to polyphase mechanical extension in the Otway Basin, creating complexity in basement-involved fault influences on Upper Cretaceous normal fault arrays. Another transition then occurs from normal-oblique extension in the western and central portions of the Otway Basin, to sinistral transtensional movement in the Shipwreck Trough. It appears as though the more complex the structural environment (i.e. pure extension being less complex than transtension), the smaller scale of normal fault segmentation.

Location	Age	Map view geometry	Typical cross-section geometry	Detached/ basement linked	Dip-linkage (inc. age of interval)	Strike linkage	Fault assemblage length
Ceduna Sub-Basin, Bight Basin	Cenomanian - Cenozoic			detached (late albian level).	Turonian - Santonian, top Santonian and Campanian - Maastrichtian.	yes (5-40 km long segments in map view)	some > 60 km
Gambier Embayment, Otway Basin	Turonian - Cenozoic			basement linked.	top Santonian and Campanian-Maastrichtian	yes (2-10 km long segments in map view)	20-30 km
Nelson Sub-Basin, Otway Basin	Turonian - latest Maastrichtian			basement linked and detached (Turonian-Santonian level).	top Santonian and Campanian-Maastrichtian	yes (3-10 km long segments in map view)	20-30 km
Shipwreck Trough, Otway Basin	Cenomanian - Palaeocene/ Eocene			cannot determine from dataset.	none	yes (0.5-5 km long segments in map view)	< 10 km

Tab. 1. Data from all 4 papers in this thesis, with the rows assigned to each study area moving from west to east along Australia's southern margin from the Ceduna Sub-Basin (row 1), to the Gambier Embayment (row 2), Nelson Sub-Basin (row 3) and finally the Shipwreck Trough (row 4). The columns assigned to different attributes of normal fault geometry and development from each study area. Note the decrease in segment size and fault assemblage length in the last two columns, moving from west to east along Australia's southern margin.

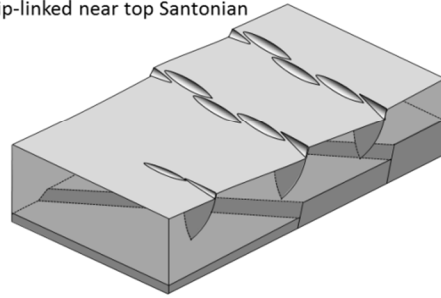
(a) Ceduna Sub-Basin, Great Australian Bight

- Gravity-driven extension/ no basement interaction
- Detached listric fault array
- Growth during thermal subsidence
- 10 km scale fault segmentation
- Vertically segmented
- Dip-linked near top Santonian



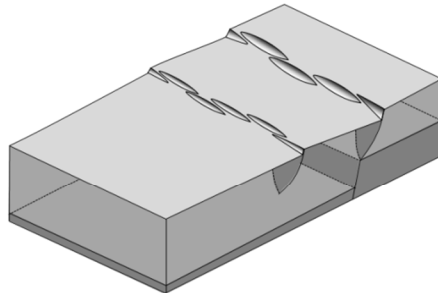
(b) Gambier Embayment, Otway Basin

- Mechanical extension, influenced by (with partial linkage to) underlying basement-involved normal faults
- Growth during rifting event
- kilometre scale fault segmentation
- Striking at 45° to underlying basement-involved faults
- Vertically segmented
- Dip-linked near top Santonian



(c) Nelson Sub-Basin, Otway Basin

- Both gravity-driven and influenced by (with linkage to) underlying basement-involved normal faults
- Growth during rifting event
- kilometre scale fault segmentation
- Striking sub-parallel to basement-involved faults
- Vertically segmented
- Dip-linked near top Santonian



(d) Shipwreck Trough, Otway Basin

- Likely both gravity-driven and mechanical extension occurring in cover sediments
- Growth during rifting event, proximal to a transtensional fault zone
- hectometre scale fault segmentation
- Higher variability in fault strike orientation
- Not vertically segmented
- Continuous growth

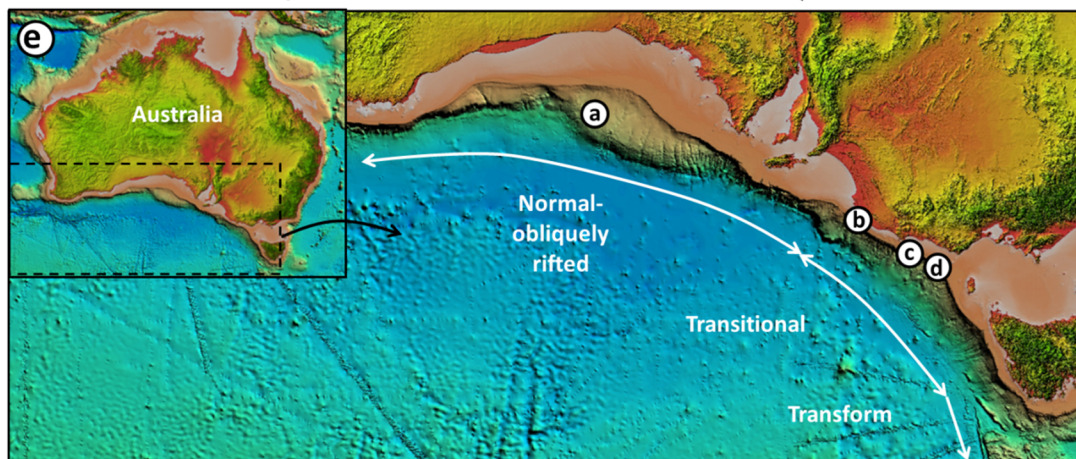
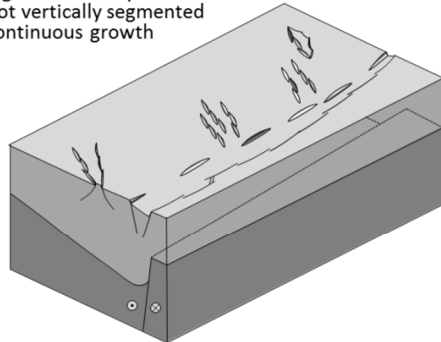


Fig. 1. Schematic 3D block diagrams (with a geometrical and development description) of the four fault arrays analysed in this thesis (a-d) and their location on the digital elevation map of Australia's southern margin below (e). Note the location of the four fault arrays in the context of the three structural domains of the southern margin (normal-obliquely rifted, transitional and transform). Also note how the fault segment size reduces from west to east (a to d).

5.6 Implications for normal fault growth and exploration

5.6.1 Implications for normal fault growth models

Throughout the four papers presented in this thesis we have tried (where possible) to assess the way in which normal fault arrays develop. Proving growth via the isolated or coherent fault model is very difficult, when error in depth conversion and seismic interpretation and fault related folding have to be taken into account. We have observed some minor evidence for the isolated fault model on one fault located in the Gambier Embayment of the Otway Basin (paper 3). All other fault assemblages analysed did not show displacement/throw deficits beyond the error range, inferring that (based on the scale of interpretation) the coherent fault model has greater support by the results of this thesis. The exact definition of the coherent fault model is never going to account for the growth and interaction of all faults and fault assemblages. However, the concept that it resembles is that faults grow in a coherent and organised fashion, resulting from a common stress field and controlled by the underlying basement terrain, the mechanical properties of the rocks in which they nucleate/propagate and the degree of sediment loading. The location of fault nucleation and the way in which a fault propagates to interact with other faults is not random. Therefore, we believe that the coherent fault model better resembles the manner in which normal faults grow and is a better way for geologists to conceptually imagine a normal fault arrays development and interaction.

5.6.2 Implications for petroleum exploration

Given that the results of this study highlights fault which have reactivated and also faults which have dip-linked, the findings of this study have direct implications for hydrocarbon migration. Faults located in the Ceduna Sub-basin and Otway Basin that are interpreted to have reactivated and propagated upwards, may have allowed the migration of hydrocarbons from deep sources rocks into shallow reservoirs. However, the independent nucleation of post-Santonian faults, without initial upward propagation of pre-Santonian faults, may have inhibited the upward migration of

hydrocarbons. Furthermore, faults located in the Ceduna Sub-Basin and Gambier Embayment of the Otway Basin have reactivated very recently, with faults penetrating well into the Cenozoic strata and some faults penetrating as shallow as ~ 70 m below the sea floor. Therefore, this highlights that recent fault reactivation and potential breach of fault dependent traps represents an important risk to the preservation of hydrocarbons in the Ceduna Sub-Basin and Gambier Embayment of the Otway Basin.

In each of the four papers presented, we have displayed surfaces interpreted using 3D seismic data to analyse the growth of normal faults. Each one of these surfaces has sizeable (kilometre scale) structural closures (fault dependent and independent), which may be trapping mechanisms for hydrocarbons. This is especially crucial for the Shipwreck trough, where we present the surface equivalent in age to the top reservoir for the Thylacine and Geographe gas fields. This surface highlights directly analogous horst and half graben structures in close vicinity to these gas fields, providing direct implication for prospectivity and Late Cretaceous play development within the Shipwreck Trough for future exploration.

References

- Baudon, C., & Cartwright, J. (2008). The kinematics of reactivation of normal faults using high resolution throw mapping. *Journal of Structural Geology*, 30(8), 1072-1084.
- Cartwright, J. A., Trudgill, B. D., & Mansfield, C. S. (1995). Fault growth by segment linkage: an explanation for scatter in maximum displacement and trace length data from the Canyonlands Grabens of SE Utah. *Journal of Structural Geology*, 17(9), 1319-1326.
- Childs, C., Nicol, A., Walsh, J. J., & Watterson, J. (1996). Growth of vertically segmented normal faults. *Journal of Structural Geology*, 18(12), 1389-1397.
- Dawers, N. H., & Anders, M. H. (1995). Displacement length scaling and fault linkage. *Journal of Structural Geology*, 17(5), 607-614.
- Jackson, C. A. L., & Rotevatn, A. (2013). 3D seismic analysis of the structure and evolution of a salt-influenced normal fault zone: A test of competing fault growth models. *Journal of Structural Geology*, 54, 215-234.
- Mansfield, C. S., & Cartwright, J. A. (1996). High resolution fault displacement mapping from three-dimensional seismic data: evidence for dip linkage during fault growth. *Journal of Structural Geology*, 18(2), 249-263.
- Ryan, L., Magee, C., & Jackson, C. A. L. (2017). The kinematics of normal faults in the Ceduna Sub-basin, offshore southern Australia: Implications for hydrocarbon trapping in a frontier basin. *AAPG Bulletin*, 101(3), 321-341.
- Rykkelid, E., & Fossen, H. (2002). Layer rotation around vertical fault overlap zones: observations from seismic data, field examples, and physical experiments. *Marine and Petroleum Geology*, 19(2), 181-192.
- Walsh, J. J., & Watterson, J. (1988). Analysis of the relationship between displacements and dimensions of faults. *Journal of Structural Geology*, 10(3), 239-247.

6. Thesis Conclusions

This thesis, together with the results of previous research, has characterised and interpreted the growth of normal fault arrays in several locations along Australia's rift-to-passive southern margin.

This has resulted in several key findings listed below.

6.1 Ceduna Sub-basin

- We have revealed the complex relationship between faults associated with the underlying Cenomanian-Santonian delta system and the overlying post-Santonian fault system, with evidence for both dip-linkage of the fault systems and complete reactivation and upward propagation of the Cenomanian-Santonian fault system into post-Santonian strata. On faults which have dip-linked, it is clear that reactivation of the Cenomanian-Santonian fault system induced the nucleation and growth of the post-Santonian fault system. Therefore, it is clear that the underlying fault system has controlled the nucleation and growth of the upper fault system.
- The post-Santonian fault system displayed much more kinematically coherent growth of strike linked fault segments, indicating that fault length was established relatively early in fault growth history without substantial displacement accumulation.
- From this study it is clear that in stacked delta system settings (i.e. Gulf of Mexico and Orange Basin, offshore Namibia), faults associated with the lower delta system will likely have a large control over the development of faults in the upper delta system, and consequently the delta system itself, with growth faults controlling sediment dispersal.
- Normal faults in the Ceduna Sub-basin have penetrated into the Cenozoic interval, displacing strata as shallow as 70m below the seafloor. This shows that reactivation of these faults occurred extremely recently, with a high potential for fault seal breach of fault dependent traps located along the faults analysed in this study, which presents an important risk to the preservation of hydrocarbons.

6.2 Otway Basin

- Upper Cretaceous normal faults that are linked to the basement-involved faults in the Otway Basin display earlier nucleation and greater overall fault throw than faults which are vertically isolated in cover sediments. This consolidates previous research showing that in an active rift setting, newly formed faults in cover sediments are more likely to initiate earlier above a reactivating basement-involved normal fault, where increased flexure of cover sediments occurs.
- By analysing the growth of a normal fault located in the Gambier Embayment of the Otway Basin, we showed that the hanging-wall depocentre of this fault has laterally increased in size through geological time, which implies this fault increased in length while accumulating significant amounts of throw until eventual linkage. This finding supports early models of normal fault growth, whereby structures nucleated and propagated independently, incidentally overlapped and geometrically linked through relay ramp breaching, referred to as the 'isolated fault model'.
- Both the process of dip-linkage and upward propagation of normal faults have previously been documented many times. However, we have shown that a normal fault in the Gambier Embayment has grown via dip-linkage of fault segments and reactivation and upward propagation of fault segments. This shows that these processes can occur on the same fault over relatively short distance (~3 km), directly highlighting the complexities of normal fault growth.
- We have created a new method for calculating throw variance as a single value to characterise a fault system, which previously had not been conducted. Using this innovative method, we have demonstrated a correlation between fault strike orientation variability and along-strike throw variability. This finding implies that faults which display greater orientation variations in map view display greater throw variability between segment

centres and linkage points. This may imply greater kinematic coherence between faults that have similar strike orientations.

6.3 Australia's southern margin

- The late Santonian continental breakup in the western portions of the southern margin (Bight Basin) had a large influence over normal fault growth in the Ceduna Sub-basin and western and central portions of the Otway Basin, with some degree of fault growth dormancy observed in all three locations at this stage.
- Continental breakup occurring in the far west of the margin (Bight Basin) during the late Santonian did not have a large effect on normal fault growth in the eastern portion of the Otway Basin (Shipwreck Trough), likely due to the distal proximity to the breakup location, transtensional movement, basin compartmentalisation and sediment loading.
- The along-strike segment size of normal faults reduces easterly, from 10 km scale in the Ceduna Sub-basin, to kilometre-scale in the western and central portions of the Otway Basin, to hectometre-scale in the Shipwreck Trough. This may be due to the transition from normal-oblique (and purely gravity driven) extension in the Ceduna Sub-basin, to polyphase mechanical extension in the Otway Basin, creating complexity in basement-involved fault influences on Upper Cretaceous normal fault arrays. Another transition then occurs from normal-oblique extension in the western and central portions of the Otway Basin, to sinistral transtensional movement in the Shipwreck Trough. It appears as though the more complex the structural environment (i.e. pure extension being less complex than transtension), the smaller scale of normal fault segmentation.